INFORMATION TO USERS

PHYSICAL VOLCANOLOGY, GEOCHEMISTRY, AND TECTONIC EVOLUTION OF
THREE SELECTED AREAS IN THE POINT LAKE AND BEAULIEU RIVER
VOLCANIC BELTS, SLAVE PROVINCE, NORTHWEST TERRITORIES, CANADA

by

Patricia Lynn Corcoran

Submitted in partial fulfillment of the Requirements
for the Degree of Doctor of Philosophy

at

Dalhousie University
Halifax, Nova Scotia
June, 2001

0-612-66650-6

Canadä

DALHOUSIE UNIVERSITY

FACULTY OF GRADUATE STUDIES

The undersigned hereby certify that they have read and recommend to the Faculty of Graduate Studies for acceptance a thesis entitled "Physical Volcanology, Geochemistry, and Tectonic Evolution of Three Selected Areas in the Point Lake and Beaulieu River Volcanic Belts, Slave Province, Northwest Territories, Canada" by Patricia Corcoran in partial fulfillment of the requirements for the degree of Doctor of Philosophy.

Dated: June 26, 2001

External Examiner:

Research Supervisor:

Examining Committee:

ii
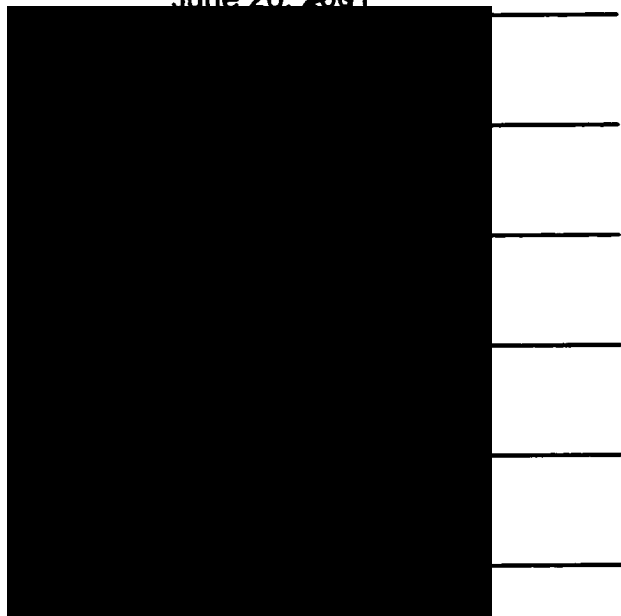
DALHOUSIE UNIVERSITY

DATE: <u>June 26th, 2001</u>

AUTHOR: <u>Patricia Lynn Corcoran</u>

TITLE: <u>Physical volcanology, geochemistry, and tectonic evolution of three selected areas in the Point Lake and Beaulieu River volcanic belts, Slave Province, Northwest Territories, Canada</u>

DEPARTMENT OR SCHOOL: <u>Earth Sciences</u>

DEGREE: <u>Doctor of Philosophy</u>   CONVOCATION: <u>October</u>   YEAR: <u>2001</u>

iii

TABLE OF CONTENTS

LIST OF FIGURES AND TABLES

List of Tables

xi

Abstract

The ca. 2.67-2.70 Ga Point Lake, Northern Beaulieu River and Central Beaulieu River volcanic belts in the Slave Province, Northwest Territories, Canada, represent portions of a continental arc to back-arc sequence that evolved over approximately 30 m.y. Inferred west-dipping subduction of an oceanic slab beneath sialic crust resulted in the development of a continental arc at least 250 km long. Physical volcanology and geochemistry of the volcanic rocks indicate that the Peltier Formation of the Point Lake belt formed in a back-arc basin overlying continental crust, the Northern Beaulieu River belt represents the transition zone between the arc and back-arc, and the Central Beaulieu River belt developed in the arc.

The Peltier Formation overlies the 3.22 Ga Augustus Granite, is interstratified with the >2.65 Ga turbiditic Contwoyto Formation, and is associated with 2.68 Ga felsic-intermediate volcaniclastic rocks of the Samandré and Beauparlant Formations. The mafic-dominated volcanic sequence is consistent with the proximal to distal portions of seamounts in deep to moderate water depths. The proximal facies include a non-vesicular pillowed sequence cut by numerous mafic intrusions, typical of the central, deep water portion of seamounts. The medial to distal, moderate depth facies are represented by pillow breccia, hyaloclastite (peperite), and pillowed and massive flows with 5-27% vesicularity. Interstratified shale units and peperite indicate contemporaneous sedimentation and volcanism. Mafic rocks in 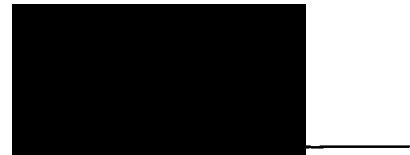the Peltier Formation range from NMORB through tholeiitic LREE-enriched EMORB with Nb and Ti depletions, to strongly LREE-enriched calc-alkaline compositions with Nb and Ti depletions. ε_{Nd} values are from -2.94 to +3.06 and increase with decreasing $(La/Yb)_n$ ratios. Insulation of the conduit walls during ascent of early magmas is considered to have limited the effects of crustal contamination over time.

The Northern Beaulieu River belt overlies the 2.95 Ga plutonic Beniah Complex, ultramafic units, and the 2.9 Ga Beniah Formation quartz arenites. Mafic volcanic facies are massive flows with subordinate pillowed flows and a paucity of fragmental debris, consistent with subaqueous fissure-fed volcanism and local seamount development. A significant mafic dyke complex indicates extension during evolution of the volcanic belt. Felsic volcaniclastic rocks are represented by a succession of planar- and cross-bedded lapilli tuff overlain by wavy- and planar-bedded coarse tuff, grading into planar-bedded

fine tuff with black tuff units, overlain by a pillowed flow. The felsic sequence represents shallow-water reworked pyroclastic deposits that accumulated along a shoreface following subaerial eruption. The fining-upward succession capped by a pillowed flow suggests drowning of the sequence. Mafic samples from the Northern Beaulieu River belt resemble NMORB and slightly LREE-enriched EMORB with negative Nb and some negative Ti anomalies. ε_{Nd} values are between +0.39 and +8.26. One felsic tuff sampled is calc-alkaline.

The Central Beaulieu River belt overlies the 2.95 Ga plutonic Sleepy Dragon Complex and a thin quartz arenite unit. Mafic volcanic facies were deposited on the medial portions of seamounts in water <200 m deep, as indicated by vesicular (5-49%) lobate-pillowed and massive flows, stratified pillow breccia and hyaloclastite. Stratified pillow breccia developed along steep flow fronts in shallow water whereas bedded hyaloclastite formed during redeposition of autoclastic hyaloclastite on seamount flanks in shallow water. Felsic volcanic facies include porphyritic flows, flow breccia, disorganized breccia, and lapilli tuff to tuff, which are consistent with the proximal to distal parts of a subaqueous dome-flow complex. Mafic samples from the Central Beaulieu River belt are tholeiitic to calc-alkaline basalts and andesites, are LREE-enriched, and display marked negative Nb and Ti anomalies. Felsic samples are calc-alkaline rhyolites, LREE-enriched, and have large negative Nb and Ti anomalies.

The study areas are best compared with the Cenozoic Japan Sea back-arc, and the Modern Japan arc, Okinawa Trough, and Havre Trough-Kermadec arc-back-arc system in the Western Pacific. These analogues involve continental crust, and are characterized by seamounts, fissure-dominated volcanism, dome-flow complexes, and shallow-water felsic volcaniclastic deposits. Geochemically, the deposits range from tholeiitic basalts to calc-alkaline rhyolites, depending on proximity to the arc. The north-south elongated, 2.7-2.72 Ga Kam Group of the Yellowknife belt proper, located approximately 150 km west of the Central Beaulieu River belt and strike-parallel to the three study areas, represents a remnant back-arc basin formed on continental crust prior to the evolution of the 2.67-2.7 Ga belts. Inferred arc migration in the western Slave Province, resulting in an arc to back-arc system that developed over ca. 50 m.y., is comparable to the scale and timing of processes operating in modern arc systems in the Western Pacific, such as Fiji and the Mariana arc.

Acknowledgments

Several people helped this thesis become a reality. Many thanks to the faculty and staff of the Earth Sciences Department at Dalhousie University and the Geology Department at Saint Mary's University in Halifax for their support, guidance and much-appreciated help with financial and registration matters over the years. A big thank you goes out to my thesis committee (J. Dostal, R.A. Jamieson, N. Culshaw, J. Waldron), especially to Jarda and Becky who pointed out all of my little errors and had no problems finding the big ones either. The dinners and squash games were great and I'm happy to have had them not only as teachers, but also as friends. To my wonderful friends in the department, especially Sarah, Charu, Gavin M., Gavin S., Eugene, and Ricardo who started out with me on this long endeavor and relate with what I've gone through every step of the way. Great parties, outburst matches, dancing, singing stupidly at the tops of our lungs, movies in English, freezing our butts off on fieldtrips, and trivia-playing made my time with you unforgettable. I wish you all the luck in the world, not that any of you will need it!

To my indispensable field assistants: 1) expert geochem. sample collector, partner in wolverine sightings, half of the reason why "DeBreast" got its name, and accidental murderer of the Beniah tiny mice, Renée-Luce. How did we ever carry those dunites anyway? 2) the world's fastest field walker, partner in riding the waves and getting scared silly over the fault zone howler, Clarence. Thanks for crushing all those samples. I couldn't have done it without you. 3) the man who added originality to our Christmas in July tree, streaked across the Beniah esker, and escorted Jarda straight to the bear, Michael. Additional thanks to everyone else who assisted me in the Slave Province over the years, Joe, Fred, Dean, Jean-Francois, Yves, Sophie, and Christine, for making that time of my life unforgettable.

Much appreciation to everyone at DIAND, especially Bill Padgham and Carolyn Relf for having so much faith in me and my projects, and to the people associated in some way with the Slave Province who visited our camps, providing ideas and guidance: Bill Fyson, C.J. Northrup, Clark Isachsen, Ned Chown, Réal Daigneault, James White, and of course, Wulf Mueller who I'll get to later...

A special thanks to my parents who taught me that I could be whatever I wanted if I worked hard enough, and to my sister for being proud of me and not asking the typical, "when will you be finished?" I thank my husband, friend, fellow geologist and (yep I can say it now) colleague, Wulf Mueller. Thanks for your knowledge, thanks for your organization, thanks for staying out of it when I asked you to (I know it mustn't have been easy), thanks for your patience although I knew it was eating you alive, thanks for taking care of the kids all the nights I had to spend at the university working, thanks for traveling with me to special places like South Africa, New Zealand, Germany, and Denmark. Thank you my boys, Andreas and Owen for not minding too much when I couldn't spend time with you, and especially to little Owen who, with his recent arrival into my life, has taught me to be more tolerant, patient, and better organized.
I'm sorry if I've forgotten anyone. I can't believe it's over. Yippee!!!

Chapter 1

INTRODUCTION

1.1   A Review of Greenstone Belts

Greenstone belts are linear sequences of supracrustal rocks predominantly containing volcanic successions that have undergone relatively low grades of metamorphism (Thurston, 1994). Although greenstone belts are generally associated with Archean terranes, they have formed throughout Earth's history from the early Archean to the Phanerozoic, and may represent a variety of tectonic settings (Taira et al., 1992). Models proposed for the formation of greenstone belts include continental rifts (Goodwin, 1981; Henderson, 1981), oceanic plateaus (Abbott, 1996; Polat et al., 1998), and convergent boundaries, including island arcs and active continental margins (Condie, 1986; Sylvester et al., 1987; Leybourne et al., 1997; Cousens, 2000). Spray (1985), Kusky (1991), and Kusky and Kidd (1992) have suggested that, following their formation, many greenstone belts were tectonically emplaced as allochthoncus sheets that were thrust over older granitoid terranes.

Ancient greenstone belts differ from their Phanerozoic counterparts as a result of specific Archean conditions. The Archean mantle is inferred to have been substantially hotter than at present, which lead to high degrees of melting (Bickle, 1986; Mackenzie and Bickle, 1988). Considering greenstone belts of all ages, only the Archean examples have preserved thicknesses >12 km (Condie, 1994). Ni, Fe, and Cr enrichments and Al_2O_3 depletions for a given Mg# in Archean basalts also support higher mantle temperatures (Arndt, 1991). With time, these high temperatures decreased, potentially as

1

a result of faster spreading, greater ridge lengths, or substantial outpouring of mafic magmas forming extensive oceanic plateaus (Thurston, 1994). The Archean was also associated with more rapid subduction (Bickle, 1978; Nisbet and Fowler, 1983), increased chemical weathering due to higher CO_2 levels (Young, 1991; Des Marais, 1994) and surface temperatures (Kasting, 1993), and increased sea floor spreading and eruption rates (Goodwin, 1977; Taira et al., 1992; Thurston, 1994). Higher eruption rates in Archean greenstone belts are supported by the predominance of ash-flow deposits (Thurston and Chivers, 1990) and a mean thickness preservation rate of 0.35 km/My, which is approximately double the mean post-Archean rate (Condie, 1994). The relatively high preservation potential may also be attributed to underplating by TTG (tonalite-trondhjemite-granodiorite) magmas, where, because of their buoyancy, the magmas rose to the base of the greenstone belts and protected them from further mantle recycling (Condie, 1994). Archean volcanic rocks are predominantly subaqueous basalts of island-arc affinity and ultramafic rocks, including komatiites, in contrast to bimodal- or calc-alkaline-dominated counterparts in post-Archean sequences (Condie, 1989; Thurston, 1994). In addition, fragmental volcanic rocks are less common in Archean deposits and where exposed, are mainly silicic (Lowe, 1994).

Archean greenstone belts have been divided into distinct assemblages, including: 1) platform assemblages, 2) mafic volcanic assemblages, 3) intermediate to felsic volcanic assemblages, and 4) late unconformable basins (Thurston and Chivers, 1990; Thurston, 1994). Platform assemblages are mainly represented by quartz arenite and orthochemical deposits, such as banded iron-formation (BIF). Tholeiitic basalts, ultramafic rocks, and minor interflow tuffs are the predominant mafic volcanic assemblages, whereas intermediate to felsic volcanic assemblages are mainly represented by fragmental deposits and minor dacitic flows. Turbidite sequences are associated with the volcanic assemblages because they were eroded during volcanism and tectonism. Late

unconformable basins, containing alluvial to shallow-water conglomerates, sandstones, and siltstones, are common components of Archean greenstone belts and are attributed to erosion of underlying mafic and plutonic rocks during tectonic uplift, commonly along strike-slip faults (e.g. Krapez and Barley, 1987; Barley, 1987; Mueller and Corcoran, 1998; Corcoran et al., 1999).

Archean crust is preserved in several places throughout the world, but is best represented in the Cathaysian, Siberian, East European, North American, African, Indian, Australian, and Antarctic cratons. The Canadian Shield in the North American craton is divided into distinct geological provinces. The Slave Province, the focus of this study, is located in the Northwest Territories, Canada, and contains numerous linear greenstone belts that present good opportunities for detailed study. Although other Archean provinces contain geochronological evidence supporting an older sialic basement, there are few like the Slave craton where the relationship between greenstone belts and older crustal material is well exposed.

1.2   Statement of the Problem

The evolution of Archean greenstone belts and the role of continental crust has long been a contentious issue. Investigating the relationship between sialic basement and overlying greenstone sequences is not possible in most Archean cratons, but the Slave Province, which is characterized by relatively abundant sialic crust, offers an opportunity to examine basement/greenstone interaction. However, projects incorporating the geochemistry, petrography, and volcanology of one or more study areas in the Slave Province to determine greenstone belt evolution and the role of sialic crust have so far been lacking.

The Yellowknife Supergroup of Henderson (1970), a well-exposed rock succession composed of volcanic and sedimentary formations near the town of Yellowknife, Northwest Territories, has been extended to include all mafic volcanic-dominated supracrustal sequences throughout the Slave Province. The compositional and physical variabilities of volcanic facies in Archean greenstone belts have led workers to assign supracrustal sequences to a range of tectonic settings. so that considering all Slave Province examples as "Yellowknife Supergroup rocks" may not be appropriate. Although several tectonic settings have been proposed for greenstone belt evolution. determining Archean tectonic environments can be problematic because metamorphism and deformation alter the compositions and original structures of volcanic rocks. *Problem:* projects comparing one or more volcanic belts with the Yellowknife Supergroup in the Slave Province are required to test the hypothesis that these belts are truly correlative.

Depositional environments of ancient volcanic successions can be elucidated using facies analyses and petrography where outcrop exposure is optimal. Identifying distinct portions of volcanic edifices. such as seamounts or dome-flow complexes. is not always a simple task in Archean sequences. but is necessary because edifice and facies types, and associated volcanic processes, commonly form in distinct tectonic settings. These volcanic features are more commonly described from Phanerozoic deposits where edifices are better preserved. *Problem:* projects documenting the physical volcanology in Archean greenstone belts need to be conducted to help clarify depositional and tectonic settings.

1.3   Purpose and Significance

Physical volcanology. geochemistry and stratigraphy are disciplines that lead to interpretations of volcanic processes, depositional settings, possible magma sources,

processes affecting parental melts, and tectonic frameworks with which specific rock types are generally affiliated.

Archean greenstone belts compare well with modern volcano-sedimentary sequences in terms of volcanic facies and crustal thickness (Thurston, 1994). Although modern examples contribute information concerning water depth, composition of unaltered volcanic material, and location of a volcano with respect to a spreading centre or arc, edifice core exposure and contact relationships between facies often cannot be determined. Cross sections through ancient rocks that demonstrate well-preserved volcanic structures contribute substantially to recognizing the processes and resulting facies that form at specific levels during edifice construction.

Geochemical studies of greenstone belts overlying sialic crust are relatively rare. Major and trace element (including rare-earth element) compositions reflect interaction with continental crust, indicating that different processes operated at the time of magma genesis than those that occurred where sialic material was absent.

This thesis presents the geochemistry and physical volcanology of felsic to mafic volcanic facies characterizing three study areas in the Point Lake and Beaulieu River volcanic belts. Slave Province. Canada. The Beaulieu River and Point Lake belts were selected for detailed study and general comparison with the Yellowknife belt because: 1) the supracrustal sequences have all been correlated with the Yellowknife Supergroup. 2) all belts occupy similar stratigraphic positions with respect to surrounding rock types, and 3) all study areas are dominated by mafic volcanic deposits.

Chapter 2 provides the general geology, stratigraphy, and ages of the Yellowknife. Central and Northern Beaulieu River, and Point Lake belts. Chapters 3-5 document the volcanic facies and geochemistry of the study areas, which leads to interpretations of the depositional and tectonic settings. Comparisons of the study areas with the Yellowknife

belt and with Phanerozoic analogues, and presentation of an overall model of Slave Province evolution between 2.66-2.7 Ga is provided in Chapter 6.

1.4   Methodology

Regional mapping was conducted at scales of roughly 1:1000 and 1:96 000 for the Point Lake belt, 1:87 000 for the Northern Beaulieu River belt, and 1:43 500 for the Central Beaulieu River belt using air photographs and previous maps by Henderson (1988), Stubley (1989) and Roach (1990). Specific localities were chosen for detailed mapping where outcrop exposure was optimal, a variety of volcanic facies types were represented, and lateral and vertical transitions were identifiable. Two localities were selected for detailed study from each of the three study areas. Outcrops were mapped at scales of 1:25, 1:30, 1:50, 1:250, and 1:350 using gridlines. Stratigraphic sections were mapped at scales of 1:250, 1:400, and 1:650 using a 60 m measuring tape. A total of 283 samples were collected from the three study areas to examine the primary and secondary mineralogy, and igneous textures in the volcanic rocks. Representative thin sections were selected for determining percentage vesicularity. Vesicle and amygdule (filled vesicle) abundances were determined by 2-dimensional counting, using 100 point grids with 1 cm and 3 mm spacing on photos, in addition to counting 500 points at every 2 mm microscopically.

One hundred and twenty-nine samples from the Beaulieu River and Point Lake belts were analyzed for major and certain trace elements (Rb, Sr, Ba, Zr, Nb, Y, La, Ce, Nd, Ga, Cu, Zn, V, Sc, Co, Cr, Ni) by X-ray fluorescence (XRF) using fused glass discs and powder pellets at the Geochemical Centre, St. Mary's University, Halifax, Nova Scotia. The precision and accuracy are illustrated in Appendix 1. Twenty-six representative samples from the Point Lake belt, 21 samples from the Northern Beaulieu

River belt, and 14 samples from the Central Beaulieu River belt were chosen for additional trace element analyses, including the rare earth elements (REE), Th, Nb, and Hf, using inductively coupled plasma-mass spectrometry (ICP-MS) at Memorial University, Newfoundland. The quality of the data and precision of the method are provided in Appendix 1. Thirteen samples from the Point Lake belt and four samples from the Northern Beaulieu River belt were selected for Sm and Nd isotope analysis using isotope dilution mass spectrometry at the AURIF lab, Memorial University, Newfoundland. Measured $^{143}Nd/^{144}Nd$ ratios were normalized to a $^{146}Nd/^{144}Nd$ ratio of 0.7219. The LaJolla standard, analyzed as part of every run, yielded average $^{143}Nd/^{144}Nd$ of 0.511849 +/-9. Initial Nd isotope ratios and εNd values were calculated using ages of 2.69 and 2.7 Ga. The analytical technique for Nd isotope analyses is described in Kerr et al. (1995), where the precision is ±0.5% or better.

Variable abundances of K, Rb, and Sr and elevated LOI values are attributed to chemical alteration and metamorphism. LOI values are <4 for >75% of the Point Lake samples, 83% of the northern Beaulieu River belt samples, and 60% of the central Beaulieu River belt samples. Highly altered rocks with LOI>8 were excluded from further consideration. Mobile elements such as K and Na, and most of the other LFSE were not used for chemical classification. Interpretations of the petrogenesis and tectonic setting are based on the less mobile high-field-strength elements (HFSE), REE, and Th.

1.5 Terminology

Several terms employed in volcanology have different connotations depending on grain size, composition, or transport process. The classification schemes are controversial and thus their usage in this thesis needs to be defined. The term "facies" refers to a distinct deposit that demonstrates consistent observable attributes, such as composition

and volcanic structure. For example, a mafic flow may be both massive and pillowed, but is represented by two facies: 1) a massive facies and 2) a pillowed facies. Similarly, a rock sequence containing massive flows that are both felsic and mafic, consists of two facies: 1) massive mafic flows and 2) massive felsic flows. "Flow units" contain numerous flows that are unseparable in the field, but are distinct petrographically. The term "volcaniclastic" refers to clastic deposits that contain predominantly volcanic components, irrespective of origin (Fisher, 1961). "Volcanic sandstones" and "volcanic breccias" are volcaniclastic rocks that range in grain size from 0.0625-2 mm and 2->64 mm, respectively (Fisher, 1961; Fisher and Schmincke, 1984). "Pyroclastic" deposits are the direct results of an explosion or the reworked products of exploded material prior to lithification (Fisher and Schmincke, 1984). Pyroclastic deposits are subdivided using the grain size classification of Fisher (1961, 1966) and Fisher and Schmincke (1984; p. 90-93), where "fine tuff" is <0.0625 mm, "coarse tuff" is 0.0625-2 mm, "lapilli" is 2-64 mm, and "breccia" is >64 mm. "Lapilli tuff" is a pyroclastic deposit containing both tuff- and lapilli-size fragments with the tuffaceous component being >25 %. "Hyaloclastite" is a fragmental deposit that forms by granulation or shattering when subaerial flows enter water, magma is erupted subaqueously, or magma is intruded through or into wet sediment (McPhie et al., 1993). The latter type of hyaloclastite is also referred to as "peperite" (Fisher, 1960).

1.6   Relationship to Published Work

Parts of this thesis have been published in two journal articles:

1) Corcoran, P.L., 2000. Recognizing Distinct Portions of Seamounts using Volcanic Facies Analysis: examples from the Archean Slave Province, Northwest Territories, Canada. Precambrian Geology, 101: 237-261.

2) Corcoran, P.L. and Dostal, J., 2001. Development of an ancient back-arc basin overlying continental crust: the Archean Peltier Formation, Northwest Territories, Canada. Journal of Geology, 109: 329-348.

Descriptions and interpretations of the mafic volcanic facies in the Point Lake and Central Beaulieu River belts from Corcoran (2000) are included in Chapters 3 and 5. Geochemical descriptions and interpretations, in addition to the tectonic model for the Point Lake belt in Chapter 3 were presented in Corcoran and Dostal (2001). Most of the text in the thesis has been modified, but some passages are included verbatim. Certain figures and photos have already been published, but the figure contents and descriptions have been slightly modified for the thesis.

Fieldwork, sampling, and research for Corcoran and Dostal (2001), in addition to the actual writing, was conducted by the first author. The second author, J. Dostal, made suggestions and provided opinions regarding the writing style and data, and was responsible for the funding of the project.

Chapter 2

GEOLOGY

2.1 Introduction to the Slave Province

The Slave Province, located in the Northwest Territories, Canada, is a relatively small Archean craton, approximately 500 km x 700 km in size (Figure 1). Plutonic suites. linear greenstone belts, and a variety of sedimentary successions including quartz arenites. extensive turbidite sequences, and late conglomeratic basins, comprise the ca. 2.58-4.0 Ga (Bowring et al. 1989; van Breeman et al.. 1992: Isachsen and Bowring, 1997) Slave Province. Several features distinguish the Slave Province from most Archean cratons worldwide. including: (1) exposed sialic basement, (2) a higher felsic/mafic volcanic rock ratio. (3) more sedimentary than volcanic rocks, and (4) abundant evolved potassium-rich granites (Henderson. 1981: Padgham. 1987: Padgham and Fyson, 1992). The oldest known rocks in the world. the 3.96-4.03 Ga Acasta gneisses (Bowring et al.. 1989; Bowring and Williams. 1998), and their >2.8 Ga counterparts (e.g. Sleepy Dragon Complex. Augustus Granite: Henderson et al.. 1987; Northrup et al.. 1999), are basement to overlying supracrustal belts in the western part of the craton (Figure 1). Mafic and intermediate volcanic rocks, ca. 2.66-2.72 Ga, dominate greenstone belts in the west. whereas ca. 2.67-2.7 Ga intermediate to felsic volcanic rocks are more common in the east (Henderson. 1981: Padgham. 1985: Padgham and Fyson, 1992). The 2722 ± 1 - 2662 ± 3 Ma (Isachsen and Bowring. 1997) Yellowknife volcanic belt can be correlated Slave-wide with the Anialik River (2687 ± 2 - 2678 ± 2 Ma; Relf et al.. 1999), Hood River (2668 ± 4 Ma; van Breemen et al., 1994), Cameron and Beaulieu River (2663 + 7/-5 Ma; Henderson et al.. 1987), and Point Lake (2690 ± 3 - ca. 2673 Ma; Northrup et al., 1999)

10
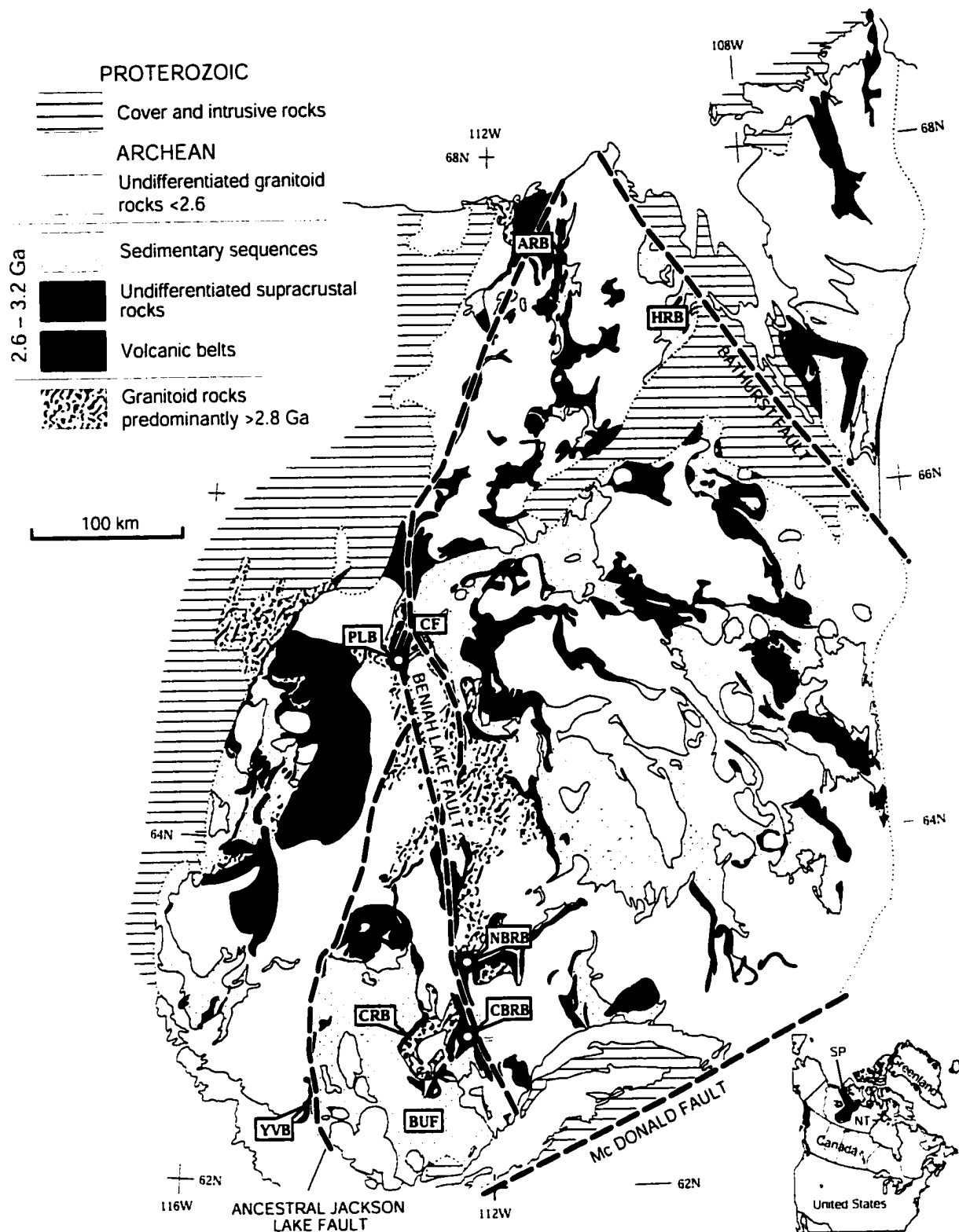
Figure 1: Lithological map of the Slave Province (SP) in the Northwest Territories (NT), Canada. Locations of the Point Lake (PLB), Northern Beaulieu River (NBRB), Central Beaulieu River (CBRB) Cameron River (CRB), Anialik River (ARB), Hood River (HRB), and Yellowknife (YVB) belts are indicated. CF, Contwoyto Formation; BUF, Burwash Formation. Circles indicate study areas. Modified from Corcoran (2000).

volcanic belts (Figure 2). The Yellowknife, Cameron River, Beaulieu River and Point Lake volcanic belts unconformably and/or structurally overlie older gneissic basement (Henderson et al., 1987; Bowring and Williams, 1998, Northrup et al., 1999), recently referred to by Bleeker et al. (1999a) as the Central Slave Basement Complex.

The Slave Province is characterized by a series of north-trending lineaments along which ca. 2.6 Ga porphyry stocks (Mueller et al., 1998), many of the volcanic belts, and most of the late-orogenic sedimentary rocks are restricted. The two most prominent lineaments are the north-trending Beniah Lake (Beaulieu River Fault Zone of Bleeker et al., 1999a) and ancestral Jackson Lake faults (Figure 1). Padgham and Fyson (1992) suggested that the Beniah Lake fault represents a significant tectonic break between an older, ca. 2.6-4.0 Ga western terrane characterized by a sialic basement and a younger, ca. 2.6-2.8 Ga eastern terrane. Compared to the eastern portion, rocks in the west produce negative ε_{Nd} values (Davis and Hegner, 1992) and higher $^{207}Pb/^{204}Pb$ ratios as determined from galena in massive sulfides (Thorpe et al., 1992). Extensive turbidite assemblages (ca. 2.71-2.65 Ga) appear to cross the boundary between the eastern and western parts of the craton, indicating that if the fault zone is 2.8 Ga or older (Padgham and Fyson, 1992) it may have undergone subsequent reactivation, resulting in the formation of 2.6 Ga tectonically-influenced sedimentary basins (Corcoran et al., 1999).

Models proposed for Slave Province evolution and for individual greenstone belts are all compatible with plate tectonic processes. Based on studies in the Yellowknife and Point Lake regions, McGlynn and Henderson (1970), Henderson (1981, 1985) and Easton (1985) suggested that the volcanic belts developed as volcanic centres along the edges of rift or fault-bounded basins (Figure 3). Older granitoid rocks, representing sialic basement crust, in addition to the overlying mafic volcanic rocks, were eroded and contributed detritus into the basin. This detritus is represented by the extensive turbidite sequences common in the Slave Province. Felsic volcanism is interpreted to have
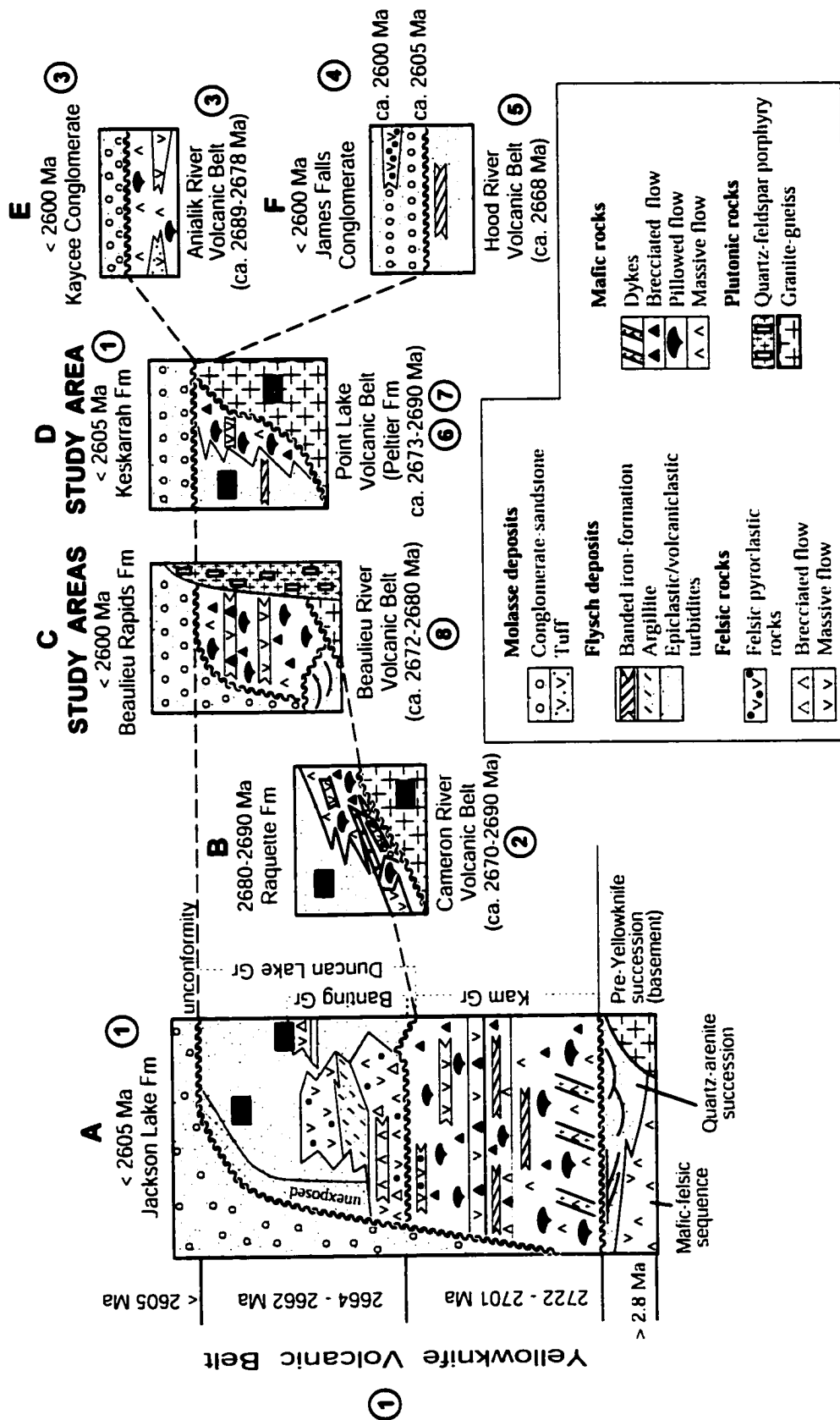
Figure 2: Stratigraphy of the Yellowknife volcanic belt and lateral pan-Slave Province correlations. References for ages: 1) Isachsen et al. (1991). Isachsen and Bowring (1994, 1997), 2) Henderson et al. (1987), 3) Relf et al. (1994), 4) Villeneuve (1994), 5) van Breemen et al. (1994), 6) Northrup et al. (1999), 7) Mueller et al. (1998), 8) unpublished data from Mueller et al. (2001). BF, Burwash Formation; CL, Clan Lake volcanic pile; SD, Sleepy Dragon Complex; CF, Contwoyto Formation; AG, Augustus Granite. Modified from Corcoran et al. (1998).
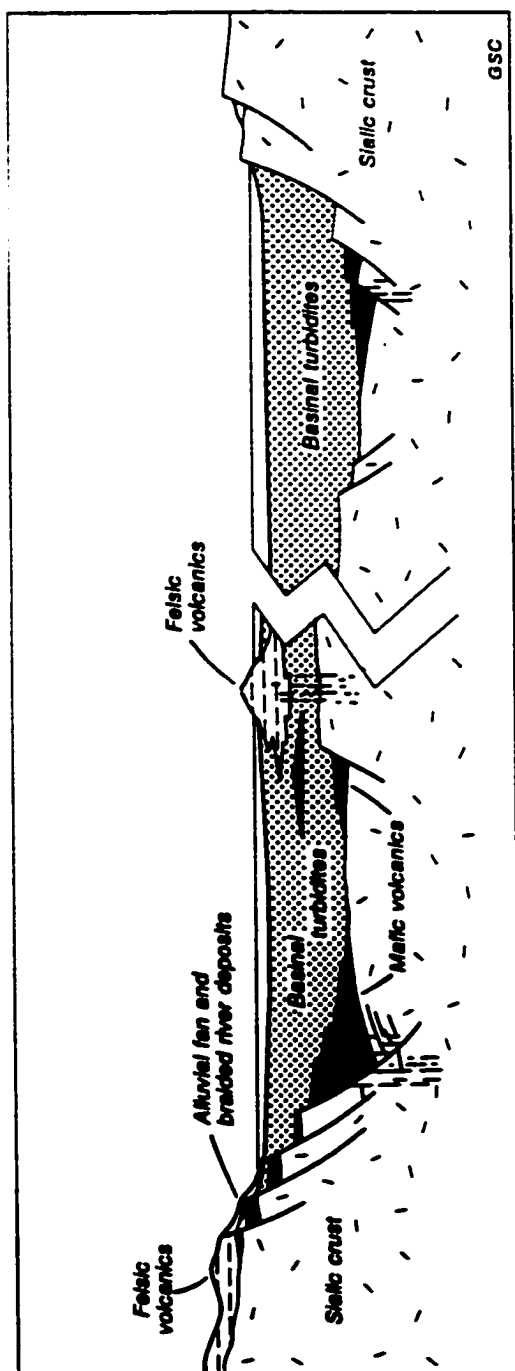
Figure 3: Fault-bounded basin model illustrating the evolution of the supracrustal sequences in the Slave Province. Rifting of sialic crust resulted in down-dropped blocks with faulted margins. Mafic volcanic deposits were erupted as volcanic centres along the faults, and with the sialic crust, were eroded and deposited into the basin. The main basin fill, represented by turbidites, was deposited during eruption of felsic volcanic material. Fluvial and shallow water sequences were deposited following breaching and further erosion of mafic centres. From Henderson (1981, 1985).

occurred during deposition of the turbidite successions. Following breaching of the mafic volcanic edifices, additional material was deposited as fluvial and shallow water deposits, represented by the ca. 2.6 Ga sedimentary formations (Henderson, 1981, 1985). Helmstaedt and Padgham (1986), MacLachlan and Helmstaedt (1995), and Cousens (2000) proposed that the Yellowknife volcanic belt formed in a back-arc basin during rifting of a continental margin arc. However, Kusky (1989) discounted the continental rift model based on the presence of contractional structures and rock types different from those typically associated with rift settings. Kusky (1989, 1990) expanded on the arc-related theory by proposing that the Slave Province evolved from accretion of several distinct terranes with significant suture zones located between the i) Anton and Contwoyto and ii) Sleepy Dragon and Contwoyto terranes (Figure 4). The Anton and Sleepy Dragon terranes, located west of the Beniah Lake fault and containing older basement, were inferred to have been subducted beneath the Contwoyto terrane, which is predominantly turbiditic with ophiolite-like slivers, interpreted as an accretionary prism complex (Kusky, 1989; Figure 5). Although the terranes contain older sialic basement, Kusky (1989, 1990) interpreted the greenstone belts as allochthonous sheets that were thrust over sialic crust. Bleeker et al. (1997a) proposed a multi-stage evolution for the Slave Province supracrustal belts, which involves interaction of basement-cover sequence microplates in the west and younger juvenile arc terranes in the east. Relf et al. (1999) inferred subduction between the ca. 2.68 Ga Anialik River belt from the eastern half of the province and the ca. 3.4 Ga gneissic Kangguyak domain in the west. The models of Kusky (1989), Bleeker et al. (1997a) and Relf et al. (1999) are similar in that the supracrustal belts are inferred to have been related to subduction that occurred between distinct eastern and western components. The rift model of Henderson (1981, 1985) is also consistent with plate tectonics, but as an extensional regime in either a continental back-arc or rifted margin setting. Subsequent lithological, volcanological, and
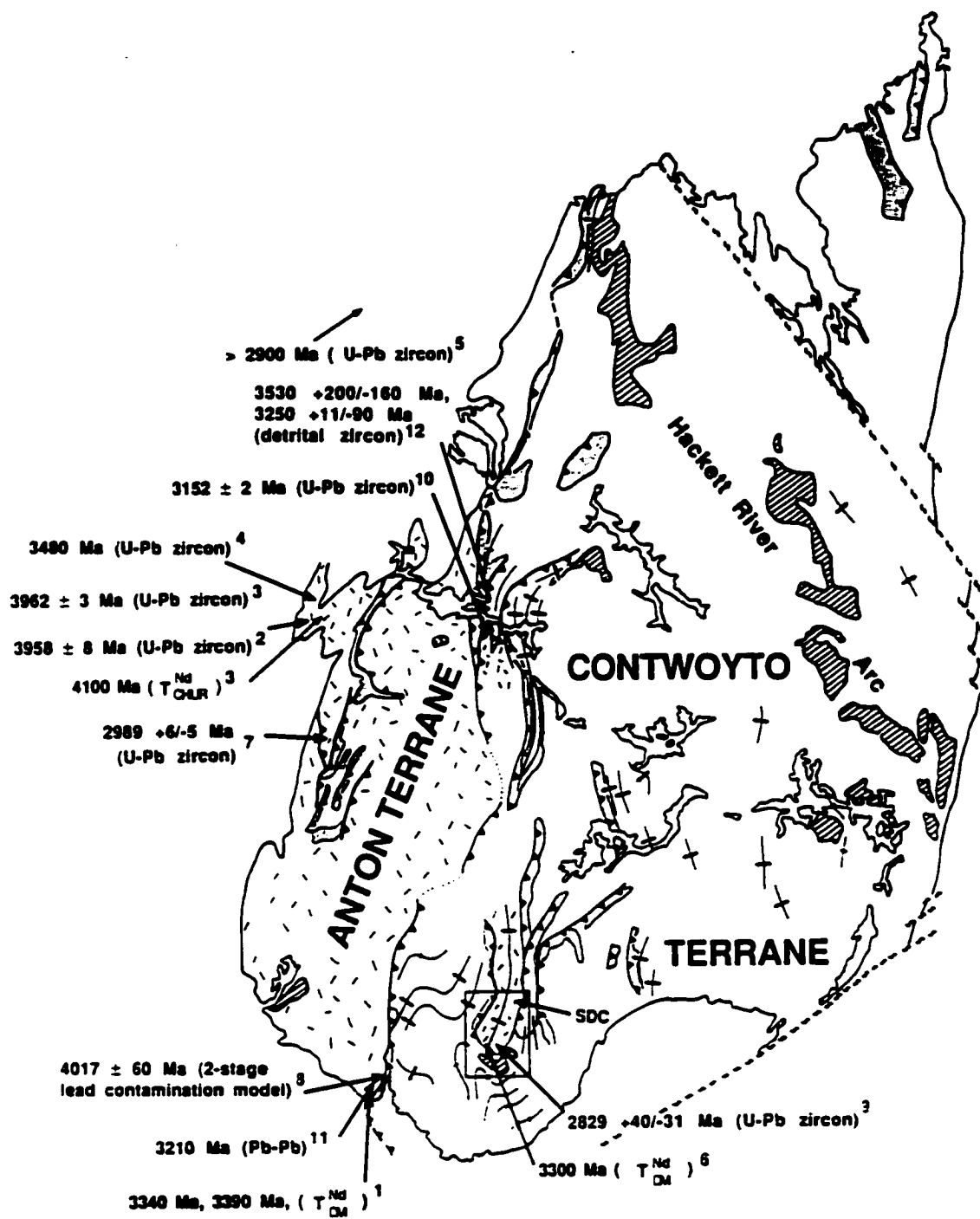
Figure 4: Map of the Slave Province illustrating the distribution of the Anton and Contwoyto terranes, Sleepy Dragon Complex (SDC) and Hackett River arc. The Anton Composite terrane (includes Sleepy Dragon terrane) is interpreted to have been subducted beneath the Contwoyto terrane. For details concerning the structures and age dates, see Kusky (1990).

Anton Composite Terrane   **Contwoyto Terrane**

A   Detour Lake Group   trench turbidites   **Hackett   River arc**
Beniah Formation
200°
500°
2.698-2.663 Ga
4.0, 3.5, 3.1,   mafic dike swarm
2.8 Ga peaks

arc volcanism superimposed
on older accreted greenstone
belts, mafic arc basement,
early thrusts

B   flysch and wildflysch
sedimentation
200°
500°
Anton

shelf drowning, ophiolite
obduction and dynamo-
thermal metamorphism

C   Sleepy Dragon Complex

Anton

syn-metamorphic thrusts,
continued overthrusting of
Anton Terrane, molasse
(Jackson Lake Formation)

D   Yk   CR   SR suture   high-angle reverse
faults
5
km
15
T$_{CHUR}^{Nd}$ > 2.7   T$_{CHUR}^{Nd}$ < 2.7   2.62-2.55 Ga

continued compression,
crustal thickening and
anatexis, granitic
plutonism, vertical
extension, lateral
escape

Figure 5: Four-stage model illustrating the evolution of the Slave Province in the Sleepy Dragon area (south). In this model, greenstone belts are considered allochthonous, having been thrust onto older basement. In (A) the Anton Composite terrane is subducted beneath the Contwoyto terrane. In (B) extensive turbidite sequences and slivers of inferred oceanic crust are formed as an accretionary prism. Compression continues in (C) with overthrusting and deposition of molasse, ca. 2.6 Ga sedimentary successions. Slave Province evolution ends with a stage of crustal thickening and extensive granitoid intrusion emplacement (D). From Kusky (1990).

geochemical studies support an arc-related model based on the presence of calc-alkaline andesites and/or basalts in certain supracrustal belts (e.g. Point Lake belt, Corcoran and Dostal, 2001; Beaulieu River and Cameron River belts, Lambert, 1988).

2.2 Yellowknife Volcanic Belt

The ca. 2662-2722 Ma (Isachsen et al., 1991; van Breemen et al., 1992; Isachsen and Bowring, 1994) Yellowknife volcanic belt (Figure 2) is considered the type section for the Slave Province-wide Yellowknife Supergroup of Henderson (1970). Inferred basement to the Yellowknife belt is represented by tonalite and granodiorite gneiss components in the Anton Complex (Isachsen and Bowring, 1997). The supracrustal assemblage also overlies two older volcano-sedimentary sequences, 1) the Bell Lake Group and 2) the Octopus Formation, but the nature of the contacts is unclear (Helmstaedt and Padgham, 1986). The Yellowknife belt is divided into the mafic flow-dominated Kam Group, the felsic volcaniclastic-dominated Banting Group and the clastic-dominated Duncan Lake Group (Helmstaedt and Padgham. 1986; Figures 2a, 6, 7).

2.2.1 Anton Complex

The Anton Complex is located along the northwest portion of the Yellowknife volcanic belt (not shown on Figure 7). U-Pb zircon ages of 2.93-3.41 Ga indicate that the granodioritic and tonalitic gneisses represent silicic basement to the Yellowknife volcanic rocks (Isachsen and Bowring, 1997). The Anton Complex also contains younger. 2642-2707 Ma granitoid intrusions (Henderson, 1985; Dudas et al., 1990). Although the contact with the overlying volcanic sequence remains enigmatic, ε_{Nd} values ranging from

Figure 6: Stratigraphy of the Yellowknife Supergroup illustrating the formations comprising the Kam, Banting, and Duncan Lake Groups. From Helmstaedt and Padgham (1986).
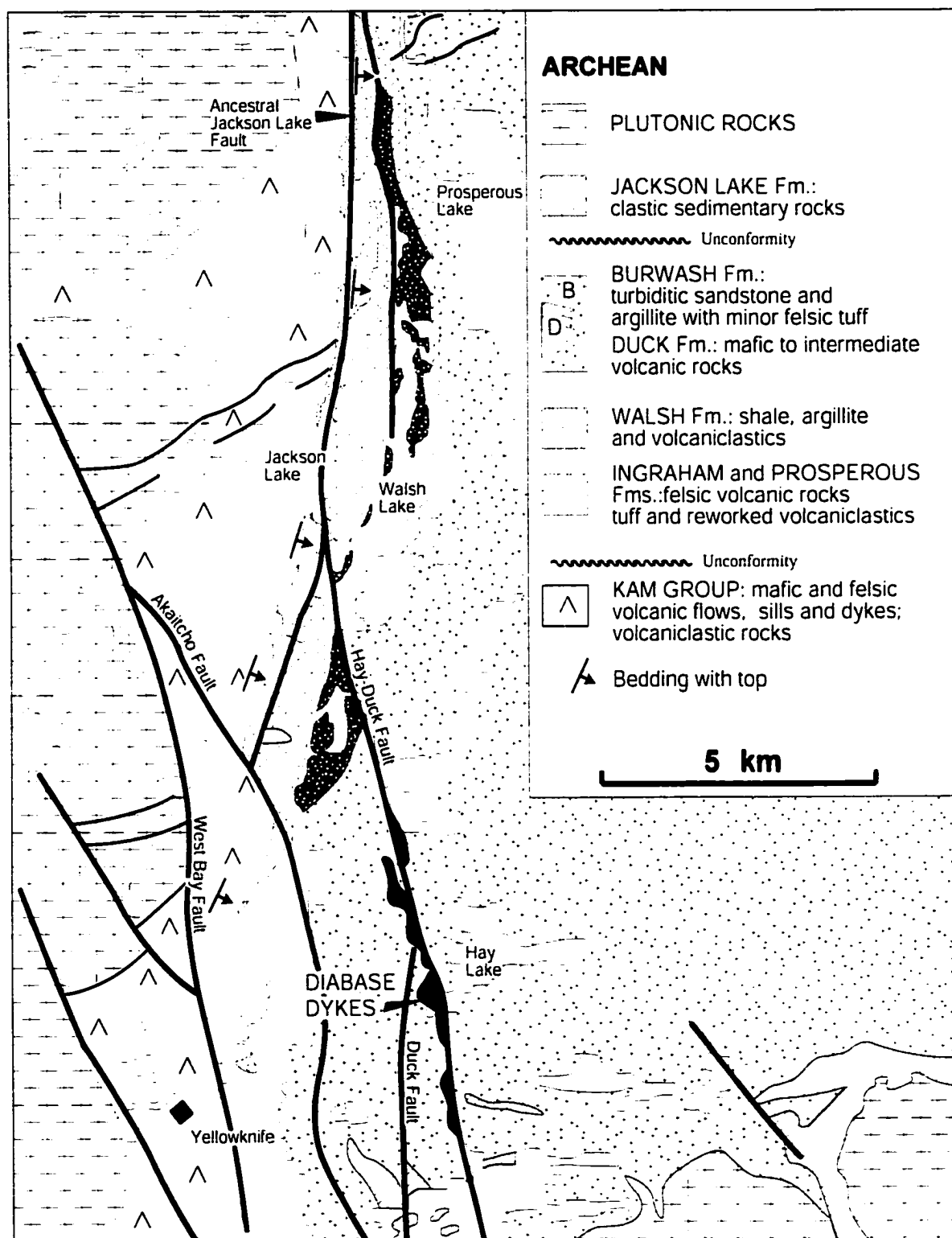
Figure 7: Regional map of the Yellowknife area showing the distribution of the Yellowknife volcanic belt formations. Modified from Henderson and Brown (1966) and Helmstaedt et al. (1980).

+5 to -3 in the mafic-intermediate rocks of the Kam Group (Cousens, 2000) further support the presence of a sialic basement.

2.2.2 Bell Lake Group

The Bell Lake Group (Isachsen and Bowring, 1997), also referred to as the Likely Formation (Padgham, 1987), Dwyer Formation (Padgham and Fyson, 1992), and Dwyer Group (Isachsen, 1992), is a <100 m-thick sequence composed of quartz arenite, felsic volcanic rocks, banded iron-formation and mafic intrusions (Helmstaedt and Padgham, 1986; Pickett, in prep.), located approximately 25 km north of Yellowknife. U-Pb detrital zircon ages of 2.92 to >3.7 Ga from the quartz arenite and an inferred unconformity between the Anton Complex and Bell Lake Group at Bell Lake (Isachsen and Bowring, 1997) indicate that the volcano-sedimentary succession is older than the Yellowknife volcanic belt (Figure 2). The Bell Lake Group, which is represented by rocks at Dwyer, Bell and Nelson Lakes, has recently been included with similar sequences at Beniah, Patterson and Brown Lakes as part of the Central Slave Cover Group of Bleeker et al. (1999a).

2.2.3 Octopus Formation

The Octopus Formation is a volcano-sedimentary succession located along the southeast margin of the Yellowknife belt. The formation, composed of amphibolites, felsic volcaniclastic rocks, siltstones, and conglomerates, was interpreted as volcanic-sedimentary remnants of a pre-Kam Group depositional cycle (Helmstaedt and Padgham, 1986). Recent geochronological data (Ketchum and Bleeker, 2000), however, indicate

that the Octopus Formation is correlative with the Yellowknife Bay Formation of the Kam Group, with an age of 2702 +8/-6 Ma.

2.2.4   Kam Group

The 10-12 km-thick Kam Group is a mafic-dominated volcanic succession divided into four distinct formations, which from base to top include: 1) the Chan, 2) the Crestaurum, 3) the Townsite, and 4) the Yellowknife Bay Formations (Figure 6).

The Chan Formation is approximately 6 km thick and consists mainly of tholeiitic mafic flows and mafic intrusions (Henderson and Brown, 1966; Helmstaedt and Padgham, 1986; MacLachlan and Helmstaedt, 1995). These intrusions display a sheeted nature, resembling typical ophiolite sheeted dyke complexes (Helmstaedt and Padgham, 1986) and some contain numerous chilled margins, consistent with multiple intrusion (MacLachlan and Helmstaedt, 1995). Based on geochemical data and the presence of numerous dyke phases, the Chan Formation is interpreted to represent the early rifting stages of a marginal or back-arc basin (Isachsen, 1992; MacLachlan and Helmstaedt, 1995).

The overlying Crestaurum Formation is composed of tholeiitic mafic flows, and cherty, felsic tuffs (Henderson and Brown, 1966; Helmstaedt and Padgham, 1986). The basal contact with the Chan Formation is marked by the Ranney chert, which yielded a maximum U-Pb zircon age of 2.72 Ga (Isachsen and Bowring, 1997). Detrital zircons within the chert yielded ages similar to those determined from the Anton Complex, indicating that the plutonic complex provided detritus to the overlying volcanic belt (Isachsen, 1992). Further support for involvement of continental crust are the ε_{Nd} values from the felsic units that range from -2.2 to -3.0. Additional inferred sources for the felsic volcaniclastic units in the Crestaurum Formation are arc-related, calc-alkaline eruptive

centres whose material was locally deposited in the marginal basin in which the Chan

Formation formed (MacLachlan and Helmstaedt, 1995).

The Townsite Formation is represented by three members, known as the Niven,

Brock, and Vee Lake lenticles. The Niven and Brock lenticles contain basalts and basaltic

andesites, whereas the Vee Lake lenticle is andesitic (Cousens, 2000). Baragar (1966)

reported calc-alkaline bulk chemistry for the entire Townsite Formation, whereas

Cousens (2000) determined that the mafic to intermediate rocks comprising the formation

follow a tholeiitic fractionation trend. Mafic rocks in the three lenticles produce positive

ε_{Nd} values, but the more felsic units have ε_{Nd} values ranging from -0.2 to -0.9 (Cousens,

2000). As for the felsic units in the Crestaurum Formation, these values corroborate the

involvement of continental crust during their development.

Massive mafic, pillowed, and pillow breccia flows predominate in the Yellowknife

Bay Formation. This uppermost formation of the Kam Group is at least 5 km thick and is

also characterized by mafic intrusions, cherty tuffs and coarse turbiditic sandstones

(Helmstaedt and Padgham, 1986). Although the Yellowknife Bay Formation is

dominated by tholeiitic basalts, some rocks are also andesitic in composition (Cousens,

2000). Negative ε_{Nd} values of -5.3 and -2.9 suggest interaction with continental basement

(Cousens, 2000).

2.2.5   Banting Group

The ca. 2662 Ma (Isachsen and Bowring, 1997), predominantly calc-alkaline

Banting Group is a 2 km-thick felsic volcaniclastic-dominated sequence divided into two

distinct formations including: 1) the Ingraham and 2) the Prosperous Formations (Figure

6). The Banting Group is discordant with the underlying Kam Group with a hiatus of 35

m.y. (Figure 2).

The Ingraham Formation is divided into the Shot Lake and Greyling Lake members. The Shot Lake member is characterized by quartz monzonite, quartz-feldspar porphyry, mafic and felsic fragmental flows, bedded tuff, and conglomerate (Helmstaedt and Padgham, 1986). This member is in fault contact with the overlying Jackson Lake Formation and is unconformably overlain by turbidites of the Walsh Formation, Duncan Lake Group (Figure 2; Helmstaedt and Padgham, 1986). The overlying Greyling Lake member features quartz-feldspar porphyry, felsic volcaniclastic rocks, mafic to intermediate pillowed flows, felsic flows, and local ash-flow units with fiamme at the top (Helmstaedt and Padgham, 1986). There is a conformable contact between the Greyling Lake member and the turbiditic Walsh Formation.

The Walsh Formation was considered part of the Duncan Lake Group according to the stratigraphy of Helmstaedt and Padgham (1986) (Figure 6), however, Padgham (1987) later characterized the formation as part of the Banting Group, as did Isachsen and Bowring (1997). This turbiditic sequence contains thin sandstone beds attributed to deposition in relatively shallow water as compared with the more extensive Burwash Formation of the Duncan Lake Group (Padgham, 1987). The Walsh Formation is conformably overlain by the Prosperous Formation.

The Prosperous Formation contains similar rock types to the Ingraham Formation, but they are considered distinct sequences as they are both locally interstratified with a homoclinal succession of Walsh and Burwash Formation turbidites (Figure 6). The Prosperous Formation is thus considered to have been deposited after initial Walsh Formation turbidite accumulation, following Ingraham Formation volcanism (Helmstaedt and Padgham, 1986).

The Banting Group is interpreted as the result of renewed arc volcanism (MacLachlan and Helmstaedt, 1995) as indicated by the calc-alkaline nature of the mafic to felsic flows (Cunningham and Lambert, 1989) and the abundance of volcaniclastic

deposits. Volcanic edifices must have been locally emergent based on the presence of wave-reworked volcaniclastic deposits and pyroclastic deposits with fiamme (Padgham, 1980).

2.2.6 Duncan Lake Group

The sedimentary-dominated Duncan Lake Group is composed of three main formations: 1) the Burwash, 2) the Duck, and 3) the Jackson Lake Formations. The Duncan Lake Group overlies the Banting Group conformably, with turbidites of the Burwash Formation locally interstratified with volcaniclastic sedimentary rocks of the Prosperous and Ingraham Formations (Helmstaedt and Padgham, 1986).

The Burwash Formation, approximately 4.5 km thick, is characterized by the graded, rippled, parallel laminated, and massive divisions typical of turbidite Bouma sequences (Henderson, 1975). It also locally contains non-turbidite, wave-developed facies close to the transition with the subaerial-subaqueous coarse clastic Raquette Lake Formation (Figure 2; Mueller and Corcoran, in press). Thin units of intraformational conglomerate and felsic tuff also characterize the sequence. The rocks are consistent with submarine fan development (Henderson, 1975) in a marginal, intra-arc, or fore-arc basin (MacLachlan and Helmstaedt, 1995; Bleeker et al., 1997a).

The Duck Formation, up to 1.5 km thick, is interstratified with the Burwash Formation east of Yellowknife (Figure 7; Easton et al., 1982). It is characterized by pillowed flows, pillow breccia, hyaloclastite, and hyalotuff cut locally by porphyritic felsic units (Helmstaedt and Padgham, 1986). Much of the formation has been extensively altered, but the least-altered rocks have a bulk chemical composition transitional between tholeiitic and calc-alkaline (Cunningham and Lambert, 1989). The Duck Formation is just one of several volcanic centres that interfinger with the extensive

Burwash Formation. Time-equivalent felsic volcanic centres at Clan (ca. 2661±2;

Mortensen et al., 1992; Figure 2) and Turnback Lakes (2663+7/-5 Ma; Henderson et al.,

1987) are consistent with complex interaction of volcanism and sedimentation.

The uppermost Jackson Lake Formation represents the youngest basin-forming

event in the Yellowknife belt with an age of <2605 Ma (Isachsen et al., 1991). It overlies

the Yellowknife Bay Formation of the Kam Group unconformably, and a 50 m.y. hiatus

is inferred between the clastic sequence and the Banting Group rocks (Isachsen and

Bowring, 1994). The Jackson Lake Formation is a 50-300 m thick sedimentary sequence

composed of conglomerate-sandstone, sandstone-argillite, and argillite-sandstone

(Henderson, 1975; Mueller et al., in press) preserved along the north-trending ancestral

Jackson Lake Fault (Figure 7). The deposits are interpreted to have formed in a wave-

and tide-influenced, high-relief basin with open ocean access (Mueller et al., in press).

2.3   Point Lake Volcanic Belt

The Point Lake volcanic belt, originally named the Point Lake Formation by

Bostock (1980) and later referred to by Henderson (1988) as the Point Lake Group, is

located approximately 300 km north of Yellowknife, along the Beniah Lake fault (Figure

1). The volcanic sequence is composed of three major formations: 1) the mafic-

dominated Peltier Formation, 2) the dacitic Samandré Formation, and 3) the rhyolitic

Beauparlant Formation (Figures 8, 9), that are inferred to overlie the 3.22 Ga (Northrup et

al., 1999) Augustus Granite unconformably. The Peltier Formation is interstratified with

the turbiditic Contwoyto Formation and contacts between the Samandré/Beauparlant and

Contwoyto Formations are, where exposed, characterized by a transition zone containing

carbonaceous, volcanic, and very fine-grained sedimentary rock (Henderson, 1998). The

Beauparlant, Samandré and Contwoyto Formations are inferred to be time-equivalent

f
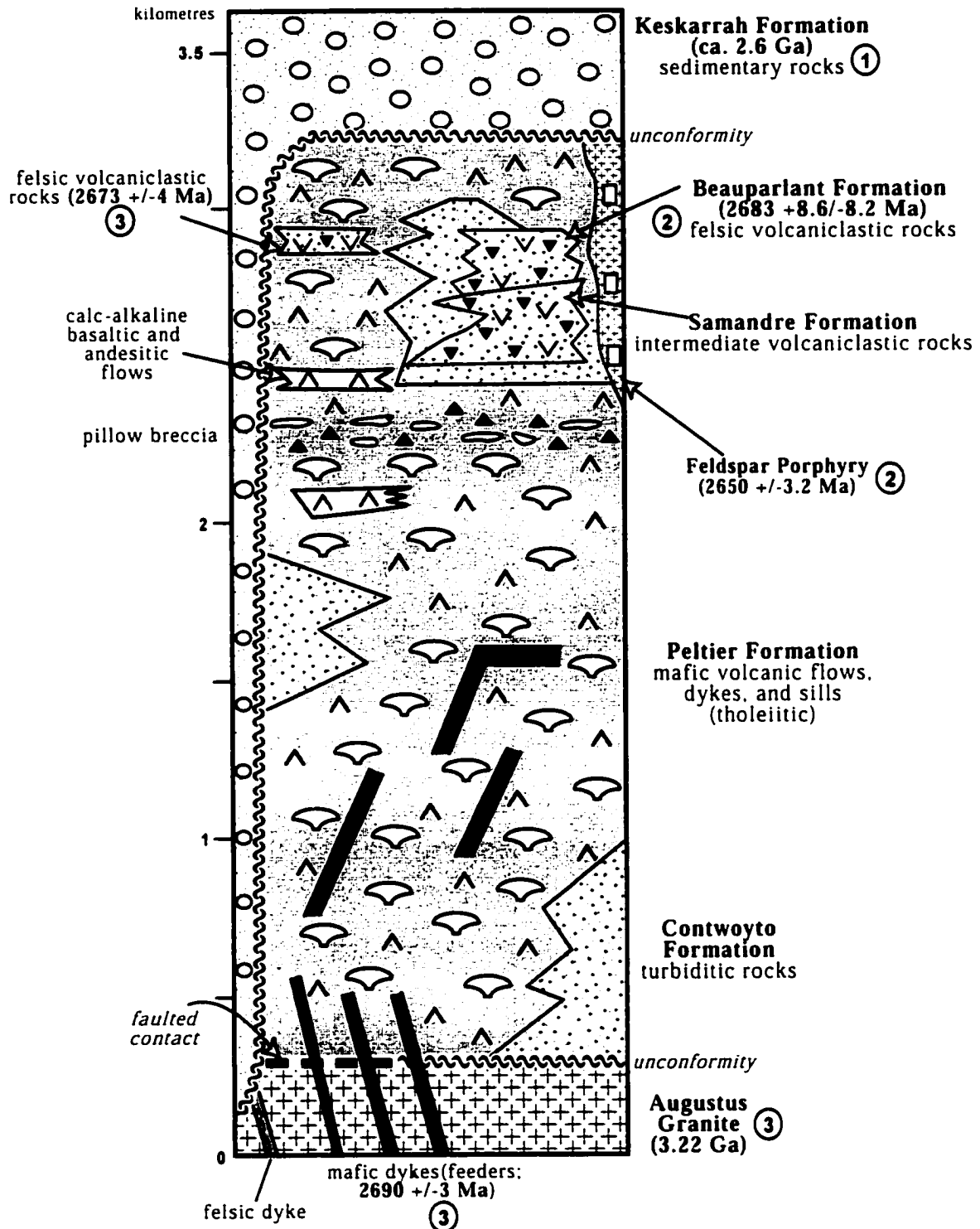
Figure 8: Schematic stratigraphy of the Point Lake volcanic belt. The Peltier, Samandre, and Beauparlant formations, interstratified with the turbiditic Contwoyto Formation, are inferred to overlie the Augustus granite unconformably. Note unconformable contacts between the Keskarrah Formation/Augustus granite, Peltier /Keskarrah formations, and Contwoyto/Keskarrah formations. Mafic and minor felsic intrusions cut the Augustus granite and are inferred feeders to the volcanic sequence. Age dates from: 1) Isachsen et al., 1991; Isachsen and Bowring, 1994, 1997, 2) Mueller et al., 2000, 3) Northrup et al., 1999. From Corcoran and Dostal (2001).
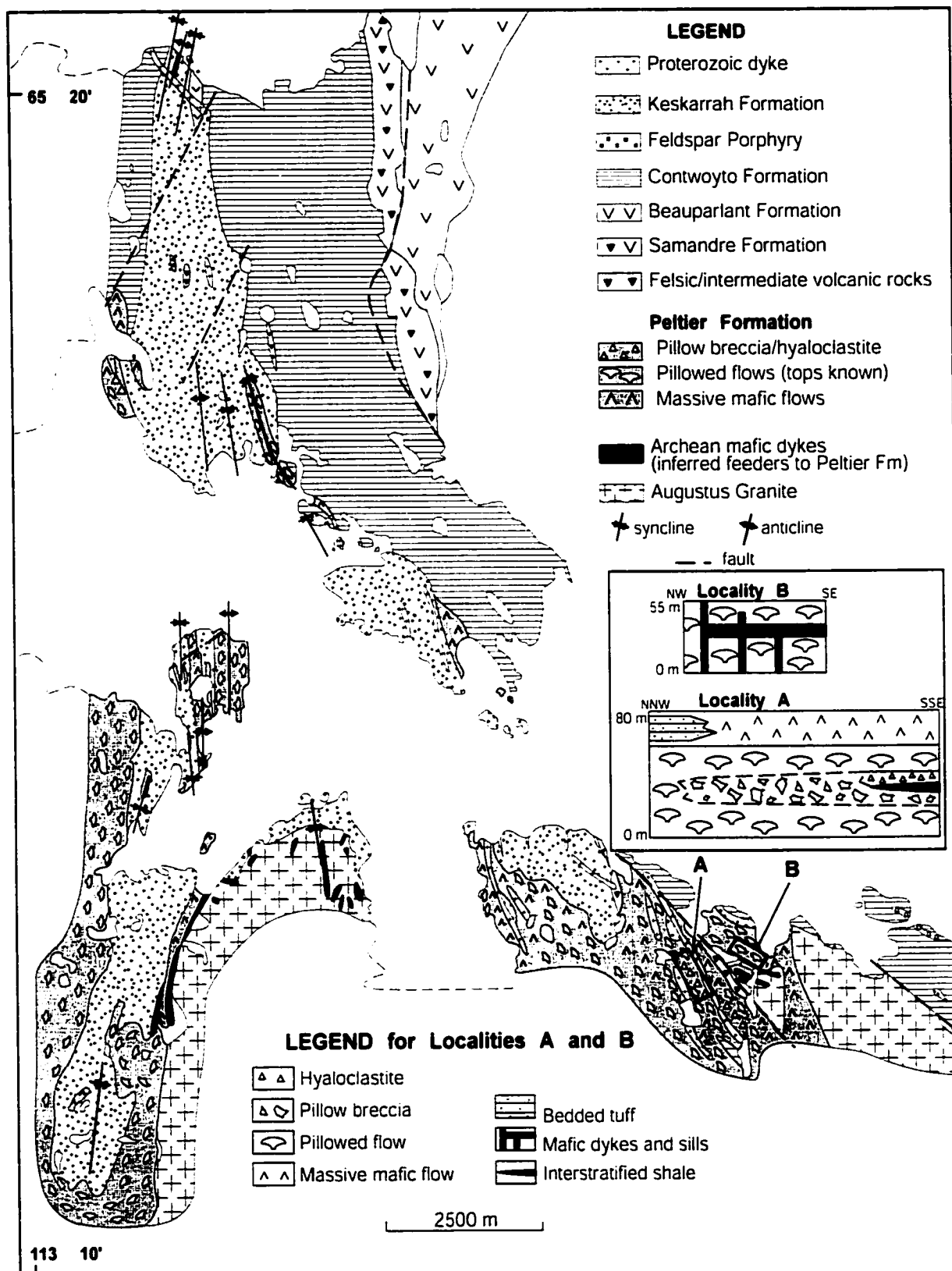
Figure 9: Lithological map of the Point Lake area. An 80 x 230 m schematic section through locality A and a 55 x 160 m section through locality B illustrate the facies architecture in the Peltier Formation. Note the location of felsic bedded tuffs interstratified with mafic massive flows at locality A. Modified from Corcoran (2000).

primarily based on the presence of volcanogenic turbidites and correlation of felsic-

intermediate rocks within the Contwoyto Formation with the Samandré and Beauparlant

Formations (Henderson 1998). A feldspar porphyry intrudes the Contwoyto Formation at

the eastern limit of the study area (Figure 9). The ca. 2.6 Ga (Isachsen and Bowring,

1994) Keskarrah Formation overlies the Peltier Formation (Figure 10), Augustus Granite

(Figure 11a), and Contwoyto Formation unconformably.

Rocks in the Point Lake area have undergone structural deformation (Jackson 1984;

Henderson 1988; Kusky 1991). The generally steeply-dipping supracrustal sequence is

characterized by small- and large-scale folds, faults and numerous high strain zones. The

region west of Keskarrah Bay is significantly more deformed than to the east, where

homoclinal successions are more common (Henderson 1998; Corcoran et al. 1998).

Structural complexity is well demonstrated on Cyclops Peninsula where Keskarrah

Formation sedimentary rocks, unconformably overlying mafic volcanic rocks of the

Peltier Formation, are preserved in tight to isoclinal folds (Corcoran et al. 1998; Northrup

et al. 1999). The highly strained amphibolitic Perrault Lithodeme marks the boundary

between the Peltier Formation and a granitoid gneiss domain to the west (Henderson

1988).

2.3.1   Augustus Granite and >2.8 Ga Granitoids

The 3.15-3.22 Ga Augustus Granite (Krogh and Gibbins, 1978; Henderson et al.,

1982; Northrup et al., 1999) is granodioritic to tonalitic in composition. The contact

between the plutonic rocks and the overlying Point Lake Group is in most cases sheared,

and is typically characterized by a fine-grained mylonite (Henderson, 1998). Although an

unconformable contact was nowhere identified, an autochthonous origin for the

greenstone belt is supported by several lines of evidence: 1) there is a range of ε_{Nd} values
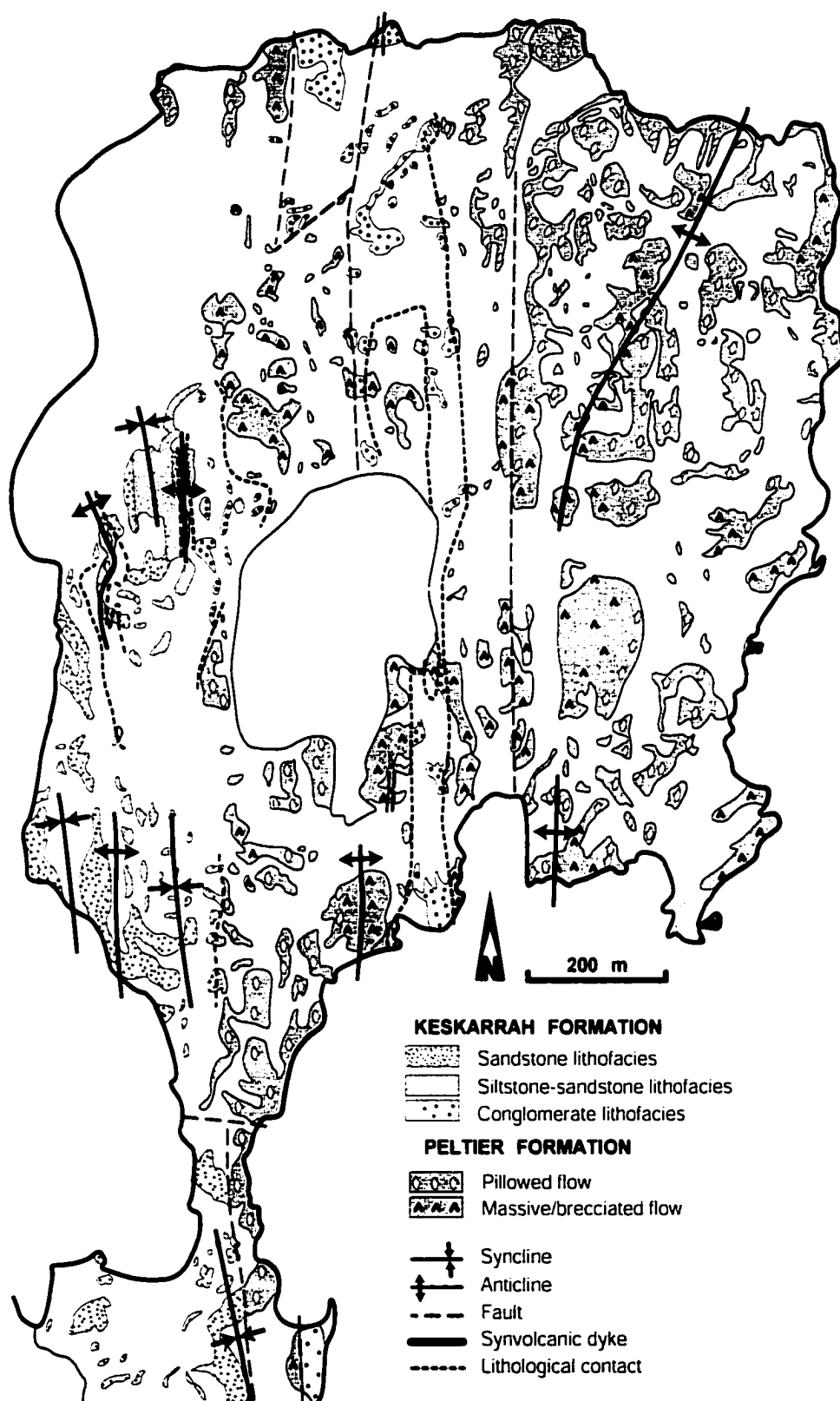
Figure 10: Lithological map of Cyclops Peninsula illustrating the folded unconformity between the Peltier and Keskarrah Formations. In all cases, the sedimentary rocks young away from the contact with their volcanic counterparts. Modified from Corcoran et al. (1998).
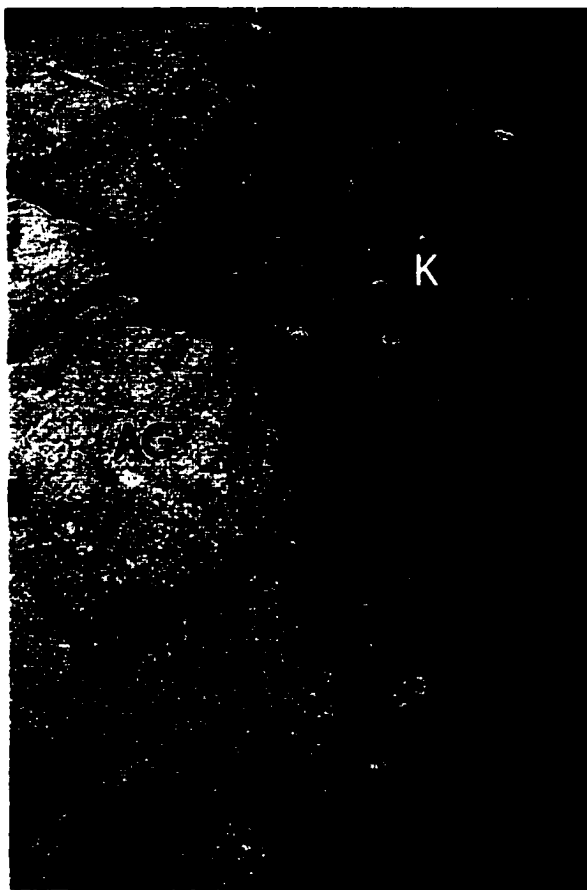
Figure 11a: Unconformity between the Augustus Granite (AG) and the conglomerate of the Keskarrah Formation (K), PLB. Arrow points to top. Scale, pencil 18 cm.
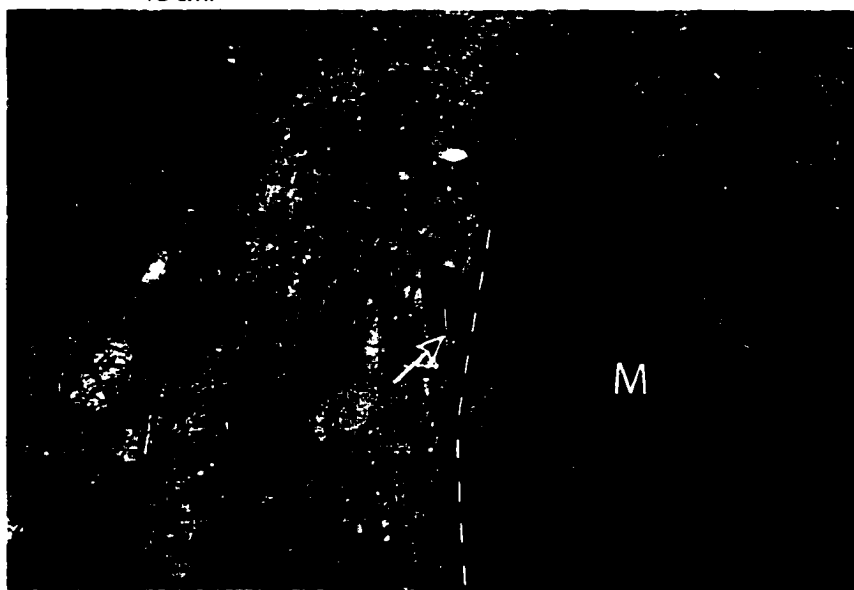
Figure 11b: Sheared unconformity (dashed line) between the mafic volcanic Peltier Formation (M) and the conglomerate of the Keskarrah Formation (K), PLB. Arrow points to top. Scale, pencil (small arrow) 14 cm.

from -6.3 to +3.06 in the volcanic rocks (Dostal and Corcoran, 1998; Northrup et al., 1999), 2) mafic dykes, interpreted as feeders to the volcanic rocks, intrude the underlying granitoid rocks, are metamorphosed to the same degree as the surrounding volcanic sequence, and are most abundant where the volcanic succession is thickest (Easton et al., 1982), 3) the Contwoyto Formation, which overlies the Augustus granite unconformably (Corcoran et al., 1998), is interstratified with the Point Lake volcanic belt (Henderson 1998; Corcoran et al., 1998), and 4) REE geochemistry of the turbiditic sequence shows that granitoid rocks were a major contributor of detritus (Easton, 1985; Corcoran and Mueller, in press). In addition to the Augustus granite, the plutonic complex at Point Lake includes abundant younger granitoid intrusions ranging from ca. 2818-3150 Ma in age (Northrup et al., 1999; Ketchum and Bleeker, 2000).

2.3.2 Peltier Formation

The Peltier Formation was the main volcanic unit studied in the Point Lake area. The mafic-dominated volcanic sequence is inferred to represent the basal part of the Point Lake volcanic belt (Figure 8) and is characterized by pillowed flows and pillow breccia, mafic massive flows, mafic dykes and sills, and minor felsic-intermediate volcanic/ volcaniclastic rocks. Mafic-intermediate dykes cutting the underlying Augustus granite and interpreted as potential feeders to the overlying Peltier Formation yielded a U-Pb age of 2690 +/- 3 Ma (Northrup et al., 1999), whereas an age of 2673 +/- 4 Ma (Northrup et al., 1999) was determined from a felsic-intermediate rock intercalated with the mafic sequence. The Peltier Formation is unconformably overlain by the sedimentary Keskarrah Formation; contacts are well-exposed on Cyclops Peninsula (Figures 10, 11b). Descriptions of the volcanology, petrography, and geochemistry of the Peltier Formation are provided in Chapter 3.

2.3.3 Samandré Formation

The Samandré Formation, accounting for less than 15% of the volcanic belt, is in conformable contact with the Beauparlant Formation in the northern part of the study area (Figure 9). Samandré deposits are mainly dacitic volcaniclastic sandstones and conglomerates with rhyolitic to basaltic fragments (Henderson, 1998). Volcanic sandstone appears massive and is highly foliated (Figure 12a), and although primary sedimentary structures were not identified during the course of this study, Henderson (1998) reported local crude bedding in volcanic breccia.

2.3.4 Beauparlant Formation

The Beauparlant Formation, comprising approximately 20% of the rocks in the volcanic belt, consists of poorly-exposed phenocrystic massive rhyolitic flows and volcaniclastic deposits (Henderson, 1998). Locally, small outcrop areas provide good exposure of volcanic conglomerate containing 0.2-15 cm-size angular felsic fragments in a chloritized felsic matrix (Figure 12b). Jigsaw fit texture and the monomictic nature of the conglomerate suggests a flow breccia origin. An age of 2683.3 +8.6/-8.2 Ma (Mueller et al., 2000) was determined from a volcanic sandstone in the Beauparlant Formation, roughly consistent with the ages obtained from the Peltier Formation.

2.3.5 Contwoyto and Itchen Formations

The Contwoyto and Itchen Formations belong to the Coghead Group of Henderson (1998) and are distinguished by the presence or absence of iron-formation (Bostock,

Figure 12a: Massive, felsic volcanic sandstone in the Samandré Formation, PLB. Scale, pencil 12 cm.
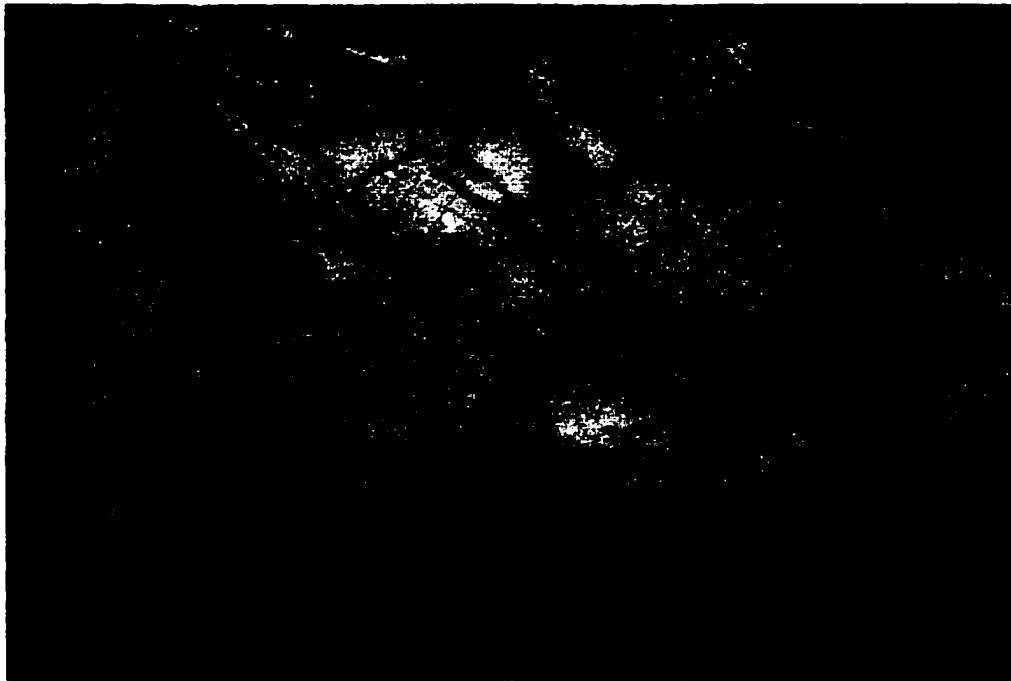
Figure 12b: Massive, felsic volcanic breccia in the Beauparlant Formation, PLB. Note the angularity and jigsaw puzzle fit of up to 10 cm-size felsic fragments (F). The felsic matrix is now chloritized. Scale, pencil 2 cm.

1980), although both formations consist predominantly of sandstone-siltstone-mudstone turbidites. The Itchen Formation is located beyond the eastern limit of the study area and is therefore not considered in detail in this thesis. The Contwoyto Formation is interstratified with the Peltier Formation as indicated by conformable, gradational changes from pillowed flows to black shale to typical turbiditic rocks, as well as intercalated black shale and pillows (Henderson, 1998). Shale beds interstratified with mafic pillow breccia, in addition to peperitic units containing fine-grained sedimentary material, further support contemporaneous volcanism and sedimentation (Corcoran, 2000). An erosional unconformity was identified between the turbiditic deposits and conglomerate of the Keskarrah Formation (Figure 13a). The Contwoyto Formation is mainly composed of thinly bedded siltstone and mudstone with thicker, up to 60 cm beds of sandstone, in addition to iron-formation. Iron-formation is either oxide-, silicate-, or carbonate-dominated and is normally interlayered with siltstone units. An example of carbonate-dominated iron-formation identified in the study area is represented by alternating beds of gray siltstone and red siderite (Figure 13b).

2.3.6 Feldspar Porphyry Stocks

A feldspar porphyry stock is located parallel to a northwest trending fault splay, near the eastern limit of the study area (Figure 9). The porphyry is a quartz diorite and contains 1-4 mm-size oligoclase phenocrysts (Simard, 2000). One sample analyzed for U-Pb zircon geochronology yielded an age of 2650 +/-3.2 Ma (Mueller et al., 2000), thus providing a minimum age for the Contwoyto Formation, which is intruded by the porphyry. Geochemically, the rocks plot in the volcanic-arc granite field on the diagram of Pearce et al. (1984), are LREE enriched, and demonstrate negative Nb anomalies,
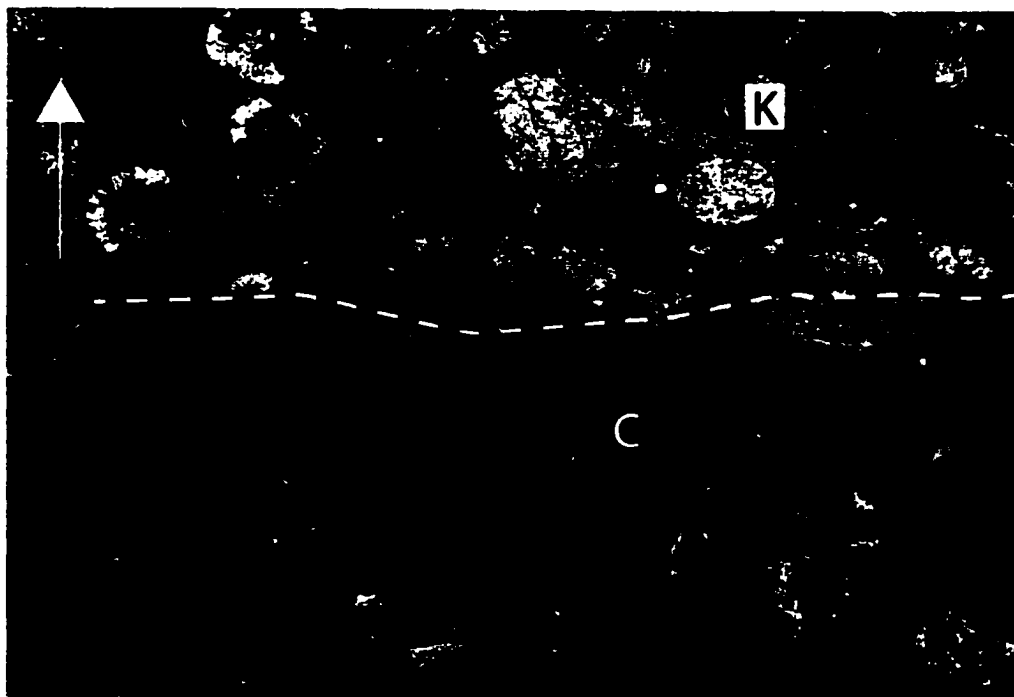
Figure 13a: Erosional unconformity (dashed line) between the Keskarrah Formation conglomerate (K) and graded beds of the Contwoyto Formation (C), PLB. Arrow indicates top. Scale, pencil 14 cm.
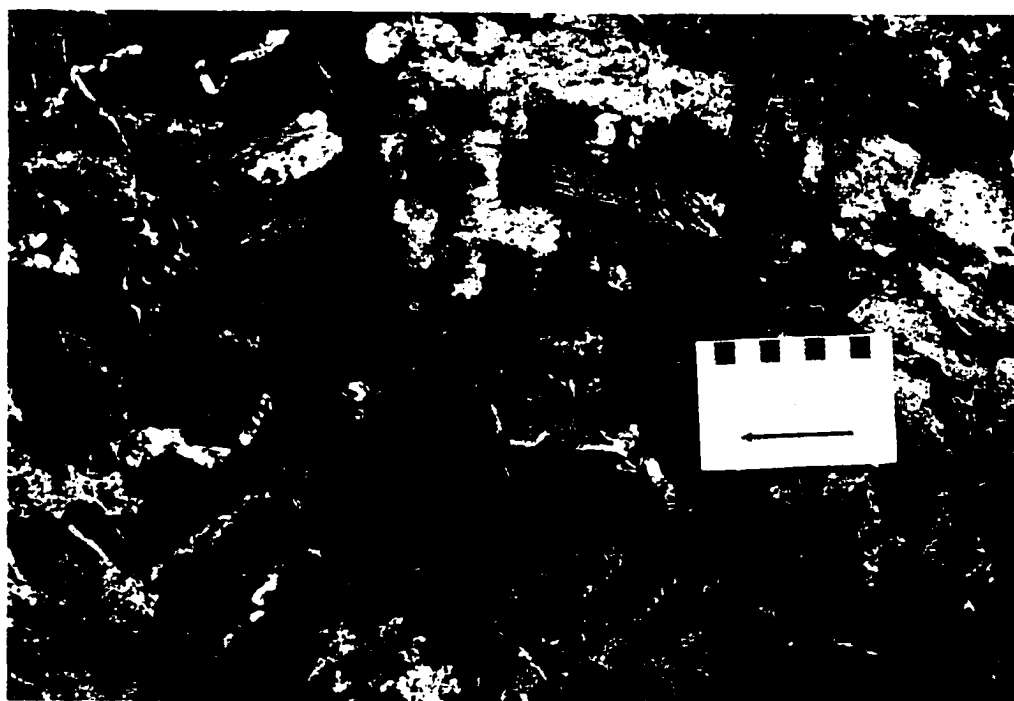
Figure 13b: Iron formation in fine-grained turbiditic deposits of the Contwoyto Formation, PLB. Iron formation is restricted to the siltstone units. Scale, card 9 cm.

suggestive of interaction with sialic crust or a subduction-related component (Simard, 2000).

2.3.7 Keskarrah Formation

The 2.6 Ga Keskarrah Formation overlies the Augustus Granite, Point Lake belt, and Contwoyto Formation unconformably (Corcoran et al., 1998). The sedimentary sequence is 5-700 m thick and is composed of conglomerate, sandstone, and siltstone-sandstone lithofacies (Figure 14a-c). The conglomerates are interpreted to have been deposited as alluvial fans and fan deltas in a high-relief setting, whereas the sandstone and siltstone-sandstone lithofacies were deposited in a shoreface to proximal offshore environment affected by waves and tides (Corcoran et al., 1998).

2.4 Northern Beaulieu River Volcanic Belt

The Northern Beaulieu River belt is located approximately 150 km northeast of Yellowknife, along the north-trending Beniah Lake fault system (Figure 15). Inferred basement is represented by granodiorite-tonalite gneisses of the Beniah Complex that are exposed north of the main part of the volcanic sequence (Figures 16, 17). The contact between the volcanic rocks and inferred basement is structural (Isachsen and Bowring, 1997). The supracrustal rocks also overlie an ultramafic layered intrusion containing dunite and pyroxenite, and the 2.9-3.1 Ga (Isachsen and Bowring, 1997) quartz arenite-dominated Beniah Formation. Detrital chromite preserved in Cr-mica laminae of the quartz-arenite suggests that the ultramafic layered intrusion is older than the sedimentary sequence. Younger, thin clastic sedimentary units are preserved along the fault zone west of Beniah Lake (Figure 17) and erode underlying quartz-arenite of the Beniah Formation.

Figure 14b: Large-scale, high- and low-angle cross-strata (Cst) and planar bedding (Pb) in the Keskarrah Formation sandstone, PLB. Arrow points to top. Scale, pencil 15cm.

Figure 14c: Planar beds (Pb) and mudstone laminae (Ml) in the Keskarrah Formation sandstone, PLB. Pencil points to top. Scale, pencil 15 cm.

Figure 14a: Massive, clast-supported conglomerate with subrounded mafic volcanic (M) clasts and plutonic (P) boulders in the Keskarrah Fomration, PLB. Scale, hammer (small arrow) 35 cm.
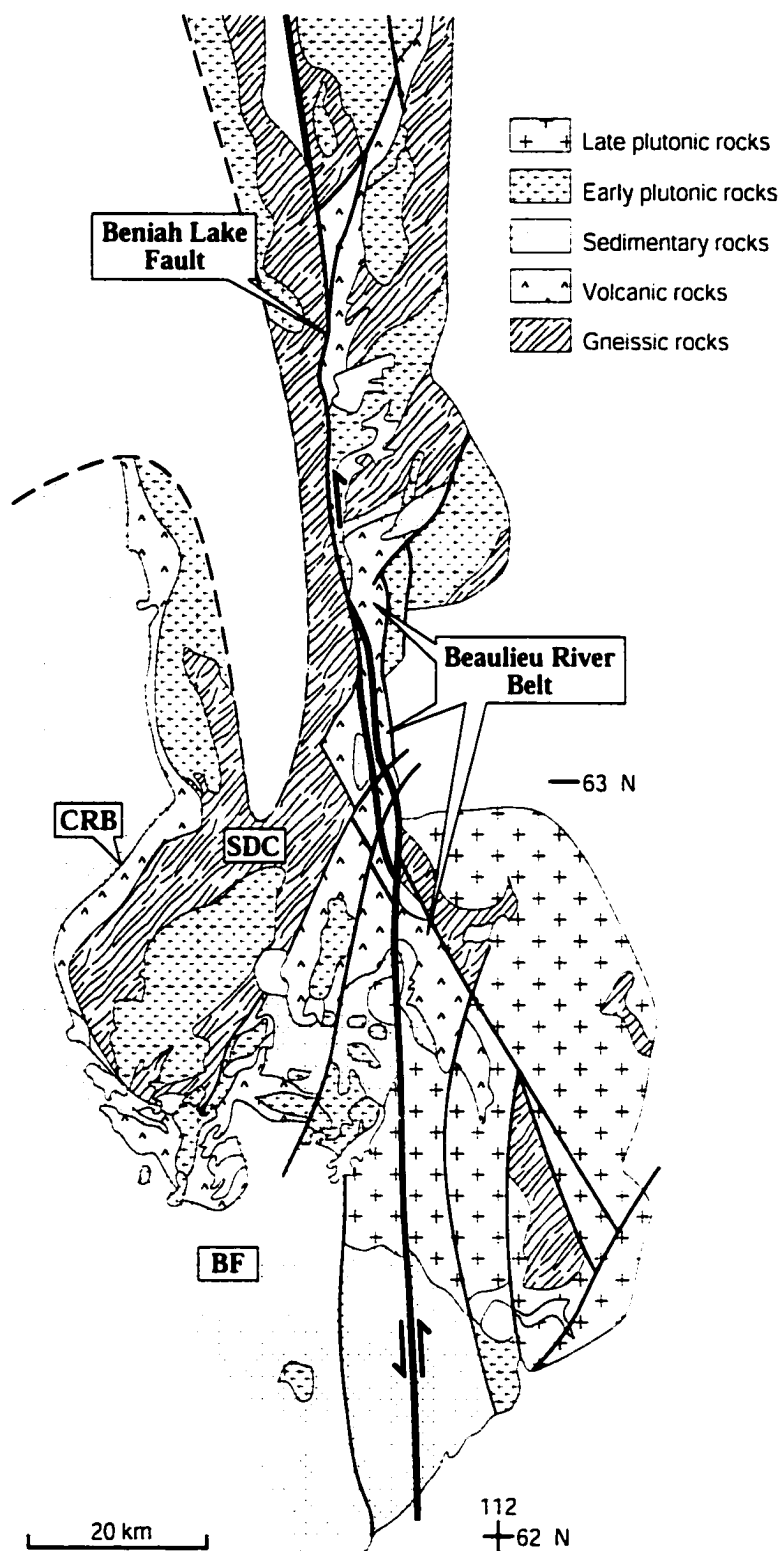
Figure 15: Regional map of the Beaulieu River belt and its stratigraphic relation to the Cameron River belt (CRB), Sleepy Dragon Complex (SDC), Burwash Formation (BF). Note the location of the Beniah Lake fault. Modified from James and Mortensen (1992).
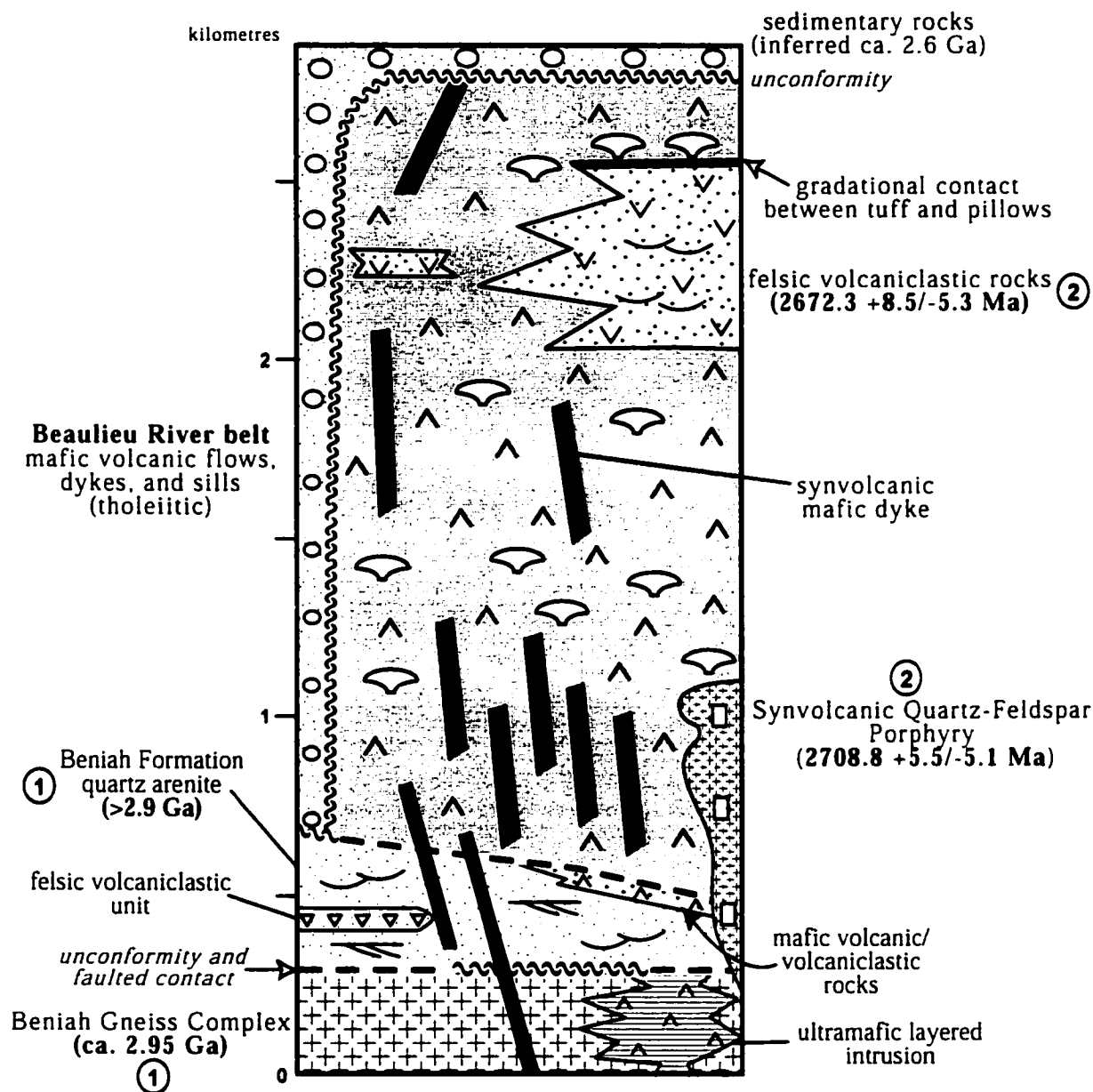
Figure 16: Schematic stratigraphy of the Northern Beaulieu River belt. The Beniah Complex and ultramafic intrusions are basement to the Beniah Formation. The mafic-dominated volcanic belt, in fault contact with the older quartz arenite, contains felsic volcaniclastic units. Mafic intrusions are abundant and cut quartz arenite and mafic flows, but are eroded by younger sedimentary rocks. Age dates from: 1) Isachsen and Bowring, 1997, and 2) Mueller et al., 2001.

41
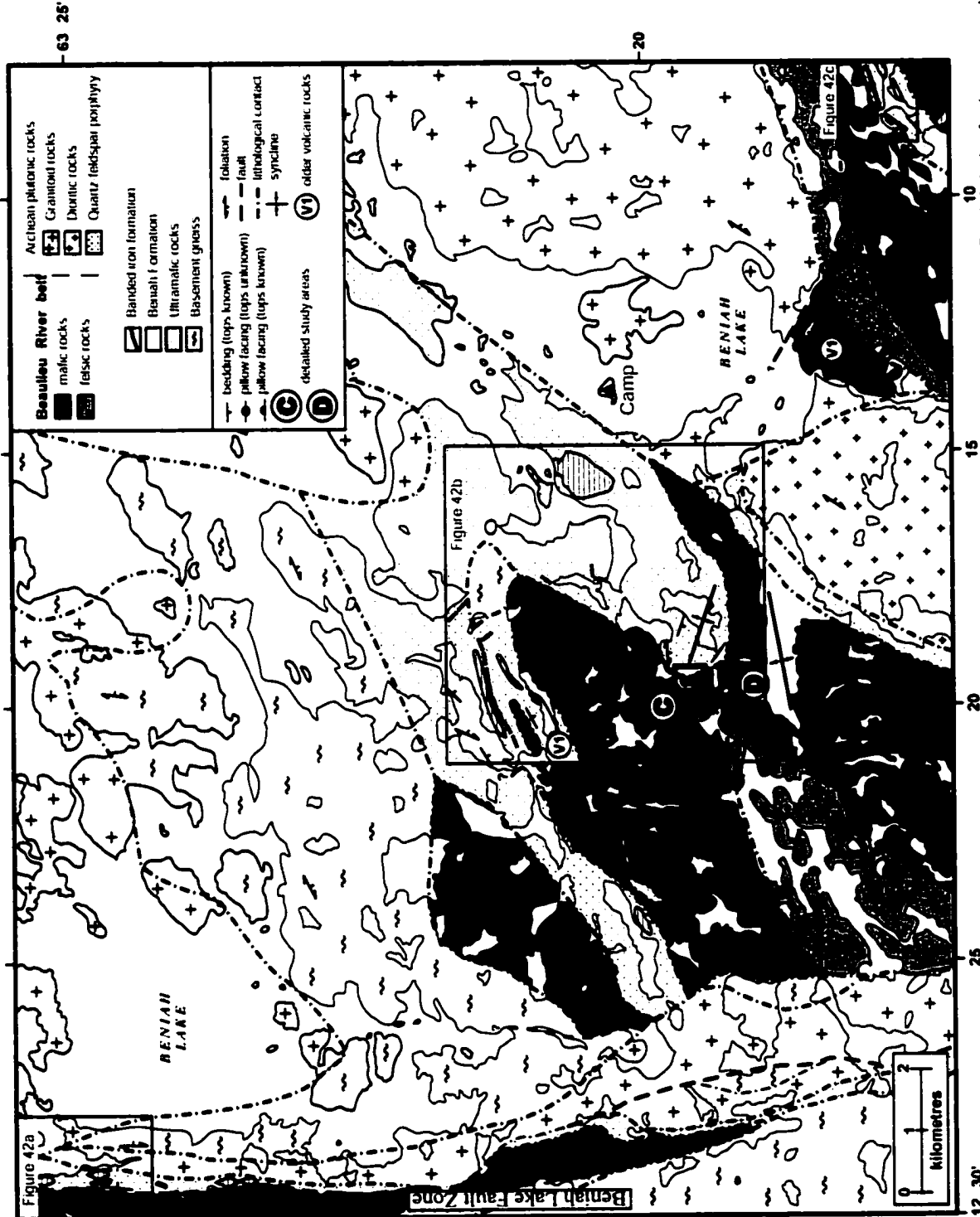
Figure 17: Regional map of the Northern Beaulieu River belt indicating the locations of Figures 42a, b, and c, the Beniah Lake fault zone, and detailed localities C and D. Modified from Roach (1990) and Pickett (thesis in progress).

These sedimentary rocks are both metamorphosed and deformed and resemble other

clastic sequences deposited along faults, such as the ca. 2.6 Ga Jackson Lake, Beaulieu

Rapids, and Keskarrah Formations (Figure 2). Abundant north-trending amphibolite

dykes cut the gneisses, ultramafic rocks, Beniah Formation, and Beaulieu River belt, but

are eroded by the younger sedimentary rocks.

In addition to the major, north-trending Beniah Lake fault and its north-trending

splays, the study area is characterized by southwest- to northeast-trending faults and

large-scale high strain zones (Covello et al., 1988; Roach, 1990). The steeply-dipping

supracrustal sequence contains at least two foliations; S1 trending roughly east-west and

S2 trending roughly northeast-southwest (Covello et al., 1988; Roach, 1990). Small- and

large-scale folds are numerous and opposing pillow younging directions indicate the

presence of synclines and anticlines where the underlying Beniah Formation quartz

arenites are either on the limbs of synformal structures or form the cores of antiformal

structures. Areas not affected by intense faulting and high strain were chosen for volcanic

facies mapping and geochemical sampling.

2.4.1 Beniah Gneiss Complex

The granodioritic-tonalitic gneiss at Beniah Lake has an U-Pb zircon age of ca. 2.95

Ga (Isachsen and Bowring, 1997), similar to the ages determined from the Sleepy Dragon

Complex. This plutonic suite constitutes part of the Central Slave Basement Complex of

Bleeker et al. (1999a), which is interpreted to have undergone a phase of plume-induced

rifting and subsidence followed by formation of shallow shelf quartz-arenite sequences.

2.4.2 Ultramafic Sequence

Ultramafic rocks (metadunite and metapyroxenite) at Beniah Lake are preserved in discrete north- to northeast-trending units that are up to 0.5 km wide and up to 1.8 km long (Figure 17). Metadunite is characterized by olivine pseudomorphs, chromite grains, and up to 20 cm-thick chromite seams (Figure 18a). Microprobe data from zoned chromite grains shows an increase in Cr_2O_3 in cores and FeO-rich rims (Appendix 2). Metapyroxenite is characterized by up to 1 cm-size pyroxene pseudomorphs (Figure 18b). Primary olivine and pyroxene in metadunite and metapyroxenite have been altered to serpentine, tremolite, talc, dolomite, and magnetite (Covello et al., 1988). Geochemically, the metadunite has SiO_2 wt % between 46 and 47 and MgO values around 5 (Appendix 3). $(La/Yb)_n$ ratios are close to 1 and there is a marked Zr depletion relative to other incompatible elements. SiO_2 wt. % in metapyroxenite varies from 45-47 and MgO values are 9-13 (Appendix 3). $(La/Yb)_n$ ratios are close to unity and Zr is depleted, similar to the metadunites.

2.4.3 Beniah Formation

The ca. 2.9-3.1 Ga (Isachsen and Bowring, 1997) Beniah Formation is a sedimentary sequence, 0.2-1 km thick, composed of four lithofacies, including 1) conglomerate, 2) quartz-arenite, 3) sandstone-siltstone, and 4) siltstone-sandstone (Pickett, thesis in progress). The formation belongs to the Central Slave Cover Group of Bleeker et al. (1999a). Quartz arenite is the most abundant lithofacies (Figure 19a) and banded iron-formation, considered part of the siltstone-sandstone lithofacies, is relatively minor (Figure 19b). The rocks are interpreted to have been deposited in a stable, shallow marine shelf setting under the influence of waves, tides and storms (Pickett, thesis in
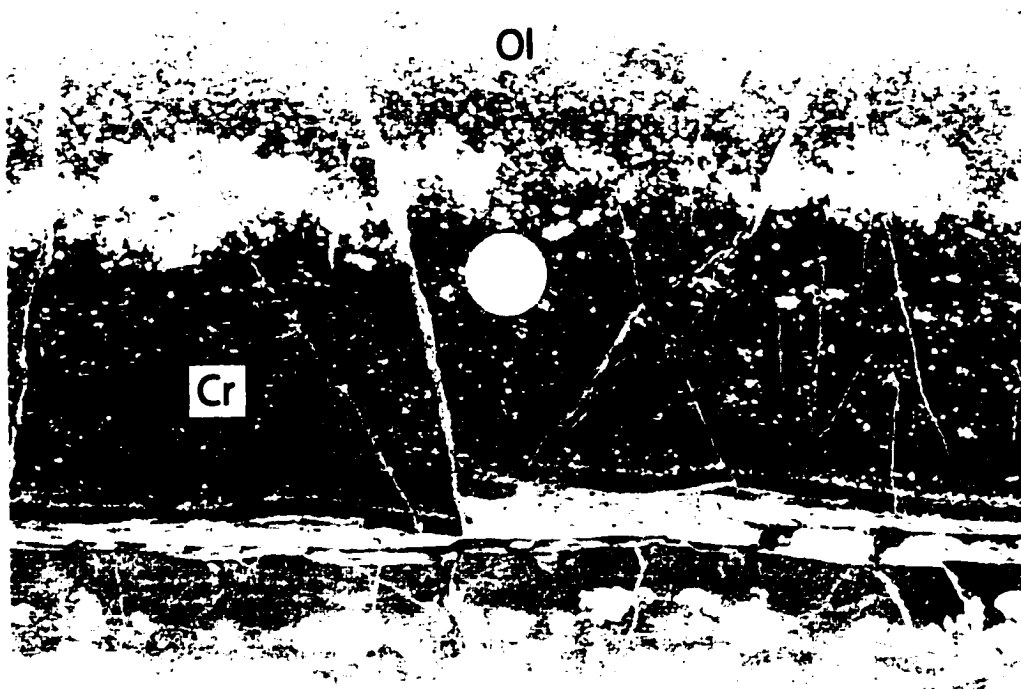
Figure 18a: Chromite seam (Cr) in altered dunite at Beniah Lake. Note the cumulate texture displayed by olivine phenocrysts (Ol). Scale, coin 2.4 cm diameter.
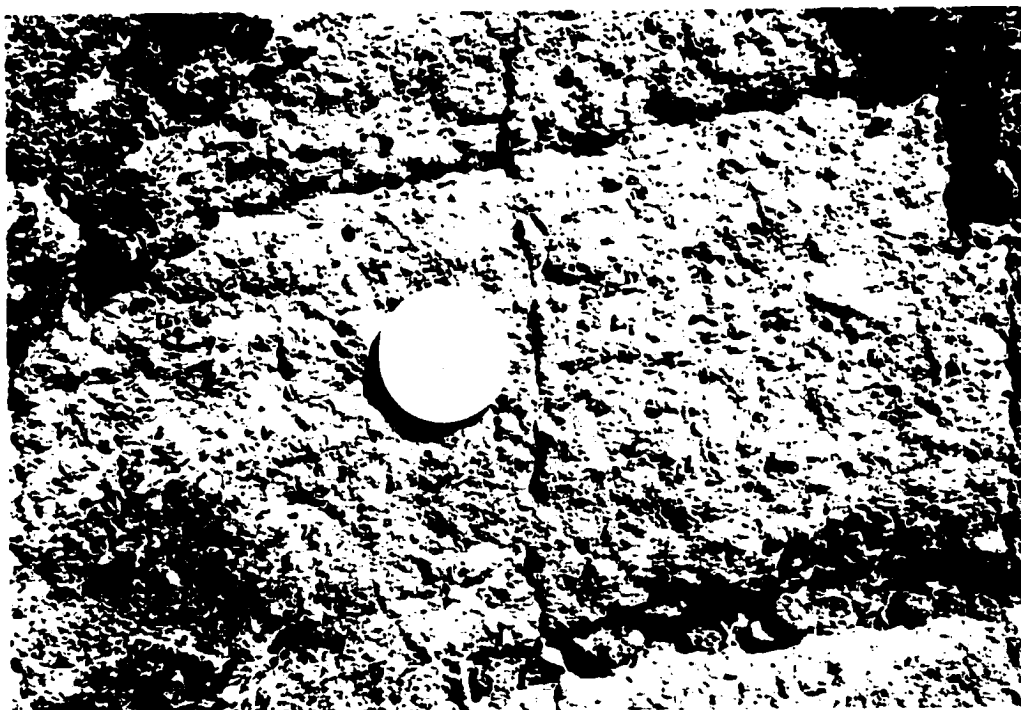
Figure 18b: Pyroxenite at Beniah Lake. Scale, coin 2.4 cm diameter.

Figure 19b: Banded iron-formation of the Beniah Formation, NBRB. Laminated magnetite-rich beds (M) alternate with chert counterparts (C). Scale, coin 2.4 cm diameter.

Figure 19a: Beniah Formation quartz arenite, NBRB, containing large-scale tabular and wavy bedforms (B) with internal low-angle to wavy bedding (W). Large arrow points to top. Scale, pen (small arrow) 15 cm.

Figure 19c: Deformed unconformity between quartz arenite (Q) and younger mafic volcanic rocks (M), NBRB. Arrow points to top. Scale, pencil 14 cm.

progress). The Beniah Formation is considered younger than the ultramafic rocks at Beniah Lake because chromite in Cr-mica laminae characterizing quartz arenite is similar in composition to the chromite seams in dunite (W. Fyson, personal communication). Locally, younger mafic volcanic rocks are structurally juxtaposed with older quartz arenite (Figure 19c).

2.4.4 Northern Beaulieu River Belt

The Beaulieu River belt at Beniah Lake has also been referred to as the Beniah Lake belt (Bleeker et al., 1999a) and as part of the Beniah Formation (Roach, 1990). The volcanic sequence, however, is laterally continuous with the Beaulieu River belt at Stanley Lake and is also adjacent to the Beniah Lake fault, suggesting that it is part of the same volcanic belt (Figures 1, 15). A U-Pb zircon age of 2672.3 +8.5/-5.3 Ma, determined from a felsic tuff, indicates the approximate age of the volcanic belt, which is similar to the ca. 2680 Ma age from felsic rocks in the Central Beaulieu River belt. Basaltic rocks predominate over felsic counterparts (Roach, 1990) and parallel mafic intrusions, akin to the dyke swarms of Lambert et al. (1992), are common features in this study area. Volcanic facies are represented by mafic massive and pillowed flows, mafic intrusions, and felsic volcaniclastic deposits. Local massive and pillowed flows with up to 3 cm-size plagioclase megacrysts were identified, but these were not studied in detail. Descriptions of the volcanology, petrography, and geochemistry of the Northern Beaulieu River belt are provided in Chapter 4.

2.4.5 Quartz-Feldspar Porphyry Stock

A polyphase quartz-feldspar porphyry stock is located parallel to a northwest trending fault splay, south of Beniah Lake (Figure 14). The porphyry phases are granodioritic, granodioritic-tonalitic, and granitic, and contain 1-3 mm-size quartz and feldspar (oligoclase and microcline) phenocrysts (Simard, 2000; Figure 20a). One sample analyzed for U-Pb geochronology yielded a crystallization age of 2708.8 +5.5/-5.1 Ma (Mueller et al., 2000). Geochemically, the rocks are LREE-enriched, display negative Nb and Ti anomalies, and fall in the volcanic arc granite field on the diagram of Pearce et al. (1984), consistent with a subduction-related evolution and/or crustal involvement (Simard, 2000).

2.4.6 Sedimentary Rocks (ca. 2.6 Ga)

Polymictic, angular to subangular clast conglomerate is preserved along the Beniah Lake fault, over an area of 40x30 m (Figure 17). The conglomerate unconformably overlies quartz arenite (Figure 20b), and a mafic dyke and contains cm- to m-size quartz arenite, siltstone, plutonic and mafic volcanic clasts. Quartz arenite clasts are subangular and contain primary bedding structures (Figure 20c), whereas mafic volcanic clasts display well-developed foliation (Figure 20d). The conglomerate matrix is composed of sandstone, in which at least one well-defined schistosity is preserved. Post-ca. 2.6 Ga rocks in the Slave Province do not exhibit similar structural features. and therefore, the polymictic conglomerate preserved along the fault at Beniah Lake is considered coeval with the Keskarrah, Beaulieu Rapids, and Jackson Lake sedimentary sequences.

Figure 20a: Quartz-feldspar porphyry south of Beniah Lake, NBRB. Note the cm-size quartz (Q) and feldspar (F) phenocrysts. Scale, coin 1.7 cm diameter.
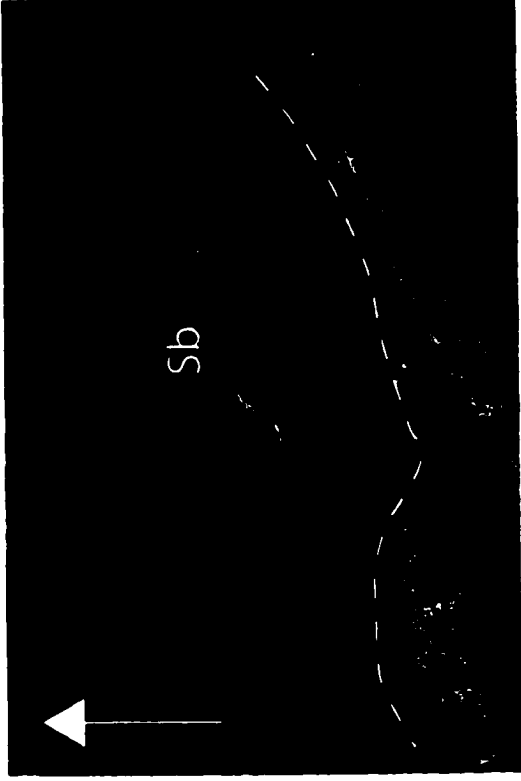
Figure 20b: Unconformable contact (dashed line) between quartz arenite (Qa) and younger sedimentary breccia (Sb) at Beniah Lake, NBRB. Large arrow points to top. Scale, pencil 14 cm.

Figure 20c: Quartz fragments in sedimentary breccia overlying the Beniah Formation, NBRB. Scale, lens cap 5.5 cm.
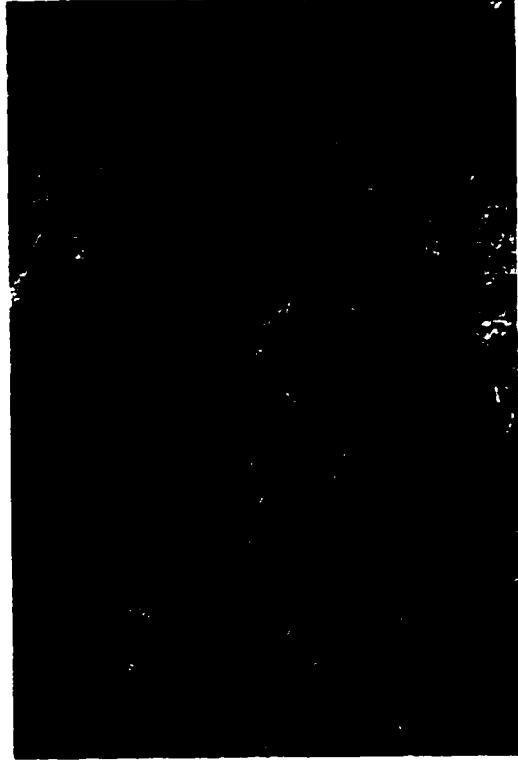
Figure 20d: Foliated mafic volcanic fragments in sedimentary breccia overlying the Beniah Formation, NBRB. Scale, lens cap 5.5 cm.

2.5   Central Beaulieu River Volcanic Belt

The ca. 2680 Ma (unpublished data from Mueller et al., 2000) Beaulieu River belt at Stanley Lake is located approximately 100 km northeast of Yellowknife (Figure 1) and 50 km south of Beniah Lake, along the north-trending Beniah Lake Fault system (Figure 15). The Beaulieu River belt is considered the eastern continuation of the 2663-2686 Ma (Henderson et al., 1987; Bleeker et al., 1997a) Cameron River belt and its lateral equivalent, the Raquette Lake Formation (Mueller and Corcoran, in press), which has an age of 2683 Ma (Bleeker et al., 1997b). The two volcanic sequences are now separated by the Sleepy Dragon Complex (Figure 15). Age dates of 2.68-2.95 Ga (Henderson et al., 1987; Lambert and van Breemen, 1991; Bleeker et al., 1999a) for the plutonic complex indicates that it may represent basement to the Cameron and Beaulieu River belts. The Beaulieu River belt at Stanley Lake is predominantly mafic, but felsic components are present locally (Figures 21, 22). The volcanic rocks are overlain unconformably by the ca. 2.6 Ga (Mueller et al., 1998) clastic Beaulieu Rapids Formation (Figures 21, 23a).

The Beaulieu Rapids area is transected by the north-trending Beniah Lake fault and its splays, which trend both northeast-southwest and northwest-southeast in the study area (Stubley, 1989; Corcoran et al., 1999). The effects of the faulting are recorded in the supracrustal sequence where foliations are largely obliterated by north-trending high strain zones close to the faults. One pervasive north- to north-northeast-trending foliation was recorded in the volcanic sequence, whereas three generations of foliations were identified in less competent siltstones of the unconformably overlying sedimentary Beaulieu Rapids Formation (Stubley, 1989). The volcanic rocks form the cores of anticlines and the limbs of synclines with the overlying sedimentary rocks. Outcrop-scale folds and crenulation cleavage are locally preserved in the volcanic sequence, but

kilometres

3 —

Beaulieu Rapids Formation
(ca. 2.6 Ga)
sedimentary rocks

unconformity

Quartz-Feldspar
Porphyry
(ca. 2.6 Ga)
④

stratified
hyaloclastite

pillow breccia

2 —

felsic volcaniclastic ③
rocks
(2676.2 +7.3/-3.4 Ma)

felsic porphyritic flows ③
(2685.5 ± 2.9 Ma)

Beaulieu River belt
mafic volcanic flows,
dykes, and sills
(tholeiitic and
calc-alkaline)

synvolcanic sill

1 —

synvolcanic dyke

Quartz arenite
(ca. 2.9 Ga)

inferred unconformity

faulted
contact

Sleepy Dragon
Complex ①
(2.8-2.95 Ga)

0 —

synvolcanic plutons ②
(ca. 2.68 Ga)

Figure 21: Schematic stratigraphy of the Central Beaulieu River belt. The Sleepy Dragon Complex is basement to the mafic-dominated volcanic belt. A ca. 2.9 Ga quartz arenite is in fault contact with the basement gneiss and overlying mafic flows. Up-section towards the unconformity with the Beaulieu Rapids Formation, there is an increase in felsic volcanic units and mafic fragmental facies. Age dates from: 1) Henderson et al., 1987; Lambert and van Breemen, 1991, 2) Henderson et al., 1987; Bleeker et al., 1999a, 3) Mueller et al., 2001, and 4) Corcoran et al., 1999.

Beaulieu Rapids Formation

[· ∴ ·] Quartz-rich sandstone

[_____] Siltstone-sandstone

[_____] Conglomerate

[▓▓▓▓] Porphyry stocks

Beaulieu River Volcanic Belt

[▓A▓A▓] Mafic volcanic rocks

[v v] Felsic volcanic rocks

[≡≡≡] Quartz arenite

[+⊹+⊹+] Gneiss (Sleepy Dragon Complex)

- - - - F1 fold axis

╈— Anticline

╈— Syncline

— — Fault

∿∿∿ Unconformity

Locality E

Locality F

1 km
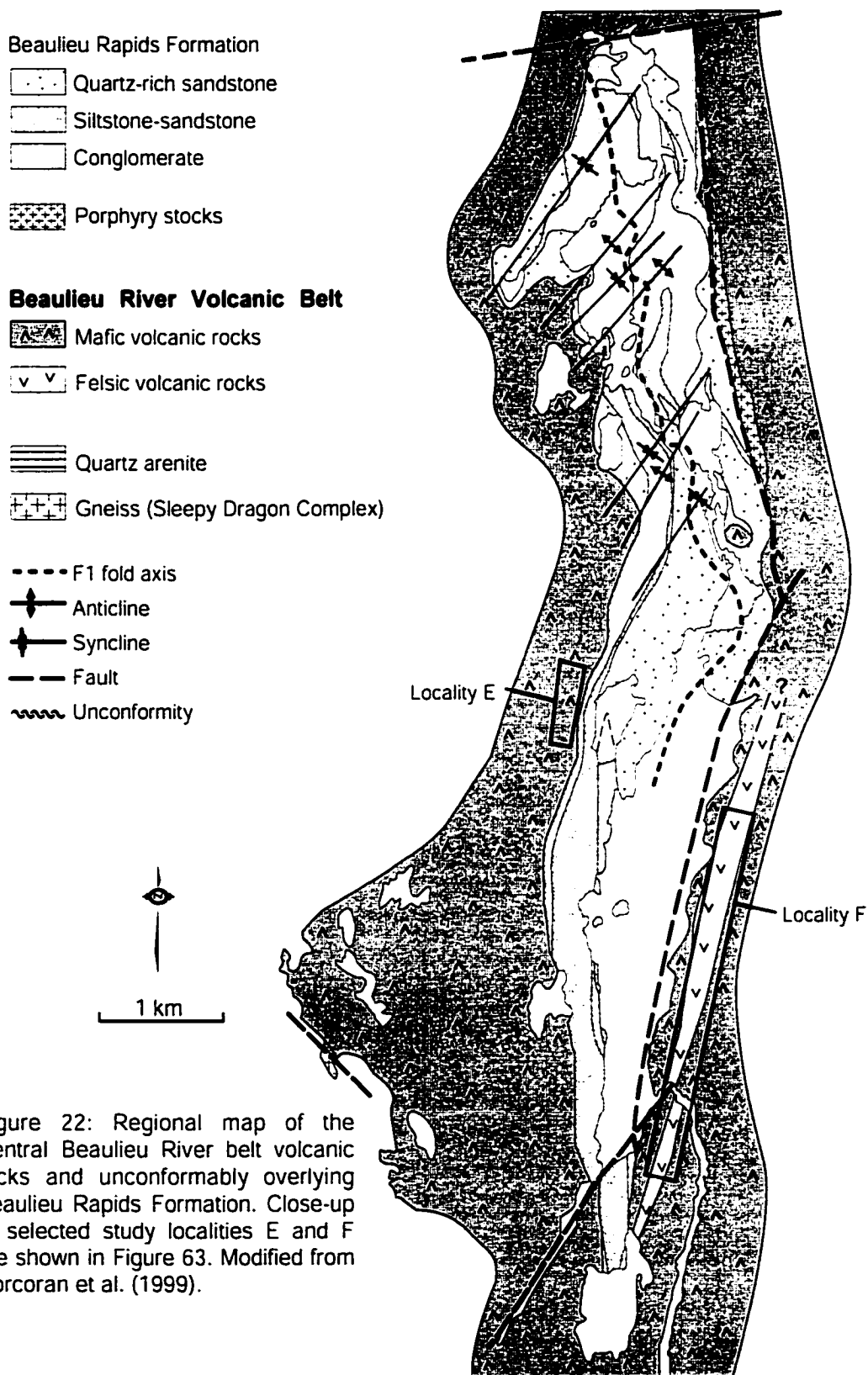
Figure 22: Regional map of the Central Beaulieu River belt volcanic rocks and unconformably overlying Beaulieu Rapids Formation. Close-up of selected study localities E and F are shown in Figure 63. Modified from Corcoran et al. (1999).

Figure 23b: Quartz-feldspar porphyry along the eastern faulted margin of Stanley Lake, CBRB. Note the abundance of quartz phenocrysts (Q). Scale, pencil 8 cm.

Figure 23a: Unconformable contact (U) between the pebbly sandstone of the Beaulieu Rapids Formation (S) and a massive flow of the Beaulieu River belt (M). Pencil points to top. Scale, pencil 10 cm.
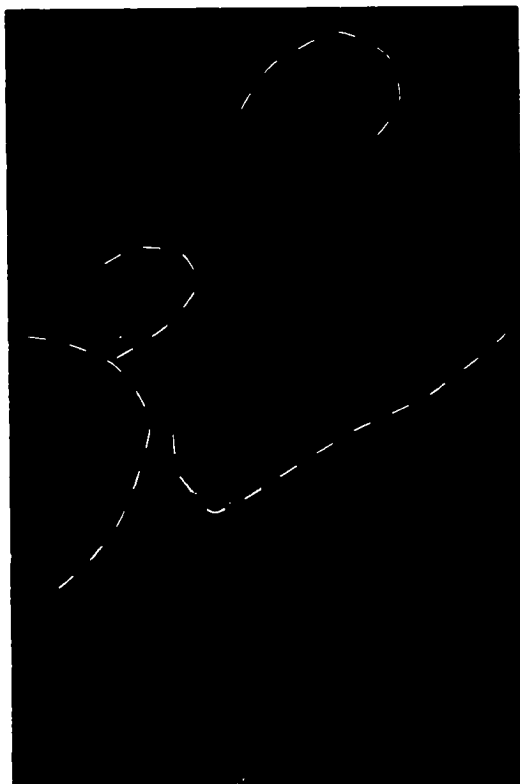
Figure 23c: Quartz-feldspar porphyry clasts (partly outlined) in conglomerate of the Beaulieu Rapids Formation, CBRB. Scale, pencil 14 cm.

homoclinal successions are readily identified using pillow younging west of the unconformity with the sedimentary rocks.

2.5.1 Sleepy Dragon Complex

The Sleepy Dragon Complex is located west of the Beaulieu River belt at Stanley Lake (Figures 15, 22). The contact between the Cameron-Beaulieu River belts and the gneissic complex is considered unconformable (e.g. Henderson et al., 1987; Lambert. 1988), and/or tectonic (e.g. Kusky. 1990; Bleeker et al.. 1999b). Highly foliated granodiorite and quartz diorite are the predominant rock types, whereas diorite and tonalite are less common (Kusky, 1990). Clasts of similar composition were identified in conglomerates of the Beaulieu Rapids Formation (Beaulieu River belt) and Raquette Lake Formation (Cameron River belt), indicating that the Sleepy Dragon Complex was probably a major contributor of detritus (Corcoran et al.. 1999; Mueller and Corcoran. in press). Several generations of dyke swarms intrude the gneissic rocks and have been interpreted as feeders to the overlying Cameron and Beaulieu River volcanic belts (Lambert et al.. 1992).

2.5.2 Central Beaulieu River Belt

The 2678.6 +4.8/-3.2 Ma (revised from 2676.2 +7.3/- 3.4 Ma by Mueller et al.. 2001) Central Beaulieu River volcanic belt lies adjacent to the north-trending Beniah Lake fault in the south-central part of the Slave Province (Figures 1, 15). Tholeiitic basalts are predominant over the entire volcanic belt, but calc-alkaline andesites. dacites. and rhyolites, and pyroclastic rocks characterize the top of the sequence (Lambert, 1988). Nd-isotope geochemistry of the volcanic rocks is consistent with mixing of a depleted

mantle source and Sleepy Dragon-type sialic crust (Lambert et al., 1992). Kusky (1990)

postulated that the Beaulieu River belt and its western counterpart, the Cameron River

belt, formed during opening and closing of an Archean ocean, based on the presence of

multiple dyke swarms interpreted as ophiolite complexes. Lambert et al. (1992)

discounted Kusky's interpretation because all isotopic evidence demonstrates that the

magmas interacted with sialic crust, and although multiple dykes are common locally,

there is no evidence for layered gabbros and ultramafic intrusions typical of ophiolites.

The Beaulieu River belt at Stanley Lake is not an area characterized by dyke swarms. The

volcanic sequence features tholeiitic basalts, calc-alkaline basalts, andesites and rhyolites,

in addition to mafic and felsic autoclastic breccia and felsic volcaniclastic rocks of

pyroclastic origin. These rock types and compositions are more consistent with a

continental arc-related setting, similar to that proposed by Mueller and Corcoran (in

press) for the Cameron River belt. A thin, up to 100 m-thick unit of quartz arenite is

located between the Sleepy Dragon Complex and the Beaulieu River belt, west of the

Beaulieu Rapids/Beaulieu River belt unconformity (Figure 22). The contact with the

quartz arenite is faulted. A more detailed description of the volcanology, petrography,

and geochemistry of the Central Beaulieu River belt is provided in Chapter 5.

2.5.3 Quartz-Feldspar Porphyry Stocks

Quartz-feldspar porphyry stocks are located along the eastern fault margin of the

Beaulieu Rapids Formation (Figure 22), consistent with local extension. The porphyries

are tonalitic and quartz dioritic in composition and contain <5 mm-size quartz and

oligoclase phenocrysts (Simard, 2000; Figure 23b). U-Pb geochronology yielded

complex zircon systematics (Mueller et al., 1998). The majority of the zircons are

inherited, implying involvement of pre-3.0 Ga sialic basement. Additional zircons

without inheritance are discordant and a preliminary age interpretation is roughly 2.6 Ga.

Locally, porphyry clasts of similar composition and texture were identified in the

Beaulieu Rapids conglomerate (Figure 23c), thus bracketing a maximum age for the

sedimentary sequence. Geochemical data from Simard (2000) corroborates the presence

of sialic crust during emplacement of the porphyries.

2.5.4 Beaulieu Rapids Formation

The ca. 2.6 Ga Beaulieu Rapids Formation overlies the Beaulieu River volcanic

belt unconformably along the western side of Stanley Lake (Roscoe et al., 1989;

Corcoran et al., 1999; Figure 22). The clastic sequence is 0.2-1 km thick and consists of a

conglomerate lithofacies I at the base, a siltstone-sandstone lithofacies, a conglomerate

lithofacies II, and a quartz-rich sandstone lithofacies at the top of the sequence (Corcoran

et al., 1999: Figures 22, 24a-c). The rocks are interpreted to have been deposited as

alluvial fans, fan deltas, sandy braidplains, and local lacustrine units in a strike-slip basin

setting (Corcoran et al., 1999).

Summary

The stratigraphy of the Point Lake, and Northern and Central Beaulieu River belts

is generally comparable with the Yellowknife volcanic belt in terms of the presence and

age of sialic basement, timing of volcanism and associated turbidite deposition, and late,

2.6 Ga unconformable deposition of coarse clastic sedimentary formations at the top of

the stratigraphic sequences. The following Chapters 3, 4, and 5 will examine in detail the

physical volcanology and geochemistry of selected areas in the Point Lake, and Northern

Figure 24b: Trough crossbedded sandstone (St) and argillite laminae (A) in the siltstone-sandstone lithofacies of the Beaulieu Rapids Formation, CBRB. Arrow points to top. Scale, knife 9 cm.

Figure 24a: Conglomerate of the Beaulieu Rapids Formation, CBRB, dominated by plutonic (P) boulders. Scale, hammer 34 cm.

Figure 24c: Large-scale, high angle sets of trough crossbeds (St) in the quartz-rich sandstone lithofacies of the Beaulieu Rapids Formation, CBRB. Arrow points to top. Scale, knife (small arrow) 9 cm.

and Central Beaulieu River belts to determine how well they compare with each other.

and whether they developed in similar depositional and tectonic settings.

Chapter 3

POINT LAKE BELT

3.1   Physical Volcanology

3.1.1   Introduction

Two study areas composed of tholeiitic basalts based on the classification of

Miyashiro (1974), and referred to as localities A and B, were selected for detailed work

(Figure 9 in Chapter 2). Although the true thickness of the Peltier Formation remains

enigmatic due to structural complexity in the Point Lake region (Henderson, 1998), the

most extensive homoclinal sequence is approximately 1.5 km thick, of which locality A

constitutes the basal part of the uppermost 700 m (Figure 9 in Chapter 2). A northwest-

trending, northeast-dipping reverse-slip fault separates localities A and B (Henderson,

1988). The study areas are composed of pillowed flows (50%), pillow breccia (20%),

mafic dykes and sills (15%), massive flows (10%), and hyaloclastite (5%). Andesitic-

dacitic volcaniclastic rocks are locally interstratified with massive flows (Figure 9 in

Chapter 2). Maps at scales of 1:100 and 1:300 in the Peltier Formation were drawn to

record lateral and vertical facies distribution and volcanic structures. The rocks

underwent greenschist facies metamorphism, as indicated by the mineral assemblage

chlorite ± epidote ± albite ± green amphibole ± carbonate, but the prefix "meta" is

omitted for simplicity.

3.2 Mafic Volcanic Facies

3.2.1 Massive Flows

Massive flows and flow units at locality A, 3-40 m thick, are up to 22% vesicular at flow bases, decreasing to 0% at flow centres and increasing to 9% near flow tops (Table 1, Figure 25). Vesicles, 0.1-1 cm in size, are locally calcite-filled. Intergranular, hyalopilitic, and ophitic textures characterize massive flows (Appendix 4). Plagioclase phenocrysts, <0.2 mm long, are surrounded by plagioclase microlites, creating an intergranular texture, whereas hyalopilitic textures are represented by plagioclase microlites in a glassy matrix. Actinolite partially enveloping plagioclase creates the subophitic texture. Volcanic facies in the Peltier Formation generally conform to the "standard" sequence of Dimroth et al. (1978), where massive parts of flows laterally and vertically become pillowed, overlain by pillow breccia, and capped by hyaloclastite or hyalotuff. All visible contacts between the massive facies and overlying pillows and pillow breccia are sharp. Bedded, fine- to medium-grained tuffs are interstratified with the uppermost massive flow unit at locality A.

Interpretation

Massive basalts represent non-channelized sheet flows that form during the initial stages of subaqueous eruption (Ballard et al., 1979; Cousineau and Dimroth, 1982) and are characteristic of higher lava effusion rates and temperatures compared to pillowed flows (Yamagishi, 1991). Massive to pillow transitions are consistent with decreasing flow rate (Griffiths and Fink, 1992). Abundant vesicles at flow bases and tops with vesicle-poor centres are common features of subaqueous massive flows (Sahagian, 1985; McMillan et al., 1987; Aubele et al., 1988). Vesicles develop when gases are trapped as

Sample/Outcrop Number	Volcanic Facies	Number of Vesicles	Total Count	Percentage Vesicularity (%)
Peltier Formation-Locality A				
PLC-96-78	massive flow (basal)	135	500	27
PLC-97-82	massive flow (middle)	44	500	9
PLC-97-84	massive flow (basal)	109	500	22
Photo 29a	pillow breccia	91	521	17
Central Beaulieu River volcanic belt-Locality E				
PLC-98-36	pillowed flow (pillow rim)	243	500	49
PLC-98-37	pillowed flow (pillow rim)	227	500	45
PLC-98-38	massive flow (basal)	183	500	37
PLC-98-39	pillowed flow (pillow centre)	103	500	21
PLC-98-40	pillowed flow (lobate part)	104	500	21
PLC-98-41	pillowed flow (lobate part)	121	500	24
Photo 29b	pillowed flow (whole pillow)	99	249	40
Photo 29c	pillow breccia	135	362	37
Photo 29d	massive flow (basal)	192	434	44

Table 1: Percentage of vesicularity in massive and pillowed flows and pillow breccia in the Peltier Formation and Beaulieu River volcanic belt.
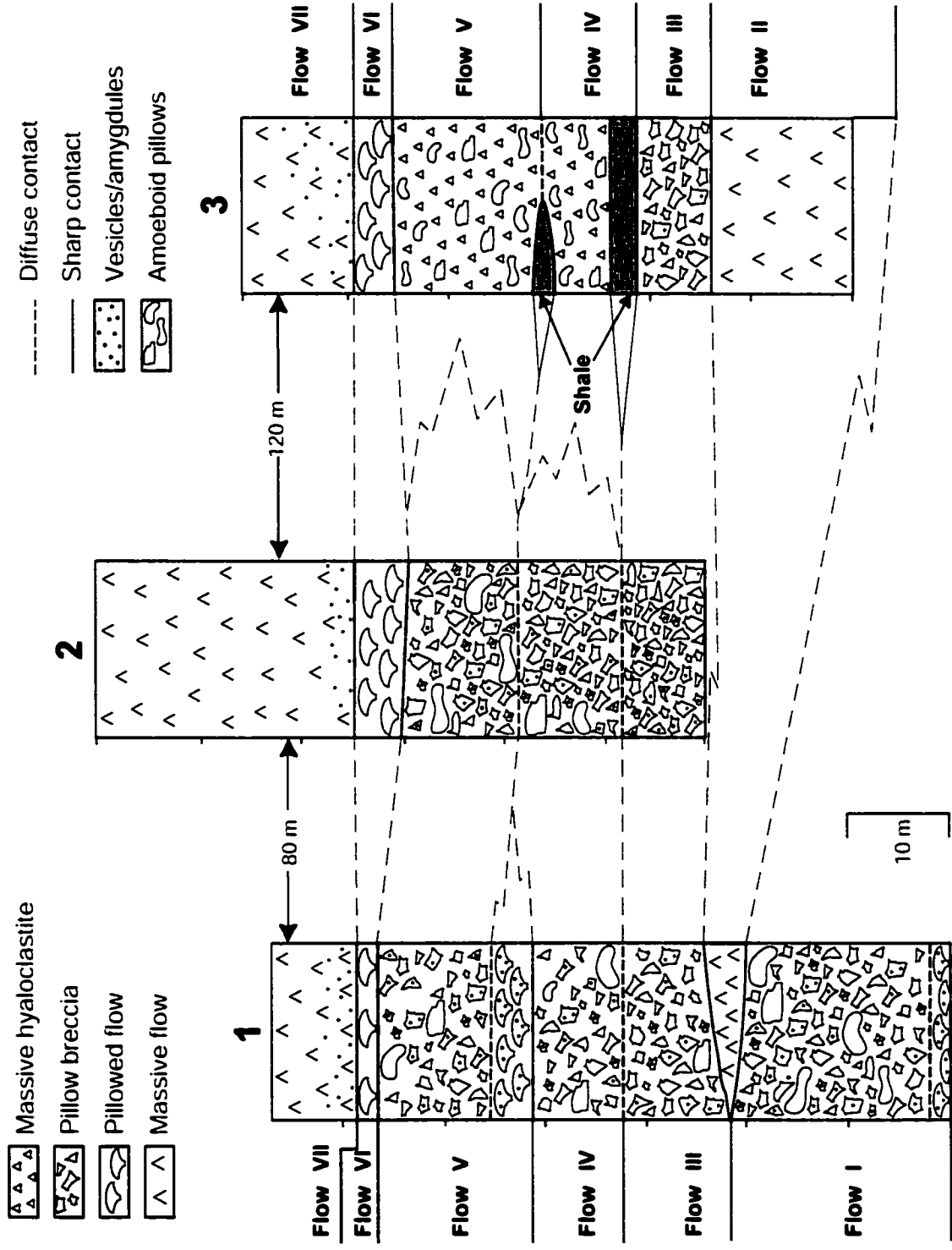
Figure 25: Vertical sections and lateral correlations based on contact relationships through pillowed and massive flows, pillow breccia, and hyaloclastite at locality A, PLB. Seven flows were recorded upsection over 68 m. Note the interstratification of shale units between flows III, IV, and V.

bubbles during cooling of a flow (Aubele et al., 1988). The bubbles rise during extrusion

and solidification; the larger bubbles rise more quickly, and become trapped in the upper

crystallization front (Sahagian, 1985). According to Sahagian (1985), the lower

crystallization front follows the direction of the upward migrating bubbles, such that it

"chases" and freezes them before they can continue their ascent. With continued cooling,

the central part of the flow eventually lacks bubbles because with increasing viscosity,

the lower crystallization front freezes them as they attempt to rise. The absence of

vesicles in flow centres depends on flow thickness because thicker flows take longer to

solidify, allowing more bubbles to migrate upwards (Walker, 1993).

3.2.2 Pillowed Flows

Pillowed flow units at localities A and B in the Peltier Formation range from 1.5-32

m thick and contain 10-90 cm-size closely-packed pillows (Figures 25, 26, 27a).

Hyaloclastite characterizes chilled margins and is present in interstices between pillows.

Percentage of vesicularity differs from 0-5% at locality B to 0-27% at locality A (Table

1) where vesicles range from 0.5-10 mm in diameter. Spherical to ovoid vesicles are

concentrically zoned from chlorite to quartz-albite or are entirely filled with calcite or

chlorite (Figure 27b). Pillowed flows in the Peltier Formation display hyalopilitic and

hyalophitic textures with plagioclase microlites, and 0.2-0.4 mm-size plagioclase

phenocrysts and secondary actinolite, respectively, in chloritized sideromelane (Appendix

4). Vertical changes from pillowed to pillow breccia flow were identified at locality A, in

addition to lateral transitions from pillowed to pillow breccia flow, locally grading into

hyaloclastite (Figure 25).

63
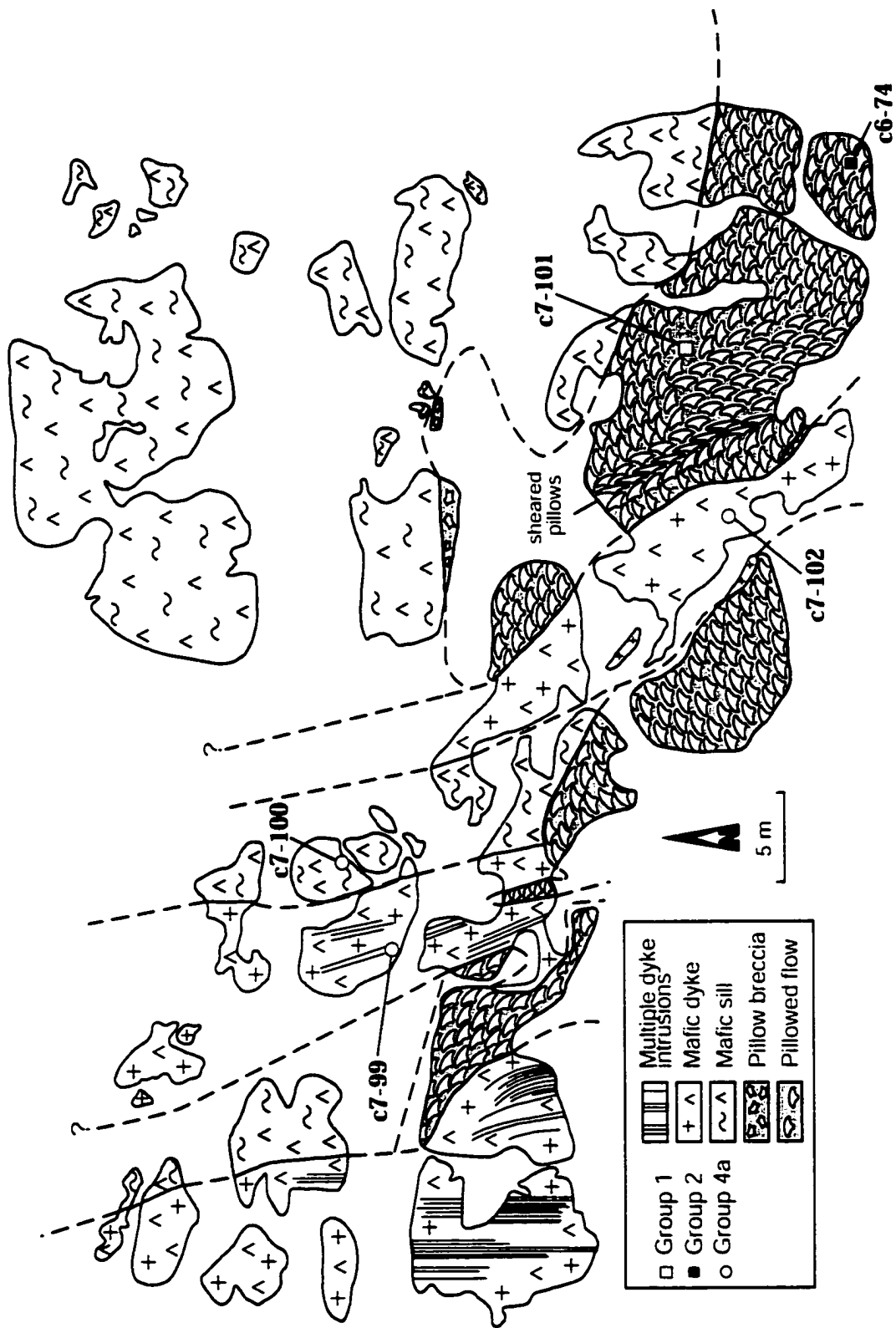
Figure 26: Mafic volcanic facies at locality B in the Peltier Formation, PLB. Three north-south trending dykes with multiple intrusions cut an east-west trending sill that has intruded a pillowed sequence. Five sample locations are indicated.

Figure 27a: Closely packed pillows in a pillowed flow from locality B, PLB Some pillows are outlined with dashed lines. Arrow points to top. Scale, fieldbook 18.5 cm.

0.25 mm
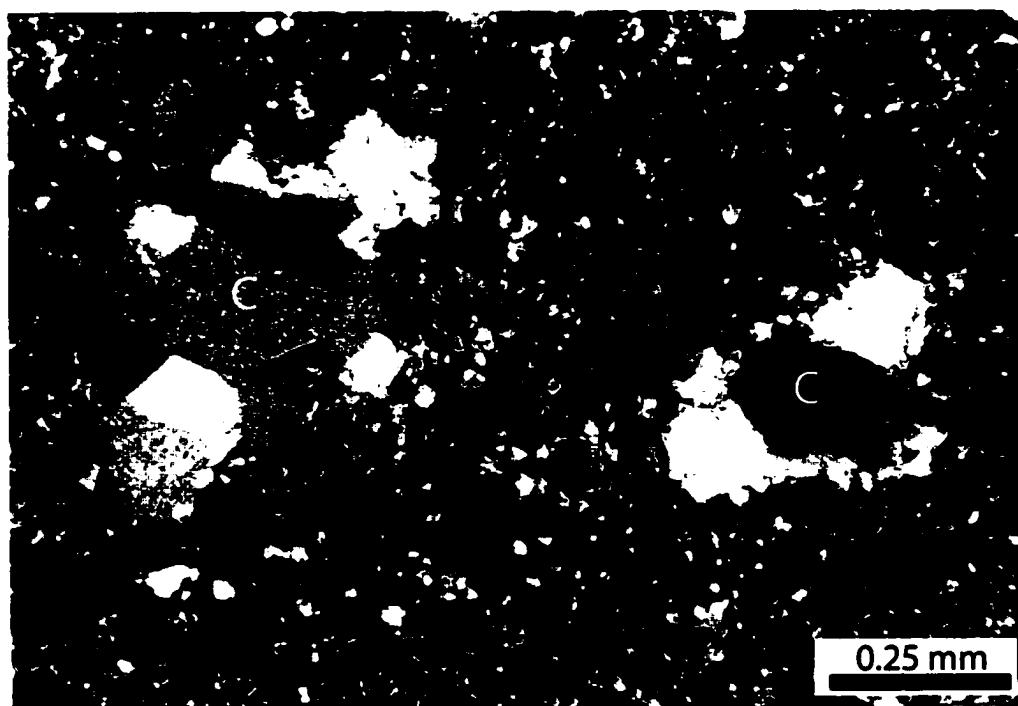
Figure 27b: Calcite-filled vesicles (C) in a pillowed flow near locality A, PLB. Thin section in xpl.

Interpretation

Pillowed flows studied extensively in both Archean (e.g. Dimroth et al., 1978; Hargreaves and Ayres, 1979; Wells et al., 1979; Cousineau and Dimroth, 1982) and Phanerozoic (e.g. Moore, 1975; Moore and Lockwood, 1978; Yamagishi et al., 1989; Yamagishi, 1991; Walker, 1992) settings form when hot lava enters into or erupts under water. Pillow lava may resemble subaerial pahoehoe flows (Wells et al., 1979; Ballard et al., 1979; Walker, 1992), but pillowed flows are distinguished by radial contraction joints (Kennish and Lutz, 1998) and the association with hyaloclastite (McPhie et al., 1993). Closely-packed pillows represent the normal, molded pillows of Dimroth et al. (1978) that are interpreted to develop when flow velocity and temperature decrease.

3.2.3   Pillow Breccia

Pillow breccia at locality A. 5-35 m thick, is composed of disorganized pillow fragments and isolated pillows (Figure 25). Pillow fragments. 2-30 cm in size, are angular to subrounded and generally lack chilled margins (Figure 28a). Whole. isolated. 20-60 cm pillows in pillow breccia are subspherical. whereas isolated. 10-40 cm amoeboid varieties are set in a matrix of massive hyaloclastite (Figure 25; section 3. flows IV and V). Vesicularity ranges from 5-17% with spherical vesicles <1 cm in size (Table 1, Figure 29). Pillow breccia matrices not composed of hyaloclastite are represented by chloritized quartz-feldspar aggregates. Thin. <1.5 m-thick units of pillow breccia at locality B locally characterize pillowed flow tops (Figure 26).

Interpretation

Pillow breccia generally develops during quench fragmentation resulting from lava-water interactions (Dimroth et al., 1978; Yamagishi, 1991). Alternatively, "pillow

Figure 28a: Pillow breccia from locality A, PLB, containing angular to subangular pillow fragments (Fr) in a mafic matrix. Arrow points to top. Scale, pencil 14 cm.

Figure 28b: Amoeboid pillow (Ap) set in a matrix of hyaloclastite (fluidal peperite), locality A, PLB. Note the intermingling of chloritized glass shards (G) and sedimentary material (S). Arrow points to top. Scale, pencil 12 cm.
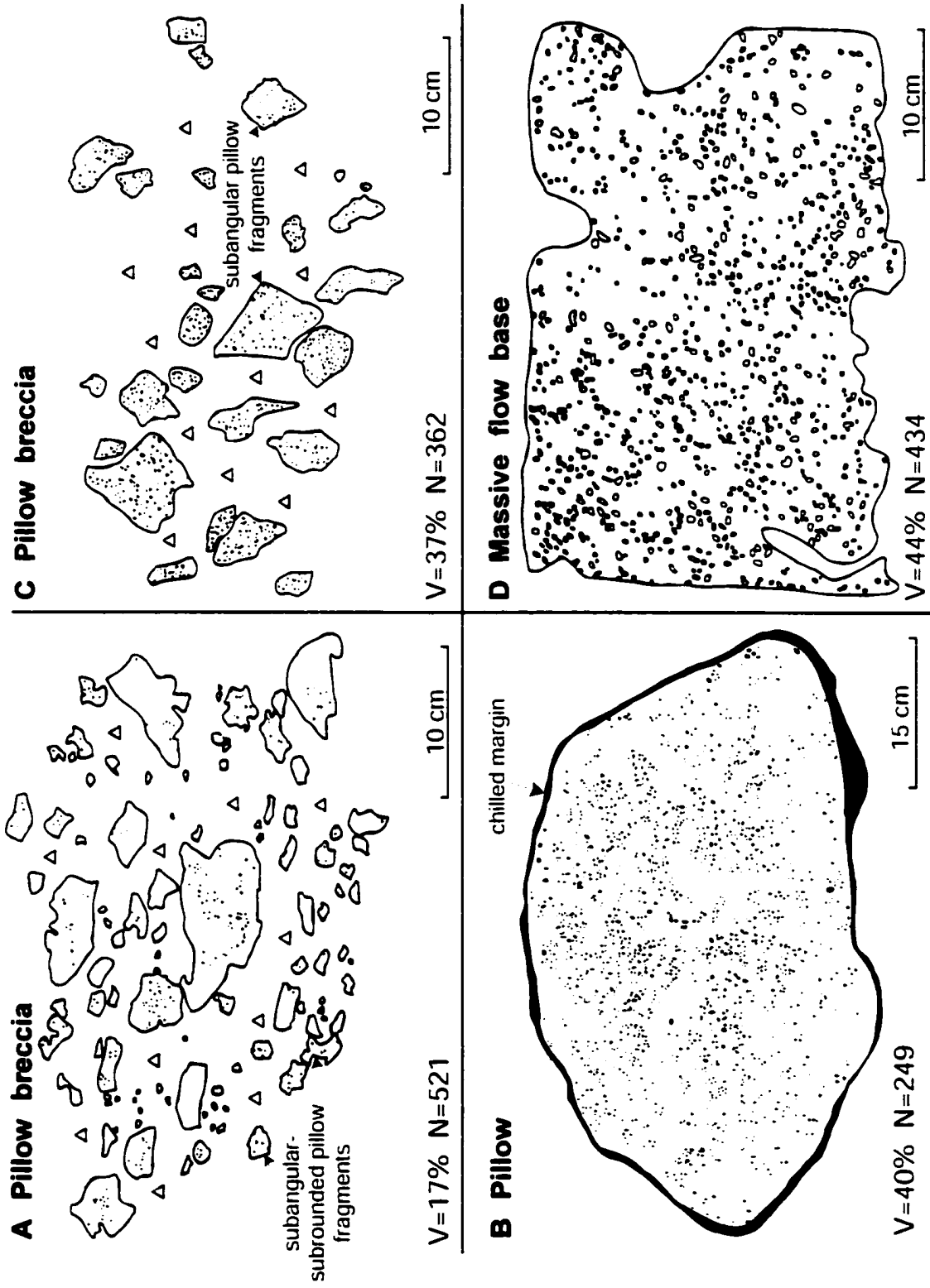
Figure 29: Vesicularity index of massive and pillowed flows and pillow breccia in the Peltier Formation and Central Beaulieu River belt (results also in Table 2). Vesicle percentage (V) and number of counts (N) are indicated. (A) Pillow breccia fragments from locality A, PLB. (B) Pillow from locality E, CBRB. (C) Pillow breccia fragments from locality E, CBRB. (D) Base of massive flow at locality E, CBRB.

A Pillow breccia

subangular-subrounded pillow fragments

V=17% N=521

B Pillow

chilled margin

15 cm

V=40% N=249

C Pillow breccia

subangular pillow fragments

10 cm

V=37% N=362

D Massive flow base

10 cm

V=44% N=434

fragment breccia" forms during mechanical disintegration of pillow lava due to slumping (Staudigel and Schmincke, 1984; Fisher and Schmincke, 1984; Busby-Spera, 1987). In addition, where lava flows into shallow water, wave or tide action combined with a steep flow front may be sufficient to break pillows into fragments (Moore, 1975; Kokelaar, 1986). Autoclastic pillow breccia and disorganized hyaloclastite at locality A are interpreted to have developed at flow tops and fronts from quench fragmentation during the late stages of an eruption and/or from slumping along the flanks of a remote part of a volcanic edifice where lava supply was decreased (e.g. Dimroth et al., 1978; Busby-Spera, 1987).

3.2.4 Hyaloclastite

Massive, non-vesicular hyaloclastite at locality A, 5-16 m thick, is characterized by isolated, amoeboid pillows (Figure 28b) and is locally interstratified with thin, 1-4 m-thick shale units (Figure 25). The hyaloclastite consists of two components: 1) chloritized sideromelane and 2) very fine-grained sedimentary material, and thus may be referred to as intrusive or peperitic hyaloclastite (McPhie et al., 1993). Convex-concave, chloritized sideromelane shards range from 0.2-3 cm in size and contain 0.02-0.05 mm-size titanite, and 0.1-0.35 mm-size plagioclase microlites (Figure 30a, b; Appendix 4). Very fine-grained sandstone and siltstone composed of microgranular quartz and feldspar, are contained in 0.5-5 cm-size globules that envelop glass shards, giving the hyaloclastite a fluidal texture. Discrete shale units, 1-4 m thick, locally separate pillow breccia and hyaloclastite (Figure 25).
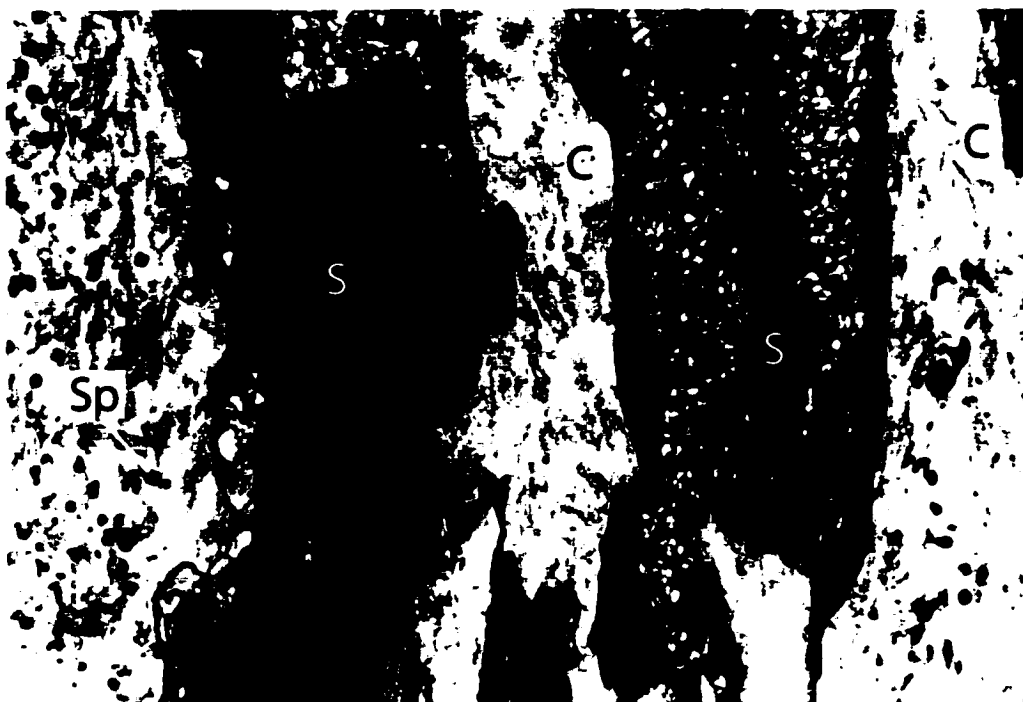
Figure 30a: Photomicrograph of disorganized hyaloclastite (fluidal peperite), containing sedimentary material (S), chloritized sideromelane (C), and sphene (Sp), locality A, PLB. Thin section in xpl.

Figure 30b: Close-up of disorganized hyaloclastite (fluidal peperite), with sedimentary material containing quartz and feldspar grains (S), and chloritized sideromelane (C), locality A, PLB. Thin section in xpl.

Interpretation

The fluidal texture resulting from the combination of devitrified sideromelane and sedimentary material in the Peltier Formation suggests that the hyaloclastite formed by autobrecciation when hot lava came into contact with cool, wet sediment, akin to the formation of peperite (e.g. Schmincke, 1967). The fluidal texture of the hyaloclastite is attributed to entrainment of very fine-grained wet sediment in a vapor film at the magma-sediment interface (e.g. Busby-Spera and White, 1987). Chlorite and sphene in sideromelane shards has been attributed to burial diagenesis and metamorphism below 500-1500 m depth (Viereck et al. 1982). Shale units intercalated with pillow breccia and hyaloclastite mark the boundaries between separate flow events, indicating periods of volcanic quiescence.

3.2.5   Dykes and Sills

Pillowed flows at locality B are cut by synvolcanic mafic dykes and sills. Dykes, 2-15 m-thick, are generally perpendicular to pillow strike and to a 20-45 m-thick massive sill (Figures 26, 31a). Numerous, mm-thick chilled margins, 10-75 cm apart, mark the presence of smaller intrusions within the central parts of most dykes. These dykes are characterized by as many as nine chilled margin contacts (Figures 31b, c) with a decrease in grain size towards individual margins. Cross-cutting relationships indicate that at locality B, the dykes were intruded after emplacement of the pillowed flows and sill. Subophitic, ophitic and intersertal dykes and ophitic sills are composed of 0.3-1 mm-size secondary actinolite and 0.1-0.8 mm-size plagioclase (Appendix 4).

Figure 31a: Contact (dashed line) between east-west trending sill (S) and north-south trending dyke (D) at locality B, PLB (see Figure 26). Scale, fieldbook 18.5 cm.

Figure 31b: Nine multiple intrusions in dyke I, locality B, PLB (see Figure 26). Scale, chisel 20 cm.

Interpretation

The intrusions at locality B are considered synvolcanic based on the presence of multiple intrusions and compositional similarities (discussed in section 3.4). Multiple intrusions are indicative of a synvolcanic, "feeder" origin (Staudigel and Schmincke, 1984; Mueller and Donaldson, 1992; Gibson et al., 1997), and are consistent with successive magma pulses where a feeder conduit was used several times to supply magma higher up in the sequence (Mueller and Donaldson, 1992). Multiple feeder dykes cutting numerous flow units associated with sills are typical of the central part of a volcanic edifice where construction is initiated (e.g. Easton, 1984).

3.3   Felsic-Intermediate Volcanic Facies

3.3.1   Peltier Volcaniclastic Rocks

Bedded, fine- to medium-grained volcaniclastic deposits are the on-strike equivalents of massive flows at locality A (Figure 19). The 10-35 m-thick, andesitic-dacitic volcaniclastic rocks are locally massive, but are generally characterized by 10-50 cm-thick planar beds (Figure 32a). The rocks are poorly sorted and contain 0.1-1.2 mm, euhedral, subangular, and broken plagioclase crystals, <1.6 mm subangular to subrounded quartz crystals (Figures 32b, 33a, b), and 0.2-2 mm subangular volcanic lithic fragments. Altered glass shards, <0.5 mm in size, were observed locally.

Interpretation

The andesitic-dacitic volcaniclastic rocks at locality A are referred to as tuffs, based on the grain size classification of Fisher (1961, 1966). The tuffs are interpreted as Bouma Ta divisions (Bouma, 1962) or S3 beds (Lowe, 1982), the results of turbidity current
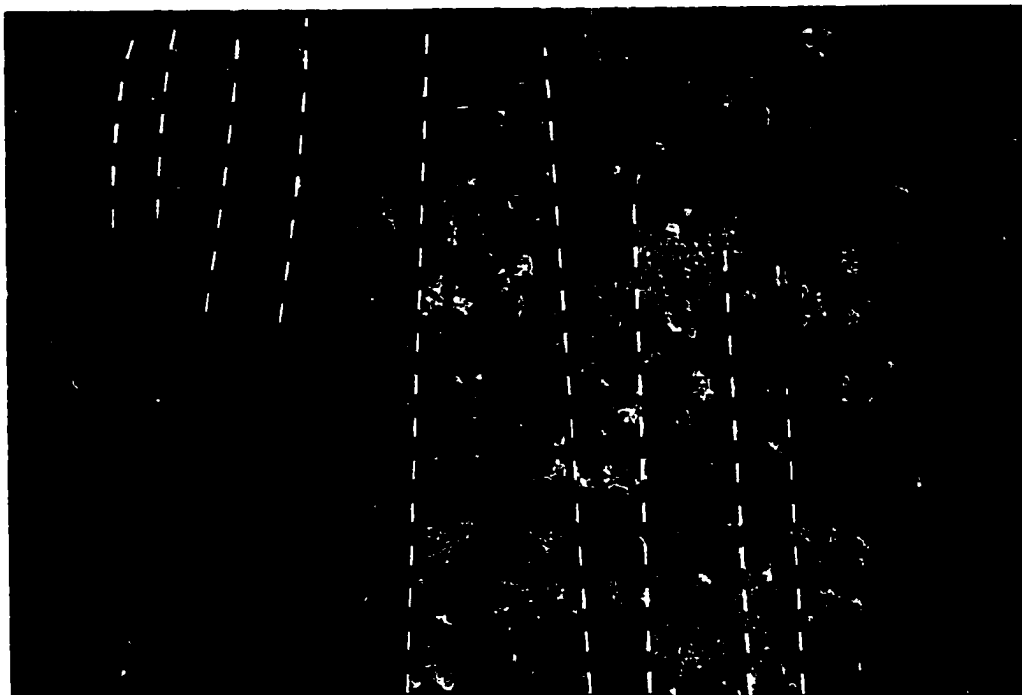
Figure 32a: Felsic bedded tuffs (dashed lines) at locality A, PLB. Scale, pencil 14 cm.
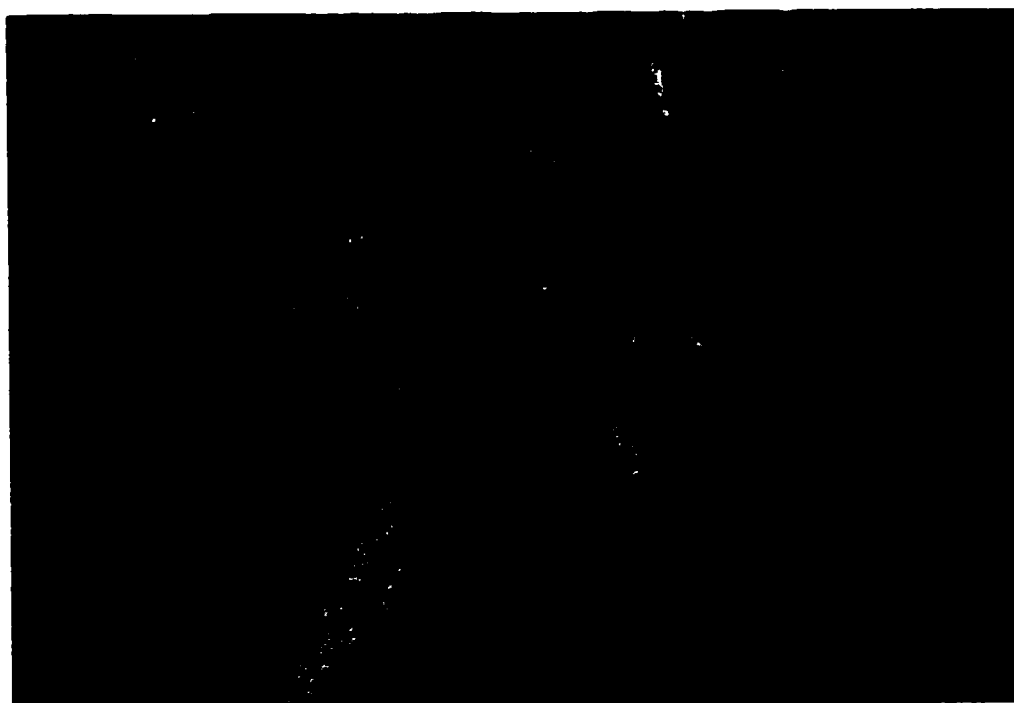
Figure 32b: Close-up of felsic bedded tuff samples, locality A, PLB. Note the subangular, mm-size quartz crystals (Q). Scale, pencil 5 cm.
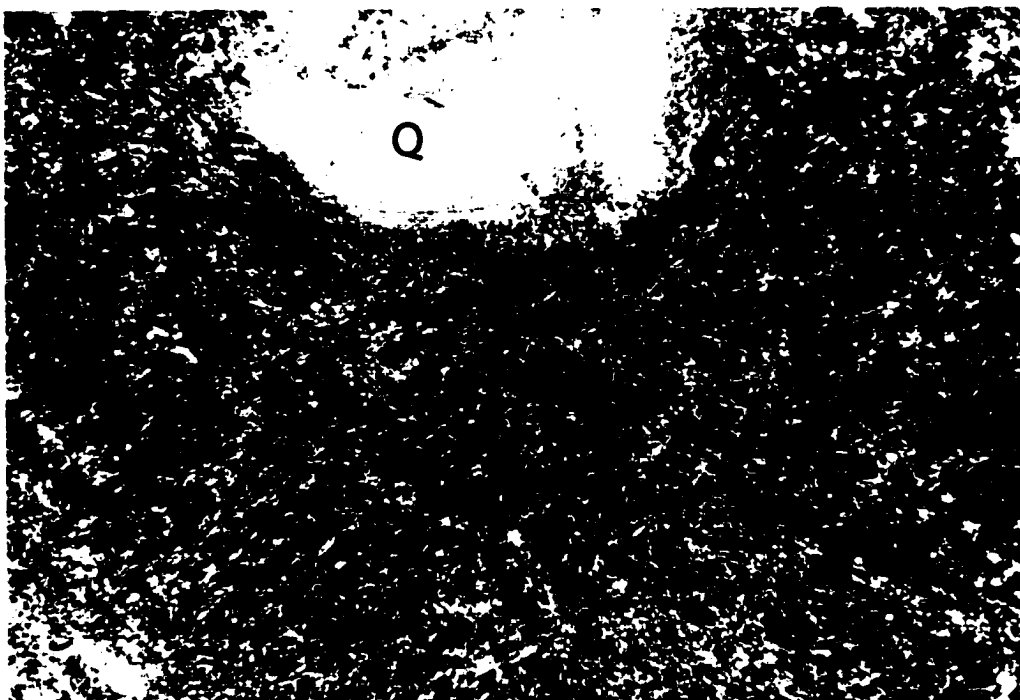
Figure 33a: Dacitic tuff containing a broken quartz crystal (Q) in a quartz-feldspar matrix at locality A, PLB. Field of view is approximately 6 mm. Thin section in xpl.
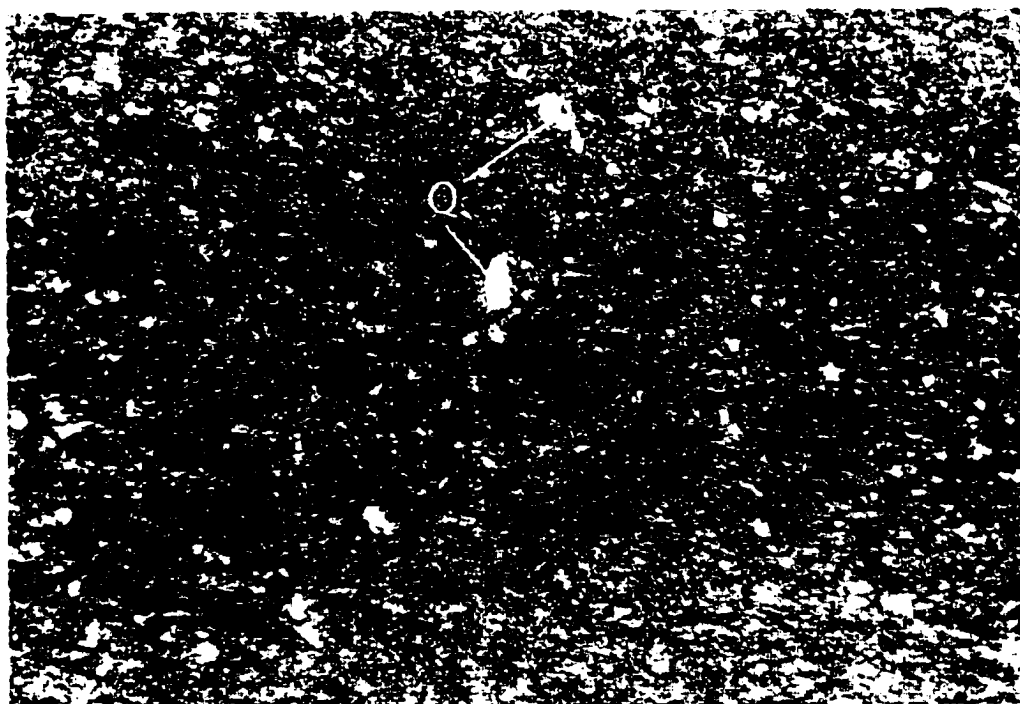
Figure 33b: Dacitic tuff containing small, subangular quartz crystals (Q) in a quartz-feldspar matrix at locality A, PLB. Field of view is approximately 6 mm. Thin section in xpl.

deposition (e.g. McPhie, 1995). Volcaniclastic rocks are typically the direct or redeposited products of subaerial and/or subaqueous eruptions, or are deposited following erosion and remobilization (reworking) of eruption products. Distinguishing between primary, redeposited, and reworked deposits is often problematic, but the abundance of angular and broken crystals in addition to lithic fragments in the tuffs argues for a primary or redeposited pyroclastic origin. Subaerial eruptions that settle through the water column are typically well-sorted and are distributed over an extensive area (McPhie et al., 1993). The poor sorting, generally unmodified to slightly modified crystal and lithic fragment shapes, and the limited extent of the bedded tuffs at locality A are consistent with deposition or redeposition from a nearby subaqueous eruption (e.g. McPhie, 1995).

3.3.2   Samandré Volcaniclastic Rocks

The Samandré volcaniclastic sample is characterized by 0.5-1.5 mm-size, subrounded, granular-textured lithic fragments in a fine-grained tuffaceous quartz-feldspar matrix. Certain lithic fragments are flattened and up to 4 mm long, possibly representing recrystallized pumice (e.g. McPhie et al. 1993; p. 139). With the limited outcrop exposure and recrystallized mineralogy, it is not possible to determine a mode of formation for the Samandré sample.

3.4   Geochemistry

3.4.1   Sampling Procedure

A total of 104 samples were collected from the Point Lake Group, but only 62 samples from the Peltier Formation and 1 sample from the Samandré Formation are

considered in this paper (Figure 34). Forty-two samples were omitted following

petrographical analysis or during sample sawing because of extreme textural

heterogeneity or silica/carbonate alteration, or following major element analysis where

LOI (loss on ignition) values were high. The samples, collected over an approximate area

of 12x18 km to achieve maximum diversity (Figure 34), were selected from outcrops

with minimal apparent chemical alteration, homogenous grain size, and low amygdule

percentages. The volcanic facies sampled include mafic pillowed and massive flows and

mafic-intermediate dykes and sills from the Peltier Formation and one felsic

volcaniclastic sample from the Samandré Formation. Only one sample was collected

from the Samandré Formation due to time constraints. The majority of the dykes and sills

are interpreted as feeders to overlying flows based on textural and compositional

similarities in the field, and the local presence of multiple intrusions (Corcoran, 2000). A

large number of samples were collected from Cyclops Peninsula, a 1.5 x 2 km area

mapped at a scale of 1:1000 (Figure 35). The peninsula was initially chosen as a prime

sampling target to determine whether the effects of chemical alteration, structural

deformation, and metamorphism were too substantial for a viable geochemical study. A

"boundary" of no sampling was designated approximately 1 km west of the western shore

of Cyclops Peninsula to avoid any effects of the shear zone located between a granitoid

domain and the Perrault Lithodeme, a highly strained unit of Peltier Formation pillowed

flows.

3.4.2   Results

Samples from the Peltier and Samandré formations are divided into four main

groups: 1) Group 1 tholeiitic basalts which are transitional into 2) Group 2 tholeiitic

basalts, 3) Group 3 calc-alkaline basalts and andesites and one rhyodacite, and 4) mafic,
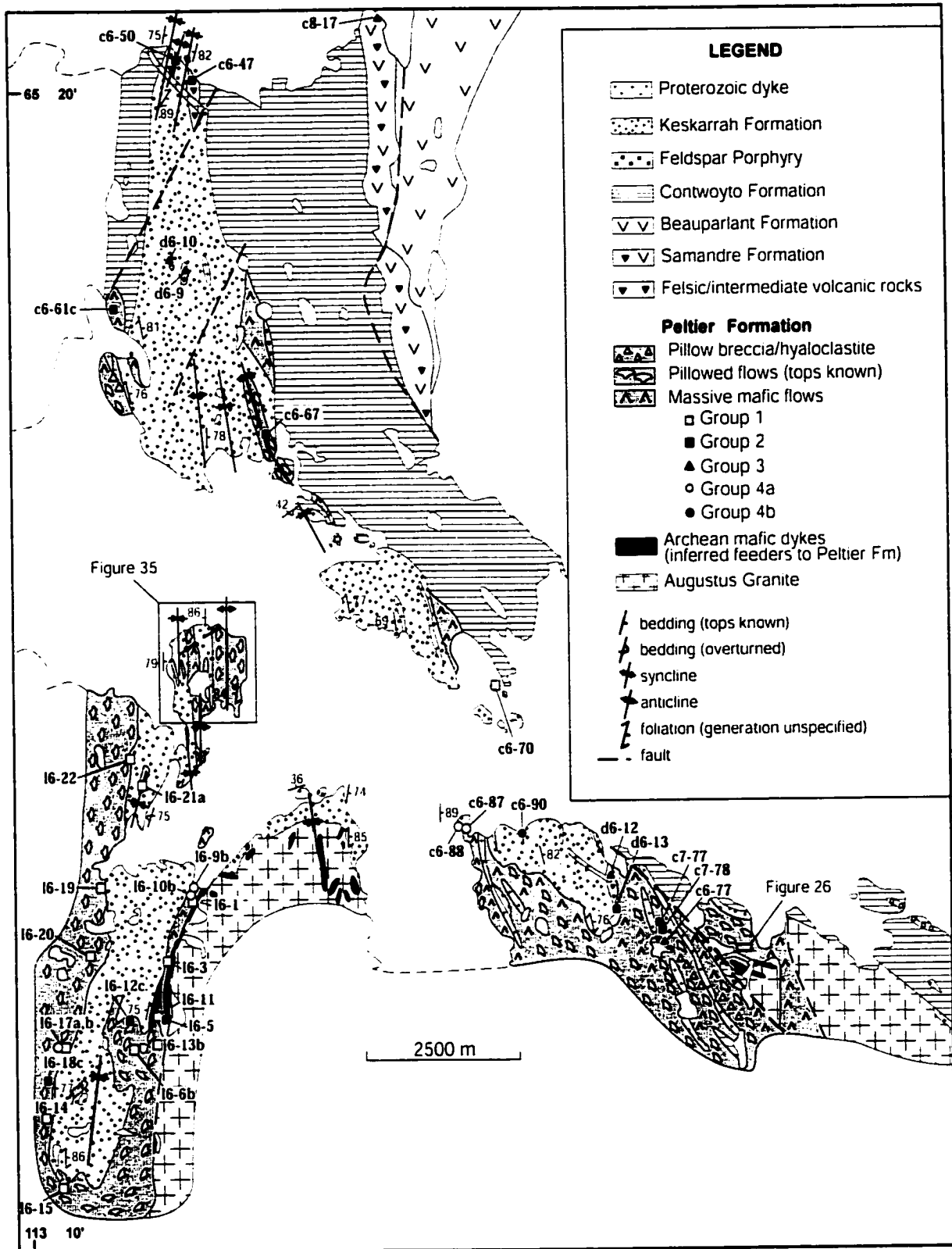
Figure 34: Lithological map illustrating 34 sample sites in the Point Lake belt. Five sample sites are shown in Figure 26 and 25 samples from Cyclops Peninsula are shown in Figure 35. Distinct groups are indicated using different symbols (see legend).
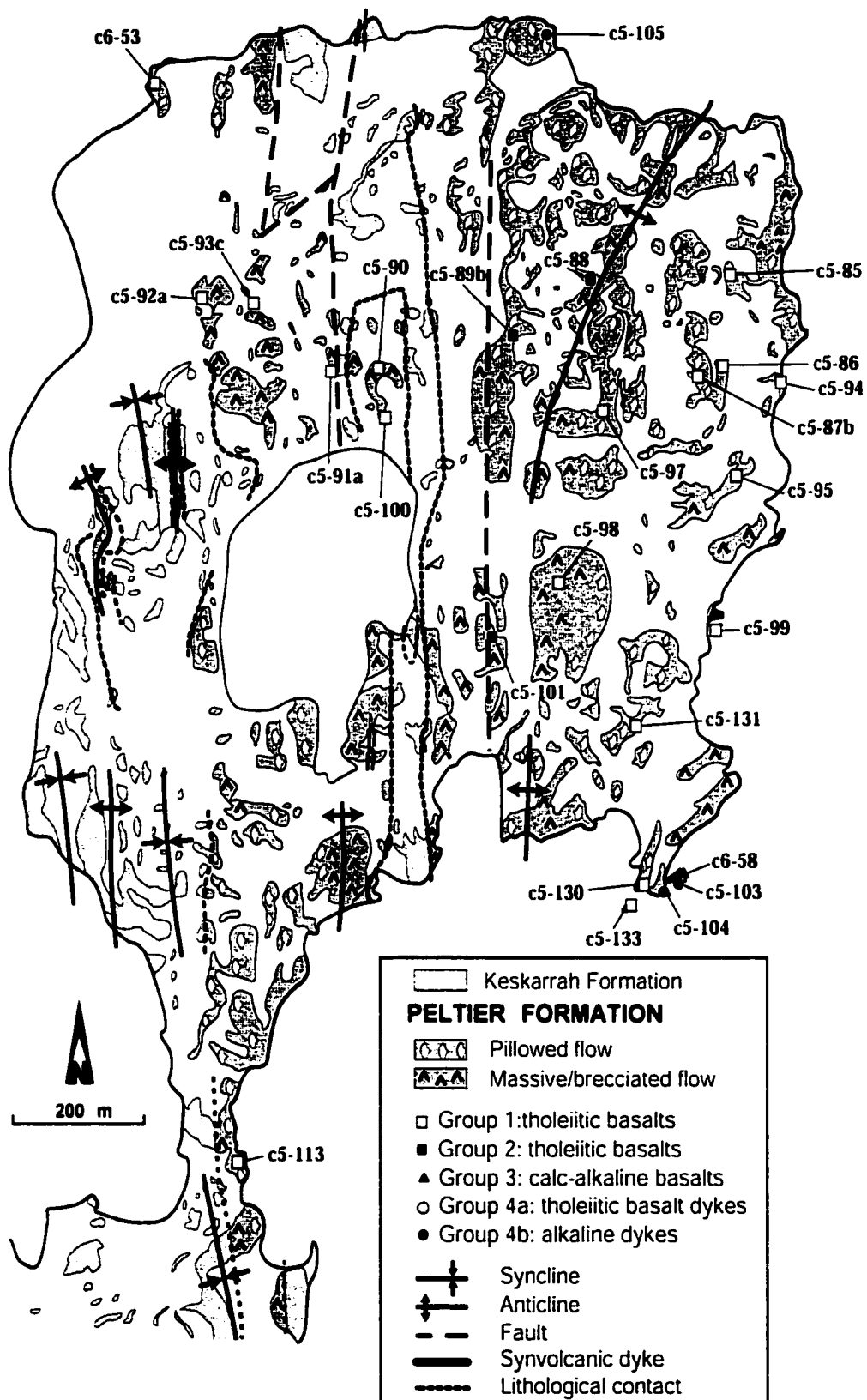
Figure 35: Lithological map of Cyclops Peninsula illustrating the locations of 25 samples. Note that most of the samples are Group 1 tholeiites.

tholeiitic dykes/sills, further subdivided into subgroup 4a basalts and 4b subalkaline

basalts (Table 2). Distinctions between Group 1 and Group 2 rocks are based on Zr/Y,

Ti/V, and $(La/Yb)_n$ ($_n$=normalized) ratios, and relative REE abundances.

Group 1 Tholeiitic Rocks

Group 1 tholeiitic basalts are mainly restricted to the southwest portion of the study

area with two exceptions, sample c6-70, located on the north segment of the study area,

and sample c7-101, collected from the southeast segment (Figure 34). Stratigraphically,

there is no distinction between Group 1 and Group 2 tholeiitic basalts. Group 1 rocks are

mainly subalkaline basalts with SiO_2 values of 45-53 wt% and FeO^*/MgO (*=total

$Fe=Fe_2O_3$ x 0.9) ratios ranging from 1.3-5. The samples demonstrate clear tholeiitic

differentiation trends on variation diagrams, with increasing FeO^*/MgO at a given SiO_2

content, and positive correlations between FeO^*/MgO vs FeO^* and FeO^*/MgO vs TiO_2

(Figure 36a-c). Group 1 tholeiites are slightly enriched in high-field-strength elements

(HFSE) and in the LREE, with $(La/Yb)_n$ ($_n$=normalized) ratios of .88-1.13, resembling

transitions between N- and EMORB (Table 3, Figure 37). The concentrations of

individual rare earth elements relative to one another remain constant, but overall sample

compositions change systematically (Figure 37). Similar phenomena are illustrated on

incompatible element diagrams where Group 1 rocks produce relatively flat patterns with

most samples displaying slight enrichments in Zr (c95-85; c95-86; c95-95; c95-99; 196-

20; 196-22) and some Nb depletions (c95-85; c95-95) relative to other incompatible

elements (Figure 38). ϵ_{Nd} values range between +0.2 and +2.23 (Table 4; Figure 39).

Table 2: Major and trace element data for samples from the Point Lake belt (ND=no data) *=total Fe as Fe2O3. C5-114, c5-115, d6-3b are examples of altered samples. Other altered samples were eliminated during sample preparation.

Sample	C5-85	C5-86	C5-87B	C5-90	C5-91A	C5-92A	C5-93C	C5-94	C5-95	C5-97	C5-98	C5-99	C5-100	C5-113
Group	Group 1	Group 1	Group 1	Group 1	Group 1	Group 1	Group 1	Group 1	Group 1	Group 1	Group 1	Group 1	Group 1	Group 1
SiO2 (wt%)	52.78	48.97	49.94	50.15	48.51	50.03	49.85	52.2	50	47.47	47.58	51.03	48.81	44.82
TiO2	0.92	1.23	0.94	1.66	1.33	1.93	1.66	1.26	0.84	2.23	1.67	2.27	1.55	1.83
Al2O3	13.77	14.16	14.27	13.93	15.15	13.57	13.55	13.33	15.11	13.21	15.01	12.34	13.8	15.12
Fe2O3*	13.25	15.11	13	15.89	15.05	17.68	15.42	15.15	11.98	18.36	16.47	19.08	16.76	19.16
MnO	0.23	0.22	0.29	0.21	0.2	0.22	0.2	0.2	0.16	0.22	0.21	0.29	0.22	0.28
MgO	6.87	6.5	6.28	5.76	5.64	4.64	5.41	5.27	7.39	5.41	5.2	3.46	5.73	5.76
CaO	7.06	9.54	8.24	7.57	9.6	7.75	8.02	8.14	9.3	9.24	8.76	6.25	6.78	7.91
Na2O	4.13	1.97	3.14	2.64	1.99	3.1	2.96	3.63	3.2	1.82	2.35	1.83	4.17	2.53
K2O	0.21	0.65	0.3	0.15	0.06	0.2	0.38	0.25	0.51	0.34	0.58	0.85	0.24	0.06
P2O5	0.09	0.11	0.09	0.17	0.13	0.19	0.14	0.15	0.07	0.1	0.13	0.29	0.15	0.15
LOI	1.76	2.22	4.02	2.64	3.07	2.32	2.88	1.48	2.15	2.75	2.62	3.42	2.76	3.13
Total	101.07	100.65	100.51	100.78	100.73	101.62	100.46	101.06	100.71	101.14	100.58	101.11	100.98	100.75
FeO*/MgO	1.74	2.09	1.86	2.48	2.4	3.43	2.57	2.59	1.46	3.05	2.85	4.96	2.63	2.99
Cr (ppm)	101	133	108	182	284	103	165	18	359	93	184	ND	175	133
Ni	90	84	173	70	60	33	52	23	107	40	54	8	66	60
Co	ND	ND	ND	ND	ND	ND	ND	ND	ND	ND	ND	ND	ND	ND
Sc	ND	ND	ND	ND	ND	ND	ND	ND	ND	ND	ND	ND	ND	ND
V	270	327	271	311	322	388	448	281	287	531	345	199	321	412
Cu	ND	ND	ND	ND	ND	ND	ND	ND	ND	ND	ND	ND	ND	ND
Pb	ND	ND	2	5	6	5	4	2	ND	5	4	ND	5	4
Zn	ND	ND	ND	ND	ND	ND	ND	ND	ND	ND	ND	ND	ND	ND
Rb	4	13	5	5	2	5	7	4	8	9	9	24	7	2
Ba	174	232	148	205	132	259	205	131	183	225	340	335	237	179
Sr	80	180	87	182	214	173	221	221	158	180	181	338	116	191
Ga	13	17	14	18	18	21	16	17	16	18	20	21	19	20
Ta	0.05	0.05	ND	ND	ND	ND	ND	ND	0.03	ND	ND	0.09	ND	ND
Nb	3.1	4.8	5.4	7	6.2	7	6.1	5.5	2	5.8	7.6	8.2	7	7.3
Cs	ND	ND	ND	ND	ND	ND	ND	ND	ND	ND	ND	ND	ND	ND
Hf	1.66	2.23	ND	ND	ND	ND	ND	ND	1.39	ND	ND	4.78	ND	ND
Zr	69	87	67	115	98	131	99	97	56	82	105	209	108	116
Y	20	24	22	34	27	38	30	34	19	24	29	54	31	37
Th	0.61	0.47	3.3	6.5	6.4	8.4	4.4	3.3	0.55	5.5	4.6	1.09	4.5	5.3
U	ND	ND	ND	ND	1.4	1.9	ND	ND	ND	ND	ND	ND	ND	ND
Zr/Y	3.45	3.63	3.05	3.38	3.63	3.45	3.3	2.85	2.95	3.42	3.62	3.87	3.48	3.14
Ti/V	20.44	22.57	20.81	32.03	24.78	29.85	22.23	26.9	17.56	25.2	29.04	68.44	28.97	26.65

Table 2: continued

Sample	C5-130	C5-131	C5-133	C6-53	C6-70	L6-1	L6-3	L6-6B	L6-11	L6-13B	L6-14	L6-15	L6-17A	L6-19	L6-20
Group	Group 1	Group 1	Group 1	Group 1	Group 1	Group 1	Group 1	Group 1	Group 1	Group 1	Group 1	Group 1	Group 1	Group 1	Group 1
SiO2 (wt%)	52.22	47.68	48.97	48.57	49.02	50.81	46.95	45.98	48	46.81	47.18	46.16	49.51	46.53	47.7
TiO2	0.69	1.85	0.97	0.88	1.01	1.13	1.12	0.9	1.08	1.57	1.46	0.81	1.13	1.1	1.66
Al2O3	11.81	13.5	14.7	15.56	14.48	15.6	13.89	14.47	13.97	14.82	14.19	15.9	15.16	13.69	13.78
Fe2O3*	13.12	18.61	11.7	11.81	11.86	11.64	12.63	12.58	13.68	14.72	14.67	12.83	11.15	13.6	13.98
MnO	0.28	0.2	0.17	0.25	0.21	0.28	0.19	0.21	0.21	0.26	0.22	0.19	0.2	0.26	0.2
MgO	8.81	5.22	6.36	7.29	3.93	4.53	5.75	8.73	6.97	6.59	6.98	7.81	5.69	5.86	6.9
CaO	7.42	7.27	8.36	7.3	9.62	8.01	10.41	11.31	7.76	9.42	9.07	9.39	11.63	9.27	6.27
Na2O	1.27	3.21	3.68	2.75	2.07	4.08	2.59	1.65	2.44	1.73	2.43	2.58	2.2	2.06	1.76
K2O	2.42	1.6	0.15	0.41	0.1	0.2	0.4	0.08	1.13	0.15	0.16	0.19	0.09	0.13	3.87
P2O5	0.05	0.15	0.09	0.06	0.08	0.08	0.08	0.06	0.08	0.14	0.12	0.06	0.09	0.08	0.15
LOI	2.54	1.66	4.7	3	5.95	2.13	4.2	2.79	3.74	3.38	2.19	2.51	1.94	5.91	5.33
Total	100.62	100.95	99.85	97.88	98.33	98.49	98.21	98.76	99.06	99.59	98.67	98.43	98.79	98.49	101.6
FeO*/MgO	1.34	3.21	1.66	1.46	2.72	2.31	1.98	1.3	1.77	2.01	1.89	1.48	1.76	2.09	1.82
Cr (ppm)	2477	123	111	300	131	261	170	337	193	236	155	185	302	171	150
Ni	254	41	172	61	87	115	48	131	65	99	64	122	140	90	74
Co	ND	ND	ND	46	50	53	35	47	49	54	40	55	50	42	45
Sc	ND	ND	ND	5	7	13	5	5	12	8	1	6	4	9	11
V	218	378	282	308	294	364	382	325	359	352	395	262	332	334	367
Cu	ND	ND	ND	30	45	112	117	35	108	85	83	166	89	98	52
Pb	3	3	1	7	8	ND	5	4	1	3	4	5	3	3	3
Zn	ND	ND	ND	103	120	101	80	104	89	116	106	160	78	105	76
Rb	27	86	3	11	15	11	14	10	29	12	14	12	10	12	63
Ba	1707	313	129	327	203	81	98	405	608	272	248	190	115	134	773
Sr	167	165	153	159	293	119	134	160	125	112	167	144	173	117	163
Ga	12	19	15	12	13	14	15	11	12	13	13	14	15	13	12
Ta	ND	ND	ND	ND	ND	ND	ND	ND	ND	ND	0.08	ND	ND	ND	0.16
Nb	4.7	7.5	5.4	11	11	7	7	3	3.4	8	5.1	6	8	8	6.4
Cs	ND	ND	ND	ND	ND	ND	ND	ND	ND	ND	ND	ND	ND	ND	ND
Hf	ND	ND	ND	ND	ND	ND	ND	ND	1.9	ND	2.49	ND	ND	ND	3.02
Zr	46	69	69	8	81	70	87	60	71	93	98	41	68	80	118
Y	16	35	22	34	25	26	24	18	22	28	26	19	20	23	31
Th	ND	5.6	ND	3	4	ND	3	2	0.54	1	0.46	1	2	1	0.64
U	ND	2.7	ND	3	2	2	1	2	3	3	2	1	1	2	2
Zr/Y	2.88	3.23	3.14	0.24	3.24	2.69	3.63	3.33	3.22	3.32	3.77	3.16	3.4	3.48	3.81
Ti/V	18.99	29.37	20.64	17.14	20.61	18.62	17.59	16.62	18.05	26.76	22.18	18.55	20.42	19.76	27.14

Table 2: continued

Sample	L6-21A	L6-22	C7-101	C5-88	C5-89B	C5-101	C6-47	C6-50	C6-61C	C6-67	C6-74	D6-13	L6-5	L6-12C	L6-18C
Group	Group 1	Group 1	Group 1	Group 2	Group 2	Group 2	Group 2	Group 2	Group 2	Group 2	Group 2	Group 2	Group 2	Group 2	Group 2
SiO2 (wt%)	48.3	49.12	44.7	47.88	50.22	49.62	50.18	45.28	49.4	53	47.71	45.5	50.23	47.41	48.78
TiO2	1.84	1.36	1.22	2.07	1.59	1.85	1.08	1.21	1.28	2.1	1.67	2.24	1.5	0.92	1.71
Al2O3	15.99	14.13	15.36	13.43	14.27	15.25	14.83	15.11	17.74	18.36	15.5	15.69	14.57	15.17	14.56
Fe2O3*	14.31	13.54	10.84	19.07	15.62	14.95	14.41	13.99	10.76	10.4	15.65	14.96	13.35	12.52	12.99
MnO	0.15	0.19	0.27	0.21	0.21	0.2	0.36	0.25	0.15	0.24	0.3	0.18	0.2	0.2	0.25
MgO	8.44	7.14	6.17	5.13	5.47	4.87	3.33	3.9	5.34	2.15	3.7	6.02	4.59	7.65	3.95
CaO	0.67	6.95	9.31	6.8	8.32	5.75	9.49	6.47	9.87	4.7	6.97	7.81	7.18	10.64	8.64
Na2O	3.98	2.12	2.54	3.25	2.61	4.4	2.42	5.02	2.1	1.38	3.64	3.16	2.41	1.26	2.66
K2O	0.03	0.01	0.81	0.42	0.25	0.43	0.34	0.23	0.39	0.97	0.03	0.17	0.95	0.02	0.19
P2O5	0.18	0.12	0.06	0.17	0.13	0.15	0.09	0.48	0.14	0.29	0.16	0.48	0.14	0.07	0.16
LOI	4.52	4.5	4.05	2.04	2.37	3.26	5.66	6.63	1.72	6.35	5	3.05	3.7	3.1	4.96
Total	98.41	99.18	99.42	100.47	101.06	100.73	102.2	98.57	98.89	99.98	100.32	99.26	98.81	98.96	98.85
FeO*/MgO	1.53	1.71	1.58	3.35	2.57	2.76	3.89	3.23	1.81	4.35	3.81	2.24	2.62	1.47	2.96
Cr (ppm)	168	147	297	84	222	241	259	137	169	183	148	109	74	330	162
Ni	99	104	124	27	60	52	63	116	29	110	145	93	47	145	70
Co	53	48	61	ND	ND	ND	42	51	41	41	43	46	35	48	46
Sc	22	7	15	ND	ND	ND	7	10	1	14	12	4	9	11	3
V	364	300	304	420	308	289	263	219	207	426	361	232	305	308	380
Cu	12	61	98	ND	ND	ND	33	81	119	25	116	28	106	59	64
Pb	4	5	9	ND	ND	ND	6	4	3	4	3	6	16	3	1
Zn	118	112	102	ND	ND	ND	91	92	98	86	86	128	178	81	106
Rb	6	8	30	13	7	5	40	10	22	18	17	13	46	10	12
Ba	494	196	374	232	229	306	512	363	292	405	136	792	347	305	227
Sr	77	142	120	128	184	70	139	129	174	126	125	717	284	180	84
Ga	16	13	15	21	18	15	20	16	11	16	16	13	15	12	14
Ta	ND	0.07	ND	0.11	0.1	0.07	0.11	0.06	0.08	ND	ND	ND	ND	ND	ND
Nb	10	5.2	5	9.5	7.4	4.1	8.7	3.4	6.2	7	6	10	10	7	10
Cs	ND	ND	0.13	ND	ND	ND	ND	ND	ND	ND	ND	ND	ND	ND	ND
Hf	ND	2.65	ND	3.59	2.91	3.19	4.25	1.94	2.7	ND	ND	ND	ND	ND	ND
Zr	119	98	55	155	127	137	167	71	101	164	125	138	139	80	138
Y	40	25	19	36	27	29	38	21	27	25	21	24	22	18	34
Th	2	0.5	1	2.36	2.01	2.09	2.9	0.99	1.43	2	4	4	5	1	1
U	2	2	0.09	ND	ND	ND	2	2	3	3	2	ND	3	2	2
Zr/Y	2.98	3.42	2.89	4.31	4.7	4.72	4.39	3.38	3.74	6.56	5.95	5.75	6.32	4.44	4.06
Ti/V	30.33	27.2	16.97	29.57	30.97	38.41	24.63	33.15	37.1	29.58	27.76	57.93	29.51	17.92	27

Table 2: continued

Sample	C7-77	C7-78	D6-9	D6-10	D6-12	C6-58	C6-77	C8-17	L6-9B	L6-10B	L6-17B	C7-99	C7-100	C7-102	CS-103
Group	Group 2	Group 2	Group 3	Group 3	Group 3	Group 3	Group 3	Group 3	Group 4a	Group 4a	Group 4a	Group 4a	Group 4a	Group 4a	Group 4b
SiO2 (wt%)	48.07	46.08	58.24	55.28	53.47	59.29	47.24	68.21	48.14	48.62	45.45	47.9	48.56	47.64	46.58
TiO2	2.092	1.964	0.62	0.82	1.08	0.73	1.11	0.39	0.58	0.88	1.07	1.01	1.3	1.09	1.83
Al2O3	14.53	13.76	17.82	16.86	14.05	16.84	15.37	14.36	15.34	14.95	15.22	14.27	14.43	14.77	7.66
Fe2O3*	13.67	14.06	4.16	6.5	7.27	5.15	13.8	5.15	11.72	12.56	14.24	12.41	15.02	14.18	16.34
MnO	0.189	0.188	0.03	0.07	0.09	0.06	0.2	0.08	0.19	0.19	0.26	0.18	0.24	0.21	0.19
MgO	6.24	6.38	2.12	4.47	7.34	3.2	8.26	1.03	8.81	6.88	7.48	7.77	5.79	6.48	14.43
CaO	7.17	7.58	5.89	6.68	6.91	6.02	4.51	1.59	7.79	10.29	10.51	9.49	7.97	10.62	9.61
Na2O	3.71	1.74	5.31	3.46	3.68	4.04	2.22	3.28	3.11	2.14	1.74	2.05	2.47	1.86	0.43
K2O	0.19	0.28	1.46	0.57	0.66	1.81	3.02	4.27	0.4	0.46	0.22	0.6	0.74	0.38	0.45
P2O5	0.421	0.395	0.23	0.21	0.27	0.17	0.07	0.13	0.04	0.06	0.08	0.07	0.13	0.09	0.2
LOI	2.31	6.04	2.03	3.73	3.49	3.23	2.12	1.1	2.62	2.45	2.37	3.43	2.43	4.52	2.77
Total	98.59	98.47	97.91	98.65	98.31	100.53	97.91	100.68	98.74	99.48	98.64	99.19	99.08	101.83	100.48
FeO*/MgO	1.97	1.98	1.77	1.31	0.89	1.45	1.5	4.5	1.26	1.64	1.71	1.44	2.33	1.97	1.02
Cr (ppm)	48	201	36	117	273	42	206	5	246	198	291	273	80	90	1492
Ni	88	87	25	89	225	109	38	8	134	87	154	110	68	114	803
Co	48	41	10	22	32	22	50	7	49	52	48	53	53	74	ND
Sc	6		6	3	7	11	15	42	13	7	7	3	8	ND	ND
V	262	227	61	131	184	75	333	5	323	309	319	329	345	281	208
Cu	30	25	8	25	13	71	17	8	79	111	63	91	139	162	ND
Pb	7	8	14	14	17	3	9	16	2	6	2	4	8	10	7
Zn	122	117	42	68	76	94	68	82	82	88	104	85	104	91	ND
Rb	12	18	28	15	21	51	31	107	15	21	14	24	30	8.8	9
Ba	520	352	747	855	452	1031	1424	834	480	400	269	290	553	ND	266
Sr	482	408	1637	1410	2811	371	1263	106	106	158	145	113	163	132.7	57
Ga	15	14	21	19	17	14	20	24	14	13	12	14	13	19	14
Ta	ND	ND	ND	0.08	0.43	ND	0.33	ND	0.03	0.03	ND	ND	ND	ND	ND
Nb	8	8	4	7	11.8	7	5.9	22	1.7	2.5	7	5	6	3.05	25.1
Cs	0.45	ND	ND	ND	ND	ND	ND	2.9	ND	ND	ND	ND	0.77	ND	ND
Hf	ND	ND	ND	3.39	4.54	ND	3.55	ND	1.01	1.63	ND	ND	ND	0.96	ND
Zr	118	109	217	124	164	138	136	588	36	59	65	62	94	29.31	171
Y	21	20	9	11	11	17	7	58	13	20	19	18	27	21.56	21
Th	-	ND	14	5.57	9.15	2	5.17	12	0.25	0.45	2	1	8	0.34	7.4
U	-	-	ND	ND	ND	1	ND	2.58	2	2	2	2	0.12	2	ND
Zr/Y	5.62	5.45	24.11	11.27	14.91	8.12	19.43	10.14	2.77	2.45	3.42	3.44	3.48	1.36	8.14
Ti/V	47.91	51.91	60.98	37.56	35.22	58.4	20	464.4	10.77	17.08	20.13	18.44	22.57	23.25	52.79

Table 2: continued

Sample	C5-104	C5-105	C6-87	C6-88	C6-90	c5-114	c5-115	d6-3b
Group	Group 4b	Group 4b	Group 4b	Group 4b	Group 4b	altered-grp.1	altered-grp.1	altered-grp.3
SiO2 (wt%)	50.78	46.82	46.89	46.35	47.48	41.69	40.99	41.94
TiO2	1.91	1.89	2.43	2.69	3.26	0.74	0.77	2.01
Al2O3	7.91	7.44	13.72	14.15	11.6	11.34	11.77	13.31
Fe2O3*	15.11	16.36	14.42	14.35	17.57	12.6	10.71	16.81
MnO	0.19	0.19	0.2	0.2	0.25	0.18	0.16	0.67
MgO	11.08	14.5	6.84	6.9	4.99	10.02	8.9	3.8
CaO	9.84	9.69	7.02	7.6	9.14	7.76	8.55	8.3
Na2O	1.52	0.39	1.73	2.57	2.18	3.32	4.23	1.11
K2O	0.93	0.45	0.21	0.78	0.63	0.32	0.05	0.42
P2O5	0.19	0.21	0.53	0.64	0.48	0.28	0.28	0.21
LOI	1.52	2.66	5.13	2.82	1.42	12.1	14.12	10.41
Total	100.98	100.6	99.13	99.05	99	100.35	100.53	98.99
FeO*/MgO	1.23	1.02	1.9	1.87	3.17	1.13	1.08	3.98
Cr (ppm)	1049	1673	246	230	15	917	904	40
Ni	217	892	141	149	17	306	290	ND
Co	ND	ND	53	53	51	ND	ND	38
Sc	ND	ND	7	6	14	ND	ND	3
V	254	209	217	257	511	200	197	401
Cu	ND	ND	37	42	505	ND	ND	97
Pb	26	7	6	6	5	4	7	8
Zn	ND	ND	138	141	112	ND	ND	196
Rb	13	9	14	23	33	20	3	24
Ba	431	268	694	708	476	177	231	259
Sr	108	56	299	401	207	509	762	73
Ga	15	13	13	13	10	13	14	13
Ta	ND	ND	0.44	ND	ND	ND	ND	ND
Nb	23.5	24.9	11.6	14	28	12.8	12.2	11
Ca	ND	ND	3.93	ND	ND	ND	ND	ND
Hf	ND	ND	3.93	ND	ND	ND	ND	ND
Zr	165	171	168	197	286	84	90	153
Y	21	21	27	29	51	17	18	31
Th	6	7.9	2.08	3	4	7	6.4	6
U	ND	ND	2	2	3	ND	ND	ND
Zr/Y	7.86	8.14	6.22	6.79	5.6	4.94	5	4.94
Ti/V	45.1	54.36	67.25	62.7	38.25	22.18	23.58	30.07

Figure 36: Variation diagrams demonstrating the behavior of (A) TiO2 wt% vs. FeO*/MgO, (B) SiO2 wt% vs. FeO*/MgO, and (C) FeO* wt% vs. FeO*/MgO in samples from Group 1 tholeiites, Group 2 tholeiites, Group 3 calc-alkaline rocks, subgroup 4a dykes/sills, and subgroup 4b dykes/sills. Good trendlines (dashed) are displayed for Groups 1 and 4a, with less reliable trends for Groups 2, 3 and 4b. Diagrams after Miyashiro (1974).

Table 3: REE data (in ppm) for selected samples from the Peltier Formation, Point Lake Belt (ND=no data)

Sample	C5-85	C5-86	C5-95	C5-99	1.6-6B	1.6-11	1.6-14	1.6-20	1.6-22	C7-101	C5-88	C5-89B	C5-101	C6-47	C6-50	C6-61C	C7-77	D6-10	D6-12	C6-77	C8-17	1.6-9B	1.6-10B	C7-100	C7-102	C6-87
Group	1	1	1	1	1	1	1	1	2	1	2	2	2	2	2	2	2	3	3	3	3	4a	4a	4a	4a	4b
La	3.93	4.63	2.88	11.03	3.02	4.12	4.82	6.17	5.05	3.17	12.51	9.08	11.03	13.62	5.37	9.16	16.75	36.5	44.8	28.91	63.26	1.72	3.09	5.72	3.74	22.13
Ce	9.8	12.03	7.24	28.96	7.84	10.35	12.97	16.45	13.47	8.06	28.51	21.39	28.96	31.47	12.48	20.57	37.07	74.27	94.33	56.34	125.9	4.69	7.85	14.88	9.58	49.88
Pr	1.44	1.82	1.08	4.35	1.21	1.53	1.97	2.47	2.01	1.22	3.86	2.88	4.35	4.23	1.73	2.82	4.98	8.86	10.79	6.4	16.09	0.73	1.18	2.26	1.47	6.5
Nd	7.21	9.22	5.49	21.79	6.24	7.73	9.96	12.4	10.09	5.86	17.71	13.34	21.79	19.57	8.2	13.25	21.27	34	38.3	23.01	61.8	3.88	6.01	10.79	7.19	28.2
Sm	2.17	2.77	1.83	6.41	2.11	2.53	3.23	3.79	3.17	1.9	4.81	3.59	6.41	5.31	2.52	3.85	4.42	5.53	5.18	3.45	12.97	1.39	2.06	3.25	2.28	6
Eu	0.81	0.99	0.64	2.09	0.74	0.84	1.09	1.3	0.96	0.76	1.52	1.13	2.09	1.84	0.88	1.26	1.67	1.45	1.44	1.06	2.94	0.56	0.74	1.18	0.9	2.1
Gd	2.83	3.67	2.57	8.14	2.83	3.41	4.22	4.94	4.03	2.48	5.72	4.28	8.14	6.39	3.26	4.53	4.39	3.74	3.28	2.24	12.47	1.94	2.81	4.42	ND	5.78
Tb	0.5	0.62	0.46	1.37	0.5	0.58	0.72	0.84	0.67	0.47	0.95	0.73	1.37	1.05	0.55	0.77	0.68	0.45	0.4	0.29	1.96	0.33	0.5	0.76	0.53	0.87
Dy	3.37	4.25	3.18	9.22	3.4	4.05	4.85	5.66	4.54	3.03	6.3	4.89	9.22	6.99	3.84	5.08	4.47	2.36	2.28	1.59	12.72	2.3	3.53	5.26	3.66	5.37
Ho	0.76	0.93	0.71	2.05	0.73	0.88	1.06	1.22	–	0.69	1.4	1.04	2.05	1.45	0.84	1.08	0.88	0.43	0.43	0.29	2.48	0.51	0.78	1.14	0.82	1.09
Er	2.26	2.82	2.09	6.09	2.21	2.59	3.14	3.56	2.89	1.97	4.13	3.23	6.09	4.3	2.48	3.2	2.54	1.15	1.17	0.82	7.17	1.53	2.32	3.34	2.4	3.14
Tm	0.32	0.42	0.3	0.88	0.32	0.38	0.46	0.53	0.42	0.3	0.6	0.46	0.88	0.62	0.35	0.46	0.34	0.16	0.17	0.11	1.04	0.22	0.34	0.49	0.34	0.46
Yb	2.13	2.7	1.99	5.89	2.09	2.56	3.04	3.47	2.84	1.92	3.94	3.03	5.89	4.04	2.39	3.06	2.34	1	1.07	0.71	6.73	1.46	2.3	3.04	2.19	2.93
Lu	0.31	0.4	0.28	0.85	0.32	0.39	0.46	0.53	0.43	0.33	0.58	0.46	0.85	0.61	0.35	0.46	0.37	0.15	0.16	0.11	1.14	0.23	0.35	0.53	0.34	0.44
La/Yb(n)	1.23	1.15	0.97	1.25	0.97	1.08	1.06	1.19	1.19	1.1	2.12	2	1.92	2.25	1.5	2	4.78	24.41	28	27.23	6.29	0.79	0.9	1.26	1.14	5.05
Tb/Yb(n)	1.04	1.01	1.02	1.03	1.06	1	1.05	1.07	1.04	1.08	1.07	1.06	1.1	1.15	1.02	1.11	1.28	1.99	1.65	1.8	1.29	1	0.96	1.1	1.07	1.31
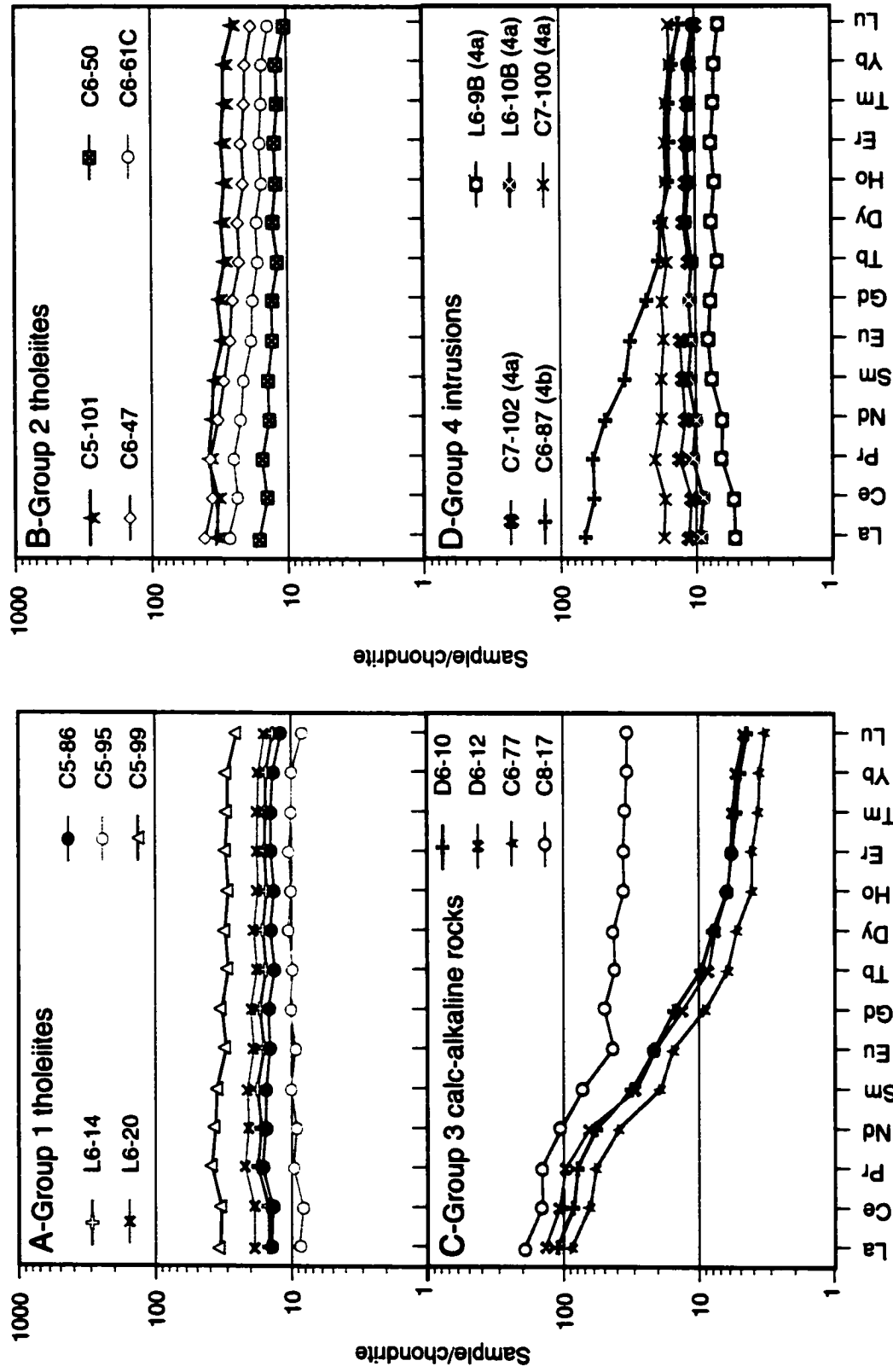
Figure 37: Chondrite-normalized REE abundances for selected Point Lake samples. Normalizing values after Haskin et al. (1968).
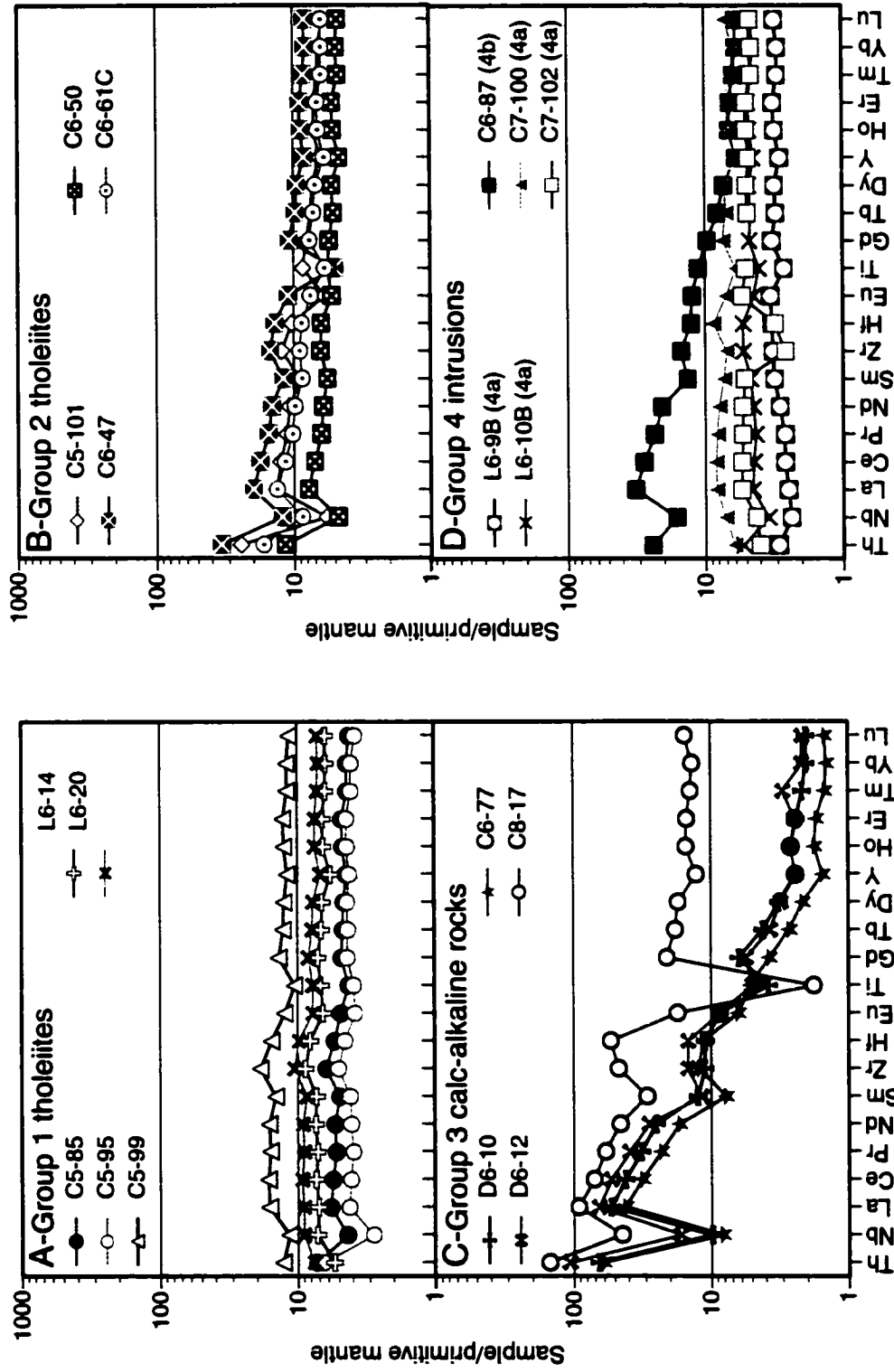
Figure 38: Primitive mantle-normalized incompatible element abundances for selected Point Lake samples. Normalizing values after Sun and McDonough (1989).

Table 4: Sm-Nd isotope systematics for selected samples from the Point Lake belt.

Sample	C5-85	C5-86	C5-95	C5-99	L6-6B	C5-88	C5-89B	C5-101	C6-47	C6-50	D6-10	D6-12	L6-9B
Group	1	1	1	1	1	2	2	2	2	2	3	3	4a
Nd (ppm)	7.04	8.82	5.42	21.06	5.73	17.62	12.80	14.45	18.39	7.01	31.10	38.08	3.18
Sm (ppm)	2.20	2.72	1.80	6.41	1.85	4.87	3.65	4.10	5.99	2.08	4.78	5.28	1.03
$^{147}Sm/^{144}Nd$	0.19274	0.19062	0.20537	0.18784	0.19914	0.17417	0.17612	0.17538	0.20119	0.18320	0.09479	0.08567	0.20016
$^{143}Nd/^{144}Nd$	0.512663	0.512632	0.512862	0.512491	0.512795	0.512131	0.512123	0.512172	0.512831	0.512419	0.510952	0.510777	0.512855
εNd	1.87	2.00	1.38	0.20	2.23	-2.08	-2.94	-1.72	2.23	0.40	2.41	2.15	3.06
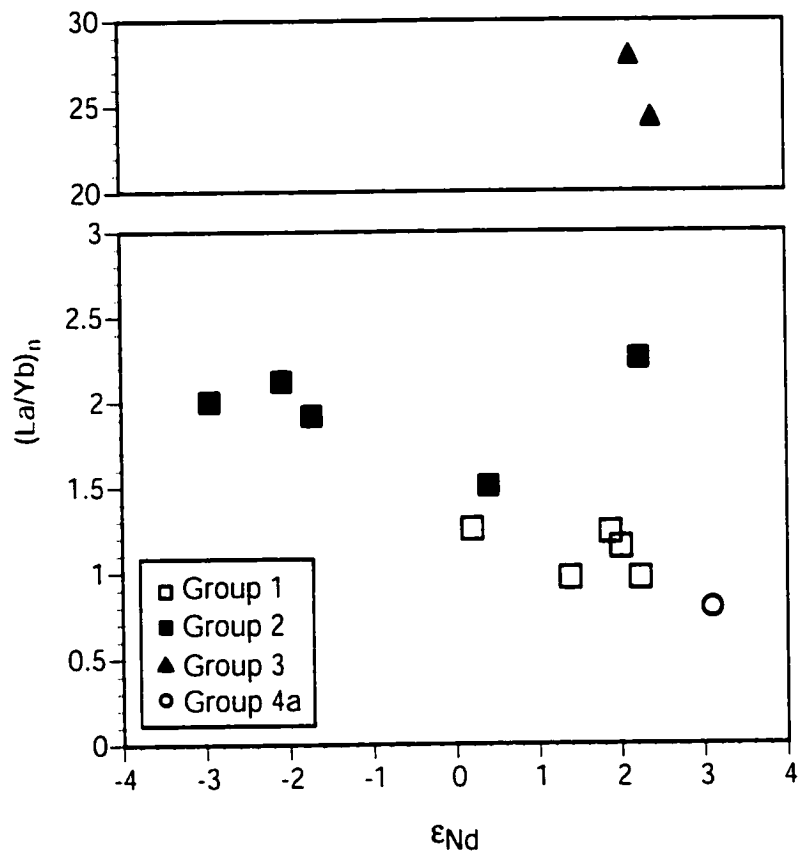
Figure 39: Initial εNd values vs. (La/Yb)n of samples from Group 1 tholeiites (open squares), Group 2 tholeiites (solid squares), Group 3 calc-alkaline rocks (triangles), and a subgroup 4a dyke (open circle) from the Point Lake belt.

Group 2 Tholeiitic Rocks

Group 2 tholeiitic basalts are dispersed throughout the study area and are locally interstratified with certain calc-alkaline rocks of Group 3 along the southeast segment (Figure 34). Group 2 samples have SiO_2 wt% ranging from 45-53 and FeO^*/MgO ratios of 1.5-4.4. These rocks demonstrate tholeiitic differentiation trends on SiO_2 vs FeO^*/MgO, FeO^* vs FeO^*/MgO, and TiO_2 vs FeO^*/MgO diagrams similar to Group 1, although Group 2 samples are slightly more scattered (Figure 36). LREE are enriched with $(La/Yb)_n$ ratios of 1.13-4.34 (Table 3). Absolute abundances of REE increase and decrease systematically, but there are few differences in the slope and curvature of the patterns (Figure 37). Incompatible trace elements are more abundant than in Group 1 tholeiites, but some samples have marked depletions in Nb (c5-88; c5-89b; c5-101; c6-47; c6-61c) and Ti (c6-47; c6-61c) relative to the REE (Figure 38). ε_{Nd} values range from -2.94 to +2.23 (Table 4, Figure 39).

Group 3 Calc-alkaline Rocks

Calc-alkaline basaltic and andesitic flows are located on the north and southeast segments, intercalated with conglomerate and tholeiitic basalts (Figure 34). One calc-alkaline rhyodacitic tuff, sample c8-17, was collected from the Samandré Formation, on the northern segment. The contact between Group 3 rocks and conglomerate was not seen; the flows may be tectonically interleaved with, or unconformably underlie the sedimentary rocks. Peltier Formation calc-alkaline samples contain 47-59 SiO_2 wt% and FeO^*/MgO ratios range from 0.9-1.8, whereas the Samandré sample contains 68% silica with an FeO^*/MgO ratio of 4.5. Sample c6-77 plots near the boundary between the tholeiitic and calc-alkaline fields on SiO_2 vs FeO^*/MgO, FeO^* vs FeO^*/MgO, and TiO_2

vs FeO*/MgO diagrams (Figure 36), but displays a REE pattern similar to other Group 3

samples (Figure 37). Group 3 samples display increasing SiO_2 with increasing

FeO*/MgO and decreasing TiO_2 and FeO* with increasing FeO*/MgO (Figure 36). The

LREE are enriched with $(La/Yb)_n$ ratios of 22.12-25.38 for the Peltier samples and 5.7 for

the Samandré sample (Table 3; Figure 37). On incompatible element diagrams, Group 3

rocks display strong depletions in Nb and Ti (Figure 38). Two calc-alkaline samples

yielded ε_{Nd} values of +2.15 and +2.41 (Table 4, Figure 39).

Group 4 Dykes/Sills

Group 4 dykes/sills are divided into two distinct sets, based on major and trace

element abundances and ratios. Subgroup 4a tholeiitic basalts with 45-46 SiO_2 wt% and

FeO*/MgO ratios from 1.2-2.3. were collected from the western segment of the study

area and from a detailed section on the eastern segment (Figure 34). These dykes and sills

cut the Peltier Formation mafic volcanic flows. Subgroup 4a intrusions display tholeiitic

differentiation trends on SiO_2 vs FeO*/MgO, FeO* vs FeO*/MgO, and TiO_2 vs

FeO*/MgO diagrams. similar to Groups 1 and 2 (Figure 36). REE patterns are relatively

flat with $(La/Yb)_n$ ratios of .71-1.14 (Table 3; Figure 37), closely resembling the patterns

of Group 1 tholeiites. Subgroup 4a intrusions are depleted in HFSE. with some samples

demonstrating slight depletions in Ti (c7-100, 16-9b, 16-10b), Nb (16-9b. 16-10b), and Zr

(c7-102) on the incompatible element diagram (Figure 38). Sample 16-9b, analyzed for

Sm-Nd isotopes, yielded an ε_{Nd} value of +3.06 (Table 4).

Subgroup 4b subalkaline basalts with 46-51 SiO_2 wt% and FeO*/MgO ratios from

1.0-3.2, were collected from the eastern segment (Figure 34) and from Cyclops Peninsula

(Figure 35). Subgroup 4b intrusions cut the Peltier and Keskarrah formations, and are

considered younger than Groups 1-4a. The subgroup displays a general tholeiitic

differentiation trend on the TiO_2 vs FeO^*/MgO plot, but the data are scattered on the

SiO_2 vs FeO^*/MgO, and FeO^* vs FeO^*/MgO diagrams (Figure 36). One sample is

enriched in LREE with a $(La/Yb)_n$ ratio of 4.58 (c96-87; Table 3; Figure 37). On an

incompatible element diagram, the sample displays depletions in Nb and Sm and does not

resemble the rocks of the other groups (Figure 38).

3.4.3 Interpretation

The association of tholeiitic basalts and minor calc-alkaline basalts and andesites,

compositional similarities between certain dykes and flows, and a spatial association

between the Peltier, Samandré and Beauparlant Formations, suggest that the volcanic

rocks at Point Lake are petrogenetically related (same evolutionary event). Rocks

belonging to Groups 1 and 2 and subgroup 4a produce relatively flat HREE patterns with

$(Tb/Yb)_n$ ratios between .93-1.24. The calc-alkaline rocks are HREE-depleted with

$(Tb/Yb)_n$ ratios significantly greater than unity (1.24-1.91; Figure 37). Relatively flat

HREE patterns like those produced by Groups 1 and 2 and subgroup 4a are typically

attributed to melting of spinel peridotite at depths of 40-60 km, in contrast to HREE-

depleted patterns like those of calc-alkaline samples d6-10, d6-12, and c6-77, which are

more consistent with melting of garnet peridotite at >80 km depth (Manetti et al., 1979;

McKenzie and O'Nions, 1991). This indicates that the magma producing calc-alkaline

rocks in the Peltier Formation was derived from deeper levels within the mantle than

those melts that formed the tholeiitic rocks. The enrichment in LREE relative to the

HREE could also be the result of contributing hydrous fluids from a subducting slab or an

OIB- (ocean island basalt) type source.

Interlayering of LREE-enriched and depleted basalts, a common feature in Archean

volcanic sequences, can easily be explained by crustal assimilation (Barley, 1986). The

process of crustal contamination is best illustrated on the incompatible element diagrams

where marked negative Nb anomalies are common in most groups (Figure 38).

Depletions in Nb relative to other incompatible elements are commonly attributed to

contamination by crustal material of granitic composition (e.g. Cox and Hawkesworth,

1985; Cousens, 2000). Negative ε_{Nd} values from three samples support the inference that

at least some of the magmas interacted with older sialic crust (e.g. DePaolo and

Wasserburg, 1976). Although crustal contamination played a significant role in the

petrogenetic evolution of the Point Lake belt, it cannot account for the calc-alkaline

component in the volcanic sequence. Calc-alkaline rocks are considered reliable

petrogenetic indicators of subduction-related processes (Wilson, 1989). These typically

demonstrate lower abundances of HFSE relative to MORB with depletions in Nb, Ta, and

Ti. Accessory minerals such as rutile are relatively insoluble in aqueous fluids associated

with subduction, and therefore remain in the subducted slab or overlying mantle wedge

(Ayers and Watson, 1991). The Nb and Ti depletions attributed to crustal contamination

in the Peltier Formation could also be imprints of subduction-related processes or

carbonatization, but the latter is discounted because Ti and Zr display constant

interelement ratios with each other and major elements such as MgO.

Linear trends produced by the Peltier tholeiitic and calc-alkaline rocks on the

FeO^*/MgO vs TiO_2, SiO_2, and FeO^* diagrams indicate mixing, fractionation, and/or

contamination processes which occurred as the magma ascended to the surface (Figure

36). Fractional crystallization affected the magmas forming each group as indicated by

the variations in REE abundances, which all increase with continued fractional

crystallization (Figure 37). Fractional crystallization, however, cannot account for the

slope variations between separate groups. Subgroup 4a dykes have similar patterns and

$(La/Yb)_n$ ratios to Group 1 tholeiitic basalts (Figure 37). Provided that the tholeiitic and

calc-alkaline rocks were derived through melting of the mantle at different depths, slope

variations in the middle to heavy REE are expected, but differences in REE patterns between Group 1 and 2 tholeiites, which are interpreted to have developed from melting of spinel peridotite, imply involvement of another process. Group 1 tholeiitic basalts resemble NMORB, whereas Group 2 tholeiites are more akin to EMORB with relative enrichments of the LREE and other incompatible trace elements. Chemical differences between N- and EMORB have mainly been attributed to differences in mantle sources (Sun and McDonough. 1989; Robillard et al., 1992). Groups 1 and 2 tholeiitic basalts at Point Lake could have been derived from a heterogeneous mantle source or may differ due to crustal contamination of Group 2 samples.

There is a clear distinction between Groups 1, 2, 3, and 4 on the $(La/Yb)_n$ vs ε_{Nd} plot (Figure 39). High $(La/Yb)_n$ ratios produced by Group 2 are consistent with some crustal contribution, as indicated by negative ε_{Nd} values. Crustal contamination during evolution of the belt is supported by a combination of stratigraphic relationships, Th enrichments. negative Nb and Ti anomalies, and negative ε_{Nd} values. The wide range in ε_{Nd} values (-2.94 to +3.06) for the Peltier Formation could be related to insulation of continental crust at different stages of development. Group 2 tholeiitic magmas, which were erupted through continental crust. could have created an insulating pathway through which subsequent magmas were emplaced (Groups 1, 3, 4). With time, the degree of crustal contribution should decrease due to increased insulation of the conduit walls (Nohda and Wasserburg, 1986). Group 3 samples have high $(La/Yb)_n$, but positive εNd values, consistent with REE enrichment by fluids derived from a subducted slab with a positive ε_{Nd}. Although several lines of evidence support interaction with continental crust, the style of contamination during magma genesis cannot be clearly determined.

3.5   Depositional Setting of the Peltier Formation

Abundant pillowed flows, pillow breccia, and hyaloclastite in the Peltier Formation and Beaulieu River volcanic belt attest to a subaqueous environment in which effusion rates were generally low (e.g. Dimroth et al., 1978; Ballard et al., 1979). The facies types, lateral and vertical facies changes, thickness of facies, and volcanic structures, are characteristic of the subaqueous portions of shield volcanoes, also known as seamounts.

Seamounts, also referred to as pillow mounds or pillow volcanoes, are mafic volcanic edifices that form on the ocean floor. These subaqueous features, varying from 0.05-10 km thick and attaining diameters as large as 100 km, are commonly associated with crustal-scale faults or rifts (Easton, 1984; Fornari et al., 1985; Chadwick and Embley, 1994; McPhie, 1995) and are generally characterized by central feeder conduits (Fisher, 1984; Head et al., 1996), in addition to predominant pillowed and sheet flows (Chadwick and Embley, 1994; Orton, 1996). Pillow breccia and hyaloclastite are commonly associated with pillowed and sheet flows on seamount flanks (Staudigel and Schmincke, 1984; Fisher and Schmincke, 1984). The volcanic facies constituting seamounts often overlie deep water sediments and/or are interstratified with sedimentary material deposited as suspension fallout during volcanism (Fisher, 1984). Seamounts, although primarily associated with mid-oceanic rift zones, have also been related to back-arc, arc, and hot spot volcanism.

Initial seamount construction in water depths below 500-2000 m is represented by locality B in the Peltier Formation, as suggested by the thick pillowed sequence, dyke/sill complex, absence of explosive debris, and low vesicularity (e.g. Moore and Schilling, 1973; Kokelaar, 1986; Staudigel and Schmincke, 1984; Fisher, 1984; Cas, 1992). Dykes and sills, salient components of seamount architecture, are interpreted to represent settings proximal to the magma source (i.e. vent) because dyke percentage decreases with

increasing distance from a volcanic centre (Walker, 1993; McPhie, 1995). These intrusions have high preservation potential, especially in ancient rocks where erosion of the subaerial deposits is extensive (Walker, 1993; Sohn, 1995). Primary eruption in seamounts necessitates a point source that may be fed directly by pipes or from an initial fissure that has collapsed, leaving only a few central conduits through which lava is supplied to the edifice (Smith and Cann, 1992; Chadwick and Embley, 1994). At locality B, magma originating from a point source is inferred to have been distributed and emplaced through a complex dyke-sill system, leading to the development of a pillow volcano or mound (Figure 40a). The minimal pillow breccia and hyaloclastite component at locality F supports a proximal setting with respect to the magma source (e.g. Wells et al., 1979; Fisher, 1984; Busby-Spera, 1987). The low vesicularity of flows suggests a deeper water environment than those envisaged for locality A because vesicularity typically decreases with increasing depth (Moore and Schilling, 1973; Staudigel and Schmincke, 1984).

An increase of pillow breccia and hyaloclastite with interstratified sedimentary deposits at locality A represents growth of a seamount outward from the source (e.g. Fisher, 1984; Figure 40b). Following quench fragmentation of pillowed flow tops and fronts, periods of volcanic quiescence ensued, resulting in the accumulation of very fine-grained sedimentary deposits between pillow breccia and hyaloclastite (Figure 40b). Massive hyaloclastite units typically accumulate at vents relatively remote from the magma source where discharge temperatures are significantly less (Lonsdale and Batiza, 1980; Busby-Spera, 1987). Effusive volcanism ensued following hyaloclastite emplacement, resulting in the deposition of massive flows. Local interstratified bedded tuffs were deposited from turbidity currents following limited subaqueous pyroclastic eruptions (Figure 40b). Volcaniclastic deposits are typically more common in remote parts of a volcanic edifice, away from the near-vent setting (McPhie, 1995; Orton, 1996).
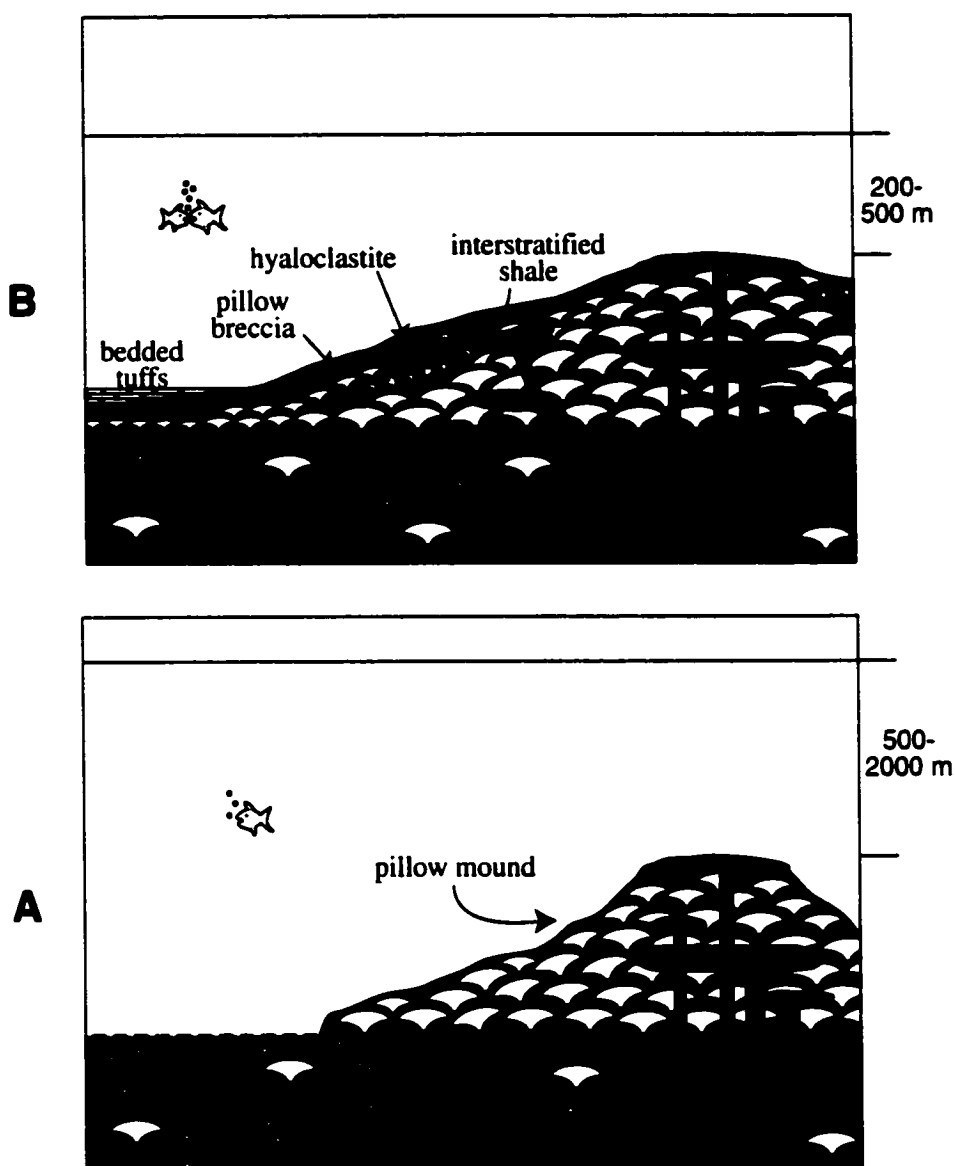
Figure 40: Models illustrating the inferred location of Peltier Formation facies on a seamount. (A) Initial seamount construction on the ocean floor, represented by locality B in the Peltier Formation. Magma originating from a point source was transported through the edifice using dykes and sills as conduits and was extruded as pillowed flows in deep water. (B) Continued effusive volcanism of a seamount in shallower water is represented by locality A. Disorganized pillow breccia and hyaloclastite accumulated on the medial portions of the seamount. Interstratified shale units indicate periods of volcanic quiescence. During deposition of massive flows, local andesitic-dacitic eruptions occurred, depositing bedded tuffs.

The increase in vesicularity (0-27%) with respect to locality B (0-5%) suggests that the pillowed and massive flows, pillow breccia, and hyaloclastite at locality A were deposited in water <500-800 m deep, but no shallower than 200 m based on the presence of non-stratified pillow breccia and interstratified shale, indicating a setting below wave base (Figure 40b).

3.6   Geodynamic Setting

Any model for the tectonic setting and evolution of the Point Lake Group must account for the fundamental stratigraphic, physical, and geochemical characteristics of the sequence, including: 1) the ascent of magma through continental crust, 2) contemporaneous subaqueous volcanism and extensive turbiditic sedimentation, 3) formation of predominantly effusive mafic flows associated with minor andesite flows and volcaniclastic material, 4) development of magmas displaying flat REE to LREE enriched patterns, with additional sources at varying depths accounting for calc-alkaline and alkalic magmas, and 5) penecontemporaneous deposition of the andesitic to rhyolitic volcaniclastic rocks that constitute one-quarter of the study area.

Ti and Zr values from Groups 1 and 2 are consistent with MORB-type rocks, from Group 3 with volcanic arc rocks, and from subgroup 4b dykes with within-plate basalts (c.f. Pearce, 1982). The latter dykes cut mafic flows in the Peltier Formation and are interpreted to have intruded the continental crust following cessation of all Point Lake belt-related (2.67-2.69 Ga) volcanic activity. Although Group 3 samples resemble arc rocks, the possibility of the volcanic succession representing an actual arc is discounted because there is a lack of abundant pyroclastic rocks of calc-alkaline composition that normally characterize arcs, and the thick interstratified turbiditic succession at Point Lake is atypical of an arc; this type of sedimentary deposit is more common in the fore-arc,

intra-arc, or back-arc regions or in the submarine trench (Mitchell and Reading, 1971; Klein, 1985). Similarly, thick turbidite sequences are not essential components of oceanic plateaus (Floyd, 1989; Storey et al., 1991). High MgO values (Storey et al., 1991), associations between tholeiitic, komatiitic and related ultramafic rocks (Storey et al., 1991; Abbott, 1996; Polat et al., 1998), flat to depleted LREE abundances (Floyd, 1989; Richards et al., 1991), and ocean island basalt compositions (Richards et al., 1991) characteristic of oceanic plateaus are not consistent with the tholeiitic-calc-alkaline compositions, low MgO values (<9 wt.%) for Groups 1 and 2, slightly LREE enriched patterns, and Nb and Ti depletions produced by the Peltier Formation samples.

The geochemistry, volcanology, and stratigraphic relationships of the Peltier Formation are consistent with deposition in a continental back-arc setting (Northrup et al., 1999). The seamount interpretation (Corcoran, 2000) is consistent with development in a rift-related setting, either at a mid-oceanic, back-arc, intra-arc, or fore-arc location. Geochemically, Groups 1 and 2, and subgroup 4a, with basalts transitional from N- to EMORB, Al_2O_3 roughly between 13-17% and MgO from 5-9%, resemble mid-oceanic or back-arc tholeiites, but the close spatial association with Group 3 calc-alkaline basalts precludes a mid-oceanic origin (e.g. Saunders and Tarney, 1984). Combinations of convergent- and rift-related rocks commonly characterize back-arc settings (Arculus, 1987). Interstratified turbiditic deposits commonly form in back-arc settings during the early to intermediate stages of opening (Klein, 1985), and although they generally contain abundant lithic fragments derived from erosion of the volcanic arc, those settings associated with deep dissection of continental material can also be rich in quartz (Condie, 1989). Ensialic basins are typically filled with thick turbiditic deposits derived from both the arc and the continent (Tarney and Windley, 1981).

A possible tectonic interpretation for the evolution of the Point Lake belt (Figure 41) involves pre-2.7 Ga accretion of an arc succession onto older continental crust
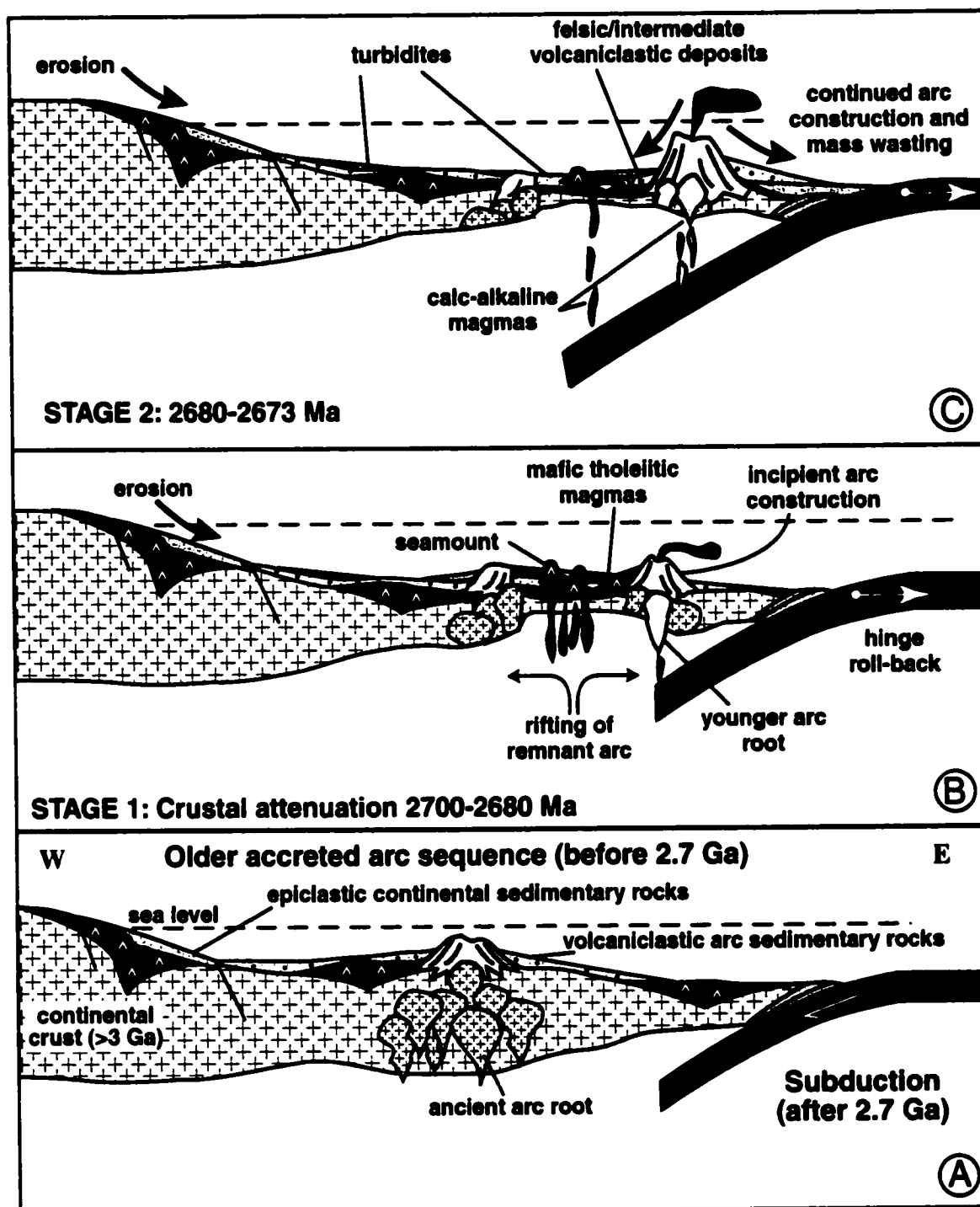
Figure 41: Schematic model illustrating Point Lake belt evolution. (A) Prior to 2.7 Ga, a volcano-sedimentary arc sequence was accreted onto >3.0 Ga continental crust. Following 2.7 Ga, subduction ensued. (B) Crustal attenuation and rifting of the early remnant arc of the crustal segment between 2700-2680 Ma, was propagated by hinge roll-back. A new arc was constructed and mafic tholeiitic magmas were erupted into the back-arc. Continental crust was eroded, material was transported by turbidity currents and was interstratified with the volcanic pile. (C) Eruption of calc-alkaline magmas through the tholeiitic sequence occurred from 2680-2673 Ma. Mass wasting of the arc led to deposition of felsic-intermediate volcaniclastic material.

represented by the 3.15-3.22 Ga Augustus granite (Figure 41a). At the eastern margin of

the continent, a subduction zone developed after 2.7 Ga (Figure 41b). Subsequently, a

younger arc-back-arc succession developed, of which the Point Lake belt is one small

subduction zone remnant. Crustal attenuation occurred between 2.7-2.68 Ga. This

extension and thinning could be attributed to injection of a diapir originating from the

downgoing slab, or convection in the mantle wedge resulting from subduction of cold

lithosphere (Moores and Twiss, 1995), or due to hinge roll-back of the subducting slab

(Hamilton, 1995). Discerning the extensional mechanism in ancient sequences is

problematic and for the sake of simplicity, hinge roll-back is the mechanism considered

for back-arc extension in the Slave Province (Figure 41b). Rifting of the older remnant

arc on the crustal segment and construction of a new, <2.7 Ga arc above the down-going

slab, resulted in the formation of a back-arc basin overlying thinned continental crust.

Mafic tholeiitic magmas, represented by Groups 1 and 2 and subgroup 4a, were erupted

through the sialic crust into the back-arc, forming an ocean floor with scattered

seamounts (Figure 41b). Some Group 2 magmas coated the walls of the plumbing system

so that penecontemporaneous magmas were insulated from the effects of crustal

contamination. Continued erosion of the continent to the west produced sedimentary

debris that was transported mainly by turbidity currents and deposited during

emplacement of the back-arc volcanic pile. These turbidites are represented by the

interstratified Contwoyto Formation. With continued subduction, the arc increased in size

and underwent extensive construction and mass wasting between 2.68-2.66 Ma, resulting

in the accumulation of felsic and intermediate volcaniclastic deposits, represented by the

Samandré and Beauparlant formations (Figure 41c). The tholeiitic rocks in the back-arc,

directly overlying the subduction zone at this stage, were intruded by calc-alkaline

magmas derived from deeper mantle levels, represented by Peltier Formation Group 3

calc-alkaline basalts and andesites (Figure 41c). The active arc probably never breached

the water surface, accounting for the paucity of felsic pyroclastic material in the study

area.

Summary

The physical volcanology and geochemistry of the Point Lake volcanic belt is

consistent with seamount construction in an ancient back-arc basin overlying continental

crust. The most significant results determined from the Point Lake belt study area are

illustrated in Table 5. The volcanic facies types and architecture are typical of

subaqueous, mafic-dominated edifices (seamounts). Geochemically, four groups of rocks

comprise the mafic-dominated Peltier Formation, represented by ca. 2.69 Ga tholeiitic,

N- and EMORB basalt dykes, sills, and flows, and ca. 2.67 Ga calc-alkaline basalt and

andesite flows. Marginally younger, ca. 2.68 Ga felsic and intermediate, calc-alkaline

volcaniclastic rocks of the Samandre and Beauparlant formations cap the volcanic

sequence. Extensive turbiditic deposits, represented by the Contwoyto Formation, are

interstratified with the volcanic rocks. Negative ϵ_{Nd} values produced by some of the

EMORB (Group 2) samples are best explained by crustal contamination. Positive values

for more NMORB-type flows and intrusions (Group 1, subgroup 4a) and calc-alkaline

flows (Group 3) are consistent with emplacement through insulated continental crust,

whereby earlier magmas coated the interior walls of the conduits.

The stratigraphy, geochemistry, and geochronology of the Point Lake belt indicate

development of a continental back-arc basin, in support of the results of Northrup et al.

(1999). 1) Prior to 2.7 Ga, an old arc succession accreted onto significantly older

continental crust. 2) Subduction and new arc construction began after 2.7 Ga. With hinge

roll-back, the crust became attenuated between 2700-2680 Ma, rifting the older remnant

arc on the crustal segment, producing a back-arc through which tholeiitic magmas were

Calc-alkaline rhyodacitic tuff, 68% SiO_2, FeO*/MgO ratio of 4.5, $(La/Yb)_n$ ratio of 5.7, strong Nb and Ti depletions relative to the REE.

Formation	Depositional setting	Chemical compositon	Geochemistry	Crustal contamination	Tectonic setting
Keskarrah Formation (2600 Ma)					
Feldspar Porphyry (2650 Ma)					
Contwoyto Formation	Locality A represents the medial to distal portions of a seamount under moderate water depth, as indicated by abundant pillow breccia, hyaloclastite (peperite), thin pillowed and massive flows, moderate vesicularity, and interbedded shale and felsic tuff. Locality B represents the proximal, deep water portion of a seamount where pillowed flows are thick and non-vesicular, pillow breccia and hyaloclastite are minimal, and intrusions with multiple chilled margins are abundant.	Groups 1 and 2: tholeiitic basalt flows; Group 3: calc-alkaline volcaniclastic basalts and andesites; Group 4a: tholeiitic basalt intrusions; Group 4b: younger unrelated subalkaline intrusions	Group 1: SiO_2 from 45-53 wt%, FeO*/MgO ratios of 1.3-5, $(La/Yb)_n$ ratios of .88-1.13, small Zr enrichments and some Nb depletions relative to the REE, ϵNd values from +0.2 to +2.23. Group 2: SiO_2 from 45-53 wt%, FeO*/MgO ratios of 1.5-4.4, $(La/Yb)_n$ ratios of 1.13-4.34, some Ti and Nb depletions relative to the REE, ϵNd values from -2.94 to +2.23. Group 3: SiO_2 from 47-59 wt%, FeO*/MgO ratios of 0.9-1.8, $(La/Yb)_n$ ratios of 22.12-25.38, strong depletions in Nb and Ti relative to REE. ϵNd values of +2.15 and +2.41. Group 4a: SiO_2 from 45-46 wt%, FeO*/MgO ratios of 1.2-2.3, $(La/Yb)_n$ ratios of .71-1.14, some slight Ti and Nb depletions relative to the REE, ϵNd value of +3.06. Group 4b: SiO_2 from 46-51 wt%, FeO*/MgO ratios of 1-3.2, $(La/Yb)_n$ ratio of 4.58, depleted in Nb and Sm relative to the REE.	As indicated by negative ϵNd values, Nb depletions, and the unconformity between the Augustus granite and turbiditic Contwoyto Formation, which is interstratified with the volcanic belt.	Continental back-arc. Mafic tholeiitic magmas (Groups 1, 2, 4a) erupted through sialic crust into a back-arc, forming an ocean floor with scattered seamounts. Conduit walls were insulated by Group 2 magmas, limiting the effects of crustal contamination on other Groups. Erosion of the continent and arc resulted in deposition of turbiditic and felsic volcaniclastic deposits, represented by the Contwoyto, Samandre and Beauparlant Formations. Calc-alkaline magmas (Group 3) from deeper mantle levels were later erupted through the tholeiitic pile.
Beauparlant Formation (2683 Ma)					
Samandre Formation					
Peltier Formation (2690-2673 Ma)					
Augustus Granite (3.22 Ga)					

Table 5: Summary reviewing the main volcanological and geochemical characteristics of the Peltier Formation, Point Lake belt.

emplaced. 3) As subduction continued between 2680-2673 Ma, calc-alkaline magmas were erupted through the tholeiitic pile, and the active arc underwent mass wasting to deposit felsic-intermediate volcaniclastic material. The continental crust was continuously eroded throughout Point Lake belt development, resulting in thick turbidite deposits interstratified with the volcanic sequence.

Chapter 4

NORTHERN BEAULIEU RIVER BELT

4.1   Physical Volcanology

4.1.1   Introduction

The northern part of the Beaulieu River volcanic belt is characterized by massive mafic flows (35%), mafic intrusions (25%), pillowed flows (15%), and felsic flows and volcaniclastic rocks (25%). Outcrop exposure is sporadic due to abundant glacial cover deposits, so that most contacts between volcanic, sedimentary, plutonic, and ultramafic rocks are inferred (Figure 17 in Chapter 2). Two representative localities with good exposure, C and D, were chosen for detailed study in the Beniah Lake area (Figure 42). Locality C, situated approximately 4.5 km southwest of the camp contains 15-60 m-thick mafic massive and pillowed flow sequences, that are locally interstratified with thin felsic volcaniclastic units. Locality D, approximately 5 km southwest of the camp (Figure 17 in Chapter 2), features a 65 m-thick transition from felsic lapilli tuffs to pillowed flows. Structural deformation at Beniah Lake is complex and with the sparse outcrop exposure, a true thickness of the belt could not be determined. Notwithstanding, an apparent homoclinal sequence, based on pillow younging, just west of localities C and D, places a maximum thickness of the belt at approximately 3 km. Outcrop maps at scales of 1:25 and 1:1000 were drawn to identify volcanic structures and determine lateral and vertical facies variations. The rocks have undergone greenschist facies metamorphism, as indicated by the mineral assemblage of green amphibole + albite + chlorite ± carbonate, but the prefix "meta" is omitted for simplicity.
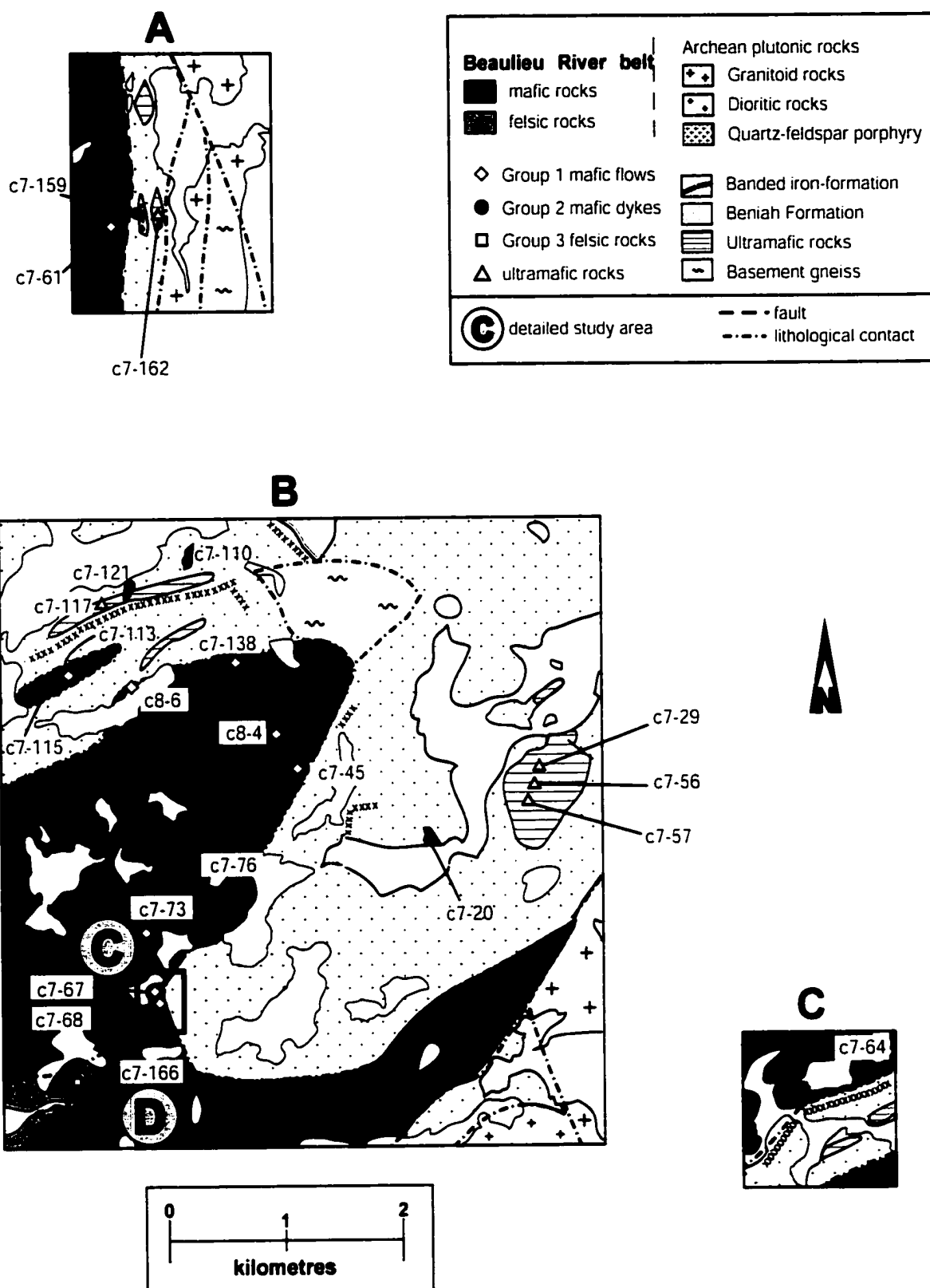
Figure 42: Locations of samples selected for geochemistry in the Northern Beaulieu River belt. For locations of A, B, and C, see Figure 17.

4.2   Mafic Volcanic Facies

4.2.1   Massive Flows

Massive flows are the most abundant volcanic facies in the Beniah Lake area. Individual flows at locality C are 10-15 m thick and locally become pillowed vertically and laterally (Figures 43, 44). Difficulties in recognizing flow transformations arise in areas where the mafic rocks were structurally interleaved with older quartz arenite (Figure 43). Individual flow margins are marked by cherty or felsic tuff horizons (Figure 44) and some flows have polygonal fracture patterns that resemble columnar jointing (Figures 44, 45a). Vesicles are uncommon in massive flows, with <5% vesicularity in the samples collected, but increased vesicularity is locally evident at flow bases (Figure 44; flow I). The majority of massive flows display granular textures, and chlorite and actinolite have in most cases obliterated the original mineralogy (Appendix 4).

Interpretation

The predominance of massive flows in the Northern Beaulieu River belt is consistent with relatively high effusion rates and temperatures, and indicate that the substrates on which the lava erupted may have been steeper than those on which pillowed flows are normally emplaced (Yamagishi, 1991; Batiza and White, 2000). Vertical and lateral flow transformations from massive to pillowed result from decreasing flow rate, which is directly related to variations in temperature and viscosity (Griffiths and Fink, 1992). The local concentration of vesicles and amygdules at flow bases and tops is consistent with the process described by Sahagian (1985) and cited in section 3.2.1.
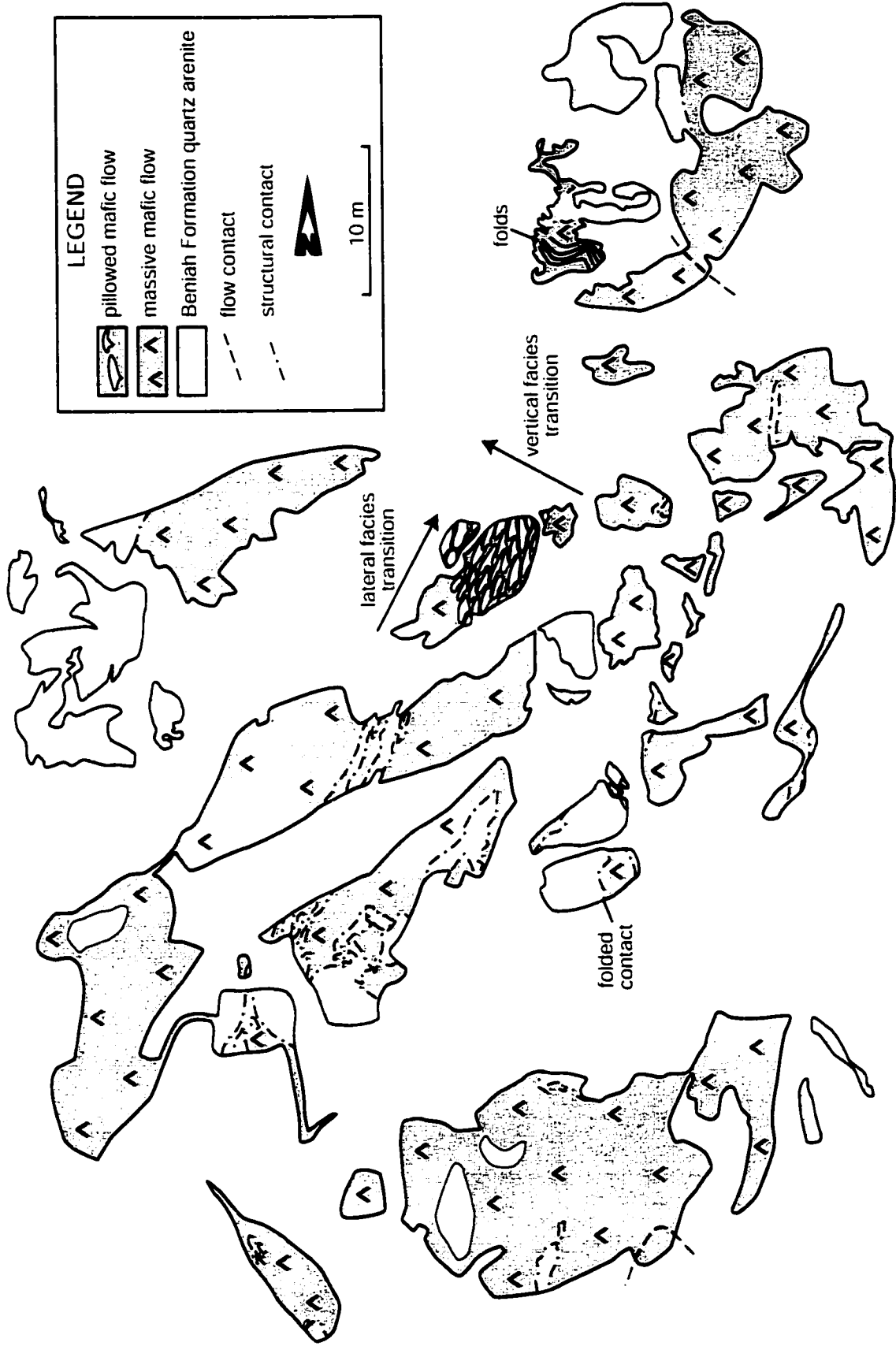
Figure 43: Mafic volcanic flows structurally interleaved with Beniah Formation quartz arenite at locality C, NBRB. Note the lateral and vertical flow changes from massive to pillowed. Outcrop is approximately 60 m east of outcrop in Figure 44.
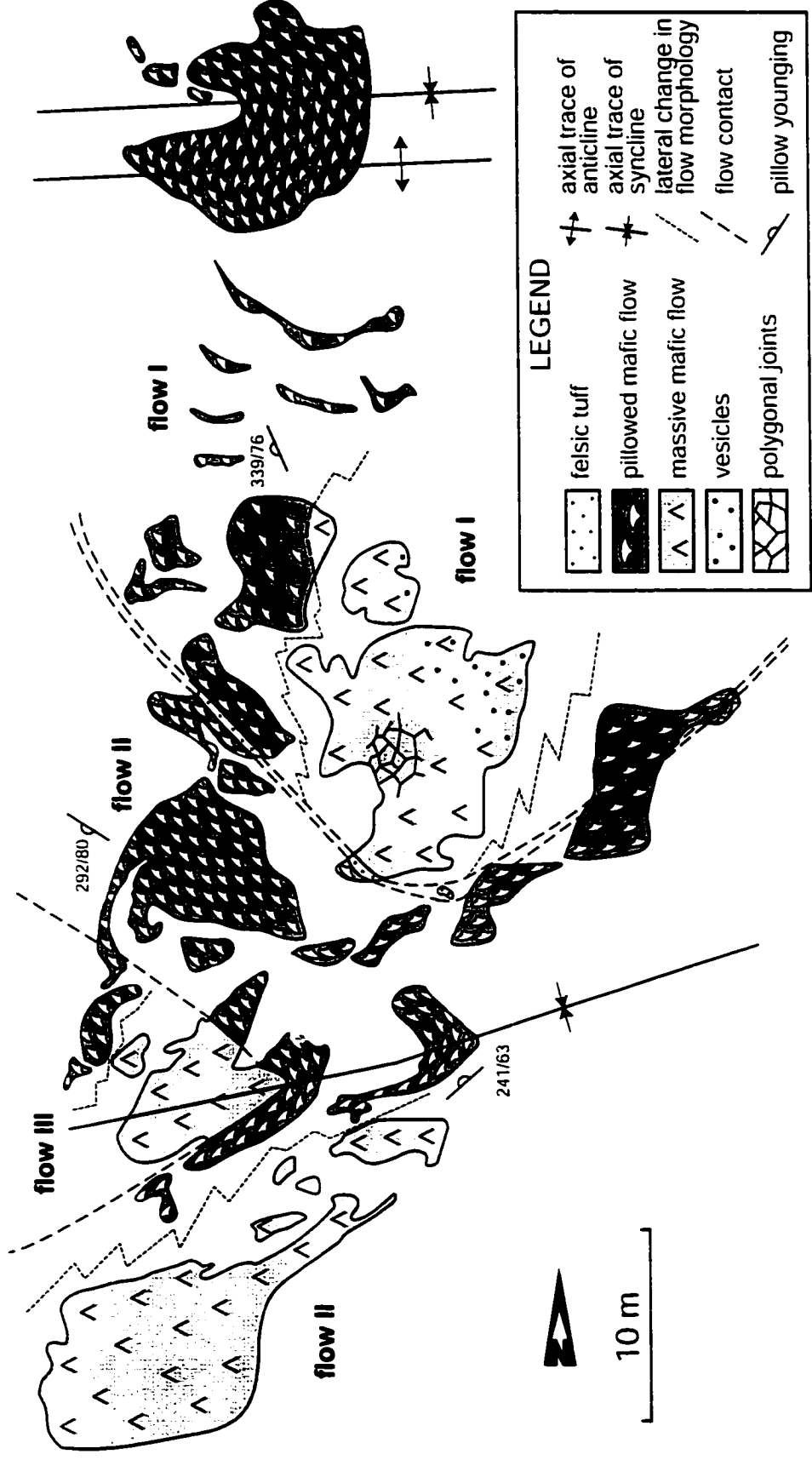
Figure 44: Mafic and felsic volcanic facies at locality C, NBRB. Note the lateral changes in flow morphology from massive to pillowed and how flow I and III are separated by a thin felsic tuff horizon. Outcrop is approximately 60 m west of outcrop in Figure 43.

Figure 45b: Pillowed flow with chloritized interstices (C) between pillows, NBRB. Arrow points to top. Scale, pencil 14 cm.

Figure 45a: Polygonal jointing (J) in massive flow I, NBRB (see Figure 44). Scale, lens cap 5.5 cm.
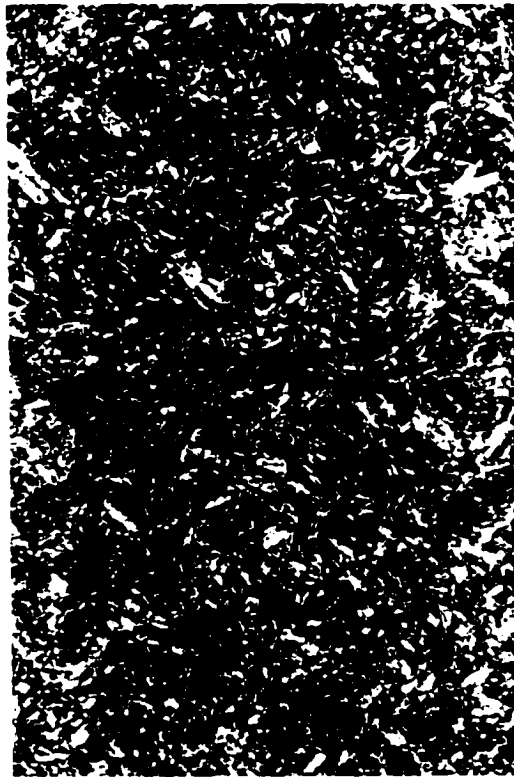
Figure 45c: Pillowed flow with intersertal texture (laths of plagioclase surrounded by dark pools of recrystallized glass) from the NBRB. Field of view is 6 mm. Thin section in xpl.

4.2.2 Pillowed Flows

Pillowed flows at locality C, 4-13 m thick, change vertically and laterally from massive flows (Figures 43, 44), and individual pillowed flows are locally separated by felsic tuff horizons (Figure 43). Transitions into pillow breccia were nowhere identified in the Northern Beaulieu River belt study area. Pillows, 0.1-1.5 m in size, are closely-packed to isolated and are commonly surrounded by chloritized hyaloclastite (Figure 45b). Isolated pillow rinds, up to 1 m long, are also common (Figure 46). Vesicles and amygdules appear to be minimal (<5%) in pillowed flows, although intense quartz-feldspar recrystallization and chlorite alteration may have masked the initial vesicularity. Pillowed flows have intersertal textures with actinolite and plagioclase in ophitic intergrowth surrounded by recrystallized, chloritized glass (Figure 45c; Appendix 4). Hyalopilitic texture is also common and some flows are aphanitic with randomly oriented plagioclase microlites. Locally, pillows contain up to 5 mm-long metamorphic actinolite porphyroblasts (Appendix 4).

Interpretation

Interstratification of pillowed flows and felsic tuff at locality C indicates that mafic and felsic volcanism was contemporaneous. Closely-packed pillows are consistent with decreasing temperature and viscosity relative to massive and lobate flows (Dimroth et al., 1978). Isolated pillows are attributed to rapid cooling and/or rapid burial by subsequent lava flows (e.g. Dimroth et al., 1978; Busby-Spera, 1987), whereas isolated pillow rinds may indicate the presence of lava tubes (e.g. Busby-Spera, 1987). The paucity of pillow breccia and hyaloclastite, which are commonly associated with pillowed flows (see Chapters 3 and 5), is consistent with a proximal setting with respect to the feeding vent or fissure (e.g. Dimroth et al., 1978, Easton 1984; Schmidt and Schmincke, 2000).
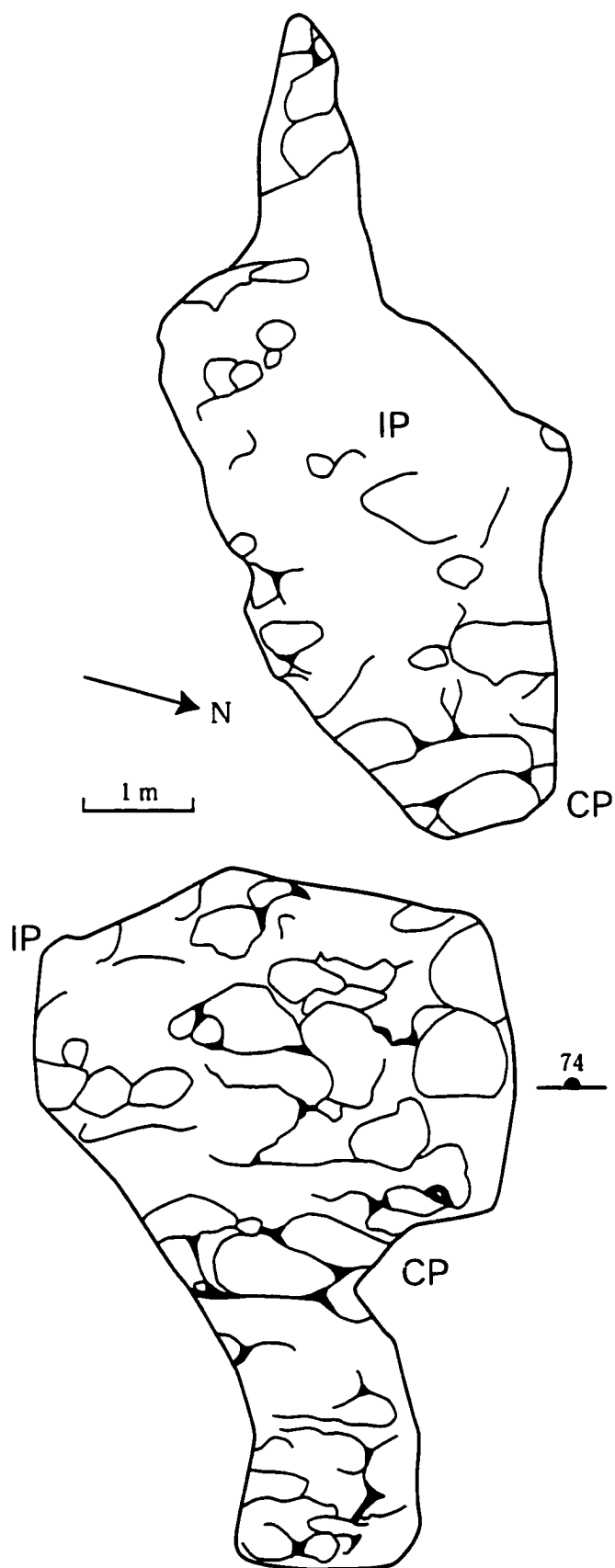
Figure 46: Example of a pillowed flow in the Northern Beaulieu River belt. Note the presence of closely-packed pillows (CP) and more isolated (IP) varieties.

4.2.3 Dykes and Sills

Distinguishing between mafic intrusions and massive flows in the field was problematic because most contacts between intrusions and other volcanic facies were irregular or unexposed. Several sharp dyke contacts were identified with the older dunite and quartz arenite (Figure 47a). The dykes are parallel, generally north-trending, and range from 3-20 m in width. These intrusions contain structural deformation features similar to those preserved in the massive and pillowed flows, suggesting that the intrusions pre-date deformation, similar to the flows. In addition, younger sedimentary breccia (interpreted as ca. 2.6 Ga) preserved along the Beniah fault zone west of Beniah Lake, was deposited unconformably on a mafic dyke, as indicated by an erosional contact. The intrusions are ophitic and subophitic with feldspar partially enveloped by actinolite, which was originally pyroxene (Figure 47b; Appendix 4).

Interpretation

Numerous parallel mafic dykes throughout the study area are consistent with crustal spreading in zones of extension over hot spots, mid-ocean ridges and back-arc basins (Carey and Sigurdsson, 1984; Forslund and Gudmundsson, 1991; Lambert et al., 1992). Abundant dyke intrusions associated with predominant massive flows suggest a proximal setting with respect to the fissure or vent (e.g. Easton, 1984; Schmidt and Schmincke, 2000) and also may indicate open-ocean spreading systems (Batiza and White, 2000). These dykes are commonly considered feeders to the overlying basaltic pile (e.g. Easton, 1984; Lambert et al., 1992).
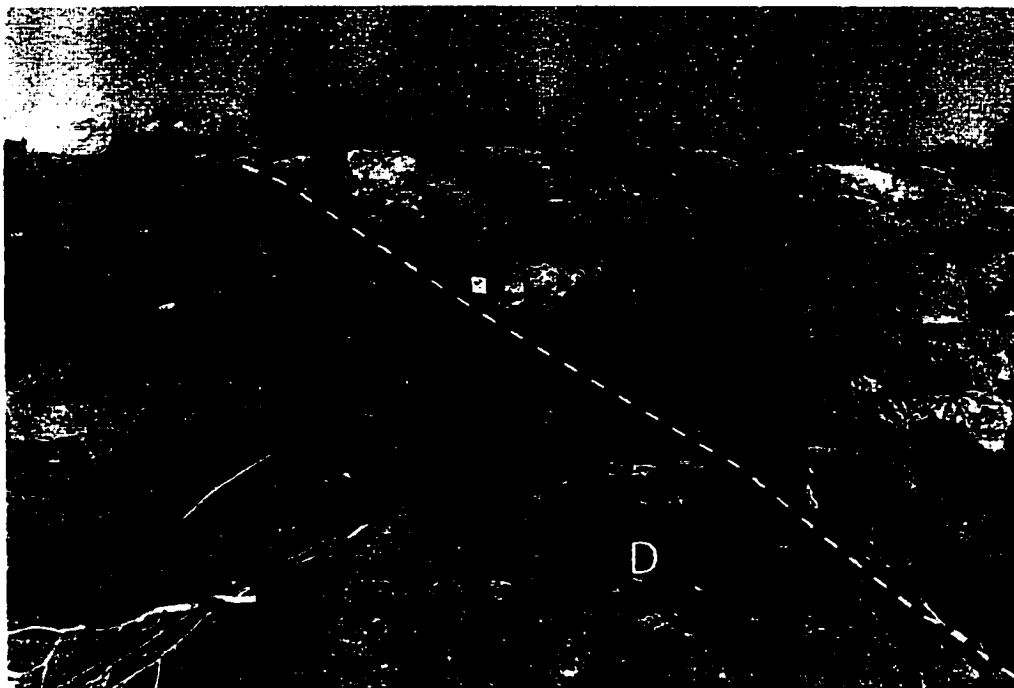
Figure 47a: Mafic dyke (D) cutting the Beniah Formation quartz arenite (Qa), NBRB. Contact is marked by the dashed line. Scale, fieldbook 17.5 cm.
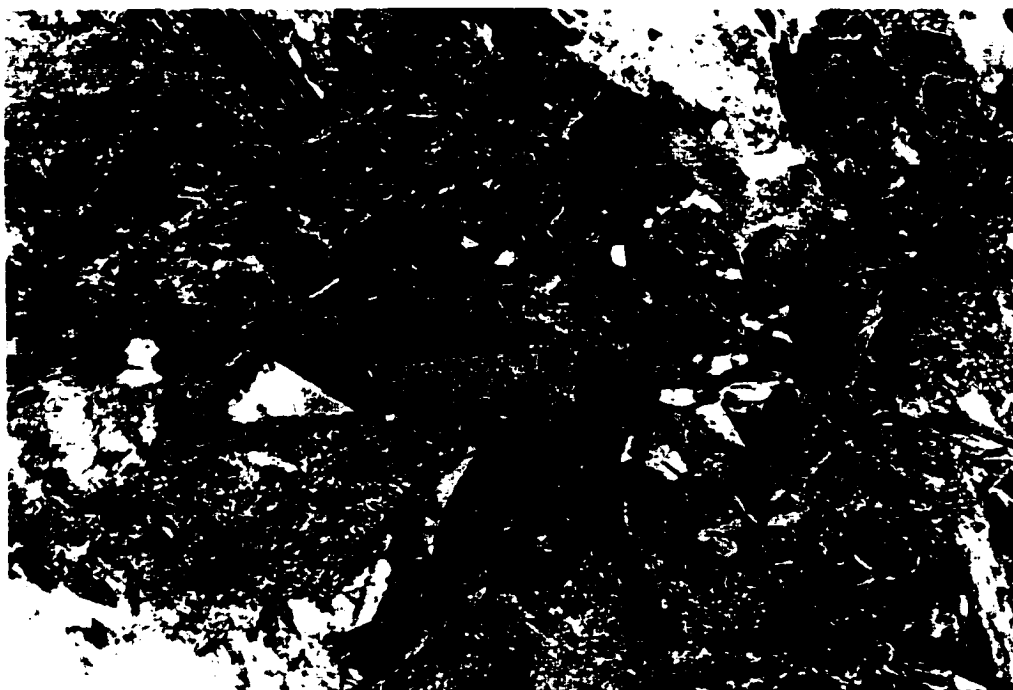
Figure 47b: Ophitic texture in a mafic dyke from the NBRB. Field of view is 6 mm. Thin section in xpl.

4.3   Felsic Volcanic Facies

4.3.1   Volcaniclastic Rocks

Felsic volcaniclastic rocks in the Northern Beaulieu River belt are represented by planar- and cross-bedded coarse and fine lapilli tuff, tabular and low-angle to wavy bedded coarse tuff, and planar laminated fine tuff (Figure 48a). At locality D, stratified tuff is erosionally overlain by planar- and cross-bedded coarse lapilli tuff (Figure 48b). Planar bedding in coarse lapilli tuff is represented by parallel beds along which subangular to subrounded, felsic fragments or weathered-out fragments, 0.5-8 cm in size, are aligned (Figure 49a). Bedsets of planar- and cross-bedded coarse lapilli tuff are 10-75 cm-thick and are separated by 2-8 cm-thick beds of fine tuff. The fining-upward transition from coarse lapilli tuff-fine lapilli tuff-coarse tuff-fine tuff is gradational over 0.5 m (Figure 49b) and occurs in 4-6 cm, small-scale fining-upward sequences (Figures 48b, 50a). Massive beds of coarse tuff, 20-100 cm thick, overlie the fining-upward sequences and contain visible felsic lithic fragments, <2 mm in size (Figure 50b). Massive beds are overlain by wavy and low-angle composite bedforms, 0.6-1.9 m thick (Figure 51) and tabular beds, 15-35 cm thick, with planar, low-angle and wavy laminae (Figure 52a). Mudstone laminae are common between bedforms (Figure 52b). Up-section, 5-16 cm long lenses of black fine tuff are intercalated with planar-bedded fine tuff (Figures 48a, 53a). Black fine tuff horizons, 0.2-1.5 m thick and containing thin parallel laminae (Figure 53b, c), become more common towards the contact with an overlying pillowed flow. The contact is irregular and gradational with intermingling of mafic and black tuffaceous material (Figure 54a, b).

An additional felsic facies in the Northern Beaulieu River belt is buff white felsic tuffaceous (cherty) horizons commonly interstratified with mafic volcanic flows (Figure
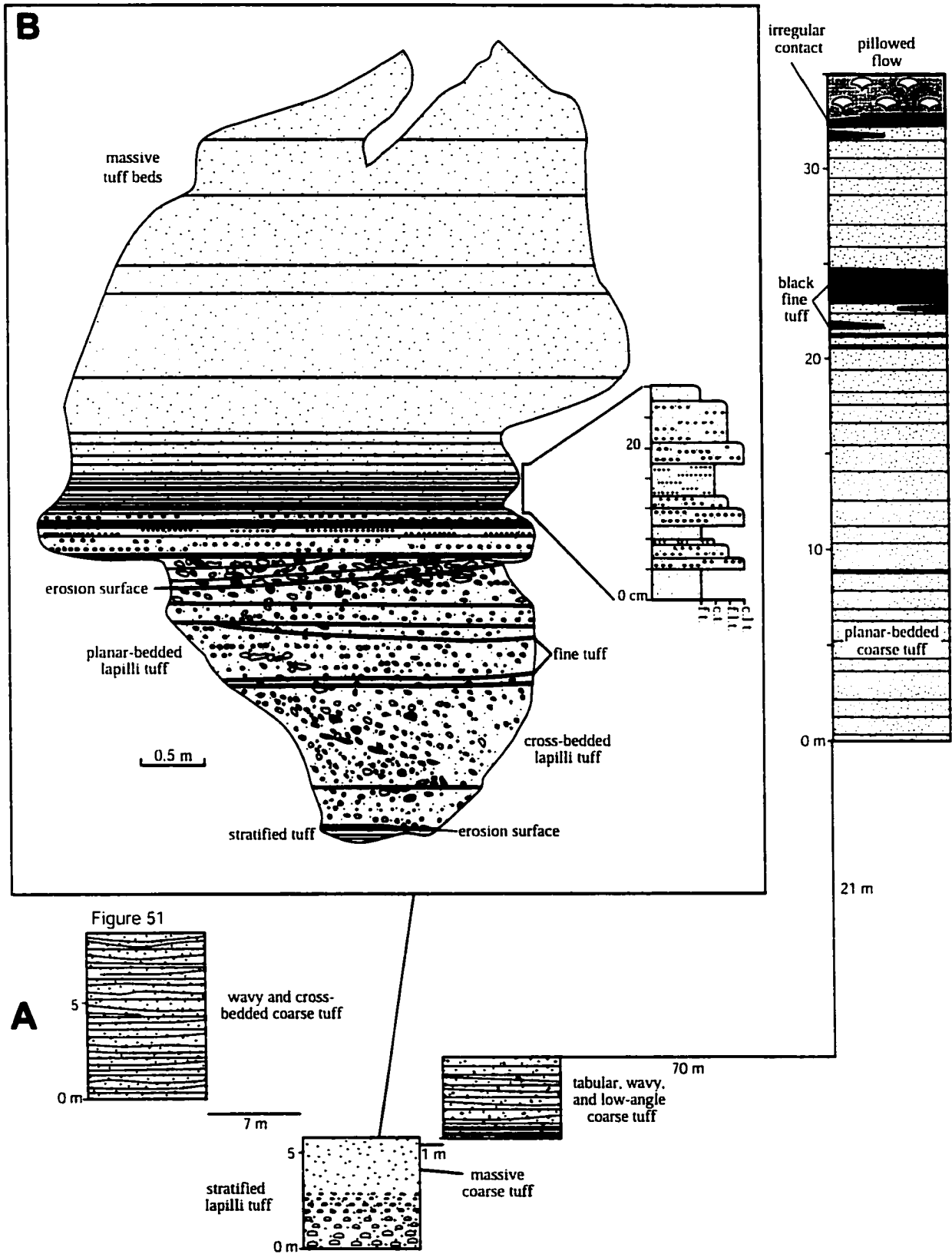
Figure 48: Felsic volcaniclastic facies at locality D, NBRB. (A) Stratigraphic section through the felsic facies. (B) Close-up of second section in A. Location of Figure 51 is indicated. f.t.: fine tuff, c.t.: coarse tuff, f.l.t.: fine lapilli tuff, c.l.t.: coarse lapilli tuff.
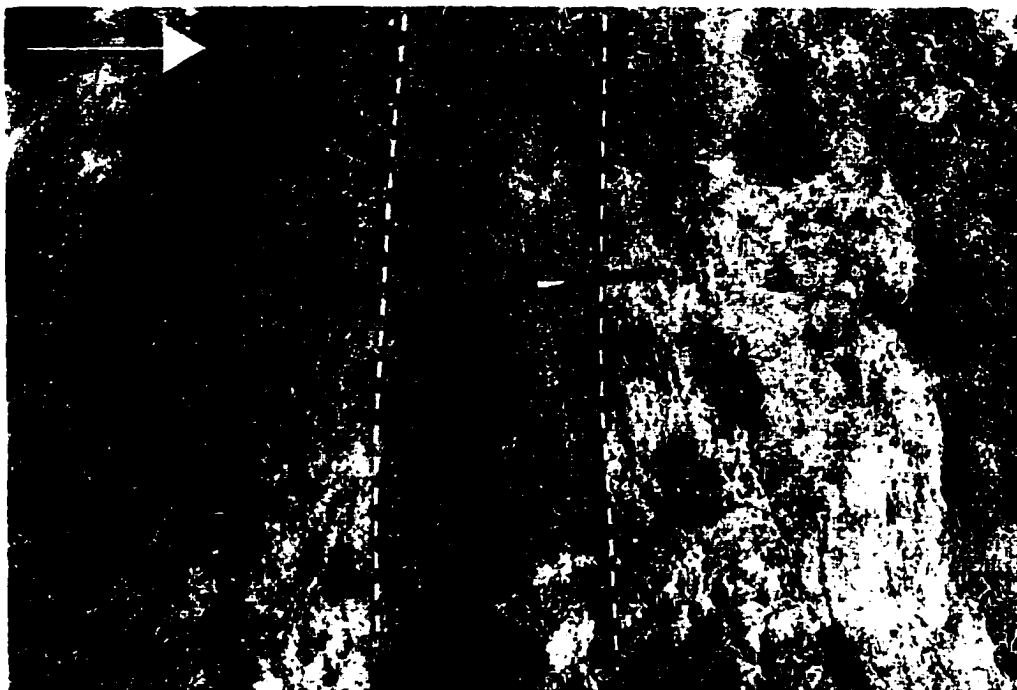
Figure 49a: Stratified felsic lapilli tuff (dashed lines) at locality D, NBRB (see Figure 48b). Arrow points to top. Scale, pencil 14 cm.
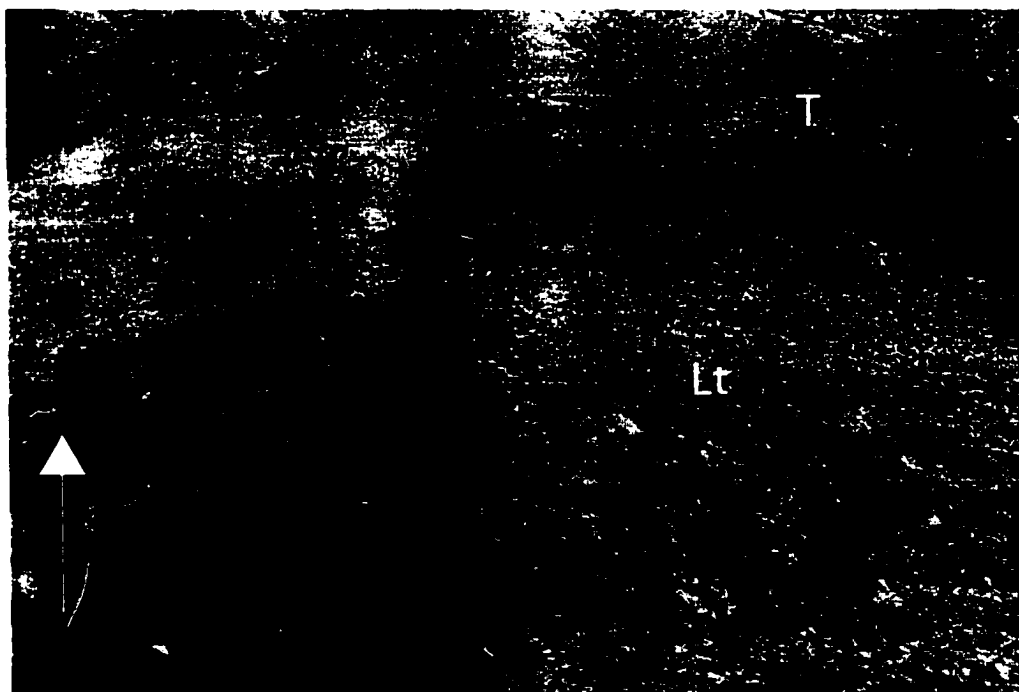
Figure 49b: Upward transition from stratified lapilli tuff (Lt) to stratified coarse tuff (T) at locality D, NBRB (see Figure 48b). Arrow points to top. Scale, pencil 14 cm.
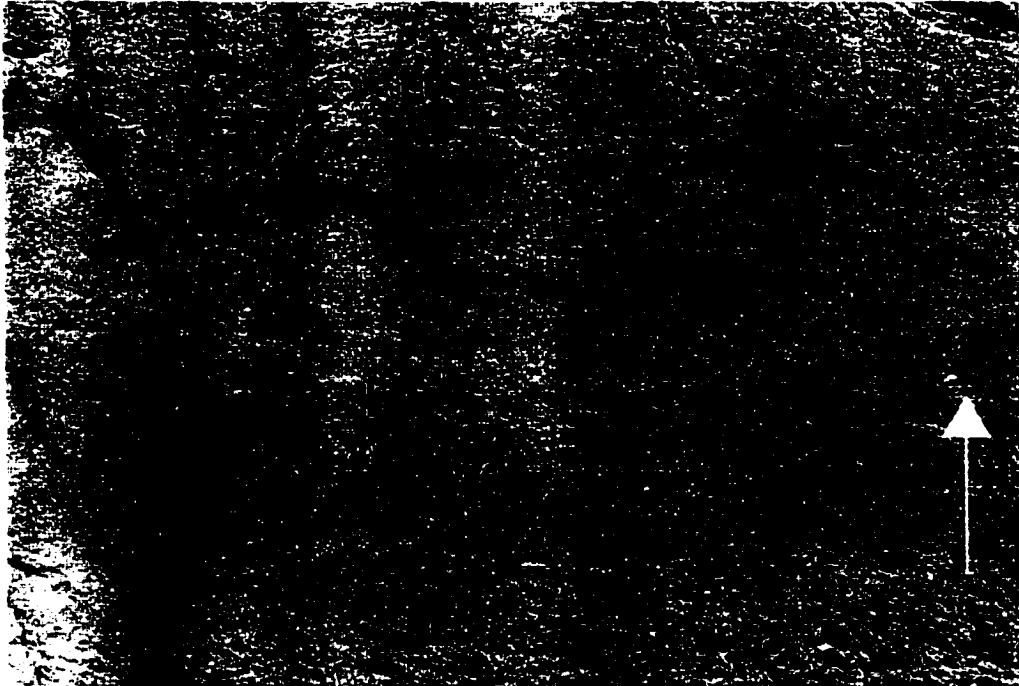
Figure 50a: A small-scale sequence of fine lapilli tuff (Lt), fine tuff (Tf), fine lapilli tuff, coarse tuff (Tc) and fine lapilli tuff beds at locality D, NBRB (see Figure 48). Arrow points to top. Scale, pencil 8 cm.
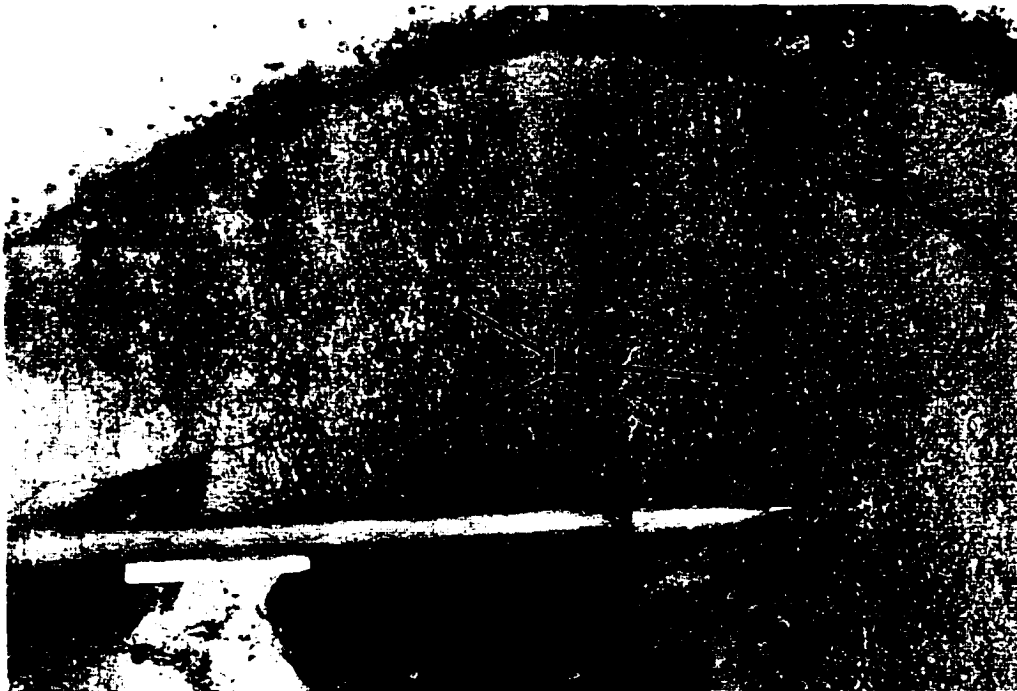
Figure 50b: Close-up of a massive felsic tuff bed at locality D, NBRB (see Figure 48b). Note the mm-size lithic fragments (Lf). Scale, pencil 14 cm.
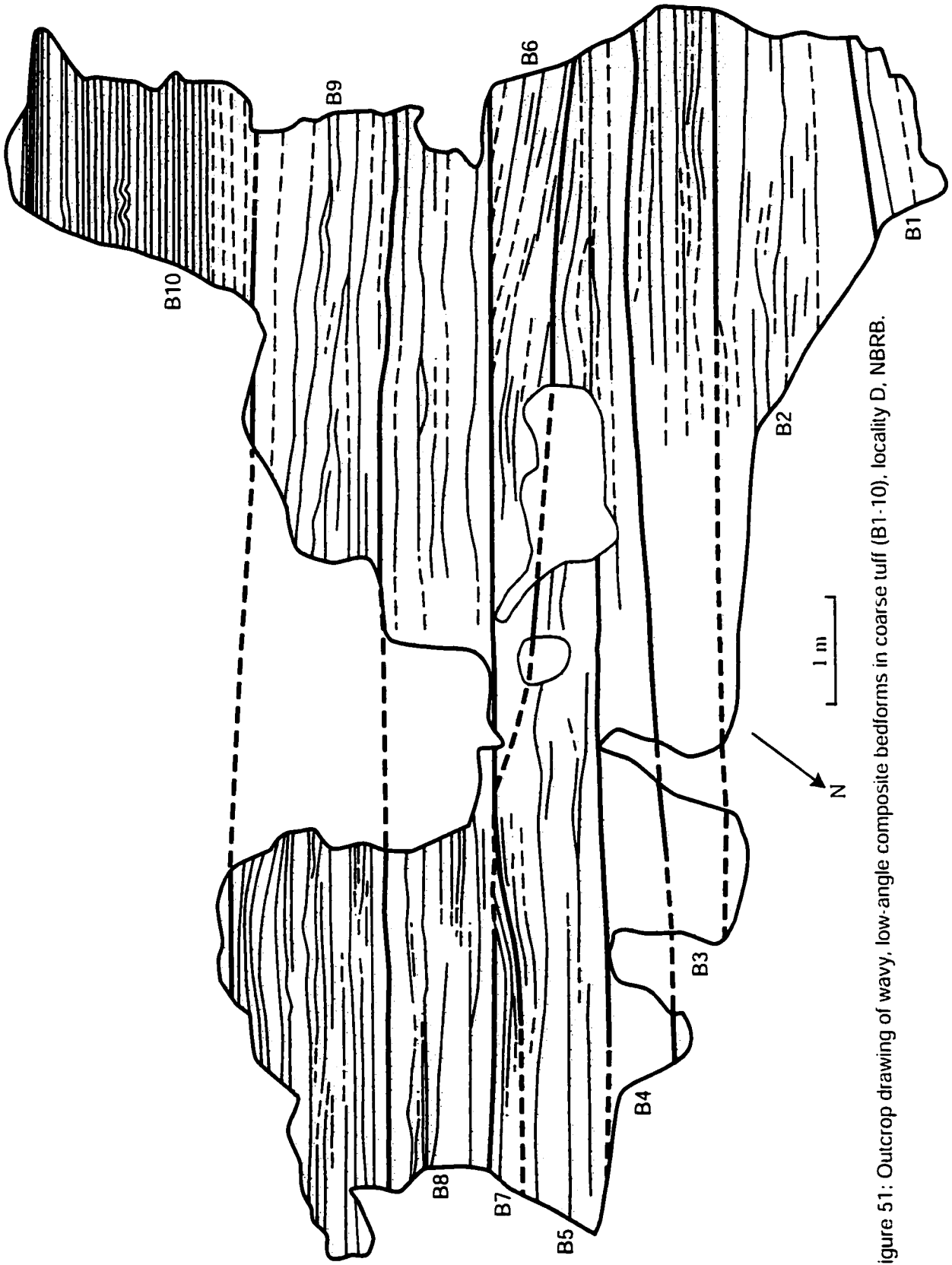
Figure 51: Outcrop drawing of wavy, low-angle composite bedforms in coarse tuff (B1-10), locality D. NBRB.

Figure 52a: Tabular bedforms (Tb) in coarse tuff with planar laminae (Pl) and wavy laminae (Wl) at locality D, NBRB. Arrow points to top. Scale, pencil 14 cm.
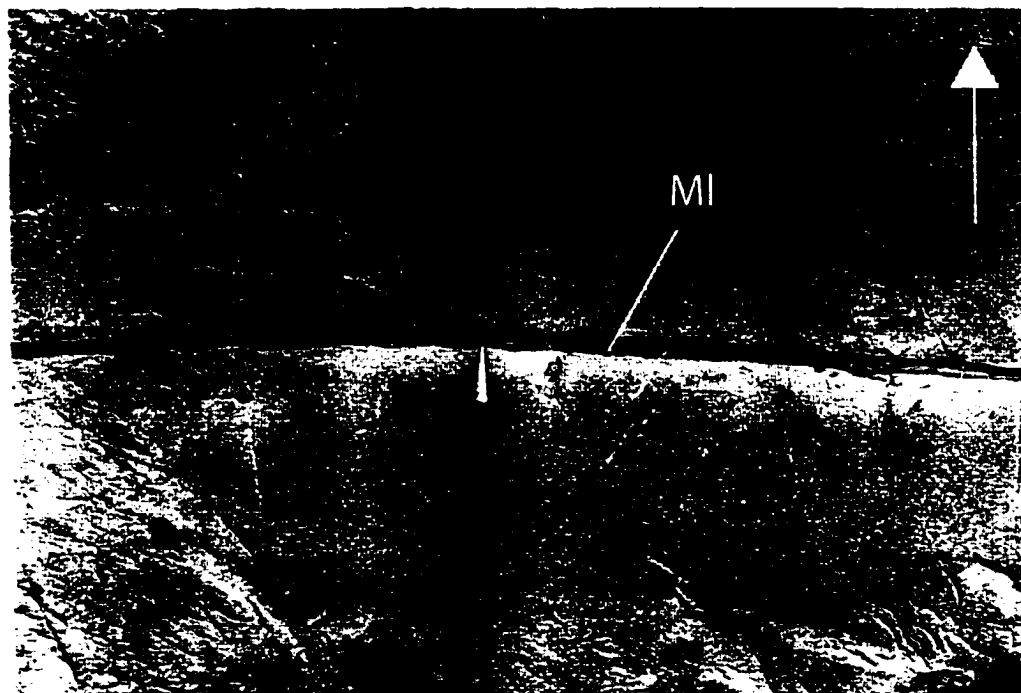
Figure 52b: Mudstone laminae (Ml) in coarse tuff at locality D, NBRB. Arrow points to top. Scale, pen, 13 cm.

Figure 53b: Black fine tuff unit 10 m below the contact between felsic tuff and mafic pillows, NBRB (see Figure 48a). Arrow points to top. Scale, pencil 10cm.

Figure 53a: Lenses of black fine tuff (Tf) in laminated coarse tuff at locality D, NBRB (see Figure 48a). Arrow points to top. Scale, pencil 14 cm.

Figure 53c: Laminae (dashed lines) in black fine tuff. Sample, 13 cm high, from locality D, NBRB.
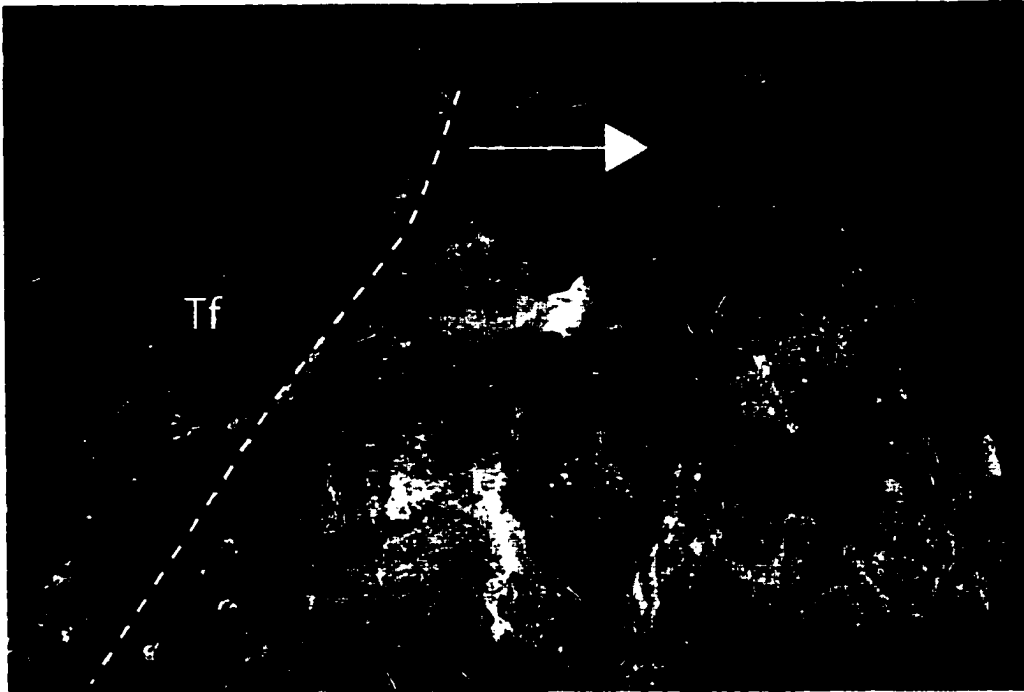
Figure 54a: Contact (dashed line) between black fine tuff (Tf) and a pillowed flow (P) at locality D, NBRB (see Figure 48a). Arrow points to top. Scale, chisel 20 cm.
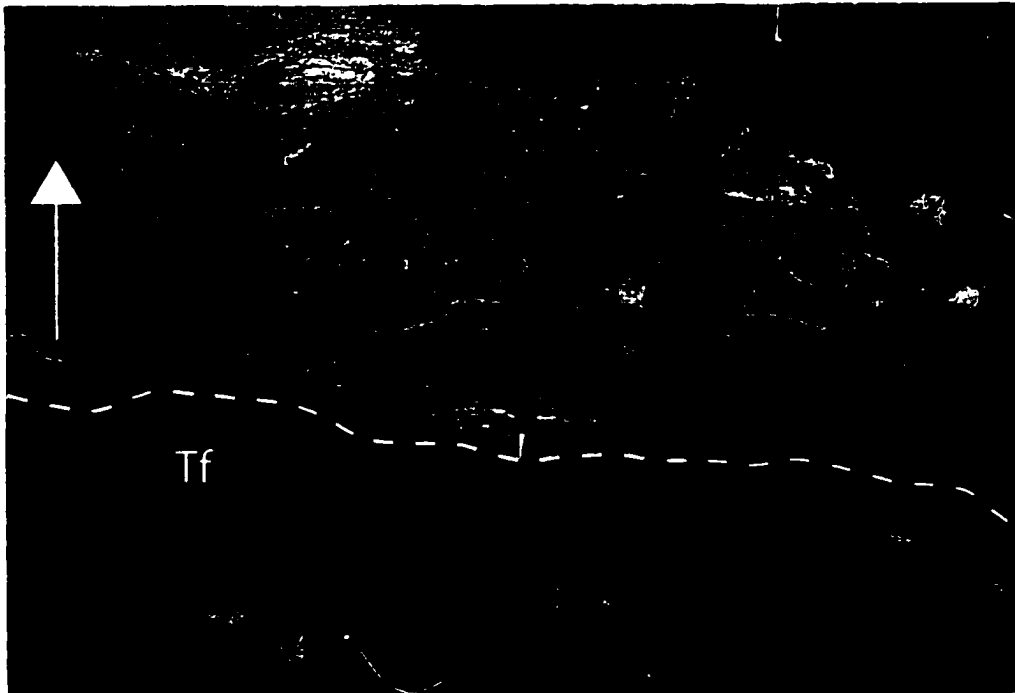
Figure 54b: Close-up of irregular contact (dashed line) between black fine tuff (Tf) and a pillowed flow (M), NBRB. Note intermingling of mafic and black tuffaceous material (gray streaks and pods in black tuff). Arrow points to top. Scale, pen 14 cm.

44). These horizons, 20-50 cm thick, are fine-grained and massive or laminated (Figure 55a) and in thin section are composed of recrystallized microcrystalline quartz (Figure 55b). The felsic tuffs at locality D, and the tuffaceous horizons interstratified with mafic flows, are vitrophyric with <0.2 mm-size monocrystalline quartz and <0.5 mm-size polycrystalline quartz and feldspar crystals, and patches of recrystallized glass (Figure 56a; Appendix 4). The glassy matrix has now been recrystallized into quartz-feldspar aggregates or displays a felty texture with interwoven randomly oriented plagioclase microlites. The lapilli are mainly subangular to subrounded felsic lithic fragments and minor subangular black tuff fragments. Black fine tuff lenses are interstratified with fine tuff upsection (Figure 56b) and contain alternating bands of fine-grained equigranular quartz and submicroscopic black material (Figure 56c; Appendix 4). The black bands are laminated on mm scale.

Interpretation

The upward transition from planar- and cross-bedded lapilli tuff to composite beds of planar-, wavy- and cross-bedded coarse tuff characterized by mudstone laminae is consistent with a shallow subaqueous setting where a combination of wave and tide influence occurs. Local cross-bedded lapilli tuff is considered the result of shoreward migration of bars on the lower shoreface under the influence of waves or during longshore and offshore drift on the upper shoreface (e.g. Bourgeois and Leithold, 1984; Hart and Plint, 1995). The fine tuff between bedforms (Figure 48b; between 2-3 m from base) is consistent with prolonged slack-water periods dominated by suspension deposition. The vertical gradation from planar- and cross-bedded lapilli tuff to planar-bedded coarse tuff can be attributed to upper flow regime turbidity current depositon during which the suspended load sedimentation rate rapidly declined (e.g. Lowe, 1988). Planar bedding is a common result of storm (e.g. Mueller, 1991) and/or wave influence
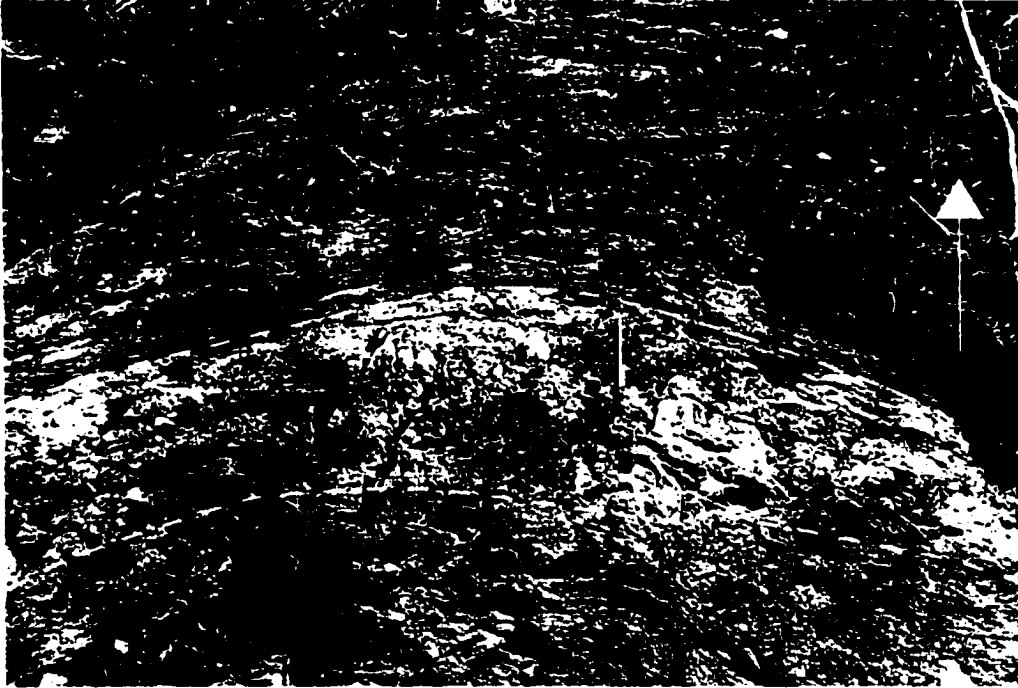
Figure 55a: Felsic tuffaceous (cherty) horizon between massive flow I and pillowed flow II (dashed lines) at locality C, NBRB (see Figure 44). Arrow points to top. Scale, pencil 14 cm.
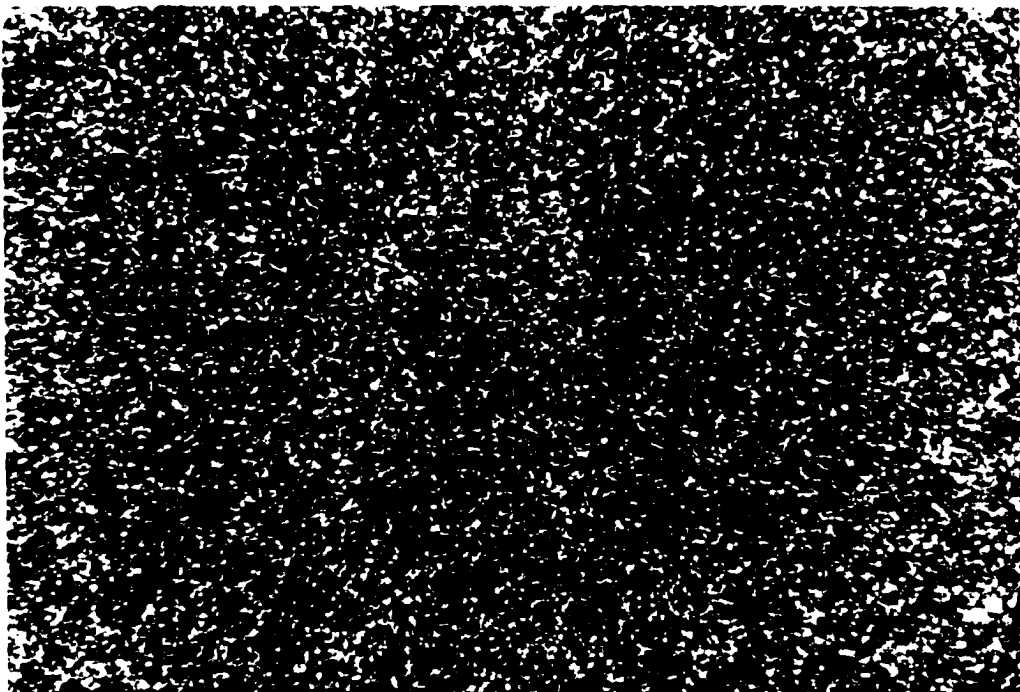
Figure 55b: Recrystallized microcrystalline quartz comprising the chert horizon interstratified with mafic flows at locality C, NBRB. Field of view is 6 mm. Thin section in xpl.
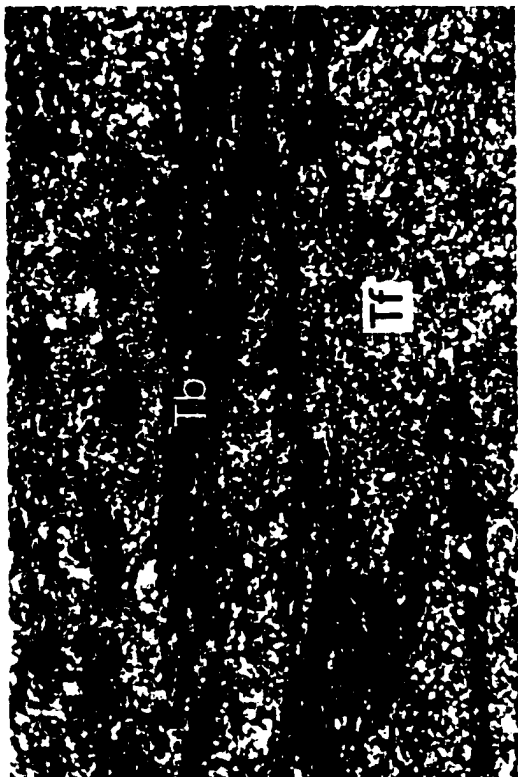
Figure 56b: Intermingled fine tuff (Tf) and black fine tuff (Tb) at locality D, NBRB (see Figure 48b). Field of view is 6 mm. Thin section in xpl.

Figure 56c: Laminated black fine tuff at locality D, NBRB (see Figure 48b). Field of view is 6 mm. Thin section in xpl.
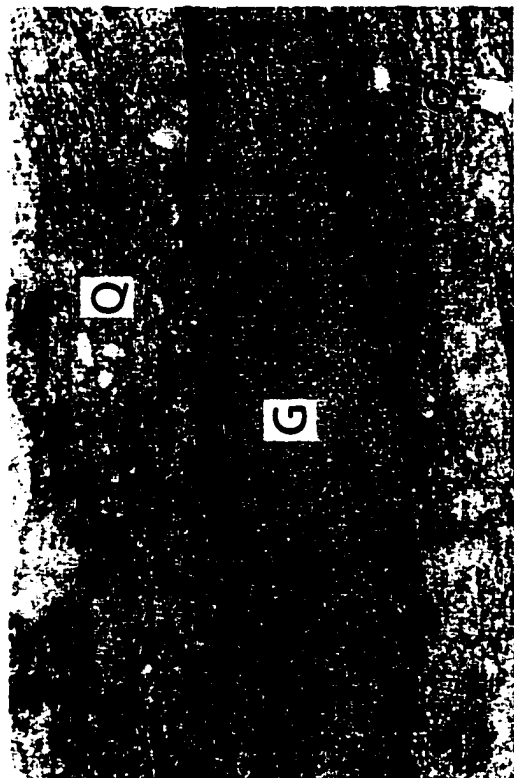
Figure 56a: Subangular, subrounded and broken quartz crystals (Q), and patches of recrystallized glass (G) in felsic tuff, locality D, NBRB. Field of view is 6 mm. Thin section in ppl.

(e.g. Howard and Reineck, 1981) in a shoreface setting. Small-scale fining-upward sequences represent successive fall-out of high- to low-concentration turbidity currents from a congested water column, which are similar to the fining- and thinning-upward sequences as described by Fiske and Matsuda (1964). However, the latter formed via subaqueous eruption in >150 m depth, whereas the deposits at locality D are interpreted to have accumulated in shallow water from subaerial eruptions. Massive coarse tuff beds represent the grain-supported deposits of sandy high-density turbidity currents when suspended load fall-out rates were high (Bouma T_a from Bouma, 1962, or S_3 beds of Lowe, 1982). Wavy composite beds containing low-angle cross-beds and wavy beds in coarse tuff are consistent with rapid flow regime variations and probably developed as asymmetrical sandwaves (e.g. Johnson and Levell, 1995; Johnson and Baldwin, 1996). Mudstone laminae between bedforms develop under highly fluctuating flow-energy conditions and calm water stages. The upward transition from coarse to fine tuff marks a significant change in sedimentary structure to planar bedding. The planar-bedded fine tuff is consistent with low concentration turbidity current deposition as the suspended load decreased, allowing for the formation of flat lamination (e.g. Lowe, 1988). Massive and laminated black fine tuff represents periods of quiescence during which fine-grained suspension deposition occurred (Bouma T_e beds; e.g. Fritz and Vanko, 1992; Allen et al., 1996). Based on their stratigraphic location, fine-grained nature, and black colour, the deposits probably represent fall-out material from a subaerial or subaqueous eruption.

Felsic tuff interstratified with mafic flows (Figure 44) is consistent with local bimodal volcanism. These thin cherty units form during periods of volcanic quiescence and mark the boundaries between separate flow events.

4.4   Geochemistry

4.4.1   Sampling Procedure

Sixty-nine samples were collected from the Northern Beaulieu River belt; 22 of these are treated in this thesis (Figure 42). Forty-seven samples were omitted based on textural heterogeneity or silica/carbonate alteration, or following major element analysis where LOI values were high (>8). The LOI cut-off of >8 was chosen in order to have enough samples for a viable geochemical study. The 69 samples were collected over an approximate area of 9x10.5 km, but those chosen for geochemistry are restricted to three main areas (Figure 42). The samples were selected where apparent chemical alteration was low, and the facies had homogenous grain size and low amygdule/vesicle percentages. The rock types sampled include mafic pillowed and massive flows, mafic intrusions, a felsic tuff, and ultramafic units. The latter are significantly older than the volcanic belt and are thus not included on the geochemical diagrams, but chemical analyses from five samples and microprobe data of chromites found in the dunite are provided in Appendices 2 and 3. One sample was collected from the western side of the Beniah Lake fault system (Figure 42a) to determine whether the volcanic rocks on the east and west are compositionally similar.

4.4.2   Results

Samples collected from the Northern Beaulieu River belt area are divided into three groups: 1) Group 1 tholeiitic basalt flows, 2) Group 2 tholeiitic basalt intrusions, and 3) a Group 3 calc-alkaline felsic tuff (Table 6). The groups are discriminated based on facies type (flow vs. intrusion), petrography, and SiO_2 wt%. The tholeiitic groups do not differ

Table 6: Major and trace element data for samples from the Northern Beaulieu River belt (ND=no data) *=total Fe as Fe2O3. All samples chosen for geochemical analysis are displayed. Altered samples were eliminated during sample preparation.

Sample	c7-45	c7-61	c7-67	c7-68	c7-73	c7-113	c7-138	c8-04	c8-06	c7-20	c7-64	c7-76
Group	Group 1	Group 1	Group 1	Group 1	Group 1	Group 1	Group 1	Group 1	Group 1	Group 2	Group 2	Group 2
SiO_2 (wt%)	51.36	48.65	46.82	49.66	50.23	47.19	46.09	50.05	49.59	51.45	49.68	50.15
TiO_2	2.46	0.86	1.17	1.08	1.97	0.7	1.24	1.15	0.74	2.33	0.76	1.3
Al_2O_3	14.62	14.11	15.52	15.95	14.97	14.6	15.23	14.9	14.36	13.21	15.23	14.13
Fe_2O_3*	13.86	12.29	12.6	13.15	14.36	15.01	14.06	13.91	11.55	17.48	12.46	15.75
MnO	0.3	0.2	0.22	0.47	0.24	0.25	0.25	0.22	0.21	0.28	0.21	0.24
MgO	4.12	8	6.17	4.79	5.36	8.89	7.29	5.83	8.09	4.73	8.47	6.39
CaO	7.06	11.03	8.23	9.66	6.86	11.89	11.68	10.34	12.01	8.86	11.67	9.99
Na_2O	4.85	1.75	2.32	1.89	2.61	1.59	1.66	2.56	2.29	2.04	2.18	2.42
K_2O	0.15	0.3	0.09	0.22	1.38	0.21	0.51	0.24	0.21	0.44	0.15	0.21
P_2O_5	0.21	0.06	0.08	0.09	0.23	0.08	0.1	0.11	0.06	0.34	0.06	0.11
LOI	0.1	0.57	5.13	3.61	0.83	0.48	0.69	0.4	0.83	0.71	0.57	0.5
Total	99.09	97.82	98.35	100.57	99.04	100.89	98.8	99.71	99.94	101.87	101.45	101.19
FeO*/MgO	3.03	1.38	1.84	2.47	2.41	1.52	1.74	2.15	1.28	3.33	1.32	2.22
Cr (ppm)	29	216	230	275	83	188	259	204	475	89	275	103
Ni	20	116	115	111	47	101	42	122	141	124	140	59
Co	73	69	55	69	57	68	46	74	59	78	62	73
Sc	12	0	8	12	12	25	10	26	6	27	10	21
V	414	290	321	370	426	227	393	313	219	379	240	344
Cu	200	109	107	61	79	26	6	133	41	59	24	114
Pb	9	3	6	0	8	7	6	13	7	8	14	6
Zn	175	76	105	1313	104	100	85	104	79	135	88	114
Rb	12	12	9	14	54	18	15	19	21	19	20	18
Ba	203	73	418	475	483	46	368	33	0	124	0	8
Sr	98	94	118	79	49	72	88	99	114	100	91	101
Ga	16	13	15	12	13	15	13	19	14	18	19	14
Nb	12.15	2.57	3.62	2.83	9.21	1.65	4.34	3.99	2.26	8.38	2.04	3.5
Zr	160	53	75	62	158	58	86	78	58	114	59	75
Y	33	17	24	20	39	35	22	38	28	47	31	39
Th	1.84	ND	0.6	ND	1.58	0.46	0.52	0.57	ND	1.99	0.56	0.31
U	0.54	0.12	0.16	0.15	0.41	0.13	0.14	0.15	0.09	0.58	0.15	0.08
Zr/Y	4.85	3.12	3.13	3.1	4.05	1.66	3.91	2.05	2.07	2.43	1.9	1.92
Ti/V	35.61	17.81	21.85	17.46	27.77	18.42	18.96	22.1	20.27	36.92	18.9	22.62

Table 6: continued

Sample	c7-110	c7-115	c7-121	c7-159	c7-166
Group	Group 2	Group 2	Group 2	Group 2	Group 3
SiO_2 (wt%)	49.81	49.36	47.72	50.5	77.94
TiO_2	1.24	1.23	2.15	1.82	0.14
Al_2O_3	5.39	18.39	12.78	12.97	10.52
Fe_2O_3*	16.77	11.66	19.37	18.92	3.25
MnO	0.29	0.19	0.29	0.26	0.03
MgO	14.42	5.8	5.85	4.58	3
CaO	11.78	10.69	9.68	9.31	1.44
Na_2O	0.44	2.53	2.5	1.91	0.42
K_2O	0.1	0.51	0.27	0.34	0.36
P_2O_5	0.09	0.19	0.16	0.16	0.01
LOI	1.34	0.58	0.2	0.3	2.3
Total	101.67	101.13	100.97	101.07	99.41
FeO*/MgO	1.05	1.81	2.98	3.72	0.98
Cr (ppm)	2523	204	63	17	4
Ni	340	53	65	25	9
Co	94	49	92	91	29
Sc	0	22	30	12	12
V	265	219	538	432	ND
Cu	29	52	144	76	8
Pb	7	11	12	9	68
Zn	142	100	149	127	118
Rb	16	25	15	16	17
Ba	0	51	60	154	432
Sr	9	154	103	110	145
Ga	11	15	20	18	24
Nb	5.36	5.8	4.92	6.14	24
Zr	73	93	94	96	214
Y	35	33	48	48	87
Th	1.34	1.66	0.53	0.5	30
U	0.08	0.41	0.14	0.1	7
Zr/Y	2.09	2.82	1.96	2	2.46
Ti/V	28.1	33.78	23.99	25.28	ND

significantly, with similar Zr/Y, Ti/V, and $(La/Yb)_n$ (n=normalized) ratios, and relative REE abundances.

Group 1 Tholeiitic Basalt Flows

Group 1 tholeiitic basalts were collected mainly from the central part of the study area, west of the camp (Figures 17, 42), but one mafic flow was sampled west of the Beniah fault zone (Figure 42a). SiO_2 values range from 46-51 wt% with FeO^*/MgO ratios of 1.3-3 (Table 6). The samples display good positive correlations between FeO^*/MgO and FeO^*, SiO_2, and TiO_2 (Figure 57). Zr/Y ratios range from 1.7-4.8 (Table 6). There is a slight enrichment in HFSE and the samples display slightly depleted to LREE-enriched patterns with $(La/Yb)_n$ ratios of .55-2.76, comparable with N- and EMORB (Table 7, Figure 58). Most of the samples produce similar patterns with negative Ce anomalies, and differ only in the concentration of REE (Figure 58). This is also illustrated on the incompatible element diagram where Group 1 samples have relatively flat patterns with small depletions in Nb and Ti (Figure 59). ε_{Nd} values range +0.39-+8.26 (Table 8). There is no significant difference in the geochemistry of the sample collected west of the fault compared with the eastern samples.

Group 2 Tholeiitic Basalt Intrusions

Group 2 tholeiitic basalt intrusions, common features in the Beniah Lake area, cut Group 1 tholeiites, as well as 2.9-3.1 Ga quartz arenite (Figure 42). Group 2 samples have SiO_2 wt% ranging from 48-51 and FeO^*/MgO ratios of 1-3.7. The intrusions display tholeiitic differentiation trends on variation diagrams, similar to Group 1 samples (Figure 57). Zr/Y ratios are between 1.9 and 2.8 (Table 6). These rocks can be further
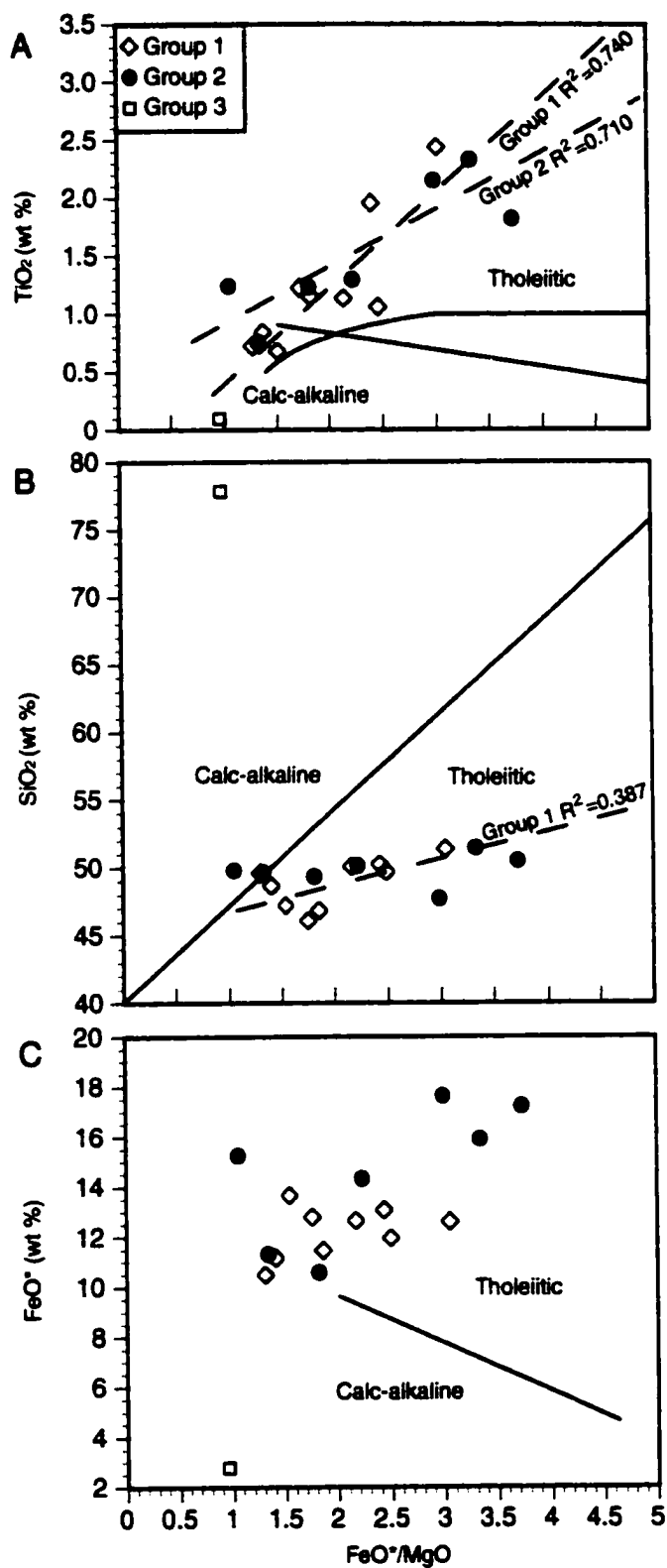
Figure 57: Variation diagrams demonstrating the behaviour of (A) TiO_2, (B) SiO_2, and (C) FeO^* vs. FeO^*/MgO in samples from Group 1 tholeiitic basalt flows, Group 2 tholeiitic basalt intrusions, and a Group 3 felsic tuff. Good trendlines (dashed) for Groups 1 and 2 are displayed in diagrams A and B. Diagrams after Miyashiro (1974).

Table 7: Rare earth element data (in ppm) for samples from the Northern Beaulieu River belt (ND=no data)

Sample	c7-45	c7-61	c7-67	c7-68	c7-73	c7-113	c7-138	c8-04	c8-06	c7-20	c7-64	c7-76	c7-110	c7-115	c7-121	c7-159
Group	Group 1	Group 1	Group 1	Group 1	Group 1	Group 1	Group 1	Group 1	Group 1	Group 2	Group 2	Group 2	Group 2	Group 2	Group 2	Group 2
La	15.42	3.16	4.74	4.24	10.67	1.82	6.92	5.35	2.86	10.93	1.69	3.85	6.04	9.46	5.56	5.82
Ce	36.70	8.30	11.82	10.31	25.67	4.75	17.46	13.19	7.16	27.56	4.58	10.25	15.06	21.43	14.68	15.4
Pr	5.73	1.42	1.93	1.64	4.12	0.77	2.80	2.15	1.15	4.1	0.78	1.65	2.24	3.01	2.44	2.47
Nd	24.32	6.44	8.62	7.65	17.67	3.9	12.37	9.51	5.32	18.96	4.18	8.57	10.13	13.23	12.23	12.58
Sm	6.29	2.02	2.60	2.39	5.00	1.38	3.24	2.86	1.60	5.08	1.65	2.8	2.9	3.4	4.02	4.15
Eu	2.10	0.80	1.01	0.91	1.73	0.64	0.96	1.05	0.66	1.65	0.66	0.99	1.52	1.05	1.28	1.36
Gd	6.78	2.60	3.45	3.24	5.75	ND	3.73	3.43	2.12	ND	ND	ND	ND	ND	ND	ND
Tb	1.11	ND	0.65	0.61	1.11	0.39	0.69	0.65	ND	0.98	0.42	0.67	0.55	0.6	0.94	0.96
Dy	6.53	3.19	3.89	3.70	6.98	2.92	4.23	4.11	2.61	6.46	2.88	4.57	3.28	4.01	6.34	6.31
Ho	1.42	0.77	0.96	0.91	1.65	0.7	0.99	0.99	0.62	1.38	0.65	1	0.65	0.84	1.4	1.42
Er	3.77	2.10	2.60	2.50	4.53	2.12	2.85	2.68	1.73	3.97	1.85	2.94	1.71	2.41	3.97	4.17
Tm	0.56	0.34	0.42	0.41	0.72	0.32	0.44	0.42	ND	0.58	0.27	0.42	0.23	0.35	0.59	0.62
Yb	3.39	2.06	2.64	2.57	4.59	2	2.72	2.65	1.76	3.62	1.77	2.74	1.36	2.24	3.69	3.96
Lu	0.55	0.36	0.44	0.41	0.73	0.32	0.48	0.45	0.29	0.58	0.28	0.43	0.2	0.35	0.59	0.64

Table 8: Sm-Nd isotope systematics for selected samples from the Northern Beaulieu River belt

Sample	c7-45	c7-61	c7-73	c8-6
Group	1	1	1	1
Nd (ppm)	24.66	15.82	30.48	18.05
Sm (ppm)	5.54	5.24	8.27	6.03
$^{147}Sm/^{144}Nd$	0.13859	0.20439	0.16747	0.20606
$^{143}Nd/^{144}Nd$	0.512026	0.512797	0.512301	0.512885
εNd	8.26	0.39	3.57	1.55
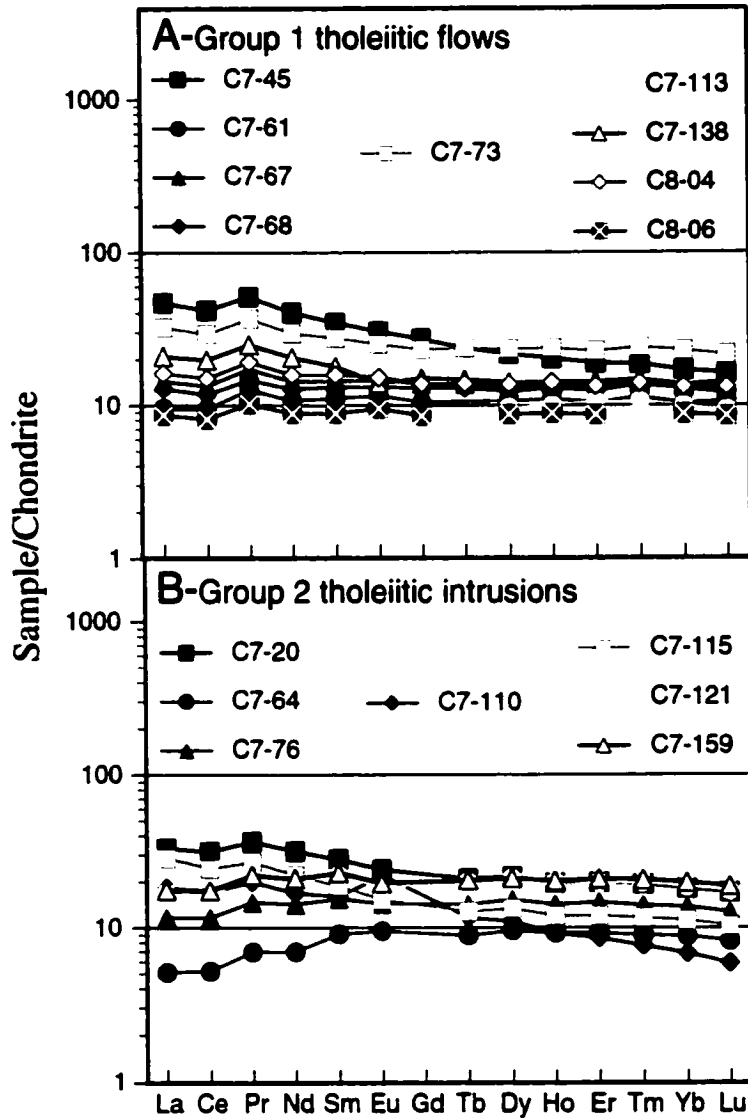
Figure 58: Chondrite-normalized REE abundances for selected NBRB samples. Normalizing values after Haskin et al. (1968).
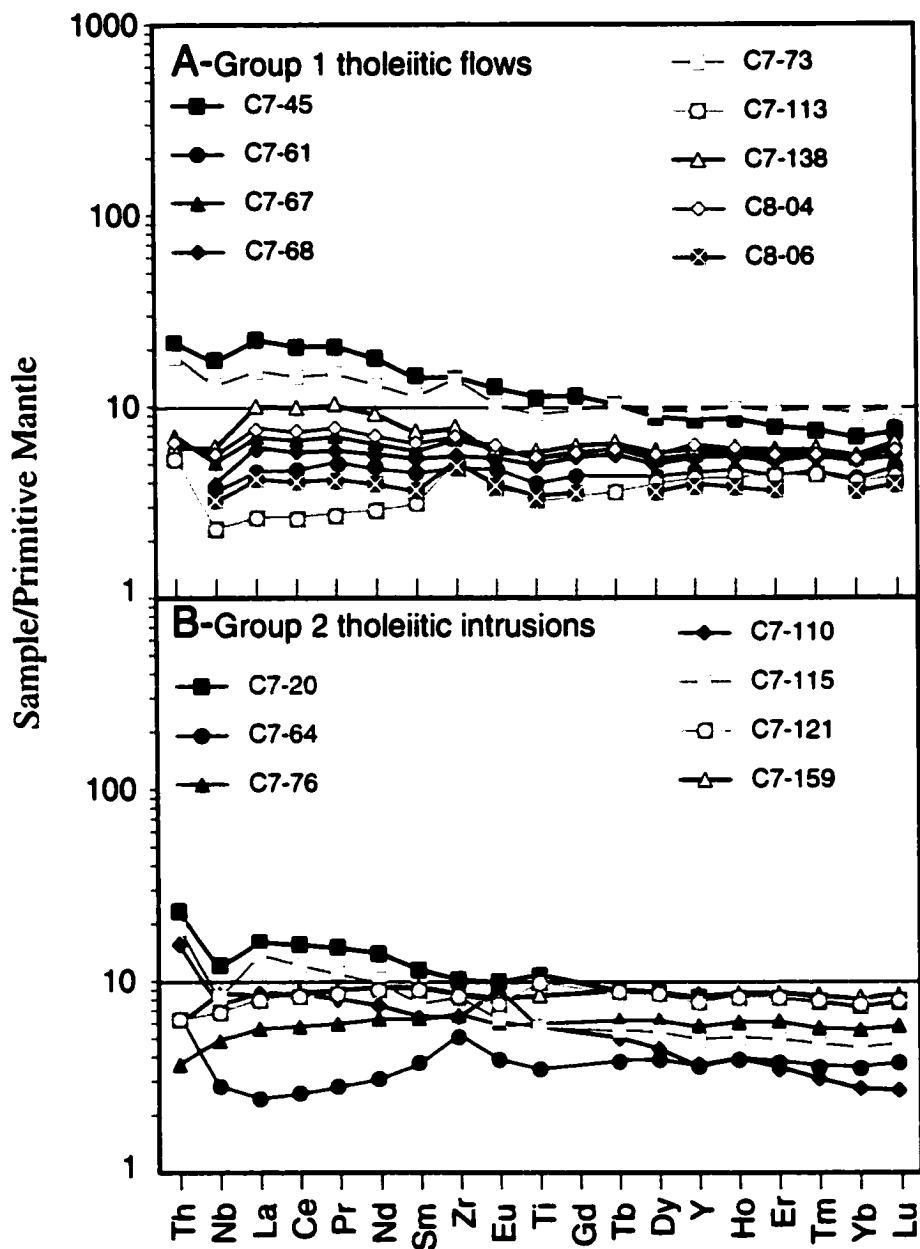
Figure 59: Primitive mantle-normalized incompatible element abundances for selected samples from the NBRB. Normalizing values after Sun and McDonough (1989).

subdivided based on $(La/Yb)_n$ ratios and Nb depletions. Samples C7-64, 76, 121, and 159

resemble NMORB as they are LREE depleted with $(La/Yb)_n$ ratios ranging from .58-.91

(Table 7, Figure 58) and do not display Nb depletions on the incompatible element

diagram (Figure 59). Samples C7-20, 110, and 115 are more similar to EMORB with

$(La/Yb)_n$ ratios of 1.83-2.69 (Figure 58) and marked Nb depletions (Figure 59). The

concentrations of REE and other HFSE change systematically within each subgroup, with

only minor variations in pattern slopes and curvatures. Group 2 samples display slight

negative Ce anomalies (Figure 58).

Group 3 Calc-alkaline felsic tuff

A felsic tuff (c7-166), collected from the basal section at locality D (Figure 42b),

contains 78 wt % SiO_2 and has an FeO^*/MgO ratio of 1 (Table 6). The high SiO_2 content

is probably the result of silicification, but the mineral components indicate that the tuff is

felsic (see section 4.3.1). The sample falls in the calc-alkaline field on the variation

diagrams of Miyashiro (1974; Figure 57). The Zr/Y ratio is 2.5, and the TiO_2 value is low

(0.14) compared with the mafic samples from the Northern Beaulieu River belt (Table 6).

The felsic sample was not analyzed for REE geochemistry because it was initially

thought that the felsic volcaniclastic rocks were related to the older Beniah Formation

quartz arenite sequence. A recent U-Pb zircon age of 2672.3 +8.5/−5.3 Ma Ma indicates

that the felsic rocks are intimately associated with the mafic volcanic succession (Mueller

et al., 2001).

4.4.3 Interpretation

Compositional similarities between tholeiitic basalt flows and intrusions and the interstratification of a calc-alkaline felsic tuff with a pillowed flow indicates that the three groups in the Northern Beaulieu River belt are petrogenetically related. Samples from Groups 1 and 2 display flat HREE patterns with $(Tb/Yb)_n$ ratios between .83-1.72 (Figure 58). These relatively flat HREE patterns are consistent with melting of spinel peridotite at depths of 40-60 km (Manetti et al. 1979; McKenzie and O'Nions 1991). Determining the source of the calc-alkaline magmas is not possible without REE data. Interstratification of EMORB and NMORB indicates either melting of a heterogeneous mantle or mixing of a MORB-like mantle and an enriched component, which could be represented by continental crust (Barley 1986), or slab-derived hydrous fluids (Miller et al., 1994; Sajona et al., 2000). A subduction-related and/or crustal component is supported by small negative Nb and Ti anomalies and the calc-alkaline composition of the felsic tuff underlying a pillowed flow is consistent with some subduction-related component in the petrogenesis of the volcanic sequence. The positive ε_{Nd} values, ranging from 0.39-8.26, indicate a depleted mantle source.

Tholeiitic differentiation trends, characterized by increasing TiO_2 and FeO and constant SiO_2 with increasing FeO^*/MgO, reflect an evolution to more evolved basaltic magmas. These trends most commonly develop due to fractionation of olivine, pyroxene, and some feldspar during evolution of the magma (Miller et al., 1994). The high FeO^*/MgO values of 1-3.7 indicate that none of the samples is strictly primitive, as a value of 0.7 is closer to equilibrium with mantle olivine (Kay et al., 1982). Fractional crystallization is also indicated on the REE diagram where the overall slopes and curvatures of the patterns are constant between samples. The only slope differences are represented by the variations in abundances of LREE between the two intrusion

subgroups (Figure 58). This indicates that some intrusions are more enriched than others, but both were derived from the same source. Relatively high Zr/Y values (up to 4.9) for the flows compared with lower values for the intrusions (<2.8) indicate that the latter are less differentiated than the flows. The values are consistent with MORB and volcanic arc basalts (cf. Pearce and Norry, 1979). Ti/V values ranging from 17-37 indicate an overlap of arclike and MORB ratios (cf. Shervais, 1982).

4.5 Depositional Setting of the Northern Beaulieu River Belt

The predominance of mafic massive flows and mafic dykes and the absence of breccias and associated fragmental deposits is inconsistent with the pillow-dominated seamount setting interpreted from physical volcanology in the Point Lake belt. A greater volume of massive flows than pillowed varieties can be a function of spreading velocity (Kennish and Lutz, 1998; Schmidt and Schmincke, 2000), magma conduit type, such as fissure or point source (Fornari et al., 1985; Smith and Cann, 1992), and effusion rate (Yamagishi, 1991). Massive flows characterize seamounts at fast-spreading zones (Ballard et al., 1979; Schmidt and Schmincke, 2000), but also form in flood basalt provinces (Hooper, 2000). These flows are commonly attributed to high eruption rates from fissures (Smith and Cann, 1992; Kennish and Lutz, 1998) and comprise geomorphic features on the ocean floor that are flatter than pillow-dominated seamounts. The subsurface features of fissures are dyke complexes (Walker, 2000) and abundant mafic dykes are associated with rifting (Carey and Sigurdsson, 1984; Walker, 1993), which occurs at mid-ocean ridges, arcs, and intra- or back-arc basins.

Wave-influenced structures in felsic volcaniclastic deposits preserved at locality D are typical of a shoreface setting in water depths between 4-10 m (e.g. Reinson, 1984). The shoreface is the zone of maximum sediment movement as a result of wave and

current action (Howard and Reineck, 1981). The fact that 65 m of felsic material is preserved with no intercalation of mafic deposits indicates congestion of the water column with felsic debris from a voluminous subaerial eruption. The material could not have been erupted subaqueously in <10 m water depth and accumulate 65 m of debris. Catastrophic input of pyroclastic material results in high rates of sedimentation over short periods of time (Smith, 1991; Mueller and Corcoran, in press). Primary deposits entering shallow water were mainly affected by turbulent flow processes at both high and low concentrations. The transition from high- (massive beds of coarse tuff) to low-concentration turbidity flows (planar-bedded fine tuff and black fine tuff), in addition to the up-section change from lapilli tuff to fine tuff, supports increased water depth or waning felsic volcanic activity. However, the overall fining-upward sequence is consistent with drowning of a subaerial edifice.

Mafic flows and abundant mafic dykes associated with shallow water felsic volcaniclastic deposits necessitate a subaerial to subaqueous depositional setting. A depositional model proposed for the Northern Beaulieu River belt is illustrated in Figure 60. Following eruption of a subaerial felsic edifice, pyroclastic debris was deposited into shallow water and was subjected to wave reworking. Mafic lavas derived from small fissure-fed edifices were emplaced on the ocean floor concommitant with subaerial eruption. Drowning of the felsic edifice due to subsidence or a rise in water level resulted in the deposition of finer-grained material overlain by pillowed flows. The subaerial to shallow subaqueous setting characterized by bimodal volcanism is consistent with deposition on a continental rifted margin or arc platform.

eruption column

massive basalt
flows

fissure

seamount

coastline

rhyolite
flow

felsic dykes

mafic dyke

felsic
lapilli tuff

felsic tuff

pillowed basalt
flows
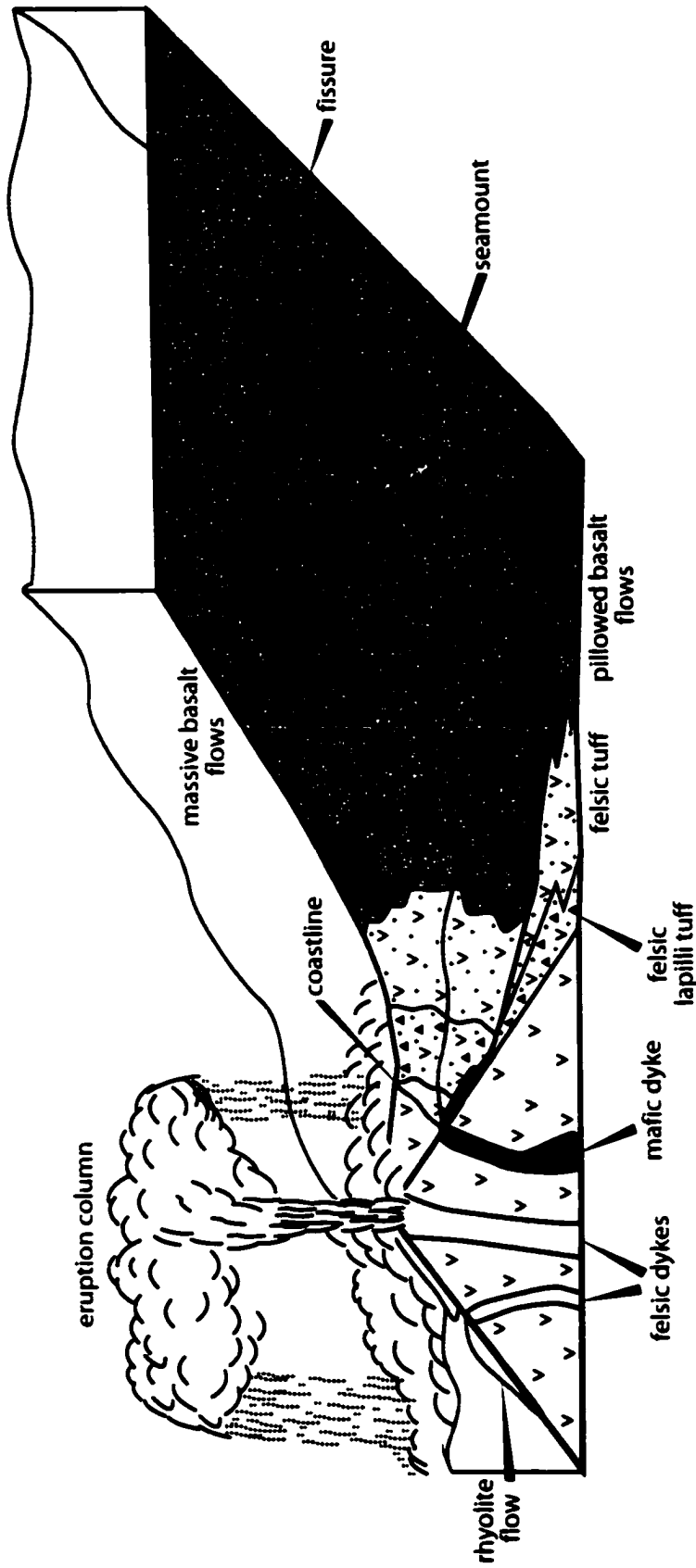
Figure 60: Depositional setting of the Northern Beaulieu River belt. A subaerial felsic edifice erupted pyroclastic material into a shallow water setting. Subaqueous mafic magmas were emplaced from fissure-dominated eruptions during deposition of the felsic debris. Local multiple pillowed basalt flows built up small seamounts on the ocean floor. Transgression, due to sea level rise and/or subsidence, resulted in drowning of the felsic edifice and deposition of pillowed flows over felsic volcaniclastic deposits.

4.6   Geodynamic Setting

A tectonic model for the Northern Beaulieu River belt must incorporate the physical

and geochemical characteristics of the volcanic succession. including: 1)

contemporaneous deposition of subaqeous mafic volcanism and shallow water felsic

volcaniclastic material. 2) predominant massive mafic flows with subsidiary pillowed

flows and a lack of breccia and hyaloclastite. 3) a significant mafic dyke complex. and 4)

interstratification of tholeiitic basalts and calc-alkaline felsic volcaniclastic rocks.

The flat to depleted LREE patterns for Groups 1 and 2 in the Northern Beaulieu

River belt are akin to NMORB or island arc tholeiities (IAT), whereas samples displaying

slight enrichments in the LREE are consistent with EMORB and IAT with moderate to

high K (e.g. Perfit et al.. 1980). This makes distinguishing between mid-oceanic and

island arc settings problematic. however. IAT generally display lower absolute

abundances of Ti. Zr. and Nb than NMORB (Perfit et al.. 1980). Most of the samples in

the Northern Beaulieu River belt are characterized by Nb and Ti depletions relative to

other incompatible elements. which may be more consistent with IAT. The presence of

one calc-alkaline felsic sample. as determined from major and trace elements (Figure 57).

which underlies a pillowed flow, tentatively supports a subduction-related component.

When plotted on Ti/Cr vs. Ni and Cr vs. Yb diagrams. the samples fall in both the ocean

floor basalt (OFB) and IAT fields, and the island arc basalt (IAB) and MORB fields,

respectively (Figure 61). Marginal basin basalts generally plot in the OFB field on the

Ti/Cr vs. Ni diagram (Beccaluva et al.. 1979) due to their compositional similarities with

MORB. Variations in basalt compositions are common in the arc to back-arc transition

zone and can occur over as little as 15 km (Gamble and Wright, 1995). MORB-type

volcanic rocks may also develop in rift grabens of young back-arc basins and are thus

associated with arc-derived deposits (Hawkins. 1995). The elements most affected by
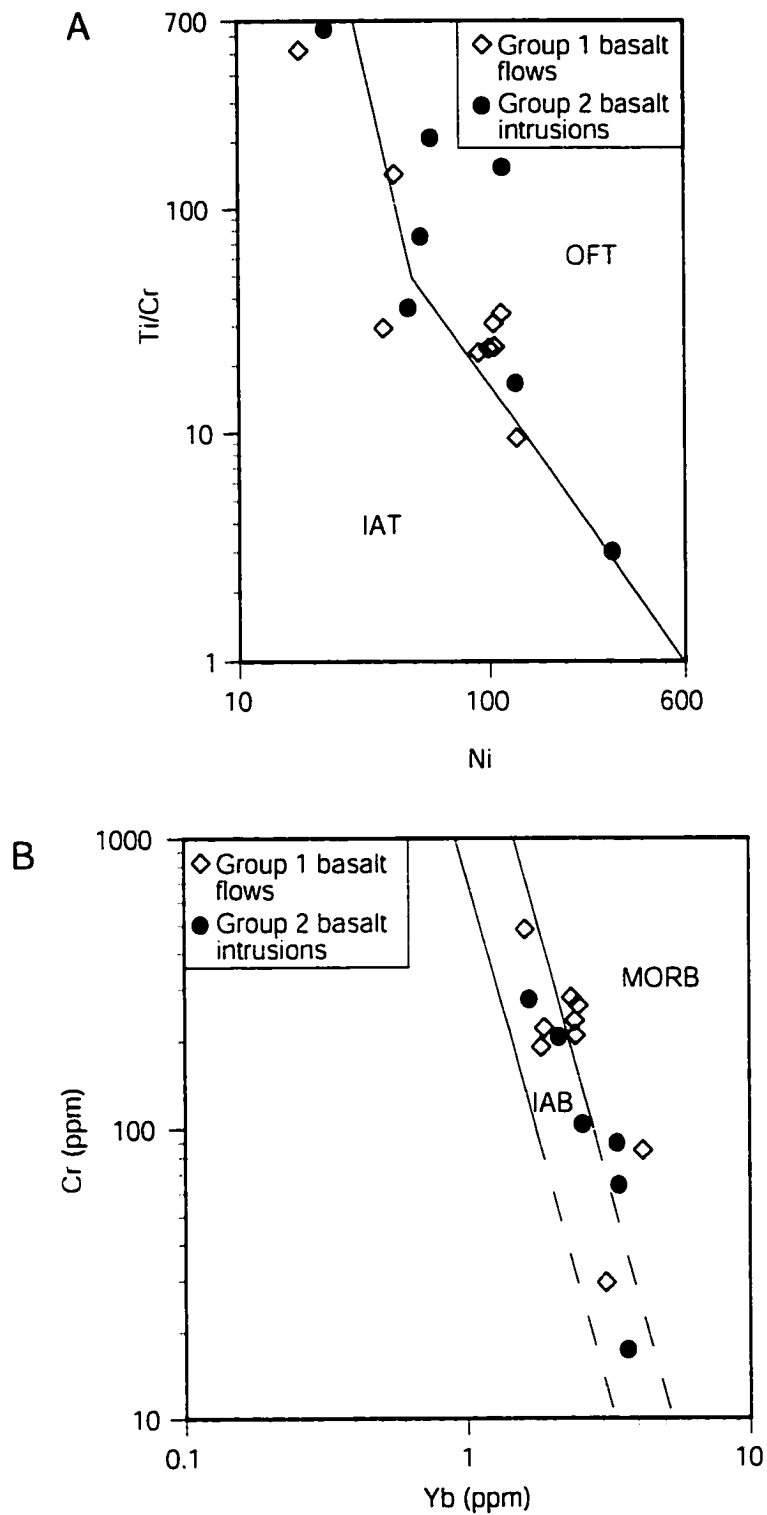
Figure 61: Discrimination diagrams distinguishing between island arc basalts (IAT, IAB) and mid-ocean ridge basalts (MORB, OFT) in the Northern Beaulieu River belt using (A) Ti/Cr vs. Ni (Beccaluva et al., 1979) and (B) Cr vs. Yb (Pearce and Parkinson, 1993).

variations in tectonic setting are the large ion lithophile elements (LILE), which unfortunately are not considered in this study because of their high mobility during submarine alteration and metamorphism (Kerrich and Wyman, 1996). The geochemical overlap of arc- and back-arc-type rocks demonstrates that a combination of stratigraphy, geochemistry and volcanology is necessary to better elucidate the tectonic setting.

The presence of shallow-water felsic volcaniclastic deposits interstratified with mafic flows is inconsistent with a mid-ocean setting. In addition, deeper water turbiditic deposits like those interstratified with the mafic volcanic rocks in the Point Lake belt, are expected in a back-arc or fore-arc setting (Klein, 1985), but they are absent in the Northern Beaulieu River belt study area. The volcanology and geochemistry of the Northern Beaulieu River belt can be associated with the fringing part of an arc, between the arc and back-arc. Tholeiitic rocks are generally the earliest components in arc evolution and form the basement on which subsequent calc-alkaline couterparts are deposited (Jakes and Gill, 1970; Jakes and White, 1972). Although the faulted basal contact between tholeiitic basalts and calc-alkaline felsic volcaniclastic rocks precludes stratigraphic determination, tholeiitic basalts are also integral components of arcs throughout their development depending on subduction rate and convergence angle (Kay et al., 1982). The entire Northern Beaulieu River belt in the Beniah Lake area contains not only abundant felsic volcaniclastic deposits, but also significant sequences of rhyolitic flows (Figure 17; Roach, 1990). The association of basalts and rhyolites, and the interstratification of mafic and felsic facies is consistent with an arc to back-arc transition zone (e.g. Miller et al., 1994; Hunter and Blake, 1995; Hunter, 1998; Rolland et al., 2000).

A possible tectonic interpretation for the evolution of the Northern Beaulieu River belt. as illustrated in Figure 62, involves subduction of an eastern slab of oceanic crust beneath continental crust from the west. The subducted slab contributed water to the
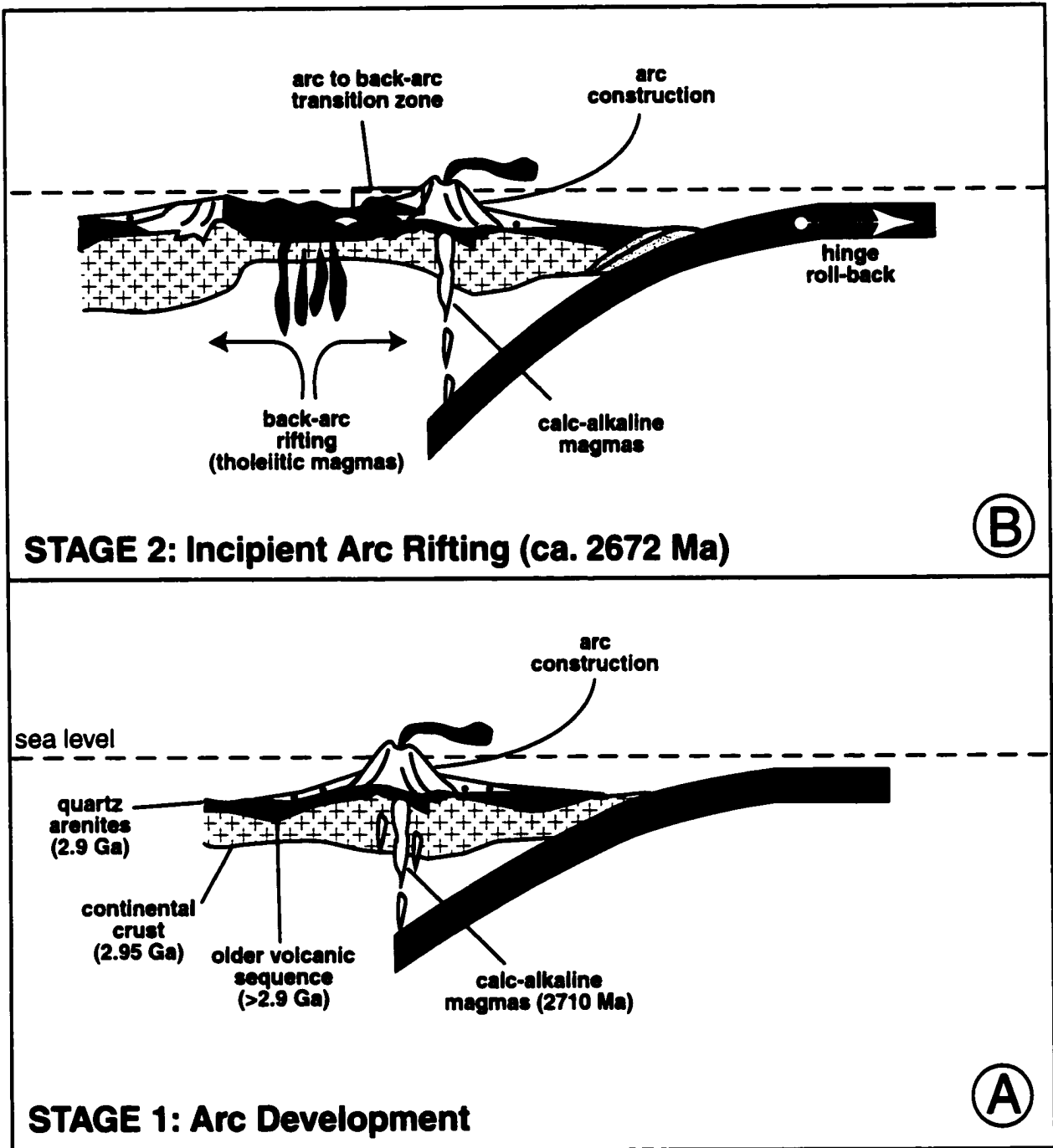
Figure 62: Schematic model illustrating Northern Beaulieu River belt evolution. (A) Subduction of oceanic crust beneath continental crust occurred around 2710 Ma. A subaqueous-subaerial arc was contructed and underwent mass wasting to deposit volcaniclastic material over an older volcanic and quartz arenite sequence (Central Slave Cover Group). (B) Crustal attenuation and rifting of the arc, propagated by hinge roll-back, created a back-arc basin. Tholeiitic magmas erupted into the back-arc and at the arc to back-arc transition zone, the tholeiitic deposits were intercalated with their calc-alkaline counterparts. This transition zone is represented by the Northern Beaulieu River belt.

mantle wedge. Melting of the wedge and partial melting of crustal material led to the formation of tholeiitic and calc-alkaline basalts and rhyolites. Possible hinge roll-back of the underlying slab caused the arc to migrate away from the continental margin, creating a back-arc basin. Back-arc extension resulted in the formation of tholeiitic magmas, which outpoured mainly from fissures during rapid magma ascent. Interstratification of tholeiitic and calc-alkaline volcanic deposits where the arc and back-arc converge makes it difficult to arbitrarily place a boundary between the two arc components. Groups 1-3 are thus placed in a transition zone between the arc and back-arc (Figure 62). Although the positive ε_{Nd} values do not support interaction with older crust, stratigraphic relationships, $(Th/La)_n$ ratios as high as 2, and comparisons with other belts interpreted to overlie the Central Slave Basement Complex support the presence of sialic crust during evolution of the volcanic sequence. This aspect will be discussed in more detail in Chapter 6.

Summary

The physical volcanology of the Northern Beaulieu River volcanic belt is consistent with fissure-dominated basalt eruptions and shallow-water felsic volcaniclastic deposition along the fringing part of an arc. Up-section transitions from shallow felsic facies to deeper water mudstone and pillowed units indicate drowning of the arc during transgression due to arc subsidence or sea-level rise. Three geochemical groups of rocks comprise the ca. 2670 Ma mafic-dominated succession, represented by tholeiitic basalt flows, tholeiitic basalt intrusions, and one calc-alkaline rhyolite tuff. The most significant results determined from localities C and D are provided in Table 9.

The stratigraphy, physical volcanology and geochemistry of the Northern Beaulieu River belt are indicative of a transition zone between an arc and back-arc overlying

	Depositional setting	Locality C represents fissure-dominated eruptions as indicated by the predominance of mafic massive flows and a mafic intrusion complex. Thin interstratified units of felsic tuff represent background sedimentation during volcanic quiescence and indicate contemporaneous felsic and mafic volcanism. Locality D represents shallow-water, reworked, felsic pyroclastic deposits derived from a subaerial eruption. Upsection gradation into finer grained deposits and a pillowed flow indicate transgression and drowning of the felsic edifice.
	Chemical composition	Group 1: tholeiitic basalt flows; Group 2: tholeiitic basalt intrusions; Group 3: a calc-alkaline rhyolitic tuff.
	Geochemistry	Group 1: SiO_2 from 46-51 wt%, FeO^*/MgO ratios of 1.3-3, $(La/Yb)_n$ ratios of 0.55-2.76, some negative Ce anomalies, Zr enrichments and small Ti and Nb depletions relative to the REE. Group 2: SiO_2 from 48-51 wt%, FeO^*/MgO ratios of 1-3.7, $(La/Yb)_n$ ratios of 0.58-0.91, some negative Ce anomalies, minor Zr enrichments and some Nb depletions relative to the REE. Group 3: SiO_2 at 78 wt%, FeO^*/MgO ratio of 1.
	Crustal contamination	As indicated by stratigraphy and some $(Th/La)_n$ values (discussed in Chapter 6). εNd values range from +0.39-+8.26.
	Tectonic setting	**Arc to back-arc transition zone** Tholeiitic and calc-alkaline magmas were erupted along an arc during subduction of an oceanic slab beneath a continental slab. With hinge roll-back the arc moved away from the continental margin and the continental slab was attenuated to create a back-arc basin. Tholeiitic magmas were emplaced in the back-arc. In the arc to back-arc transition zone, both calc-alkaline and tholeiitic magmas were erupted (Groups 1-3). Shallow water setting indicates that the deposits formed along the fringing part of the arc.

Conglomerate Sequence

Northern Beaulieu River Belt (2672 Ma)

Quartz-Feldspar Porphyry (2710 Ma)

Beniah Formation (Central Slave Cover Group; 2.9 Ga)

Ultramafic Sequence

Beniah Complex (2.95 Ga)

Table 9: Summary reviewing the main volcanological and geochemical characteristics of the Northern Beaulieu River belt.

continental crust. 1) Subduction of an oceanic slab beneath continental crust resulted in development of an arc with tholeiitic and calc-alkaline affinities. 2) With hinge roll-back, the arc migrated away from the continental margin and the crustal slab was attenuated, creating a back-arc through which tholeiitic magmas were emplaced. 3) Tholeiitic basaltic and calc-alkaline silicic material was interstratified in the transition zone between the arc and back-arc.

Chapter 5

CENTRAL BEAULIEU RIVER BELT

5.1 Physical Volcanology

5.1.1 Introduction

Two study areas in the Central Beaulieu River belt were selected for detailed study. Locality E, approximately 85 m thick and locality F, approximately 250 m thick, are located northwest and east of Stanley Lake, respectively (Figures 63, 22 in Chapter 2). Five mafic volcanic facies comprise the sequence at locality E: 1) pillowed-lobate flows (50%), 2) pillow breccia (20%), 3) massive flows (20%), 4) synvolcanic mafic dykes (5%), and 5) stratified hyaloclastite (5%). Three felsic facies characterize the sequence at locality F: i) massive porphyritic flows (50%), ii) massive tuff-lapilli tuff (25%), and iii) massive volcanic breccia (25%). The felsic rocks are classified mainly by textures and mineral components due to the paucity of exposed volcanic and sedimentary structures. Locality E was mapped at scales of 1:20 and 1:100 to constrain lateral and vertical facies distribution and to document volcanic structures. The rocks underwent greenschist facies metamorphism, as indicated by the assemblage albite ± chlorite ± epidote ± green amphibole ± carbonate, but the prefix "meta" is omitted for simplicity.
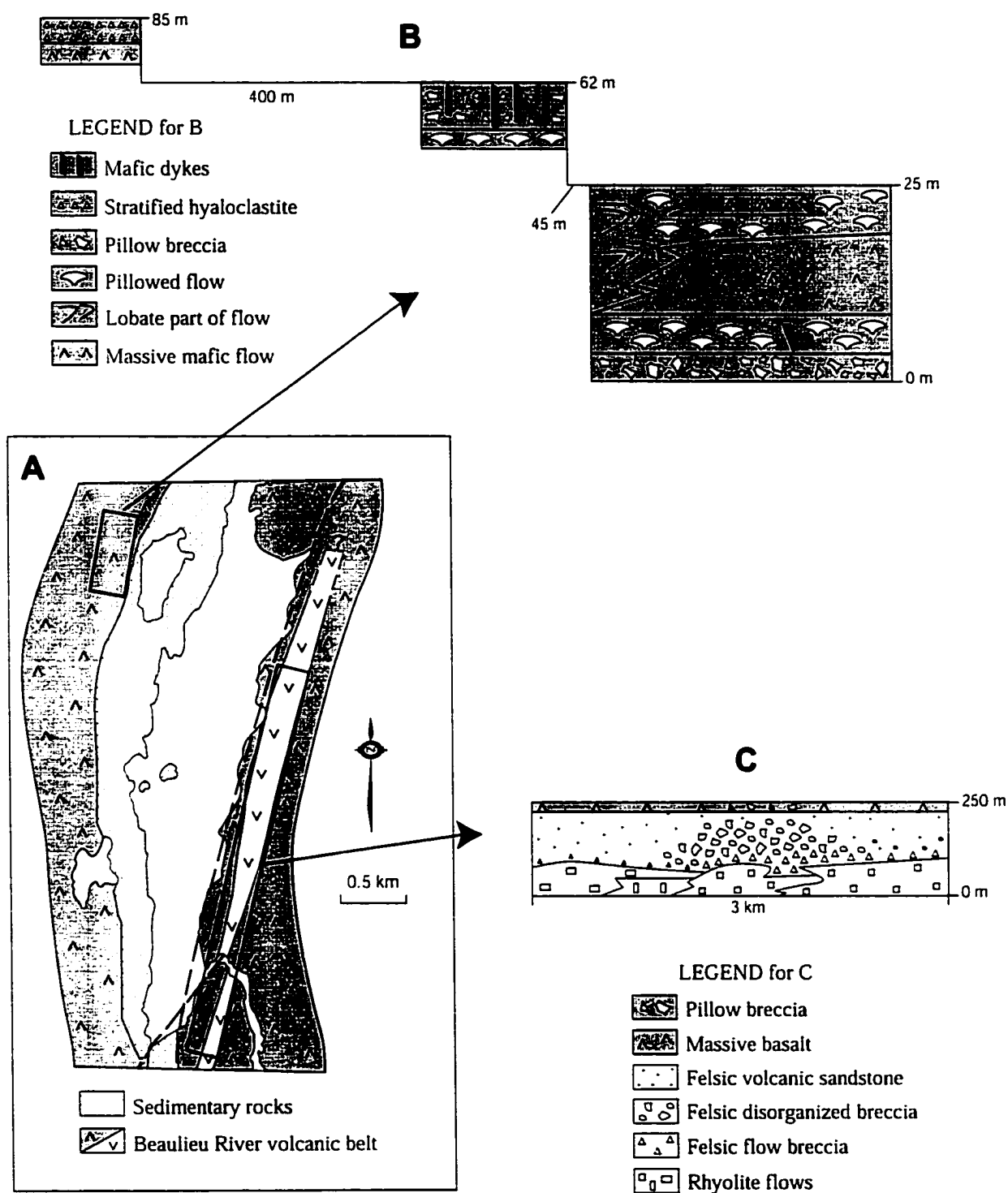
Figure 63: (A) Location of detailed localities E and F in the Central Beaulieu River belt. (B) Schematic diagrams illustrating the mafic volcanic facies comprising locality E. (C) Schematic diagram showing the felsic volcanic facies that characterize locality F and the upsection transition into pillow breccia and mafic flows.

5.2   Mafic Volcanic Facies

5.2.1   Massive Flows

Individual massive flows at locality E are 6-20 m thick (Figure 64). The flows are vesicular and amygdaloidal with vesicularity ranging from 5% at flow centres to 35-44% at flow tops and bases (Table 1 and Figure 29 in Chapter 3, Figure 64). Spherical to ovoid vesicles, 0.5-1.2 cm in size, are locally filled with calcite (Figure 65a) and chlorite. Stubby plagioclase phenocrysts or plagioclase microlites in chloritized sideromelane produce intersertal to hyalopilitic textures (Appendix 4). Massive parts of flows laterally and vertically become lobate or pillowed, are sharply overlain by pillow breccia, and/or are capped by hyaloclastite (Figure 64).

Interpretation

Massive basalt flows at locality E are comparable with their equivalents at locality A in the Point Lake belt. Vertical and lateral transitions from massive to lobate to pillowed are consistent with decreasing flow rate as a result of lower temperature and higher viscosity (Griffiths and Fink. 1992). Vesicle and amygdule concentrations at the bases and tops of flows and near pillow margins are attributed to the process described by Sahagian (1985) and cited in section 3.2.1.

5.2.2   Lobate-Pillowed Flows

The 3-15 m-thick pillowed flows at locality E contain closely-packed pillows, "isolated" pillows, and lobe structures (Figure 64). Closely-packed pillows, similar to close-packed pillows illustrated by Yamagishi (1994; p. 66), range in size from 20-150

vesicular base

dyke

10 m

pillow breccia

flow IV

flow III

flow II

flow I

sharp contact

closely-packed pillows

lobe structures

isolated, incompletely-formed pillows
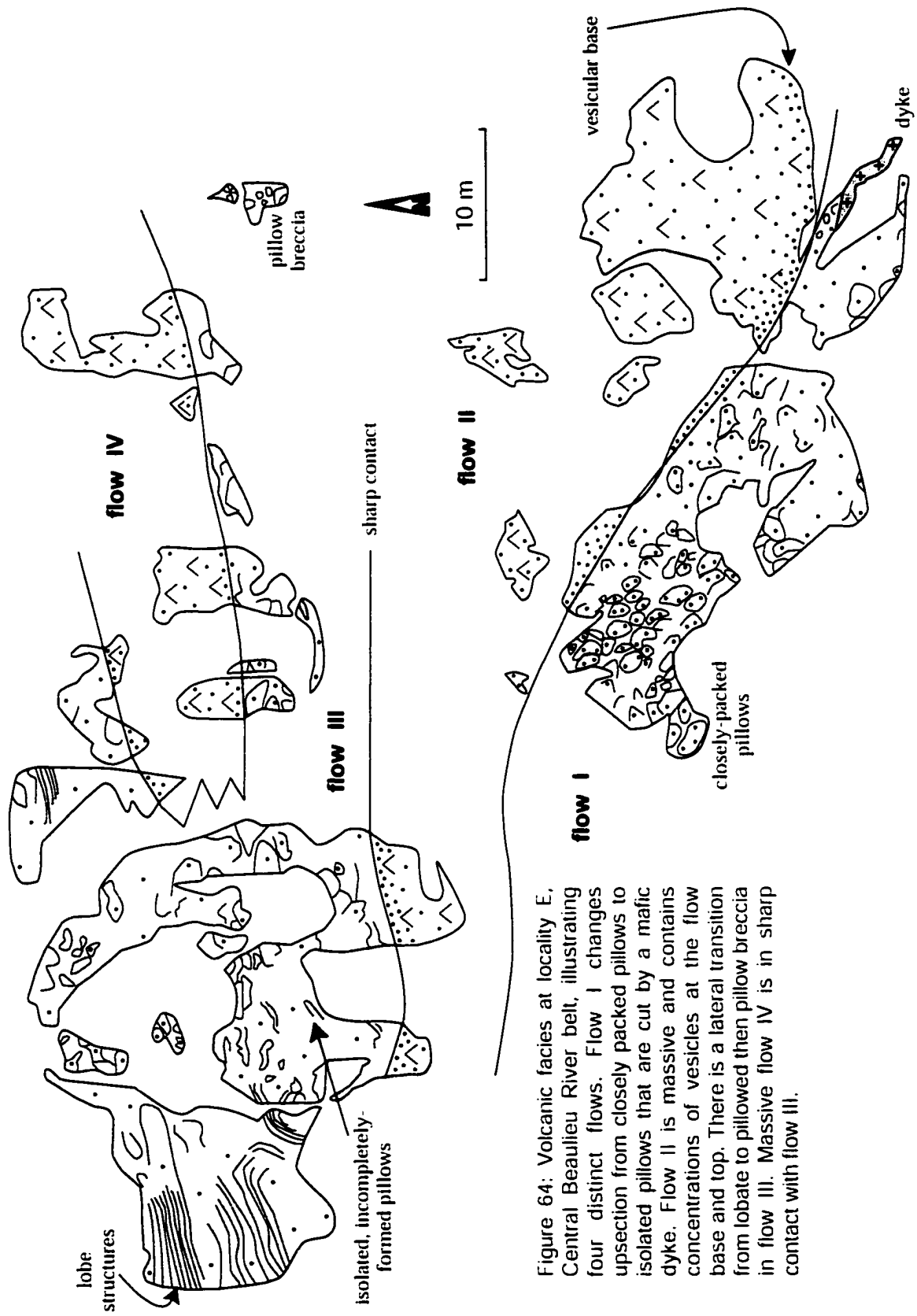
Figure 64: Volcanic facies at locality E, Central Beaulieu River belt, illustrating four distinct flows. Flow I changes upsection from closely packed pillows to isolated pillows that are cut by a mafic dyke. Flow II is massive and contains concentrations of vesicles at the flow base and top. There is a lateral transition from lobate to pillowed then pillow breccia in flow III. Massive flow IV is in sharp contact with flow III.

Figure 65b: Closely-packed pillows in pillowed flow I, CBRB (see Figure 64). Large arrow points to top. Scale, pencil (small arrow) 14 cm.

Figure 65a: Calcite amygdules (A) from the basal part of massive flow IV, CBRB (see Figure 64). Scale, pencil 13 cm.

Figure 65c: Thermal contraction fractures (Ft) in a pillow from flow I, CBRB (see Figure 64). Arrow points to top. Scale, pencil 14 cm.

cm, are characterized by 1-2 cm-thick chilled margins and some contain thermal contraction fractures (Figure 65b, c). Lateral transitions from lobate to pillowed (isolated pillows), to pillow breccia (Figure 64; flow III), and vertical changes from pillowed to pillow breccia (Figures 66, 67), were identified. Lobe structures, 0.5-5 m long, were distinguished by discontinuous, 0.25-1 cm-thick vesicular flow bands that are parallel to upper and lower flow margins and are locally folded (Figure 68a, b). Isolated pillows, <20 cm in size, are formed along lobe margins (Figure 64; flow III), resembling the lava lobes of Yamagishi (1994; p. 42). Vesicles, comprising 21-49% of pillowed flows (Table 1 in Chapter 3), are spherical to ovoid and <0.5-15 mm in size (Figure 29 in Chapter 3, Figure 69a). Calcite and chlorite fill vesicles, and although common throughout pillows, vesicles tend to be concentrated in pillow centres (Figure 29 in Chapter 3). Pillow centres are chiefly composed of microgranular plagioclase, whereas stubby plagioclase and plagioclase microlites in a glassy matrix are predominant near pillow rims (Appendix 4). The lobate part of the flow is characterized by microgranular plagioclase. Vesicles are either concentrically zoned with mineral assemblages quartz+chlorite-calcite, chlorite-calcite, and chlorite-quartz, or simply contain calcite (Figure 69b, c; Appendix 4).

Interpretation

Isolated pillows, analogous to incompletely formed or welded pillows of Dimroth et al. (1978) or pillow "ghosts" as described by Busby-Spera (1987), are the results of cooling that was too rapid to allow for complete formation (e.g Dimroth et al., 1978) or rapid burial by overlying lava during high eruption rates leading to incomplete chilling (e.g. Busby-Spera, 1987). Apparent massive areas between isolated pillows may mark the location of lava tubes (e.g. Busby-Spera, 1987) or welded megapillows (e.g. Dimroth et al., 1978). Fractures in pillows developed from thermal contraction during cooling (e.g. Wells et al., 1979; Yamagishi, 1991). Large vesicles at pillow centres represent coalesced
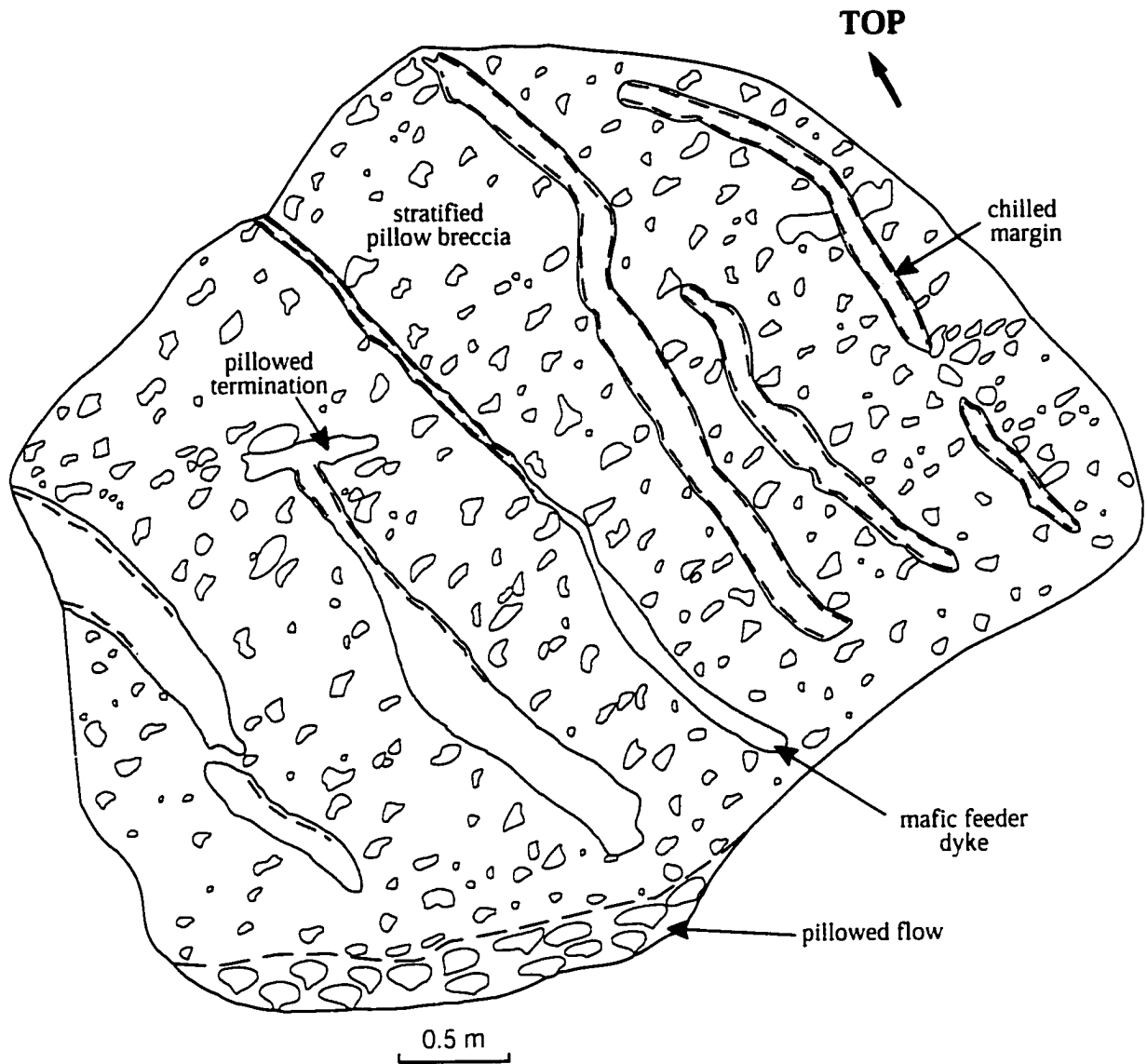
Figure 66: Outcrop sketch of the relationship between mafic feeder dykes, pillow breccia, and a pillowed flow at locality E, Central Beaulieu River belt. Crudely bedded pillow breccia overlies a pillowed flow. Feeder dykes have chilled margins and locally propogate into individual pillows.
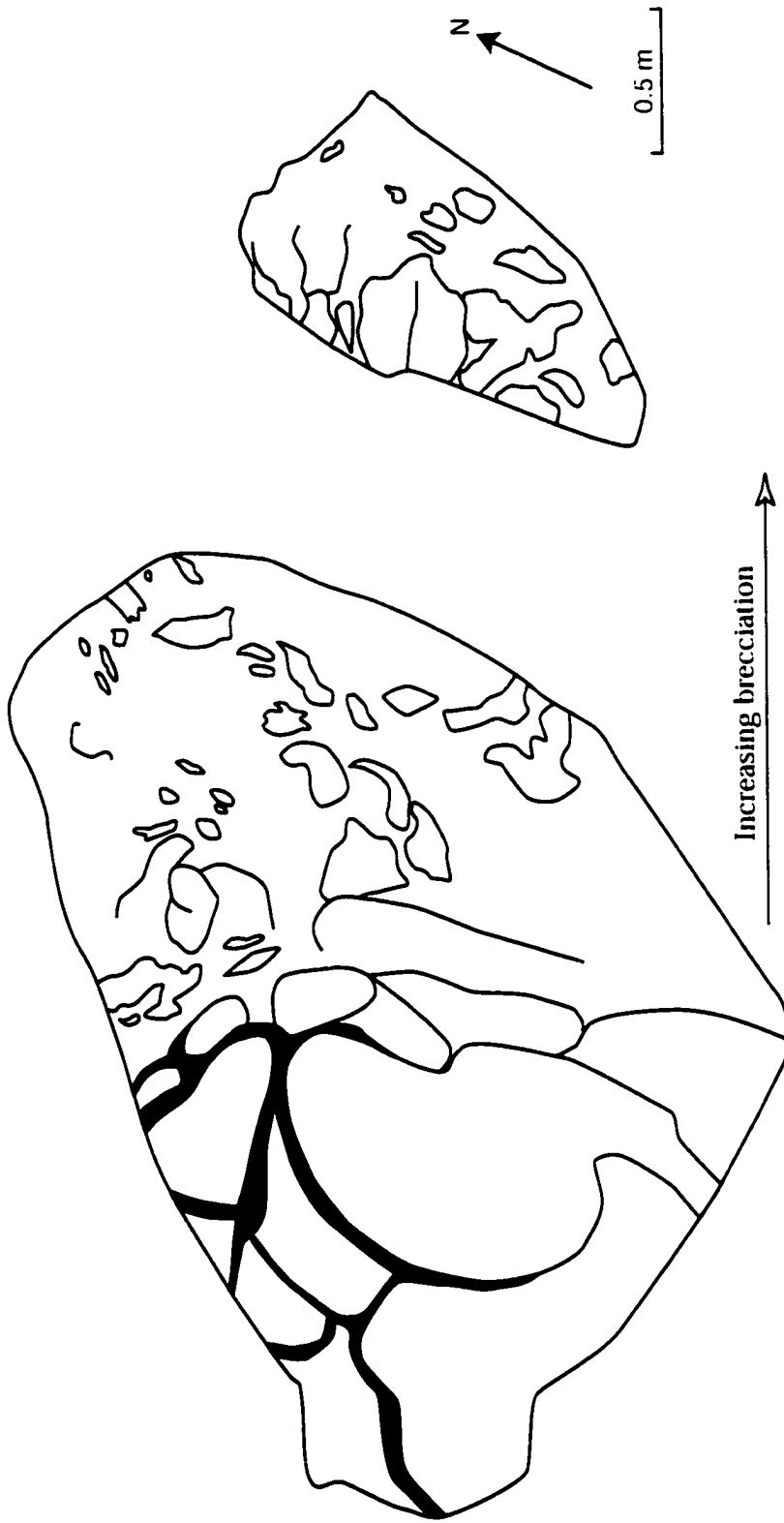
Figure 67: Vertical transition from pillowed flow to pillow breccia at locality E, Central Beaulieu River belt. Pillows are closely packed and pillow breccia contains subangular to subrounded pillow fragments.
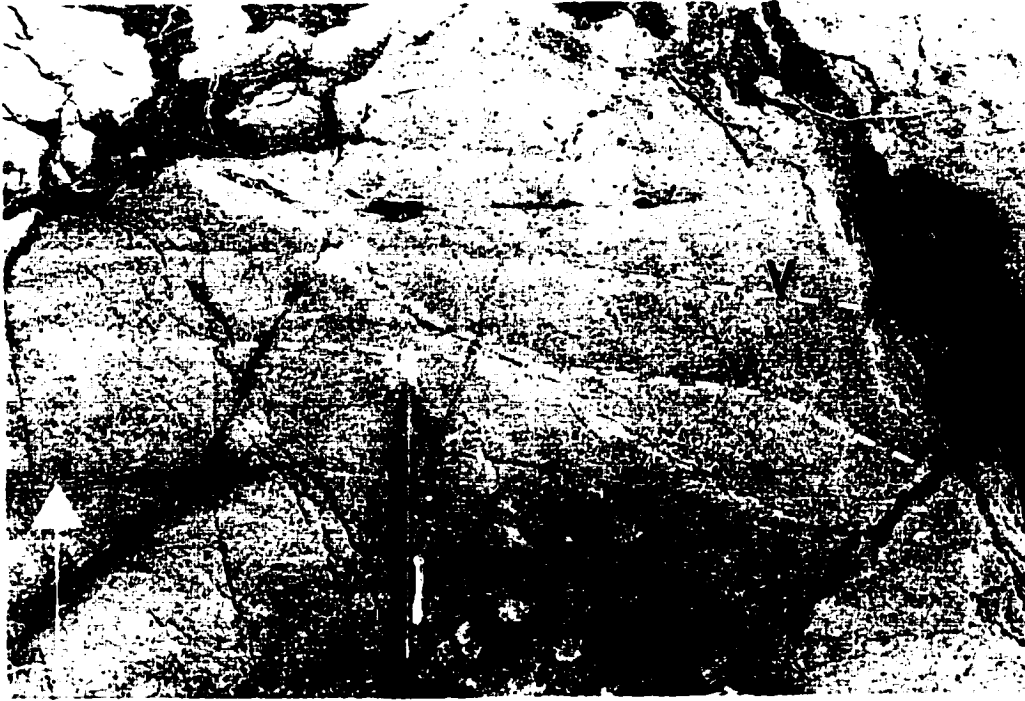
Figure 68a: Lobe structures (dashed lines) emphasized by concentrations of vesicles (V) in mafic flow III, CBRB (see Figure 64). Arrow points to top. Scale, pencil 14 cm.

Figure 68b: Lobe structures (dashed lines) that laterally become pillowed in flow III, CBRB (see Figure 64). Arrow points to top. Scale, pencil 14 cm.

Figure 69a: Vesicles (V) and a chloritized chilled margin (Cm) of a pillow from flow I, CBRB (see Figures 29b, 64). Arrow points to top. Scale, pencil 14 cm.

Figure 69c: Photomicrograph of a calcite-filled (Ca) vesicle and a concentrically zoned amygdule with chlorite + quartz (Ch + Q) along the rim and calcite (Ca) in the core (xpl). Taken from a pillow, CBRB.
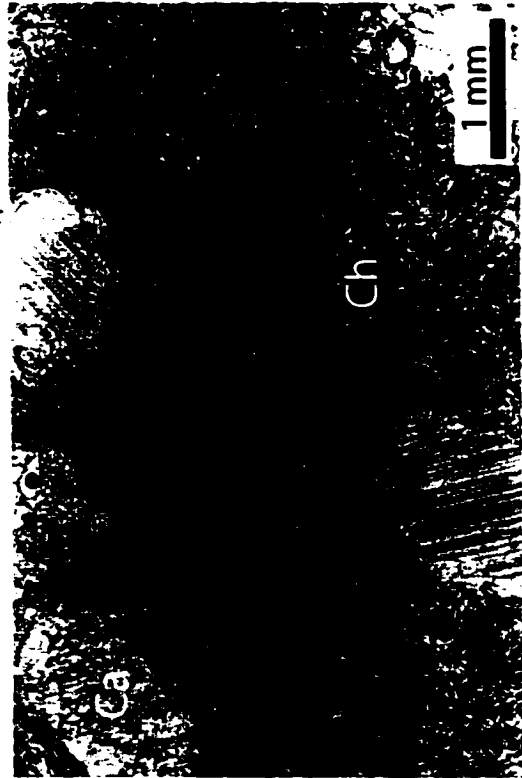
Figure 69b: Photomicrograph of chlorite-filled (Ch) and calcite-filled (Ca) vesicles near the rim of a pillow, CBRB. Thin section in xpl.

bubbles that did not have enough time to migrate toward the upper pillow margin before it cooled and crystallized.

5.2.3 Pillow Breccia

At locality E, crudely stratified pillow breccia, 0.5-6 m thick, contains whole pillows and pillow fragments (Figures 66, 67, 70a). Whole pillows with 0.5-1.5 cm-thick chilled margins are either 10-15 cm long and sub-spherical, or 10-25 cm long and amoeboid (Figure 70b) and are locally associated with <30 cm-thick hyaloclastite. Pillow fragments, 1-18 cm in size, are subangular to subrounded and locally lack chilled margins (Figure 70c). Vesicles, <1.5 cm in size, are common in whole pillows and pillow fragments, in which vesicularity ranges from 20-37% (Table 1 and Figure 29 in Chapter 3). Hyalopilitic texture is common in fragments, in addition to pilotaxitic texture where plagioclase microlites display sub-parallel alignment consistent with flow (Appendix 4). The matrix of pillow breccia is chiefly composed of microgranular plagioclase.

Interpretation

Vertical transitions from pillows to pillow breccia are explained by changing discharge rates during single eruptive events, and lateral changes indicate slope differences and/or diminishing magma supply at the distal parts of flows as a result of increasing surface area (Cas, 1992). Crudely bedded pillow breccia in the Beaulieu River volcanic belt suggests either gravity-induced deposition along seamount flanks in shallow water (e.g. Staudigel and Schmincke, 1984; McPhie et al., 1993) or may represent flow-front deposits where pillow breccia formed the foresets of shallow water lava deltas (e.g. Dimroth et al., 1985).

Figure 70a: Very vesicular (V), subangular to subrounded fragments in pillow breccia at locality E, CBRB (see Figure 29c). Arrow points to top. Scale, pencil 14 cm.

Figure 70b: Amoeboid pillow breccia fragments at locality E, CBRB. Arrow points to top. Scale, pencil 14 cm.

Figure 70b: Vesicular, amoeboid pillow in pillow breccia (outcrop in Figure 66). Note the chilled margin (Cm) and the largest vesicles (V) in the pillow centre. Arrow points to top. Scale, pencil 6 cm.

5.2.4 Hyaloclastite

Stratified hyaloclastite at locality E is characterized by 1-4 cm-thick vesicular

layers in 0.5-3 m-thick units (Figure 71a). Principal components include 0.3-4.5 mm

scoria containing quartz-albite-filled vesicles (Figure 71b), 0.1-0.35 mm-size plagioclase

crystals, and <0.1 mm-size bubble-wall and cuspate glass shards in a matrix of

microgranular feldspar. The stratified hyaloclastite overlies a massive flow, but could not

be traced laterally.

Interpretation

Hyaloclastite generally develops as a response to thermal contraction at flow tops

and fronts where the magma flows into water, is erupted subaqueously, or is emplaced

into cool, wet sediment (Dimroth et al., 1978; McPhie et al., 1993). Hyaloclastite may

also form as a result of subaqueous lava fountaining (Smith and Batiza, 1989). The

stratified hyaloclastite in the Beaulieu River volcanic belt is attributed to deposition of

reworked pillow breccia and hyaloclastite by waves in relatively shallow water, based on

the stratified nature of the deposit (e.g. McPhie et al., 1993).

5.2.5 Dykes

Synvolcanic mafic dykes at locality E, 0.03-0.4 m wide, cut pillow breccia and

pillowed flows (Figures 64, 66). Locally, the dyke/flow contacts are irregular, appearing

to "mold" around individual pillows (Figure 72a, b). The intrusions begin and terminate

within the same flow with local propagation into individual pillows (Figures 66, 72c).

Transitions from dykes to overlying flows were nowhere evident, although the dykes are

generally perpendicular to flow tops. Porphyritic and glomeroporphyritic textures are
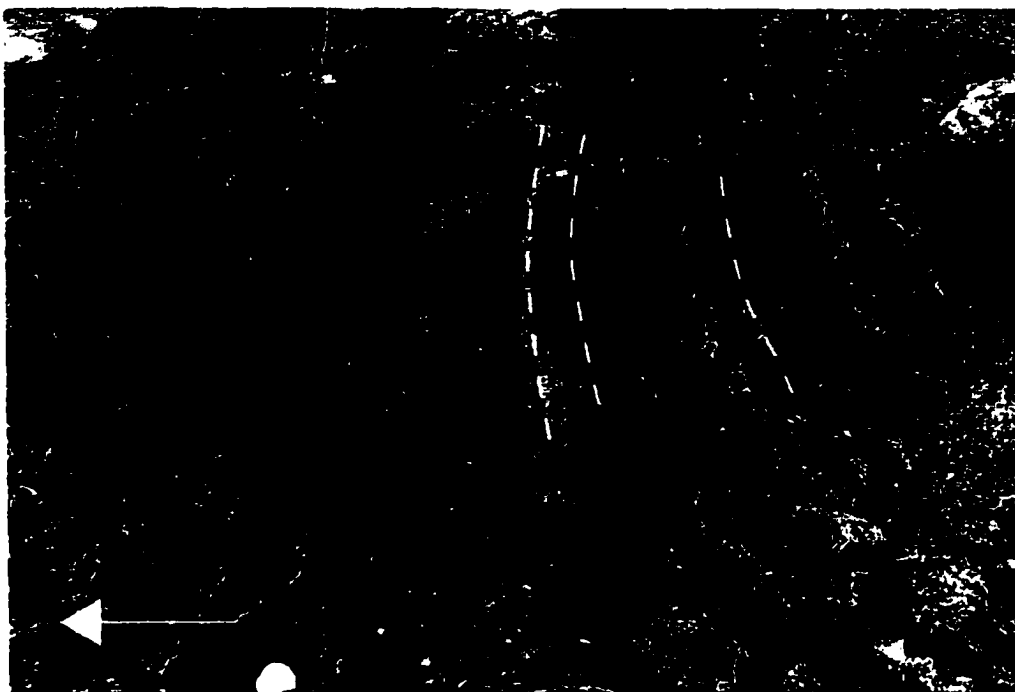
Figure 71a: Stratified hyaloclastite (dashed lines) at locality E, CBRB. Arrow points to top. Scale, knife 9 cm.

Figure 71b: Photomicrograph of a scoria lapillus in stratified hyaloclastite, CBRB. Note the abundance of vesicles and their coalescing nature (Vc). Thin section in xpl.

Figure 72b: Dyke (D)/pillow flow (Pf) contact, CBRB. The irregular contact and preservation of a small pillow (P) suggests that the flow was not fully consolidated during dyke injection. Scale, pencil 14 cm.

Figure 72c: Dyke (D) propagating into a pillow (P) in pillow breccia, CBRB (see Figure 66). Arrow points to top. Scale, pencil 14 cm.

Figure 72a: Dyke (D) cutting pillowed flow (Pf) I, CBRB (see Figure 64). Scale, pencil 14 cm.

predominant with 0.2-2.5 mm-size plagioclase phenocrysts and 1-3.5 mm-size phenocryst clusters, respectively, in matrices of feldspar microlites. Ophitic and sub-ophitic textures are also common (Appendix 4).

Interpretation

Similarities in compositions of flows and dykes, and restriction of dykes within single flow units justify a synvolcanic interpretation. Dyke discontinuity is typical of narrow intrusions that inject for short distances before cooling and solidifying (Bruce and Huppert, 1990). Intrusions oriented perpendicular to bedding and terminating with blunt ends or propagating into pillows are often classified as feeder dykes (Yamagishi, 1991; Kano et al.. 1993). These parallel dykes indicate the manner in which overlying flows were fed. Irregular contacts between intrusions and flows indicate that the flows were not completely solidified during dyke injection.

5.3   Felsic Volcanic Facies

5.3.1   Massive Volcaniclastic Rocks

Felsic tuff-lapilli tuff at locality F is up to 60 m thick. but is generally poorly exposed. The deposits appear massive with no evidence of grading or stratification and contain <3 mm-size quartz crystals. These volcaniclastic deposits overlie massive breccia and are locally interstratifed with mafic pillow breccia (Figures 73, 74a). The contact between felsic and mafic units is irregular, but abrupt (Figure 74a). Pillow breccia fragments at locality F are similar to those at locality E in terms of form and vesicularity. Vesicles, 1-5 mm in size, comprise up to 40% of pillow breccia fragments at locality F (Figure 74b). Lapilli tuff contains 2-45 mm-size, rounded felsic fragments in a fine- to

30m—

pillow breccia

Figure 74b

interstratification
of felsic and mafic
facies

irregular contact
(Figure 74a)

felsic coarse
tuff

0m—
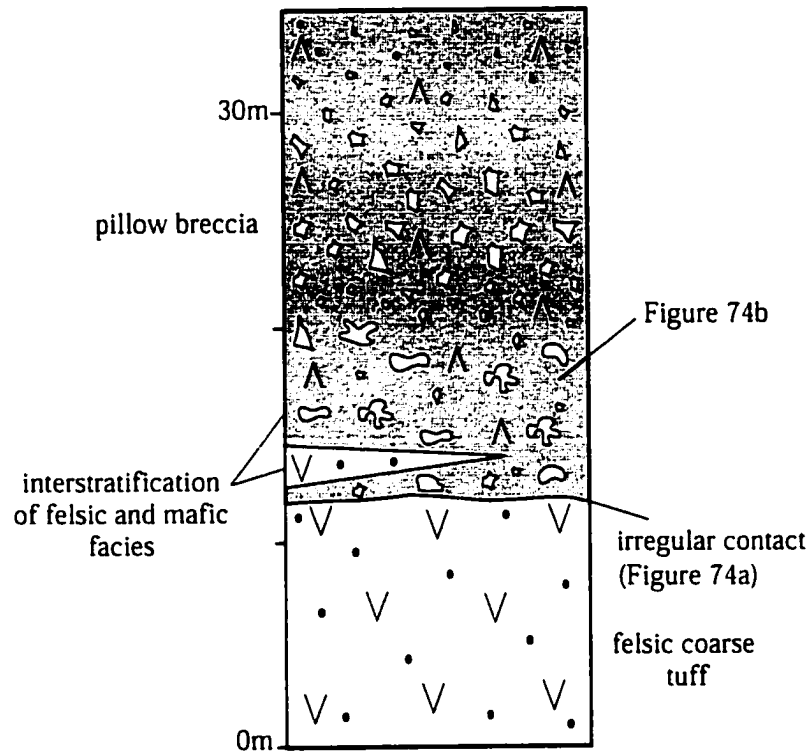
Figure 73: Sketch of the contact and intercalation of felsic tuff
and mafic pillow breccia at locality F, Central Beaulieu River belt.

Figure 74a: Depositional contact (dashed line) between felsic tuff (F) and mafic pillow breccia (M), locality F, CBRB (see Figure 73). Scale, pencil 14 cm.

Figure 74b: Vesicular mafic fragment (M) in pillow breccia 2 m from contact with felsic tuff, locality F, CBRB. Scale, pencil 4 cm.

coarse-grained matrix (Figure 75a), and overlies massive breccia. Petrographically, the

tuff-lapilli tuff contains up to 25% quartz and feldspar crystals, and lithic fragments.

Quartz crystals are anhedral and broken and are 0.1-3 mm in size, whereas 0.1-1.5 mm

plagioclase crystals are subhedral and broken (Appendix 4). Lithic fragments, 2-45 mm

in size, exhibit a granular texture with quartz and feldspar crystals (Figure 75b). The

carbonate/chlorite-altered matrix is composed of recrystallized quartz and feldspar with

dark patches or "wisps" of altered glass.

Interpretation

The gradational contact between the felsic tuff and overlying pillow breccia and the

paucity of explosive debris support a subaqueous depositional setting. The apparent

massive nature of the tuff-lapilli tuff and the anhedral to subhedral broken crystals are

consistent with deposition under debris flow conditions where material may have

slumped down from a subaqueous felsic edifice. However, the rounded pebble-size

fragments indicate that local reworking must have occurred. Unfortunately, the lack of

outcrop precludes an unambiguous interpretation of the depositional process. Three lines

of evidence support a synchronous origin for the tuff-lapilli tuff, felsic flows, and felsic

breccia: 1) the three facies are spatially restricted within one narrow area (locality F), 2)

the crystals, lithic fragments, and pebbles in the tuff-lapilli tuff are all silicic in

composition, and 3) the granular texture of some lithic fragments suggest a cognate

origin, whereby pieces of a felsic edifice were eroded during magma ascent. The

volcaniclastic deposits are thus considered pyroclastic in origin and can be classified as

tuff to lapilli tuff, based on the classification of Fisher (1961).
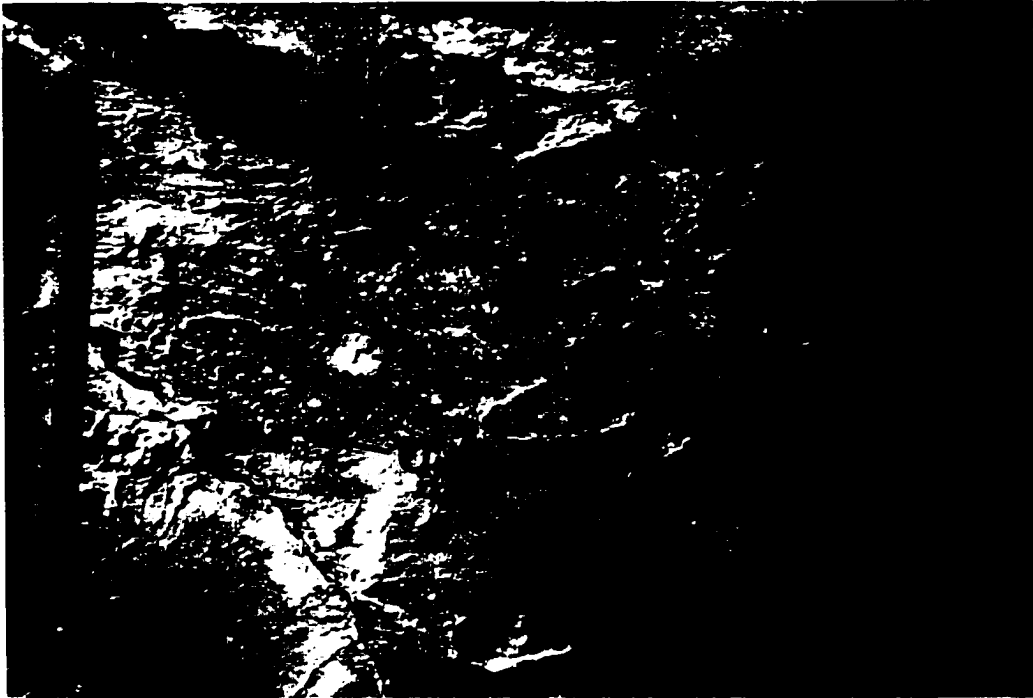
Figure 75a: Felsic lapilli tuff with rounded felsic fragments (F) and quartz crystals (Q) in a fine tuff matrix, locality F, CBRB. Scale, pencil 14 cm.
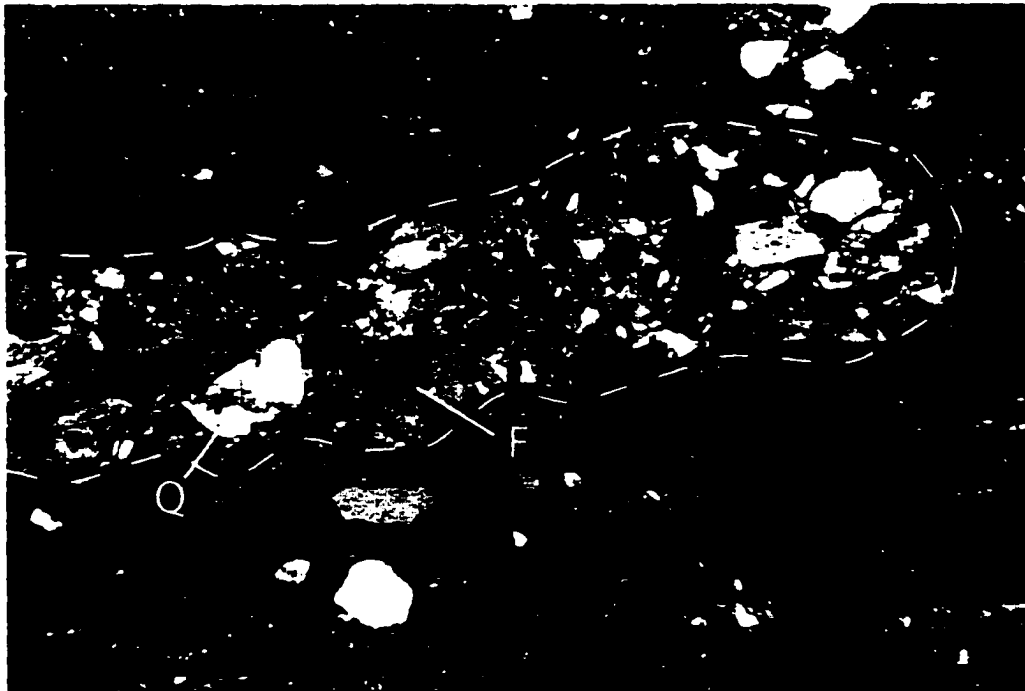
Figure 75b: Lithic fragment (outlined) in felsic lapilli tuff containing quartz (Q) and feldspar (F). The granular texture may indicate a cognate origin. Field of view is 6 mm. Thin section in xpl.

5.3.2   Massive Porphyritic Flows

Massive porphyritic flow units at locality F, up to 40 m thick, are characterized by 0.2-5 mm-size quartz and feldspar phenocrysts (Figure 76a, b). An upper contact between a porphyritic flow and felsic volcanic breccia is gradational, but basal contacts with other felsic and mafic facies were not identified. In thin section, individual flows can be distinguished based on phenocryst type and percentage. Three separate flow types were identified: 1) flows with <5-10%, 0.2-5 mm quartz phenocrysts in a micropoikilitic matrix, 2) flows with <5 %, 0.2-2 mm quartz and feldspar phenocrysts, and up to 2.5 mm glomerophenocrysts in a recrystallized quartz-feldspar matrix, and 3) flows with 10-30%, 0.7-2.5 mm quartz and feldspar phenocrysts, and 1-3.5 mm glomerophenocrysts in a recrystallized quartz-feldspar matrix. The latter flows contain devitrification rims around quartz phenocrysts (Figure 76c; Appendix 4). Feldspar phenocrysts in all flows are subhedral to euhedral.

Interpretation

Below its liquidus temperature, the viscosity of a silicic lava is strongly affected by melt temperature and water content. When these factors decrease, short, thick flows or domes with carapace breccias will result (Fink, 1983; Yamagishi and Dimroth, 1985). The ambient hydrostatic pressure of seawater is generally higher than the volatile content of the magma (Cas, 1992) so that subaqueous explosive facies are less common than in subaerial settings. The upper, gradational flow/breccia contact at locality F is consistent with high viscosity/low temperature extrusion of silicic lava followed by quench fragmentation of lava surfaces (autobrecciation) (Fink, 1983). The absence of flow banding and lobes, typical features of silicic flows and domes, and flow top breccia in some areas, indicates that the porphyritic units could be intrusive. However, these units

Figure 76c: Quartz-feldspar porphyritic flow containing quartz phenocrysts (Q) with devitrification rims (R) from locality F, CBRB. Field of view is 1.5 mm. Thin section in xpl.

Figure 76a: Quartz-feldspar porphyritic flow from locality F, CBRB. Note the up to 5 mm-size quartz phenocrysts (Q). Scale, pen 14 cm.

Figure 76b: Quartz-feldspar porphyritic flow containing subhedral quartz (Q) and plagioclase feldspar (F) phenocrysts. Field of view is 6 mm. Thin section in xpl.

are considered extrusive because no chilled margins were found and there are no intervening mafic deposits which would support an intrusive origin. Variations in the amounts and types of phenocrysts reflect the presence of at least three separate flow or dome types.

5.3.3 Massive Volcanic Breccia

Massive felsic breccia units at locality F are divided into two distinct subfacies based on textures. percentage matrix. and contacts with overlying and underlying units. Coherent breccia. 5-20 m thick. gradationally overlies felsic flows and is composed of angular to subangular. 4-15 cm-size felsic fragments (Figure 77a). The fragments and matrix are both beige. making it difficult to distinguish individual boundaries. A jigsaw fit texture is common and the fragments are locally flow banded (Figure 77b). Both the matrix and the fragments have undergone granular crystallization where the original glassy matrix is recrystallized to equigranular quartz and feldspar (Appendix 4). Disorganized felsic breccia. up to 60 m thick, is overlain by coarse tuff-lapilli tuff. but the upper contact was not identified. Subrounded to subangular fragments, 2-20 cm in size. are randomly set in a fine-grained quartz-feldspar matrix altered by silica. sericite. and carbonate. The fragments are chiefly composed of microcrystalline quartz and the elevated silica content (see section 5.4.2; sample w9-42) indicates that the deposits have undergone significant silicification.

Interpretation

The gradational contact between a felsic flow and overlying breccia, the jigsaw fit texture, and the fact that all fragments are compositionally similar to felsic flows. indicates that the coherent breccia is an autoclastic flow breccia (e.g. Fisher and

Figure 77a: Felsic breccia at locality F, CBRB, containing subangular fragments (some outlined) that are the same composition as the matrix. Scale, pen 14 cm.
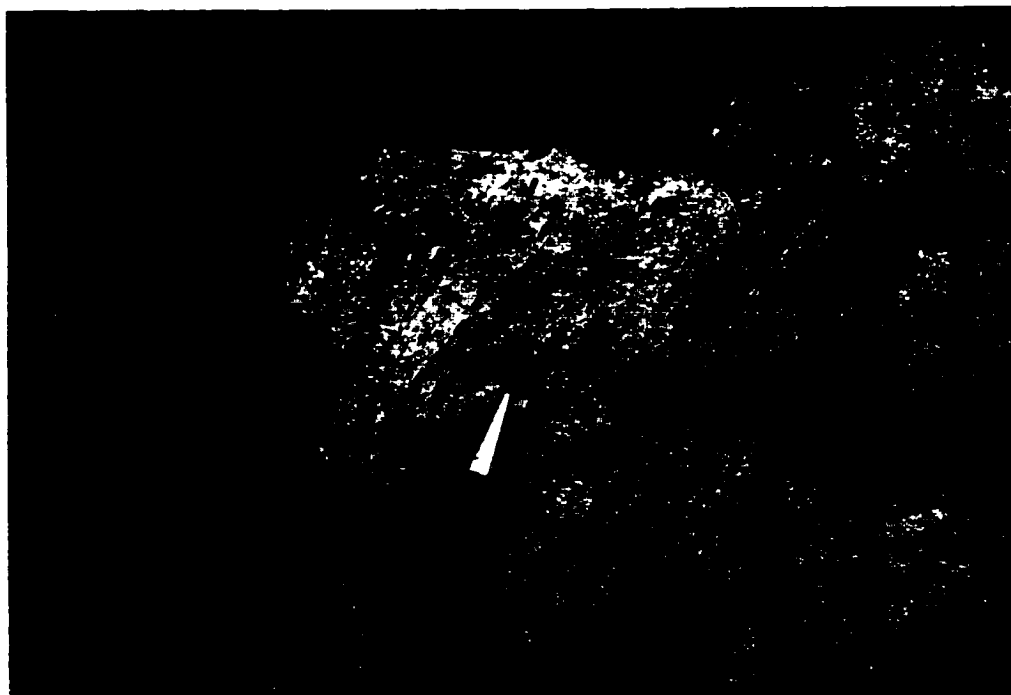
Figure 77b: Flow banded (dashed lines) fragment in felsic breccia, locality F, CBRB. Scale, pen 7 cm.

Schmincke, 1984; McPhie et al., 1993). Flow breccia commmonly characterizes the margins of lava flows and develops due to chilling of a flow surface, thus increasing the viscosity. The liquid flow interior brecciates the solidified top as it moves beneath it (Fink, 1983; Gibson, 1999; Ayres and Peloquin, 2000). In contrast, the subangular to subrounded fragments and their random orientation in the disorganized breccia is consistent with fracturing and avalanching at flow or dome fronts (e.g. De Rosen-Spence et al., 1980; Ayres and Peloquin, 2000). A pyroclastic origin with minimal reworking is inferred based on the monolithic nature of the breccia and the close spatial association with the felsic tuff-lapilli tuff, porphyritic flows, and flow breccia.

5.4   Geochemistry

5.4.1   Sampling Procedure

A total of 31 samples was collected from the Beaulieu River belt at Stanley Lake; 15 are presented in this thesis (Figure 78). Eleven samples were collected west of the Beniah Lake fault system and unconformity between the sedimentary and volcanic rocks, and four samples were collected east of the fault (Figure 78). Only a small number of samples is considered because high degrees of carbonatization, silicification and sulfide alteration significantly changed the composition of most of the rocks in the study area. The samples selected are the least altered, show generally homogeneous grain size, and have the lowest amygdule/vesicle percentages in the study area. The volcanic facies sampled include mafic pillowed and massive flows, mafic dykes, felsic massive flows, and a felsic tuff.

Beaulieu Rapids Formation

Quartz-rich sandstone

Siltstone-sandstone

Conglomerate

Porphyry stocks

Beaulieu River Volcanic Belt

Mafic volcanic rocks

Felsic volcanic rocks

□ Group 1 tholeiitic to calc-alkaline basalt to andesite flows

○ Group 2 tholeiitic to calc-alkaline basalt dykes

△ Group 3 calc-alkaline rhyolites

Quartz arenite

Gneiss (Sleepy Dragon Complex)

1 km

Figure 78: Lithological map illustrating 15 sample sites in the Central Beaulieu River belt. Distinct groups are indicated using different symbols (see legend).

5.4.2 Results

Samples from the Central Beaulieu River belt are divided into three main groups: 1) Group 1 tholeiitic to calc-alkaline, basalt to andesite flows, 2) Group 2 tholeiitic to calc-alkaline basalt dykes, and 3) Group 3 calc-alkaline rhyolites (Table 10). Tholeiitic and calc-alkaline basalts and andesites are grouped together because there were difficulties in distinguishing between them using major and trace elements. Most of the samples collected are transitional between tholeiitic and calc-alkaline.

Group 1 Tholeiitic to Calc-alkaline, Basalt to Andesite Flows

Samples from Group 1 were collected east and west of Stanley Lake, but the eastern samples were too altered for geochemical analysis. Based on the minimal sample set, there are no compositional changes with stratigraphy. Group 1 rocks are basaltic to andesitic with SiO_2 values ranging from 50-61 wt% and FeO^*/MgO ratios of 0.8-2.4. On FeO^*/MgO vs FeO^*, FeO^*/MgO vs TiO_2, and FeO^*/MgO vs SiO_2 variation diagrams, only samples c8-28, c8-29, and c9-38 plot consistently as tholeiitic, whereas sample c8-26 falls in the calc-alkaline field on all three diagrams (Figure 79). The remaining four samples plot in both the tholeiitic and calc-alkaline fields on different diagrams, suggesting a transitional nature. When plotted on a La/Yb diagram, sample c8-28 falls in the transitional field, c9-47 is on the border between transitional and tholeiitic, whereas the other five samples plot in the calc-alkaline field (Figure 80). Determining differentiation trends is problematic because of the small sample suite and scatter. Most Group 1 rocks are enriched in the LREE, with $(La/Yb)_n$ ratios of 3.7-5.72 (Figure 81; Table 11). The patterns are smooth, and concentrations of the REE remain constant with respect to one another. Samples c8-28 and w9-47 have different slopes with $(La/Yb)_n$

Table 10: Major and trace element data for samples from the Central Beaulieu River belt (ND=no data) *=total Fe as Fe2O3. All samples chosen for geochemical analysis are displayed. Altered samples were eliminated during sample preparation.

Sample	C8-26	C8-28	C8-29	C8-30	W9-38	W9-39	W9-47	W9-49	C8-21	C8-27	C8-32	W9-42
Group	Group 1	Group 1	Group 1	Group 1	Group 1	Group 1	Group 1	Group 1	Group 2	Group 2	Group 2	Group 3
SiO2 (wt%)	60.87	50.34	50.11	52.27	54.12	59.01	52.23	53.75	51.45	49.28	53.94	86.65
TiO2	0.98	1.28	1.2	1.37	2.16	1.15	0.95	1.19	1.19	1.76	1.08	0.09
Al2O3	13.76	15.26	13.65	16.66	13.28	12.16	15.24	15.58	18.46	14.55	15.97	6.09
Fe2O3*	9.53	12.31	10.63	9.41	14.16	8.02	8.56	11.4	9.16	14.73	10.82	0.48
MnO	0.25	0.17	0.25	0.23	0.18	0.2	0.23	0.13	0.18	0.2	0.14	0.02
MgO	7.14	5.92	4.31	4.57	5.32	3.8	4.05	5.92	5.14	5.68	5.58	0.34
CaO	0.52	4.5	7.42	6.97	5.81	5.33	7.88	5.92	5.63	5.78	5.36	0.64
Na2O	1.82	3.88	3.73	0.9	2.7	3.87	3.73	3.12	4.49	3.66	2.6	1.41
K2O	1.08	0.23	0.46	1.46	0.79	0.11	0.18	0.66	0.49	1.93	0.64	2.72
P2O5	0.26	0.15	0.23	0.24	0.36	0.45	0.12	0.21	0.23	0.31	0.2	0.03
LOI	3.98	6.68	7.9	6.22	1.67	5.72	6.82	2.7	4.34	-	3.51	1.09
Total	100.19	101.72	99.8	100.3	100.55	99.82	99.99	100.5	100.76	98.88	99.84	99.56
FeO*/MgO	1.2	1.87	2.22	1.85	2.4	1.9	1.9	1.73	1.6	2.33	1.75	1.27
Cr (ppm)	19	173	27	134	42	122	304	130	76	118	181	<4
Ni	21	97	35	86	30	48	175	77	67	88	89	<3
Co	41	59	42	46	59	40	60	58	44	72	51	<5
Sc	ND	ND	14	ND	ND	ND	ND	ND	ND	ND	ND	ND
V	152	208	200	227	307	151	197	190	193	271	186	12
Cu	46	57	57	26	29	8	106	35	40	35	37	22
Pb	16	12	8	25	15	7	6	8	13	13	10	112
Zn	16	108	11	172	131	105	98	114	95	122	104	32
Rb	91	4	32	48	19	3	3	24	13	86	16	49
Ba	26	71	269	604	428	92	62	376	313	330	260	309
Sr	482	60	142	408	289	167	157	307	337	64	272	28
Ga	18	15	14	19	19	17	15	17	21	19	20	4
Ta	0.76	ND	ND	0.59	0.59	0.66	ND	0.53	0.63	0.61	0.52	0.82
Nb	10.58	5.19	21	8.73	10.7	13.25	2.98	7.9	9.2	10.07	7.72	8.05
Cs	0.42	0.22	ND	3.19	4.13	0.67	0.12	4.93	2.47	3.35	2.59	0.14
Hf	4.87	2.63	ND	3.8	3.68	4.07	1.56	3.5	3.96	3.82	3.49	2.22
Zr	194	98	144	159	149	180	58	152	168	159	145	71
Y	29	29	31	23	33	33	29	25	28	34	23	27
Th	5.7	1.74	2	2.78	3.07	2.27	0.56	2.63	3.84	1.47	2.79	13.57
U	1.57	0.37	1	0.7	0.75	0.58	0.16	0.62	0.88	0.36	0.67	5.35
Zr/Y	6.69	3.38	4.65	6.91	4.52	5.45	2	6.08	6	4.68	6.3	2.63
Ti/V	38.68	36.92	36	36.21	42.21	45.7	28.93	37.58	36.99	38.97	34.84	45

Table 10: continued

Sample	W9-45	W9-46	W9-51
Group	Group 3	Group 3	Group 3
SiO2 (wt%)	64.4	66.19	66.59
TiO2	0.6	0.56	0.55
Al2O3	15.35	13.93	12.89
Fe2O3*	4.95	5.58	5.66
MnO	0.05	0.15	0.08
MgO	3.87	5.25	6.66
CaO	1.49	0.22	0.17
Na2O	0.18	2.71	ND
K2O	5.53	2.57	2.63
P2O5	0.13	0.12	0.12
LOI	3.22	2.38	3.78
Total	99.77	99.66	99.13
FeO*/MgO	1.15	0.96	0.76
Cr (ppm)	78	69	26
Ni	33	24	11
Co	17	23	26
Sc	ND	ND	ND
V	98	91	78
Cu	22	84	6
Pb	6	73	15
Zn	55	166	73
Rb	118	73	78
Ba	449	539	217
Sr	5	24	ND
Ga	21	15	18
Ta	0.96	0.94	1.27
Nb	12.06	11.11	11.87
Cs	2.43	0.82	0.51
Hf	5.23	5.05	5.21
Zr	191	190	186
Y	26	13	39
Th	14.62	7.46	15.25
U	3.96	3.61	6.01
Zr/Y	7.35	14.62	4.77
Ti/V	36.73	36.92	42.31
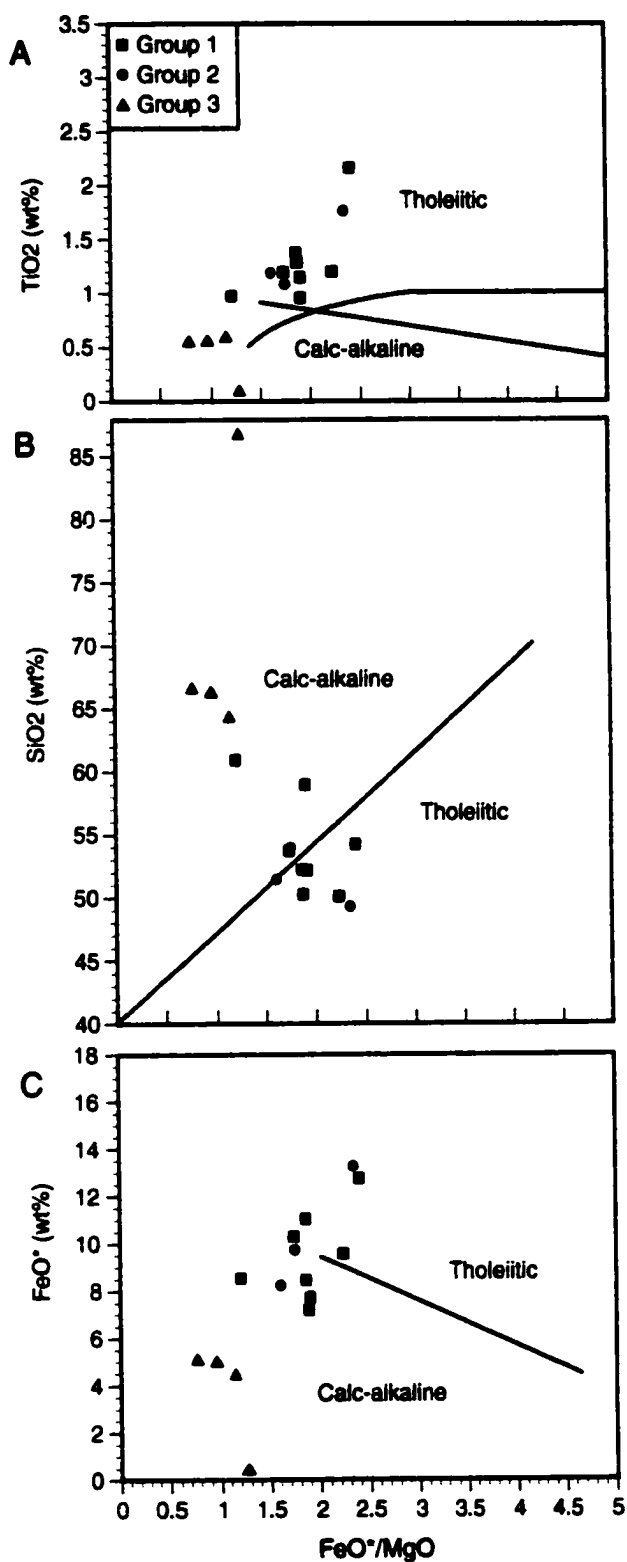
Figure 79: Variation diagrams demonstrating the behaviour of (A) TiO2 wt% vs. FeO*/MgO, (B) SiO2 wt% vs. FeO*/MgO, and (C) FeO* wt% vs. FeO*/MgO in samples from Group 1 tholeiitic to calc-alkaline basalt to andesite flows, Group 2 tholeiitic to calc-alkaline basalt dykes, and Group 3 calc-alkaline rhyolites. Sample set is too small to determine tholeiitic or calc-alkaline trends. Diagrams after Miyashiro (1974).
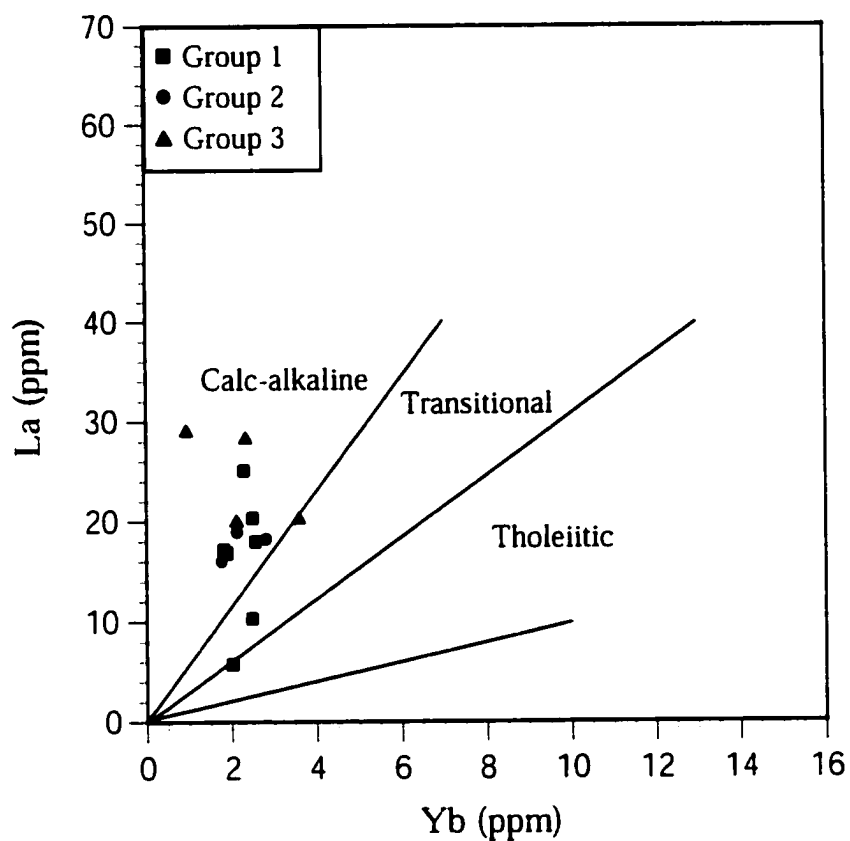
Figure 80: Variation diagram illustrating the behaviour of La vs. Yb in samples from Group 1 tholeiitic to calc-alkaline basalt to andesite flows (squares), Group 2 tholeiitic to calc-alkaline basalt dykes (circles), and Group 3 calc-alkaline rhyolites (triangles) in the Central Beaulieu River belt. Diagram after Barrett and MacLean (1997).
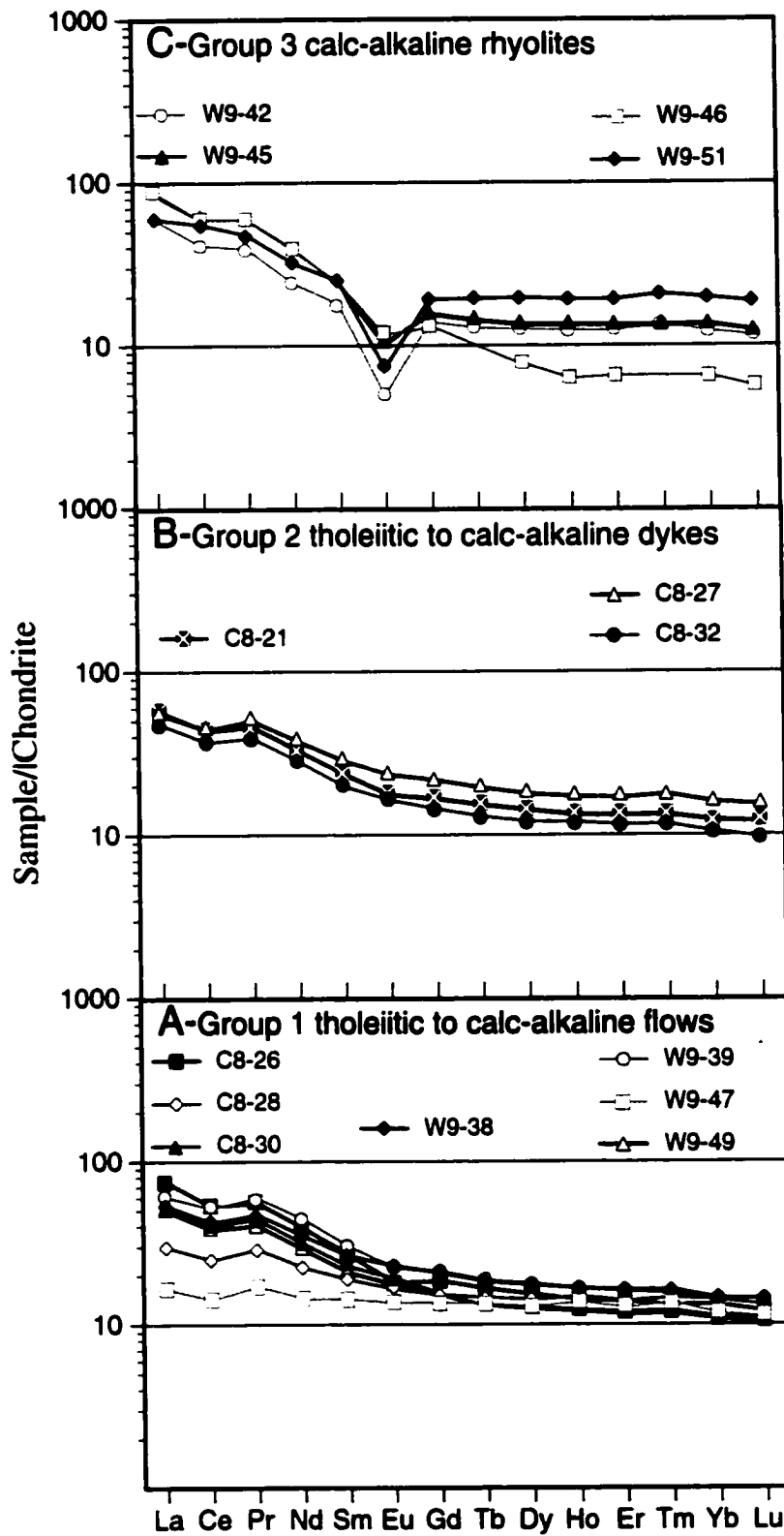
Figure 81: Chondrite-normalized REE abundances for samples from the CBRB. Normalizing values after Haskin et al. (1968).

Table 11: REE data (in ppm) for samples from the Central Beaulieu River belt

Sample	C8-26	C8-28	C8-30	W9-38	W9-39	W9-47	W9-49	C8-21	C8-27	C8-32	W9-42	W9-45	W9-46	W9-51
Group	Group 1	Group 1	Group 1	Group 1	Group 1	Group 1	Group 1	Group 2	Group 2	Group 2	Group 3	Group 3	Group 3	Group 3
La	24.84	9.91	16.87	17.7	20.05	5.5	16.6	18.58	17.96	15.71	19.59	28.02	28.68	19.82
Ce	46.61	21.98	35.41	37.13	45.63	12.58	33.36	38.01	38.32	32.4	36.14	52.26	52.15	48.76
Pr	6.27	3.25	4.94	5.28	6.72	1.94	4.52	5.17	5.56	4.41	4.4	6.65	6.66	5.35
Nd	23.39	13.44	18.74	20.91	26.64	8.66	17.37	19.64	22.29	16.96	14.51	23.29	23.23	19.27
Sm	4.83	3.42	4.09	4.77	5.49	2.59	3.75	4.25	5.09	3.59	3.24	4.39	4.42	4.51
Eu	1.24	1.15	1.32	1.58	1.53	0.94	1.21	1.21	1.6	1.13	0.34	0.7	0.8	0.5
Gd	4.6	3.8	3.83	5.16	5.28	3.4	3.78	4.14	5.37	3.59	3.46	3.88	3.22	4.79
Tb	0.78	0.69	0.61	0.86	0.88	0.63	0.61	0.72	0.91	0.61	0.6	0.67	ND	0.91
Dy	4.59	4.32	3.73	5.24	5.38	3.88	3.85	4.27	5.34	3.63	3.78	4.02	2.33	5.91
Ho	1	1.04	0.84	1.17	1.16	0.97	0.85	0.93	1.2	0.84	0.87	0.94	0.44	1.35
Er	2.76	2.79	2.3	3.28	3.22	2.54	2.38	2.63	3.38	2.31	2.47	2.66	1.3	3.84
Tm	0.4	0.44	0.35	0.49	0.46	0.41	0.36	0.4	0.53	0.35	0.41	0.4	ND	0.62
Yb	2.63	2.82	2.15	2.9	2.83	2.34	2.21	2.47	3.16	2.1	2.45	2.69	1.3	3.92
Lu	0.41	0.45	0.35	0.49	0.49	0.38	0.38	0.41	0.52	0.33	0.39	0.42	0.19	0.63
La/Yb(n)	5.72	2.13	4.76	3.7	4.29	1.42	4.55	4.56	3.44	4.53	4.85	6.31	13.37	3.06
Tb/Yb(n)	1.26	1.04	1.21	1.26	1.32	1.15	1.17	1.24	1.23	1.24	1.04	1.06	ND	0.99

ratios of 2.13 and 1.42, respectively (Figure 81). All of the samples from Group 1 show a negative Ce anomaly. On the incompatible element diagram, the samples have pronounced Nb and Ti depletions, and most are enriched in Zr (Figure 82).

Group 2 Tholeiitic to Calc-alkaline Basalt Dykes

Group 2 samples were collected west of Stanley Lake. These basalt dykes cut mafic flows and terminate within them, and contain the same foliation patterns as the surrounding volcanic units, indicating a synvolcanic origin. Group 2 samples have SiO_2 wt% ranging from 49-54 and $FeO*/MgO$ ratios of 1.6-2.3, and plot in both the tholeiitic and calc-alkaline fields on SiO_2 vs $FeO*/MgO$, $FeO*$ vs $FeO*/MgO$, and TiO_2 vs $FeO*/MgO$ diagrams (Figure 79). All dykes fall in the calc-alkaline field on the La/Yb plot (Figure 80) and are LREE enriched with $(La/Yb)_n$ ratios of 3.44-4.56 (Figure 81; Table 11). REE patterns are smooth with negative Ce anomalies and overall REE abundances increase and decrease systematically (Figure 81). The three dykes sampled display Nb and Ti depletions and Zr enrichments on the incompatible element diagram (Figure 82), similar to Group 1 flows.

Group 3 Calc-alkaline Rhyolites

Calc-alkaline rhyolitic flows (w9-45, w9-51), a tuff (w9-46), and volcanic breccia (w9-42) were collected near the eastern shore of Stanley Lake (Figure 78). The felsic sequence is interstratified with mafic rocks as indicated by the gradational contact between felsic volcanic sandstone and mafic pillow breccia. Group 3 samples contain 64-
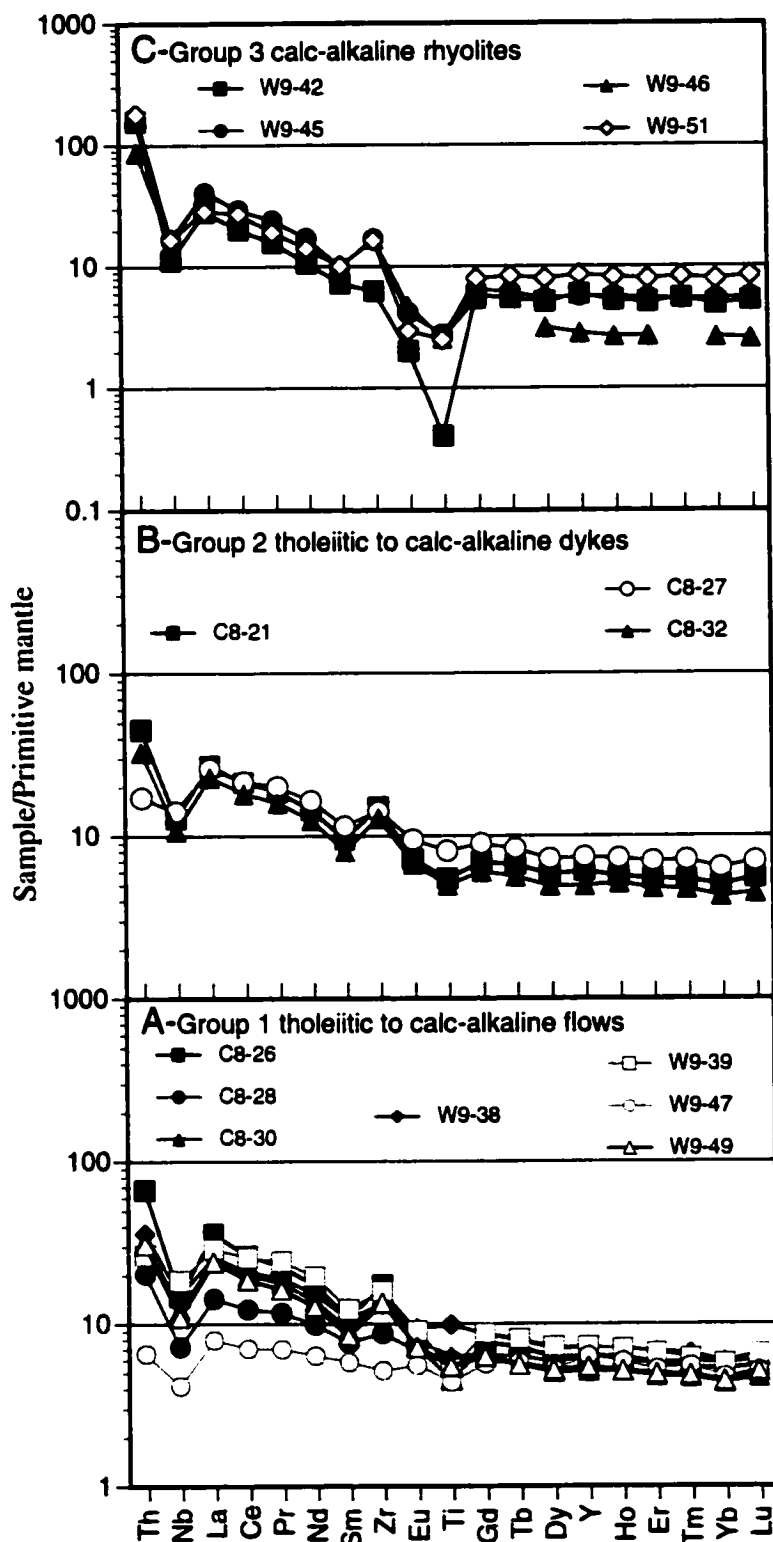
Figure 82: Primitive mantle-normalized incompatible element abundances for samples from the CBRB. Normalizing values after Sun and McDonough (1989).

87 % SiO_2, but the latter value, determined from separated breccia fragments, is probably a result of silicification. FeO^*/MgO ratios range from 0.7-1.3. All four felsic samples plot in the calc-alkaline fields on SiO_2 vs FeO^*/MgO, FeO^* vs FeO^*/MgO, and TiO_2 vs FeO^*/MgO diagrams, but w9-42 has lower TiO_2 and FeO^* values and a significantly higher SiO_2 value than the other samples (Figure 79). Group 3 rocks are scattered from calc-alkaline to transitional on the La/Yb plot (Figure 80). This scatter is reflected in the $(La/Yb)_n$ ratios of 3.06-6.31 for three of the samples and 13.37 for w9-46 (tuff), whereas $(La/Sm)_n$ ratios are very similar, ranging from 2.41-3.56 (Table 11). The samples are LREE enriched and display relatively smooth patterns with some slight Ce depletions relative to the other REE and significant negative Eu anomalies (Figure 81). On the incompatible element diagram, Group 3 rocks display strong depletions in Nb and Ti and are enriched in Zr (Figure 82).

5.4.3   Interpretation

The interstratification of tholeiitic and calc-alkaline basalts, andesites and rhyolites, and similar compositions for mafic dykes and mafic flows indicate that the volcanic units at Stanley Lake are petrogenetically related. LREE enriched samples from Groups 1 and 2 have relatively flat HREE patterns with $(Tb/Yb)_n$ ratios of 1.04-1.32 (Table 11). Samples w9-47 and c8-28, which are only slightly enriched in LREE, have similar $(Tb/Yb)_n$ ratios of 1.15 and 1.04, respectively. These are the only two samples that plot close to the tholeiitic field on the La/Yb diagram and fall in the tholeiitic field in at least 2 of the 3 variation diagrams (Figures 79, 80). The lower $(La/Yb)_n$ ratios, but similar HREE abundances indicate that there was no difference in source, but instead, the variations may be artifacts of crustal contamination (e.g. Barley, 1986). Lambert et al. (1992) showed that Nd-isotope geochemistry of the volcanic rocks in the Beaulieu River belt

indicates mixing of a depleted mantle source with sialic crust. Additional support for

crustal contamination is illustrated on the incompatible element diagram where negative

Ti anomalies characterize Groups 1 and 2 (Figure 82). $(Th/La)_n$ ratios as high as 1.4 for

the basalts and andesites and 5 for the rhyolites are consistent with crustal contamination.

ε_{Nd} values were not determined for the Central Beaulieu River belt because most of the

samples underwent substantial alteration, as evident from the sample scatter on the

variation diagrams and by some major and trace element discrepancies. For example,

decreases in MgO and TiO_2 are expected with an increase in Zr, which would reflect the

removal of pyroxene, olivine, and Fe-Ti oxide, but the data are not consistent with the

expected trend (Table 10).

Although crustal contamination may have played a role in the development of the

Central Beaulieu River belt, the Nb and Ti depletions are also consistent with subduction-

related processes. The subduction imprint is further supported by the presence of calc-

alkaline basalts, andesites and rhyolites. The calc-alkaline rhyolites of Group 3 have

$(Tb/Yb)_n$ ratios of 0.99-1.06, except for sample w9-46 whose $(Tb/Yb)_n$ ratio could not be

determined, but whose $(Gd/Yb)_n$ ratio is 1.99. This discrepancy can be attributed to the

fact that w9-46 is a volcaniclastic rock, and therefore may contain components derived

from a wider variety of sources than the felsic flows and autobreccia sampled. The HREE

for Group 3 samples are very similar to those of the samples from Groups 1 and 2,

indicating that the basalts, andesites, and rhyolites all had a common source (e.g. Kay et

al., 1982). This is further displayed on a Zr vs. $(Ce/Yb)_n$ diagram, where most samples

display a positively correlated array with only w9-42 (felsic breccia) and w9-46 (felsic

tuff) plotting apart from the dominant trend (Figure 83). The negative Eu anomaly

associated with Group 3 calc-alkaline samples reflects the retention of Eu in a feldspar-

rich source (continental crust) during partial melting and/or the removal of feldspar

during crystal fractionation (e.g. Rollinson, 1993).
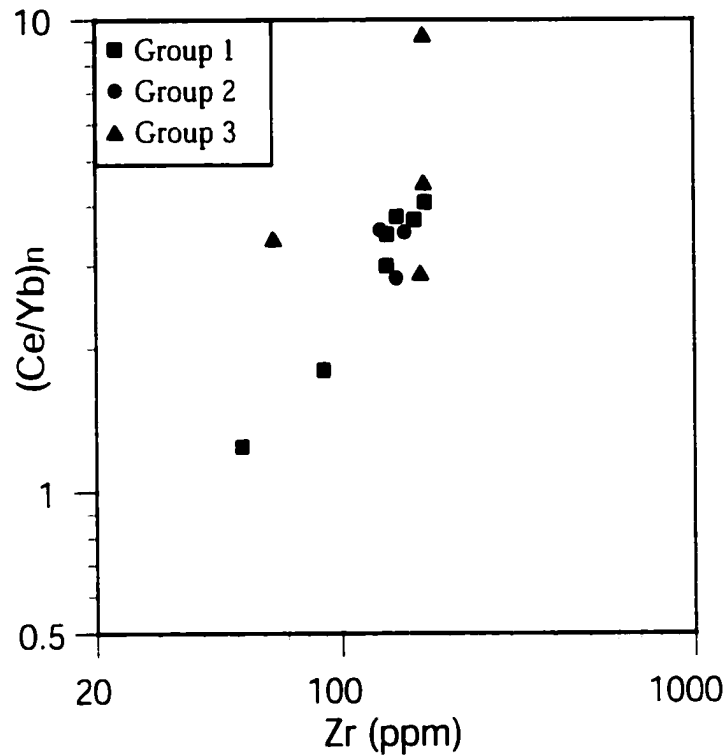
Figure 83: (Ce/Yb)n vs. Zr for samples from Group 1 tholeiitic to calc-alkaline basalt to andesite flows (squares), Group 2 tholeiitic to calc-alkaline basalt dykes (circles), and Group 3 calc-alkaline rhyolites (triangles) from the Central Beaulieu River belt. Diagram after Miller et al. (1994). Most of the samples plot in a positively correlated array, indicating that they had a common source. Only the felsic breccia and tuff depart from the general trend, suggesting that they had mixed sources or sources not represented in the sample set.

Tholeiitic basalt magmas are generated by melting of mantle peridotite, which is controlled by the composition and temperature of the mantle (Grove, 2000). The relatively flat HREE patterns for the more basic rocks in the study area can be attributed to melting of spinel peridotite at depths of 40-60 km (e.g. Manetti et al. 1979; McKenzie and O'Nions 1991). Crystallization of basaltic magma combined with partial melting of crustal material leads to silica-rich compositions and the formation of dacites and rhyolites (Rogers and Hawkesworth, 2000). Formation of calc-alkaline intermediate and silicic magmas is complex and is often the result of processes that occur at convergent margins. In this type of setting, the generation of magma is dependent on fluid interaction with the mantle when H_2O is released from the subducted slab. Slight negative Ce anomalies for all groups can be attributed to interaction with seawater where trivalent Ce is oxidized to an insoluble tetravalent state (e.g. De Baar et al., 1983). Alternatively, the apparent negative anomalies could be related to analytical error of Pr.

5.5   Depositional Setting of the Central Beaulieu River Belt

Mafic volcanic facies at locality E in the Central Beaulieu River belt resemble the thin pillowed and massive flows and abundant pillow breccia at locality A in the Point Lake belt. Although the two study areas can be compared with mafic subaqueous volcanism on a seamount, the relative variations of facies types, volcanic structures, and percentage of vesicularity are characteristic of different depths and locations with respect to the source.

Stratified pillow breccia and hyaloclastite and high vesicularity in the Central Beaulieu River volcanic belt are characteristic features of the uppermost parts of subaqueous edifices (e.g. Staudigel and Schmincke, 1984; Figure 84a). Scoriaceous, glass shard-rich, stratified hyaloclastite developed from wave reworking and redeposition
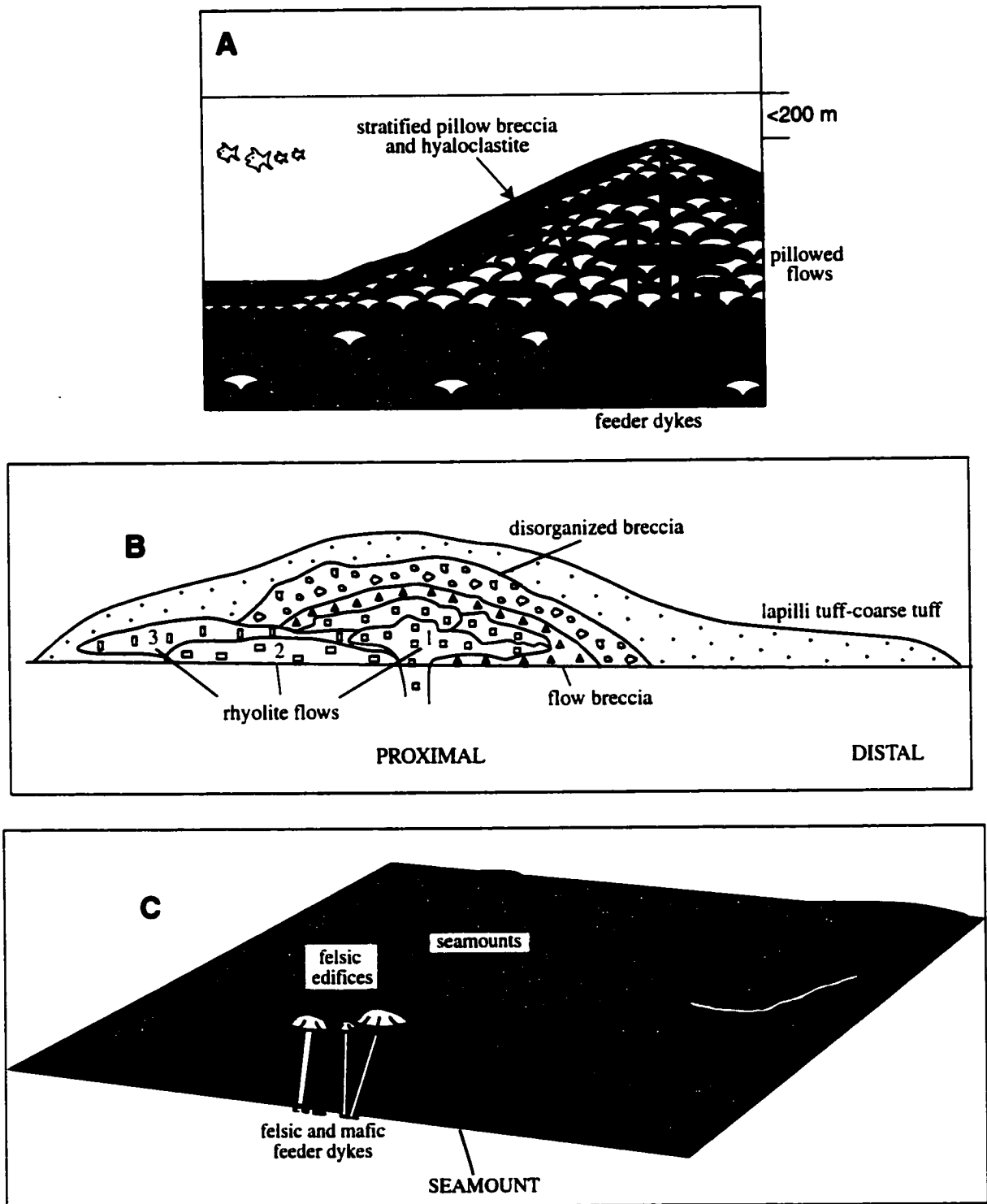
Figure 84: Depositional setting of the Central Beaulieu River belt. (A) Model illustrating the inferred location of locality E on a seamount. The study area is represent by the uppermost facies (thin pillowed and massive flows, abundant stratified pillow breccia and hyaloclastite). (B) Model demonstrating the felsic facies associated with the inferred dome-flow complex at locality F. (C) Subaqueous depositional setting of the Central Beaulieu River belt illustrating the development of felsic edifices at the top of a seamount.

along the flanks of an edifice in relatively shallow water (<200 m). Based on the lateral and vertical facies associations with coherent pillowed flows, the stratified pillow breccia is interpreted to have developed at the head of steep flow fronts in shallow water (e.g. Dimroth et al., 1978). In addition, high vesicularity (20-49%) in pillowed-lobate and massive flows, and in pillow breccia, supports a shallow water setting (e.g. Moore and Schilling, 1973). Locality E in the Beaulieu River volcanic belt is a good representative of the topmost portion of a seamount (Figure 84a).

Subaqueous silicic lavas form as domes, cryptodomes, or tabular masses (flows) (De Rosen-Spence et al., 1980; Yamagishi and Dimroth, 1985; Cas, 1992; Gibson, 1999). Domes are "mounds of volcanic rock that form as lava flows onto the surface and amasses over a vent" and a cryptodome is " an accumulation of molten material just beneath the surface" (Fink and Anderson, 2000). Cryptodomes are normally characterized by hyaloclastite and peperite at the interface between the intruding magma and the sedimentary material into which it intrudes (Cas, 1992; McPhie et al., 1993). Distinguishing between lava flows and domes, however, is problematic because domes are commonly composed of numerous flows and the facies associated with flow advance and dome extrusion are similar. Remnant feeder dykes, if preserved, may differentiate domes from flows (McPhie et al., 1993). Massive flows, hyaloclastite, autobreccia, feeder dykes, and reworked debris are all common components of dome complexes (Cas, 1992). These complexes are associated with short (<2 km) flows that develop proximal to the feeding vent or fissure (Gibson, 1999). The domes may comprise sequences of different lavas that are distinguished based on phenocryst abundance and size (Cas, 1992). Unlike basaltic flows that can travel great distances from the source, silicic flows and domes are good indicators of vent proximity (McPhie et al., 1993).

The felsic flow-autobreccia-disorganized breccia-coarse tuff to lapilli tuff sequence at locality F in the Beaulieu River volcanic belt is consistent with deposition in a dome-

flow complex (Figure 84b). At least one dome is represented by the transition from massive porphyritic flow to flow breccia to disorganized breccia to coarse tuff. Massive flows characterize the core of the dome and autobreccia forms at the dome margins (e.g. De Rosen-Spence et al., 1980; Yamagishi and Dimroth. 1985; McPhie et al., 1993). More "distal" facies. with respect to the vent. include disorganized breccia caused by avalanching of fragments along the steep dome front. and coarse tuff to lapilli tuff representing the reworked counterparts of underlying flows and breccias (e.g. De Rosen-Spence et al., 1980). Although reworking occurred. the narrow spatial restriction of the facies sequence and the absence of basalt fragments suggest that the transport distance was relatively minimal. The two massive porphyritic units not associated with disorganized breccia (Figure 84b) represent distinct flows that advanced concommitant with dome formation. The spatially narrow felsic dome-flow complex associated with relatively shallow-water (<200 m) mafic facies indicates bimodal volcanism near the upper portion of a mafic-dominated edifice (Figure 84c).

5.6   Geodynamic Setting

An interpretation of the tectonic setting and evolution of the Central Beaulieu River belt must account for the stratigraphic. physical, and geochemical characteristics of the volcanic sequence. including: 1) contemporaneous subaqeous basaltic to rhyolitic volcanism, 2) formation of predominantly effusive flows associated with local volcaniclastic material, 3) development of tholeiitic to calc-alkaline magmas from a similar source, and 4) crustal contamination as indicated from previous Sm-Nd isotope studies (Lambert et al., 1992).

The transitional to calc-alkaline nature of the volcanic sequence and the negative Nb and Ti depletions are consistent with an arc setting (e.g. Wilson, 1989; Pearce, 1996).

In addition, arcs commonly contain a combination of basalts, andesites, and rhyolites (Perfit and Davidson, 2000). Most Ti/Zr ratios from Groups 1-3 are consistent with volcanic arc rocks (c.f. Pearce, 1982). Groups 1-3, with basalt to rhyolite compositions, display increasing Zr with increasing $(Ce/Yb)_n$, which supports a calc-alkaline evolution (e.g. Miller et al., 1994). This positive correlation is consistent with arc rocks that evolved through fractional crystallization, assimilation and mixing (e.g. Huijsmans and Barton, 1989). Unlike the Point Lake volcanic sequence, which contains $(La/Yb)_n$ values consistent with NMORB to EMORB and is interstratified with extensive turbidite deposits, the Central Beaulieu River belt produced higher $(La/Yb)_n$ values and is relatively distal with respect to the turbiditic Burwash Formation (Figure 15), consistent with a tectonic setting closer to the arc. Thick turbiditic successions are more typical of the back-arc or fore-arc regions (Klein, 1985). The interstratification of felsic and mafic facies in the Central Beaulieu River belt resembles features observed in arc-related settings (e.g. Smith et al., 1990; Miller et al., 1994; Ayres and Peloquin, 2000; Lafrance et al., 2000).

The Central Beaulieu River belt study area represents a small part of an arc that developed on continental crust. The presence of an older sialic basement during evolution of the volcanic belt is supported by previous mixing models using Nd isotopic data (Lambert et al., 1992), relatively high $(Th/La)_n$ ratios for some samples, and the stratigraphy in the study area. This aspect will be elaborated in more detail in Chapter 6. A schematic model involves subduction of an eastern slab of oceanic crust beneath a western continental slab (Figure 85). Hydration of the mantle wedge and crust by fluid and volatiles from the subducted slab resulted in tholeiitic to calc-alkaline magma genesis. Seamounts composed of tholeiitic to calc-alkaline basalts and andesites developed in relatively shallow water (<200 m) and represent the basal part of the arc,
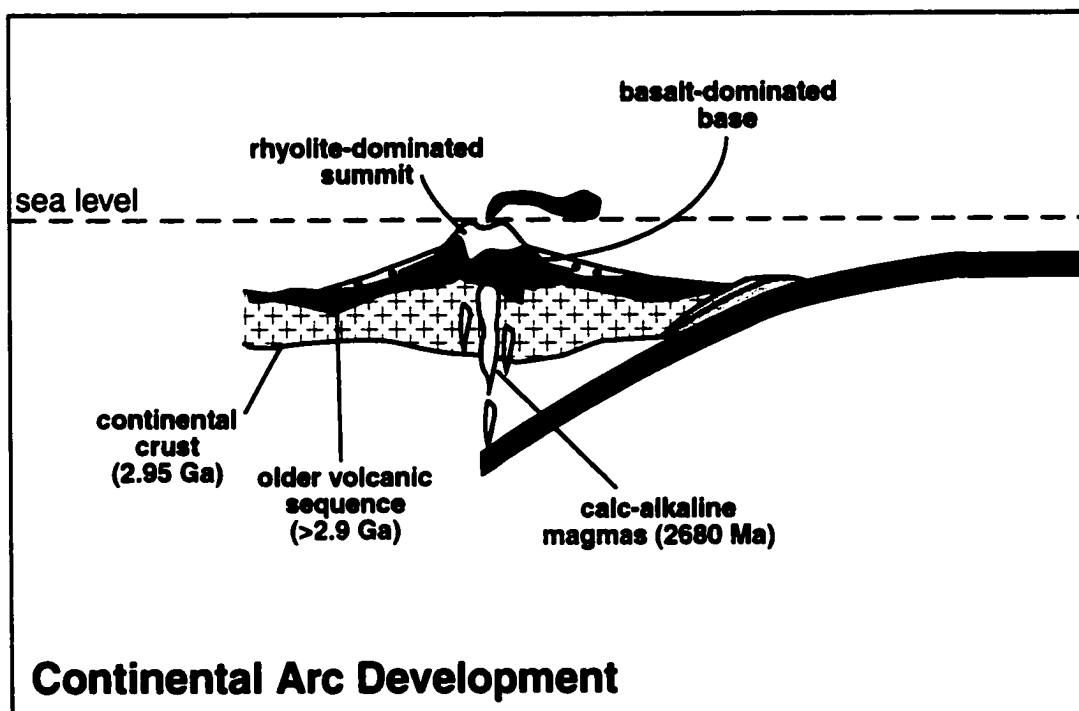
Figure 85: Schematic model illustrating Central Beaulieu River belt evolution. (A) Subduction of oceanic crust beneath continental crust resulted in deposition of a tholeiitic basalt base overlain by calc-alkaline basalt to rhyolite flows in relatively shallow water (less than 200 m). Seamounts represent the basal parts of the sequence on which smaller felsic edifices developed. Mafic and felsic flows were locally reworked by waves, creating stratified mafic deposits, and felsic breccia, lapilli tuff and tuff near the topmost portions of the arc edifices.

whereas calc-alkaline rhyolitic dome-flow complexes formed at the tops of seamounts and were intercalated with later intermediate lavas during arc evolution (Figure 85).

Summary

The physical volcanology of the Central Beaulieu River belt is consistent with effusive-dominated basaltic to intermediate eruptions on seamounts in relatively shallow water (<200 m). Silicic dome construction occurred on the topmost portions of the seamounts. Geochemically, three groups of rocks constitute the ca. 2680 Ma volcanic sequence, represented by tholeiitic to calc-alkaline, basalt to andesite flows, tholeiitic to calc-alkaline basalt dykes, and calc-alkaline rhyolite flows and volcaniclastic deposits. The most significant results determined from the Central Beaulieu River belt study area are listed in Table 12.

The interstratification of tholeiitic to mainly calc-alkaline basalts, andesites and rhyolites, significant negative Nb and Ti anomalies, and previous Sm-Nd isotope results indicate that the Central Beaulieu River belt represents a small part of a continental arc. Subduction of an oceanic slab beneath continental crust resulted in the formation of an arc with a tholeiitic base overlain by mixed tholeiitic to calc-alkaline deposits.

Characteristic	Description
Depositional setting	**Locality E** represents the medial portion of a seamount in shallow water, as indicated by stratified pillow breccia, stratified hyaloclastite, thin pillowed and massive flows, and high vesicularity. **Locality F** represents a felsic dome-flow complex, as indicated by massive porphyritic flows, flow breccia, disorganized breccia and tuff-lapilli tuff. Felsic domes developed at the upper most part of a seamount.
Chemical composition	**Group 1**: tholeiitic to calc-alkaline, basalt to andesite flows; **Group 2**: tholeiitic to calc-alkaline basalt dykes; **Group 3**: calc-alkaline rhyolitic flows, breccia, and tuff.
Geochemistry	**Group 1**: SiO_2 from 50-61 wt%, FeO^*/MgO ratios of 0.8-2.4, $(La/Yb)_n$ ratios of 3.7-5.72, negative Ce anomalies, Zr enrichments and Nb and Ti depletions relative to the REE. **Group 2**: SiO_2 from 49-54 wt%, FeO^*/MgO ratios of 1.6-2.3, $(La/Yb)_n$ ratios of 3.44-4.56, negative Ce anomalies, Zr enrichments and Nb and Ti depletions relative to the REE. **Group 3**: SiO_2 from 64-87 wt%, FeO^*/MgO ratios of 0.9-1.8, $(La/Yb)_n$ ratios of 22.12-25.38, strong depletions in Nb and Ti relative to REE.
Crustal contamination	As indicated from mixing models using Nd isotope data and negative εNd values from mafic dykes in the Sleepy Dragon Complex (Lambert et al., 1992), some $(Th/La)_n$ values, and stratigraphy (more details in Chapter 6).
Tectonic setting	**Continental arc.** Subduction of oceanic crust beneath a continental slab resulted in the development of a continental arc. Tholeiitic to transitional basalt-dominated seamounts represent the basal part of the arc, whereas calc-alkaline andesites and rhyolites represent dome-flow complexes that were emplaced over the more mafic deposits.

Beaulieu Rapids Formation (<2600 Ma) — **Quartz-Feldspar Porphyry (2600 Ma)** — **Central Beaulieu River Belt (2680 Ma)** — **Sleepy Dragon Complex (2.8-2.95 Ga)**

Table 12: Summary reviewing the main volcanological and geochemical characteristics of the Central Beaulieu River belt.

Chapter 6

DISCUSSION

6.1   Comparison of the Three Study Areas

6.1.1   Continental Crust

The Point Lake, Northern Beaulieu River and Central Beaulieu River volcanic belts are

considered by Bleeker et al. (1999a) to overlie the Central Slave Basement Complex.

Ages of 3.22 Ga for the Augustus Granite (Northrup et al., 1999), 2.95 Ga for the Beniah

Complex (Isachsen and Bowring, 1997), and 2.8-2.95 Ga for the Sleepy Dragon Complex

(Henderson et al., 1987; Lambert and van Breemen, 1991; Bleeker et al., 1999a) indicate

the presence of older sialic basement in all three study areas. Sm-Nd isotope systematics

support enriched sources for rocks in the Point Lake belt (Northrup et al., 1999; Corcoran

and Dostal, 2001). Lambert et al. (1992), in their study of dyke swarms in the Cameron

and Central Beaulieu River belts, reported a range in ε_{Nd} values from –2.0 (mafic dykes

in Sleepy Dragon Complex) to +4.11 (dyke in volcanic belt) and proposed a mixing

model with both crustal and mantle components. The positive ε_{Nd} values for four samples

from the Northern Beaulieu River belt indicate a depleted mantle source. Some samples

from the Point Lake belt also produce positive ε_{Nd} values, which are attributed to

insulation of conduit walls over time (see Chapter 3), and this process may in part be

responsible for the positive ε_{Nd} values from the Northern Beaulieu River belt. Although

the positive values do not support contamination by older crust, some samples have

$(Th/La)_n$ ratios up to 1.72, consistent with crustal interaction. In addition, the stratigraphy

194

of the study areas is similar. Quartz arenites were identified by Bleeker et al. (2000) south

of the Point Lake study area discussed in this thesis. These rift-related deposits overlie

plutonic basement in the Northern Beaulieu River belt (Covello et al., 1988; Pickett,

thesis in preparation; Figure 17 in Chapter 2), and were also identified between the

Central Beaulieu River belt and Sleepy Dragon Complex (Figure 22 in Chapter 2). These

quartz arenite sequences are referred to as the Central Slave Cover Group and are

associated with the Central Slave Basement Complex. The stratigraphic sequence of

plutonic basement overlain by quartz arenites, which are overlain by greenstone belts,

was also identified at Bell. Dwyer. Patterson, and Brown Lakes (Helmstaedt and

Padgham, 1986; Jackson, 1996; Isachsen and Bowring, 1997; Bleeker et al., 1999a), in

the western half of the Slave Province. The absence of similar stratigraphic sequences in

the eastern portion of the craton supports the presence of at least two distinct Archean

terranes. as previously proposed by Padgham and Fyson (1992).

6.1.2   Volcanology

The Point Lake, Northern Beaulieu River and Central Beaulieu River belts contain

distinct volcanic facies types and architecture, textural features, and volcanic structures

that are typical of specific depositional settings. The Point Lake and Central Beaulieu

River belts are predominantly composed of pillowed flows, whereas the Northern

Beaulieu River belt is chiefly characterized by massive flows. Multiple pillowed flows

develop from point sources and construct pillow mounds on the ocean floor. also referred

to as seamounts. The volcanic facies on a seamount change as a function of water depth

and proximity to the vent. Although both the Point Lake and Central Beaulieu River belts

evolved as one or more seamounts, the latter contains thinner flows, abundant stratified

breccia and hyaloclastite, and higher vesicularity, consistent with a shallower water

setting (<200 m depth). Subordinate pillowed flows in the Northern Beaulieu River belt probably developed as isolated seamounts, but the area was dominated by fissure eruptions producing abundant massive flows. A dyke/sill complex associated with fissure eruptions is consistent with significant extension.

Fissure-dominated volcanism associated with multiple intrusions can occur in a variety of tectonic settings, but the shallow-water (<10 m depth), wave-influenced depositional setting of the interstratified felsic lapilli tuff and tuff indicates that the volcanic sequence was deposited at a shoreface along the margin of an arc or continent. In contrast, the felsic sequence of flows, breccia, lapilli tuffs and tuffs interstratified with mafic facies in the Central Beaulieu River belt is consistent with a dome-flow complex that developed at the summit of a seamount. Felsic deposits are not components of the Peltier Formation, but andesitic tuffs interstratified with mafic pillowed and massive flows were deposited distal to an edifice during reworking of pyroclastic material immediately following an eruption.

6.1.3   Geochemistry

The Point Lake, Northern Beaulieu River and Central Beaulieu River volcanic belt study areas contain a range of rock compositions from basalt to rhyolite. The Peltier Formation, Point Lake belt, is composed of basalts and minor andesites, whereas the Samandré Formation, also of the Point Lake belt, contains rhyodacite. The Northern Beaulieu River belt is composed of basalts and rhyolites, with a lack of intermediate compositions. Basalts, andesites, and rhyolites comprise the Central Beaulieu River belt. Both tholeiitic and calc-alkaline compositions are represented in the three study areas in varying proportions. From the sample sets collected, approximately 90% of the Peltier Formation is tholeiitic with only 10% calc-alkaline rocks. The Samandré sample is calc-

alkaline. Although the Northern Beaulieu River belt has a tholeiitic to calc-alkaline ratio of 19:1 based on the sample set, this is an artifact of selective sampling. If all of the felsic units in the Beniah Lake area are calc-alkaline in composition, the ratio would be significantly lower. Finally, because of the transitional nature of many samples from the Central Beaulieu River belt, a reliable estimate of tholeiitic to calc-alkaline proportions cannot be made. However, the geochemistry indicates that the study area is dominated by deposits of calc-alkaline affinity.

REE patterns of tholeiitic basalts from the three study areas are consistent with melting of spinel peridotite (Figure 86). FeO*/MgO values of 0.9-5 for the Point Lake belt, 1-3.7 for the Northern Beaulieu River belt, and 0.8-2.4 for the Central Beaulieu River belt, indicate that the rocks underwent significant fractionation during their evolution. Intrusions from the Point Lake and Northern Beaulieu River belts have lower FeO*/MgO values than the flows, reflecting their more primitive nature, whereas flows and dykes from the Central Beaulieu River belt display similar FeO*/MgO values. Similarly, Zr/Y values are higher for the flows than for the intrusions in the Point Lake and Northern Beaulieu River belts. Basalts from these belts display tholeiitic fractionation trends (Figures 36, 57), whereas basalts from the Central Beaulieu River belt are more consistent with a calc-alkaline evolution when plotted with the andesites and rhyolites (Figure 83). Evolution of calc-alkaline basalts, andesites and rhyolites from the same source is further displayed on the REE diagrams where the patterns for the Central Beaulieu River basalt to andesite dykes, basalt to andesite flows, and rhyolite flows and tuffs are similar in shape and slope, with variations only in the overall REE abundances (Figure 86). In contrast, calc-alkaline rocks in the Peltier Formation have significantly higher slopes than their tholeiitic counterparts, indicating the involvement of two distinct sources (Figure 86).

Figure 86: Chondrite-normalized REE abundances for (A) mafic flows and (B) mafic intrusions from the Point Lake (Peltier Fm), Northern Beaulieu River (NBRB) and Central Beaulieu River (CBRB) belts, and (C) calc-alkaline rhyolites from the Central Beaulieu River belt, and calc-alkaline basalts and andesites (Peltier Fm) and one rhyodacite (Samandré Fm) from the Point Lake belt. Normalizing values after Haskin et al. (1968).

The presence of calc-alkaline rocks in the three study areas, in addition to negative Nb and Ti anomalies for most samples (Figure 87), supports a subduction-related component in their evolution. Negative Nb and Ti anomalies are more pronounced for the Central Beaulieu River belt samples and almost all of the samples from the three belts display a positive Zr anomaly relative to Sm and Eu (Figure 87). This Zr anomaly is also evident in rocks from the Kam Group, Yellowknife volcanic belt (Cousens, 2000), indicating that the Slave Province may have been characterized by a subcontinental lithosphere enriched in Zr.

The physical volcanology combined with geochemistry reflects a back-arc setting for the Peltier Formation, Point Lake belt, a transitional setting from arc to back-arc for the Northern Beaulieu River belt, and an arc setting for the Central Beaulieu River belt. Sm-Nd isotope systematics from the Point Lake and Central Beaulieu River belts support interaction with continental crust. The presence of older, 2.95-3.22 Ga plutonic rocks in all three areas suggests that the arc-back-arc sequences probably developed on sialic basement. A summary comparing the Point Lake, Northern Beaulieu River and Central Beaulieu River belts is provided in Table 13.

6.2   Comparison with the Yellowknife Volcanic Belt

The Point Lake, Northern Beaulieu River and Central Beaulieu River belts display similar characteristics to specific parts of the well studied Yellowknife volcanic belt. These four belts have been consistently referred to as "Yellowknife Supergroup-type" basalt-dominated sequences, which are distinguished from the felsic-dominated "Hackett River-types" of Padgham (1985) that characterize the eastern half of the Slave Craton. The question is: are these belts similar enough to be grouped together under one general heading?

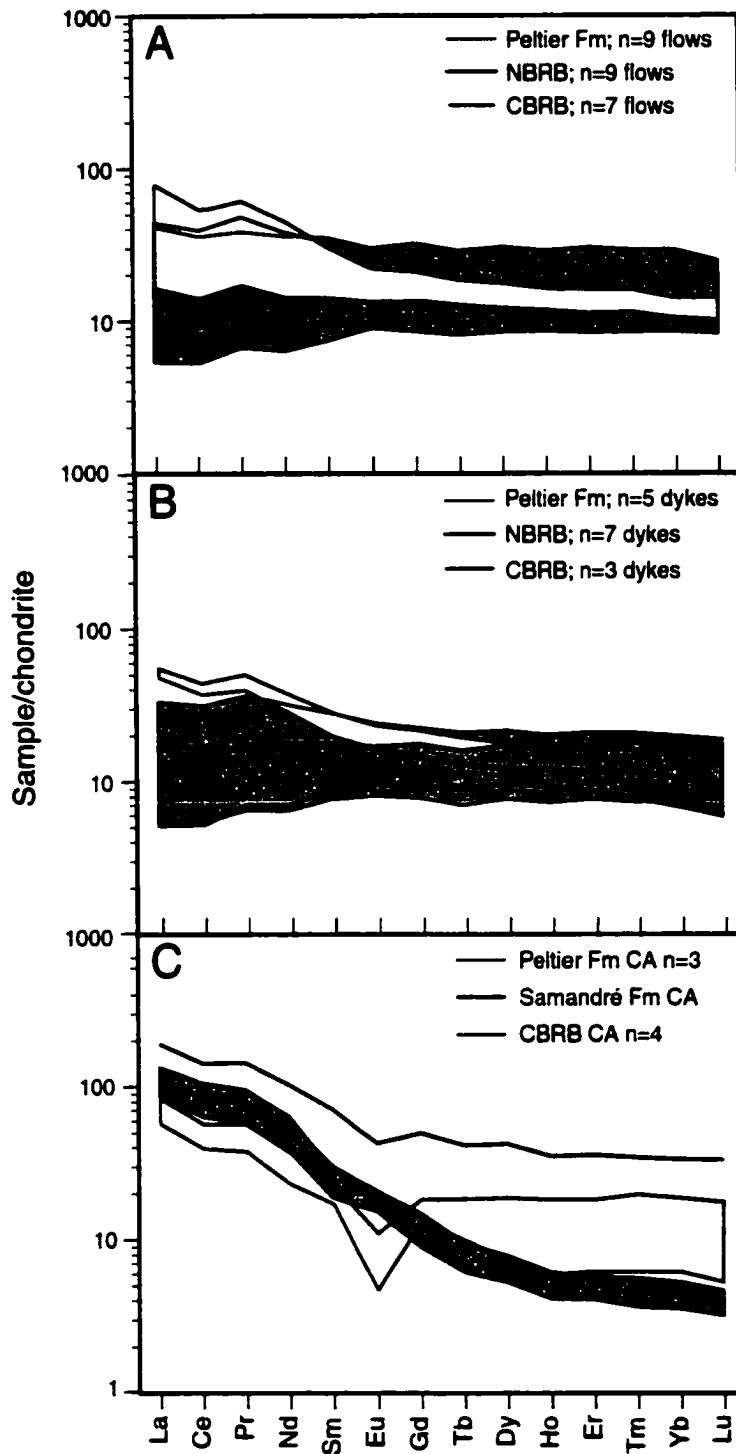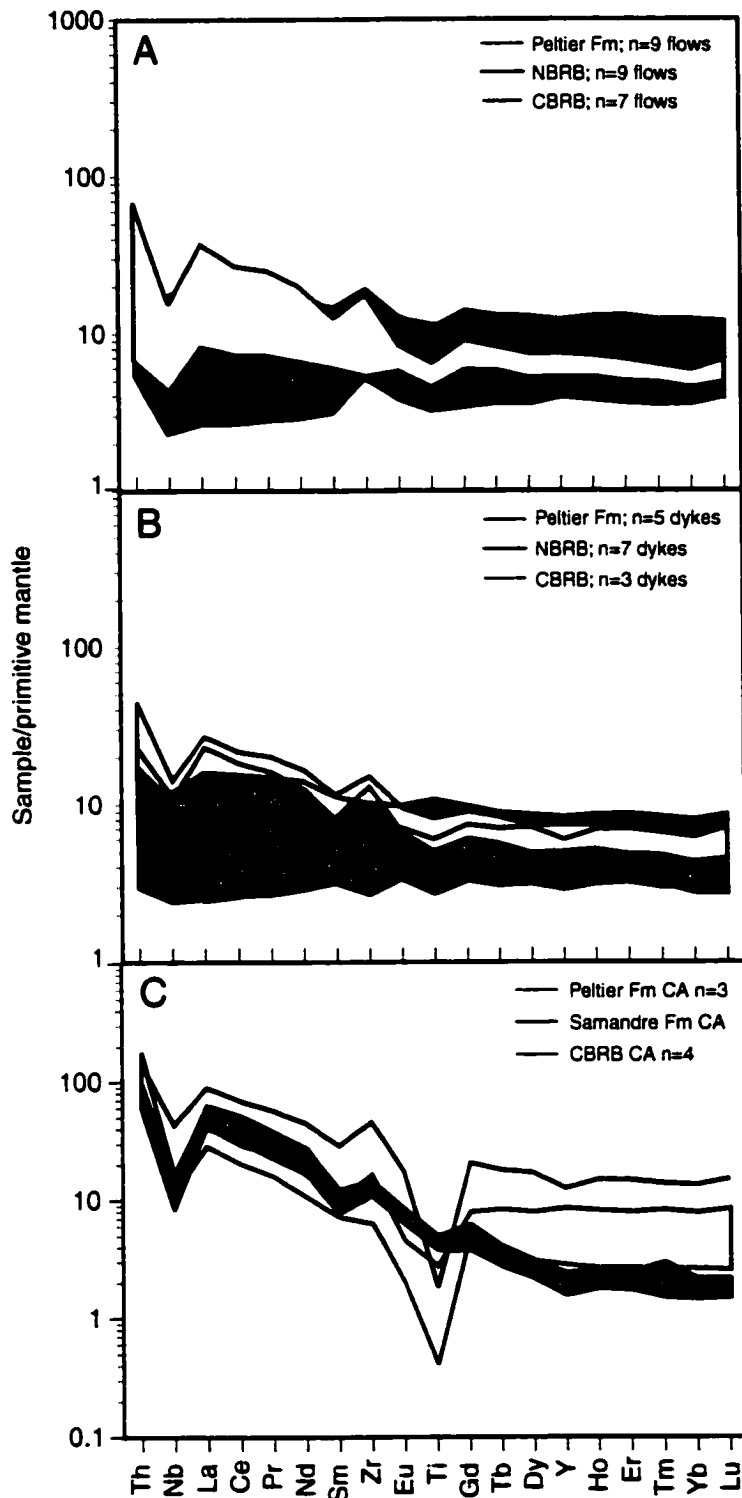Figure 87: Primitive mantle-normalized incompatible element abundances for (A) mafic flows and (B) mafic intrusions from the Point Lake (Peltier Fm), Northern Beaulieu River (NBRB) and Central Beaulieu River (CBRB) belts, and (C) calc-alkaline rhyolites from the Central Beaulieu River belt, and calc-alkaline basalts and andesites (Peltier Fm) and one rhyodacite (Samandré Fm) from the Point Lake belt. Normalizing values after Sun and McDonough (1989).

Study Area	Geochemistry	Volcanology	Depositional Setting	Tectonic Setting
Peltier Formation, Point Lake volcanic belt	*Mainly tholeiitic basalts (resembling N- and EMORB) with minor calc-alkaline basalts and andesites from two distinct sources. *Most samples display negative Nb and Ti anomalies and positive Zr anomalies relative to the REE.	*Predominant pillowed flows, pillow breccia, hyaloclastite, minor massive mafic flows, mafic multiple intrusions. *Andesitic bedded tuffs.	*Seamounts in deep to moderate water depths (200-2000 m below sea level). Proximal and distal locations relative to vent.	Continental back-arc.
Northern Beaulieu River volcanic belt	*Tholeiitic basalts (N- to EMORB) and one calc-alkaline rhyolite. *Most samples display negative Nb and Ti anomalies and positive Zr anomalies relative to the REE.	*Predominant mafic massive flows, a mafic dyke complex, subordinate pillowed flows. *Interstratified thin felsic tuff beds. *Felsic lapilli tuff and tuff grading up into a pillowed flow.	*Fissure-dominated eruptions with local small pillow-dominated seamounts. *Shallow water (<10 m), wave-influenced shoreface setting for the felsic facies.	Continental arc to back-arc transition.
Central Beaulieu River volcanic belt	*Mainly calc-alkaline and transitional basalts, andesites and rhyolites that evolved from the same source. *Strong negative Nb and Ti anomalies and positive Zr anomalies relative to the REE.	*Thin pillowed and mafic massive flows, abundant stratified pillow breccia and hyaloclastite. *felsic porphyritic flows, felsic breccia, lapilli tuff, and tuff.	*Seamounts in relatively shallow (<200 m) water. Medial location relative to vent. *Dome-flow complex.	Continental arc.

Table 13: Summary reviewing the characteristics of the three study areas.

Stratigraphically, the four volcanic sequences are generally comparable, as they all overlie older granitic basement and are capped by ca. 2.6 Ga sedimentary sequences. Ages ranging from 2690-2672 Ma for the Point Lake, and Northern and Central Beaulieu River belts fall between the ages determined from the 2722-2701 Ma Kam Group and the 2664 Ma Banting Group, so that a time correlation is problematic. Notwithstanding, different parts of the Kam Group are comparable with the Point Lake, and Northern and Central Beaulieu River belts based on volcanic rock types and compositions. The lowermost 6 km-thick Chan Formation was deposited on an older rift-related sequence, represented by the Dwyer Formation (MacLachlan and Helmstaedt, 1995). The Chan Formation is characterized by massive and pillowed basalt flows with a sheeted dyke complex akin to an ophiolite sequence (Helmstaedt and Padgham, 1986; Helmstaedt et al., 1986). The basalts are tholeiitic with some small negative Nb anomalies (Cousens, 2000). These are all characteristic of the Northern Beaulieu River belt, which overlies older rift-related quartz arenite (Beniah Formation), contains a dyke complex, and is composed of tholeiitic basalts with some negative Nb depletions. In addition, both the Chan Formation and the Northern Beaulieu River belt study area are characterized by interstratified felsic deposits. The Chan Formation is interpreted to have formed in a marginal basin setting, analogous to the Mesozoic Rocas Verdes basin (Helmstaedt and Padgham, 1986; Helmstaedt et al., 1986). The uppermost felsic unit in the Chan Formation is interpreted to have been derived from a nearby arc (MacLachlan and Helmstaedt, 1995), consistent with the felsic lapilli tuffs and tuffs in the Northern Beaulieu River belt, which are also arc-derived deposits.

From the base to the top, the Kam Group becomes more arc-like in composition (MacLachlan and Helmstaedt, 1995) and is unconformably overlain by the arc-related volcanic deposits of the Banting Group. The transition from tholeiitic mafic-dominated sequences to calc-alkaline felsic-dominated sequences is recorded in the Point Lake belt.

Tholeiitic basalts that formed in a back-arc basin (Peltier Formation) are overlain by younger felsic, calc-alkaline rocks (Samandré and Beauparlant Formations), although there is no unconformity between the lower and upper sequences. EMORB compositions and small negative Nb anomalies, which characterize the Point Lake and Northern Beaulieu River belts, are common throughout the Yellowknife sequence (Cousens, 2000), and positive Zr anomalies are typical of all four belts. The Peltier, Samandré and Beauparlant Formations are interstratified with turbidite deposits (Contwoyto Formation), as is the Banting Group with turbidites of the Burwash Formation (Helmstaedt and Padgham, 1986). Cousens (2000) attributes the geochemical composition of the Kam Group to a combination of fractional crystallization and crustal assimilation processes.

The Central Beaulieu River belt is marginally different from the Point Lake and Northern Beaulieu River belts and Kam Group because it is dominated by basalts, andesites and rhyolites that follow a calc-alkaline fractionation trend. In terms of geochemistry, these deposits are better compared with the Banting Group, although the Central Beaulieu River belt is mafic-dominated and the Banting Group is felsic-dominated. The Banting Group has been interpreted as an arc sequence (MacLachlan and Helmstaedt, 1995).

A review of the similarities between the Yellowknife, Point Lake, and Northern and Central Beaulieu River belts shows that the greenstone belts are analogous, not only in terms of composition, but also stratigraphy. Although no rocks between the ages of 2701-2664 Ma have been dated in the Yellowknife belt, the time span of Yellowknife belt evolution overlaps with the ages determined from the three study areas. This would suggest that it is appropriate to refer to all four localities as "Yellowknife Supergroup-type", and their spatial relationships indicate that the development of the Yellowknife belt was possibly related to the evolution of the Point Lake, Northern Beaulieu River and Central Beaulieu River belts (see section 6.4).

6.3   Analogues

The physical volcanology, depositional environments, geochemistry, and tectonic settings of the study areas can be compared with Phanerozoic and Modern analogues. The following analogues are grouped into two sections: 6.3.1) volcanology and depositional setting, irrespective of tectonic origin, and 6.3.2) geochemistry and tectonic setting. Table 14 provides a summary of analogues for the Point Lake, Northern Beaulieu River and Central Beaulieu River belts.

6.3.1   Volcanology and Depositional Settings

Seamounts

Mafic volcanic facies in the Point Lake and Beaulieu River volcanic belts resemble those of Phanerozoic seamounts or pillow volcanoes that develop on the ocean floor in a variety of tectonic settings. Mid-oceanic analogues include modern seamounts associated with the Mid-Atlantic (Smith and Cann, 1992; Head et al., 1996) and Juan de Fuca (Chadwick and Embley, 1994) ridges, and the East Pacific Rise (Lonsdale and Batiza, 1980; Hekinian et al., 1989; Smith and Batiza, 1989), in addition to Mesozoic-Cenozoic seamounts in the Canary Islands (Staudigel and Schminke, 1984) and Cyprus (Eddy et al., 1998). Further comparisons can be made to modern arc-backarc-related seamounts in the Mariana Trough (Fryer, 1995), and the Lau Basin (Hawkins, 1995), and to Cenozoic seamounts in southwest Japan (Kano et al., 1993) and in the Japan Sea (Sohn, 1995).

Study Areas	Analogues
Depositional Settings in the Point Lake and Central Beaulieu River belts	*Modern seamounts:* -Mid-Atlantic ridge (Smith and Cann, 1992; Head et al., 1996) -Juan de Fuca ridge (Chadwick and Embley, 1994) East Pacific Rise (Lonsdale and Batiza, 1980; Hekinian et al., 1989; Smith and Batiza, 1989) -Mariana Trough (Fryer, 1995) -Lau Basin (Hawkins, 1995). *Phanerozoic seamounts:* -the Canary Islands (Staudigel and Schminke, 1984) -Cyprus (Eddy et al., 1998) -southwest Japan (Kano et al., 1993) -the Japan Sea (Sohn, 1995) *Phanerozoic dome-flow complexes:* -Island of Ponza, Italy (Scutter et al., 1998) -Ushikiri Formation, SW Japan (Kano et al., 1991)
Depositional Setting in the Northern Beaulieu River belt	*Modern fissure-dominated volcanism:* -East Pacific Rise (Lonsdale and Batiza, 1980; Hekinian et al., 1989) -Galapagos Rift Valley (Ballard et al., 1979) *Shallow-water felsic volcaniclastic deposits:* -Late Cenozoic central part of Northern Honshu, Japan (Sato and Amano, 1991) -Naktul unit, Late Cretaceous Dras arc complex, Ladakh Himalayas (Robertson and Degnan, 1994).
Geochemistry and tectonic setting of Point Lake belt	*Back-arc basins:* -Modern Okinawa Trough (Letouzey and Kimura 1985; Honma et al. 1991; Sibuet et al. 1995) -Tertiary Yamato Basin in the Sea of Japan (Pouclet and Bellon 1992; Cousens and Allan 1992; Tamaki 1995)
Geochemistry and tectonic setting of the Northern Beaulieu River belt	*Back-arc to arc transition zone:* -Early Cretaceous Peninsula Hardy, Chile (Miller et al., 1994) -Modern Havre Trough-Kermadec arc-backarc system (Gamble and Wright, 1995).
Geochemistry and tectonic setting of the Central Beaulieu River belt	*Arc volcanoes:* -Modern Towada Volcano, northeast Japan (Hunter and Blake, 1995) -Modern Aso Volcano, southwest Japan (Hunter, 1998)

Table 14: Modern and Phanerozoic analogues for the depositional and tectonic settings of the three study areas.

The pillowed flow-dominated sequence at locality A in the Point Lake belt is similar to <45 m-thick pillow mounds on the Cleft segment of the Juan de Fuca Ridge (Chadwick and Embley, 1994), 50-650 m-high pillow-dominated seamounts in the rift valley of the Mid-Atlantic Ridge (Smith and Cann, 1992; Head et al., 1996), and the 200 m-high Alestos Hill seamount in an inter-graben zone of the Troodos ophiolite, Cyprus (Eddy et al., 1998). Edifices in these settings are either inferred or proven to be fed by magma migrating through feeder dyke/sill complexes. Mafic edifices characterized by abundant feeder dykes and sills indicate extension associated with rifting (Walker, 1993). Extensive disorganized autoclastic pillow breccia and hyaloclastite associated with coherent massive and pillowed flows at locality B resemble the Trachyte I lithofacies of the inferred 2000 m-high, back-arc Tok Island volcano, Korea, which represents a subaqueous effusive episode before the onset of explosive shallow-water to emergent volcanism (Sohn, 1995). The interstratification of bedded tuffs and massive flows at locality B is comparable to the relationship between distal volcaniclastic deposits and volcanic flows in the >1500 m-thick, inferred island-arc seamount on the Shimane Peninsula, southwest Japan, as described by Kano et al. (1993). Interstratified sedimentary deposits recording volcanic quiescence are comparable to those now accumulating on seamount summits 800-2500 m deep near the East Pacific Rise (Lonsdale and Batiza, 1980; Smith and Batiza, 1989).

Stratified hyaloclastite and pillow breccia associated with coherent pillowed and massive flows at locality E in the Central Beaulieu River volcanic belt are analogous to the intermediate-shallow water flank deposits of the 1800 m-thick, Pliocene seamount sequence at La Palma, Canary Islands (Staudigel and Schminke, 1984). Both the Point Lake and Central Beaulieu River belt examples are best compared with the seamount at La Palma, which is characterized by a deep-water, basal pillowed sequence intruded by dykes and sills, overlain by in-situ hyaloclastite and pillow breccia, changing up-section

into intermediate-shallow water, stratified, reworked deposits (Staudigel and Schminke, 1984).

Fissure-dominated volcanism

The inferred fissure-dominated volcanism responsible for the abundant mafic massive flows and intrusions in the Northern Beaulieu River belt is common at spreading centres such as the East Pacific Rise and the Galapagos Rift Valley, where sheet flows develop as a result of faster spreading rates (Ballard et al., 1979; Kennish and Lutz, 1998). The paucity of mafic explosive debris in the Point Lake, Northern Beaulieu River and Central Beaulieu River volcanic belts indicates that either 1) none of the seamounts or fissure-fed edifices breached the water surface, or 2) the emergent portions of the edifices have been eroded.

Dome-flow complexes

The dome-flow complex preserved in the Central Beaulieu River belt is comparable with the Pliocene subaqueous succession on the Island of Ponza, Italy (Scutter et al., 1998), and Miocene subaqueous block lavas of the Ushikiri Formation, SW Japan (Kano et al., 1991). Scutter et al. (1998) recognized four distinct facies groups of which the "older dome facies association" and the "lava flow facies association", best resemble the deposits of the Central Beaulieu River belt. Gradational changes from coherent rhyolite to talus breccia to reworked breccia are consistent with proximal to distal dome facies. Coherent rhyolite changing into jigsaw-fit breccia, clast-rotated breccia, and reworked breccia and sandstone reflect the proximal to distal facies of a major submarine lava flow. Similar changes from massive rhyolite to jigsaw-fit breccia, talus breccia, and reworked tuffs were identified in the Central Beaulieu River belt at locality F. Similar facies types in subaqueous rhyolite flows characterize the Ushikiri Formation, which was deposited in

water depths between 200-1000 m. This edifice is 600 m high and 4 km wide and is composed of three units containing lavas, breccias, and hyaloclastite (Kano et al., 1991). The lavas are characterized by an outer reworked volcanic breccia and are considered the subaqueous counterparts of subaerial block lava.

Shallow water shoreface deposits

The felsic, shallow water, reworked pyroclastic deposits that characterize locality D in the Northern Beaulieu River belt can be compared with similar depositional settings in the Late Cenozoic central part of Northern Honshu, Japan (Sato and Amano, 1991) and the Naktul unit of the Late Cretaceous Dras arc complex in the Ladakh Himalayas (Robertson and Degnan, 1994). Deposits belonging to the back-arc basin opening stage of Sato and Amano (1991) in Northern Honshu are extensive mafic lavas erupted in the submarine back-arc associated with shallow marine felsic volcaniclastic deposits along the volcanic front (Backbone Ranges). This stage marks a transgression with advanced rifting, during which mafic and felsic debris was deposited. The Naktul unit in the Dras arc complex is mainly composed of volcaniclastic deposits that were deposited on a proximal volcaniclastic apron in a fore-arc setting (Robertson and Degnan, 1994).Volcaniclastic turbidites exhibit Bouma A-D divisions and mudstone units are interstratified with fine-grained turbidites. The volcaniclastic deposits overlie pillowed and massive flows that represent the base of the volcanic arc.

6.3.2   Geochemistry and Tectonic Settings

Back-arc basins

Development of the Point Lake ensialic back-arc basin can be compared with analogues that are associated with back-arc rifting or crustal thinning and sialic crust,

such as the modern-day Okinawa Trough in the west Pacific (Letouzey and Kimura,

1985; Honma et al., 1991; Sibuet et al., 1995) and the Tertiary Yamato Basin in the Sea

of Japan (Pouclet and Bellon, 1992; Cousens and Allan, 1992; Tamaki, 1995). The

Okinawa Trough is a modern example of a back-arc basin that formed during continental

extension related to the subduction of the Philippine Sea plate beneath the Eurasian plate.

The trough, which has already extended between 74-80 km (Sibuet et al., 1995) behind

the Ryukyu volcanic chain and trench in the west Pacific, contains basaltic magmas

similar to those that form in intra-oceanic back-arc basins, such as the Mariana Trough

(Honma et al., 1991). Like the Peltier Formation Groups 1 and 2 and subgroup 4a, basalts

in the Okinawa Trough are chemically similar to NMORB (Honma et al., 1991). The

ascent of basaltic magma was facilitated through a normal fault system where the

continental crust was thinnest (Sibuet et al., 1995). Spreading along normal faults created

grabens, half-grabens and other rift-related structures. The net extension of the

continental crust to form the back-arc basin is estimated at 100 km in the southeast and

200 km in the north of the Okinawa Trough (Sibuet et al., 1995). The sediment is

between 3-8 km thick (Letouzey and Kimura, 1985). Like the turbiditic succession at

Point Lake, the sediments in the Okinawa Trough are intercalated with volcanic rocks

that overlie continental basement in the east and northeast (Letouzey and Kimura, 1985).

Tholeiitic basement material recovered from the Yamato Basin, Sea of Japan,

yielded trace element patterns resembling enriched NMORB with slight negative Nb and

positive Th anomalies (Pouclet and Bellon, 1992; Allan and Gorton, 1992), similar to

Peltier Formation Groups 1 and 2, and subgroup 4a. Emplacement of tholeiitic basalts in

the Yamato Basin is interpreted to have occurred during extension and thinning of the

lower crust (Pouclet and Bellon, 1992, Tamaki, 1995). Opening of the Japan Sea was

instigated by strike-slip faulting in continental crust during the India-Eurasia collision

(Tamaki, 1995). Geophysical data indicate that the crust beneath the Yamato Basin is too

thick (12-16 km; Tamaki, 1995) to represent oceanic crust. This basin is interpreted to overlie thinned continental crust intruded by basaltic magmas, as continental rafts are common in the Sea of Japan (Cousens and Allan, 1992; Tamaki, 1995). Topographic highs represented by ca. 2.7 Ga continental crust are characteristic features of the Yamato Basin (Tamaki, 1995). The back-arc basin is characterized by seamounts and thick turbidites (up to 2.5 km; Tamaki, 1995), features consistent with the Point Lake sequence. Although post-rifting volcanism in the Sea of Japan from Miocene to present is dominated by alkaline and potassic compositions, basaltic rocks representing the phases of rifting and spreading are characteristic of the basement (Pouclet et al., 1994).

Back-arc to arc transition zones

The transitional arc to back-arc setting of the Northern Beaulieu River belt is analogous to the characteristics of the Early Cretaceous deposits on Peninsula Hardy, Chile (Miller et al., 1994), and the modern Havre Trough-Kermadec arc-backarc system north of New Zealand (Gamble and Wright, 1995). The Hardy Formation, preserved as a 600 m-thick sequence on Peninsula Hardy, represents an arc that developed along the western margin of South America. The basalt to rhyolite succession interfingers with the Yahgan Formation, interpreted as marginal basin fill. Tholeiitic basalts that are mainly LREE depleted are typical of the Yahgan Formation, whereas calc-alkaline samples displaying LREE enrichments and negative Nb-Ta and Ti anomalies belong to the Hardy Formation. The interstratification of tholeiitic and calc-alkaline volcanic rocks is attributed to temporal variations during marginal basin evolution. The calc-alkaline rocks are interpreted to have been erupted near the active arc and the tholeiitic basalts erupted in the back-arc when the basin was wider. Although the Northern Beaulieu River belt includes only one calc-alkaline sample in this study, the shallow water setting (<10 m depth) of the felsic volcaniclastic rocks necessitates a subaerial to subaqueous transition

where tholeiitic and calc-alkaline magmas are intercalated. The transitional arc to back-arc setting proposed by Miller et al. (1994) is a good analogue.

The Havre Trough-Kermadec arc-backarc system is located at the convergence of the Pacific and Australian plates. The southern portion of the arc-backarc system marks the transition between continental and oceanic crust, which has resulted in a wider range of compositions (basalt to rhyolite) in the former than in the latter (basalt and basaltic andesite; Gamble et al., 1995). Lavas that erupted along the eastern escarpment of the Ngatoror rift system, southern Havre Trough, display similar geochemistry to the Kermadec arc lavas, with negative Nb and Ti anomalies. The eastern escarpment is closest to the volcanic arc, whereas the western escarpment, only some 10-15 km away, contains MORB-like basalts. This indicates how arc to back-arc transition zones are characterized by mixtures of volcanic rocks with both tholeiitic and calc-alkaline affinities.

Arc volcanoes

The geochemistry of the Central Beaulieu River belt can be compared with the Towada and Aso Volcanoes in Japan (Hunter and Blake, 1995; Hunter, 1998). Aso Volcano in southwest Japan is developed on a basement composed of metamorphic and plutonic complexes and contains both tholeiitic and calc-alkaline basalts with similar REE patterns. This similarity in slope and curvature, and varying only in overall REE abundances, indicates that the rocks were derived from a common parental magma (Hunter, 1998). A mixed tholeiitic/calc-alkaline sequence is also recorded at Towada Volcano in NE Japan. Both volcanoes are located 20 km behind the volcanic front. Early volcanism was basaltic and andesitic and felsic deposits are preserved at the edifice summits (Hunter and Blake, 1995). The transition from tholeiitic to calc-alkaline has been attributed to combined crustal assimilation and fractional crystallization (AFC).

Although the Japan analogues are subaerial, and thus contain more pyroclastic debris, their compositions are strikingly similar to the Central Beaulieu River belt study area which features a tholeiitic to calc-alkaline continuous arc series overlying continental crust.

6.4   Geodynamic setting

Plate tectonics are inferred to have occurred in the Slave Province, with geodynamic settings ranging from continental rifting (Henderson. 1981, 1985) to consuming margins with crustal interaction (Kusky, 1989, 1991; MacLachlan and Helmstedt, 1995; Cousens. 2000), and combinations thereof (Isachsen and Bowring, 1994, 1997; Mueller et al., 2001). The three study areas represent different sectors of an arc-back-arc system floored by >2.8 Ga continental crust, where the Point Lake Belt is closer to the back-arc spreading center, the Northern Beaulieu River belt represents the back-arc to arc transition zone. and the Central Beaulieu River belt is better compared with the arc (Figure 88). The change in geodynamic setting indicates variation in migration or shift of the arc and rifting of the continent.

Extension is an important tectonic regime at convergent margins, although the entire arc system advances over time (Hamilton, 1995). The hinge roll-back causes intra- and back-arc spreading, which is accompanied by migration of the arc (Dewey, 1980). Different types of arcs are formed depending on the types of interacting plates (i.e. ocean-ocean or ocean-continent). The study areas are consistent with an Andean-type margin or continental arc. as indicated by the isotope systematics, geochemistry, N-S distribution of the continental crust (Bleeker et al., 1999a), quartz arenite sequences overlying basement (Bleeker et al., 1999a; Pickett, thesis in preparation), unconformities between basement and greenstone belts (Corcoran et al., 1998; Mueller and Corcoran, in press), and physical

Continental Arc with Marginal Basin
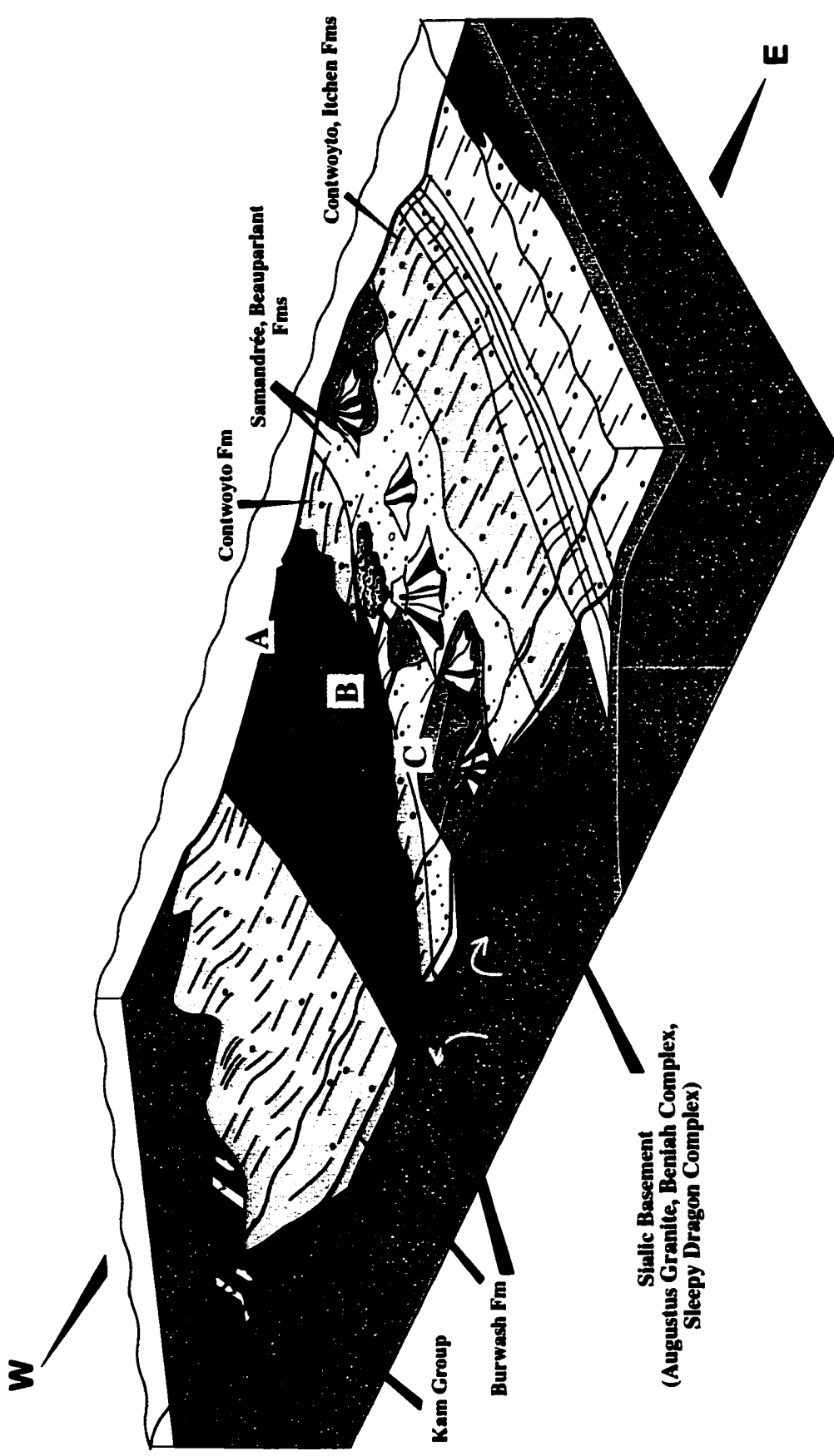
Figure 88: Geodynamic setting of the three study areas in the Slave Province. The Point Lake belt (A) formed in a back-arc, the Northern Beaulieu River belt (B) formed in the arc to back-arc transition zone, and the Central Beaulieu River belt (C) formed on the arc. Modified from Moores and Twiss, 1995.

volcanology. Ages from the study areas indicate an evolution between 2690-2670 Ma, which compares favorably with the ca. 15-25 m.y. time span for modern arc-backarc systems in the westen Pacific (Leitch, 1984; Saunders and Tarney, 1984; Wharton et al., 1995). The 20 m.y. time span suggests that the arc migrated and evolved into a mature marginal basin with a thick turbidite sequence and rift-related basalts at Point Lake. The arc, due to hinge roll-back, migrated over time and caused crustal attenuation, similar to a Japan-type arc setting.

The older ages from the Kam Group of the Yellowknife volcanic belt, its interpretation as a continental marginal basin (Helmstaedt and Padgham, 1986; Cousens, 2000), and its N-S trend parallel to the Point Lake, Northern Beaulieu River and Central Beaulieu River belts, indicates that it developed during earlier splitting of an active continental arc prior to the 2.69-2.67 Ga subduction event. The spatial relationship between the Kam Group and the study areas suggests eastward migration of the subduction zone over 30-50 m.y. The evolution of parallel series of arcuate arc-back-arc sequences is a classical feature of asymmetrical arc spreading centers in the western Pacific Ocean (e.g. Karig, 1971; Karig et al., 1978; Hathway, 1994; Hawkins, 1995). The Slave Province records the evolution of an ancient arc system from ca. 2720-2670 Ma, during which a continental margin attenuated, an arc developed, and a back-arc basin formed (Kam Group). Later volcanism occurred in the eastern part of the older rifted arc, represented by the Central Beaulieu River belt. With continued hinge roll-back, the younger arc split and a second back-arc basin developed (Point Lake belt). The Northern Beaulieu River belt records the volcanism that occurred in the younger arc to back-arc transition zone. The younger, ca. 2662 Ma Banting Group is not related to the evolution of the three study areas, and may represent a later phase of rejuvenated arc volcanism.

Chapter 7

SUMMARY AND CONCLUSIONS

This thesis presents the physical volcanology, depositional settings, geochemistry, and tectonic settings of three portions of Archean greenstone belts in the Slave Province, Northwest Territories, Canada. The Point Lake, Northern Beaulieu River, and Central Beaulieu River belt study areas are characterized by distinct volcanic facies and rock compositions that are related to arc-back-arc evolution that occurred over 20 m.y. between 2.67-2.69 Ga.

Stratigraphy

1. Older, >2.8 Ga continental crust is preserved in the Point Lake, Northern Beaulieu River and Central Beaulieu River belt study areas. The volcanic belts all overlie quartz arenite sequences, are overlain by ca. 2.6 Ga sedimentary deposits, and are roughly time correlative.

Physical Volcanology and Depositional Setting

2. Thick pillowed flows, abundant intrusions, the absence of fragmental deposits, and low vesicularity at locality A in the Peltier Formation, Point Lake belt, are consistent with a deep water, proximal seamount setting where edifice growth was intiated.

3. Thin pillowed and massive flows, abundant pillow breccia, hyaloclastite, interstratified felsic volcaniclastic deposits, and moderate vesicularity at locality B in the Peltier

215

Formation, Point Lake belt, represent the moderate water depth, medial to distal portion of a seamount. Intercalation of sedimentary and volcanic material (peperite) and shale interbeds, deposited during periods of volcanic quiescence, show contemporaneity of Peltier Formation volcanism and Contwoyto Formation sedimentation.

4. Abundant massive basalt flows and subordinate pillowed flows in the Northern Beaulieu River belt indicate a subaqueous depositional setting where fissure eruptions were dominant and small local seamounts developed. A mafic dyke complex indicates significant extension.

5. Wavy-, planar- and cross-bedded lapilli tuff and coarse tuff grading upsection into fine tuff with black mudstone beds, conformably overlain by a pillowed flow at locality D in the Northern Beaulieu River belt, are consistent with a transgressive sequence in a shallow water shoreface setting.

6. Thin pillowed and massive flows, abundant stratified pillow breccia and hyaloclastite, and high vesicularity at locality E in the Central Beaulieu River belt represent a shallow water, medial seamount setting. Synvolcanic dykes are interpreted as feeders to the overlying volcanic pile.

7. Felsic porphyritic flows, associated with autoclastic felsic breccia, grading into disorganized felsic breccia, overlain by felsic tuff are consistent with a dome-flow complex. Interstratification of the felsic tuff with overlying pillow breccia indicates contemporaneous felsic and mafic volcanism.

Geochemistry and Tectonic Setting

8. Point Lake belt: Group 1 is composed of tholeiitic basalt flows. $(La/Yb)_n$ ratios resemble NMORB, but some of the samples have Nb depletions relative to the REE. The samples produce positive ε_{Nd} values. Group 2 contains tholeiitic basalt flows with $(La/Yb)_n$ ratios resembling EMORB and some Ti and Nb depletions relative to the REE. ε_{Nd} values are both negative and positive. Group 3 rocks are calc-alkaline volcaniclastic basalts and andesites with high $(La/Yb)_n$ ratios and negative Nb and Ti anomalies. The samples produce positive ε_{Nd} values. Group 4a is composed of tholeiitic basalt intrusions that resemble Group 1 flows. Group 4b contains younger unrelated subalkaline intrusions. One calc-alkaline rhyodacitic tuff from the Samandré Formation has a high $(La/Yb)_n$ ratio with negative Nb and Ti anomalies. The mainly tholeiitic rock compositions are consistent with a continental back-arc setting where the effects of crustal contamination decreased over time due to insulation of conduit walls.

9. Northern Beaulieu River belt: Group 1 is composed of tholeiitic basalt flows resembling NMORB, but with very minor negative Ti and Nb anomalies. Four samples produced positive ε_{Nd} values. Group 2 rocks are tholeiitic basalt intrusions of the dyke complex. These intrusions resemble NMORB with some negative Nb anomalies. Group 3 is represented by a calc-alkaline rhyolitic tuff. The sample set is represented by tholeiitic basalts, but much of the Northern Beaulieu River belt is composed of felsic volcanic units. The presence of at least one calc-alkaline sample indicates a subduction-related component. The volcanology indicates a shallow to deeper water transition which is

consistent with the fringing part of an arc. The volcanology combined with geochemical results is consistent with a back-arc to arc transition zone.

10. Central Beaulieu River belt: Group 1 rocks are tholeiitic to calc-alkaline, basalt to andesite flows with negative Nb and Ti anomalies and high $(La/Yb)_n$ ratios. Group 2 rocks are tholeiitic to calc-alkaline basalt dykes similar in composition to Group 1 flows. Group 3 is composed of calc-alkaline rhyolitic flows, breccia, and tuff with very high $(La/Yb)_n$ ratios and marked negative Nb and Ti anomalies. The geochemistry is consistent with a continental arc setting.

Geodynamic Setting

11. The Point Lake, Northern Beaulieu River and Central Beaulieu River belts represent parts of a continental arc to back-arc setting. The volcanic belts, distributed over approximately 250 km, are the products of an inferred west-dipping subduction zone that, over ca. 20 m.y., resulted in arc migration and evolution into a mature arc-back-arc. The volcanology and geochemistry of the 2.72-2.70 Ga Kam Group is comparable to the study areas, and it has been interpreted as a back-arc basin. The location and age of the Kam Group indicate that it may represent a remnant back-arc that formed during the early stages of western Slave arc system evolution. This is confirmed by the major 35 m.y. hiatus between the Kam Group and the study areas, and the unconformity between the Kam and Banting Groups of the Yellowknife volcanic belt.

APPENDICES

Appendix 1: Accuracy and Precision of ICP-MS and XRF data

ICP-MS Data

The samples are compared to the Canadian Centre for Mineral and Energy Technology, Mines and Resources standard MRG-1, which is a gabbro from Mount Royal, Montreal. Standard values are from Govindaraju (1994). Column A is the assumed true value of MRG-1. Column B is the measured value on the Takla Group sample. Column C is the difference A-B. Column D is the accuracy, which is the difference expressed as a percentage of the true value of the standard, i.e.

$$100 * (A-B)/A$$

Column E is the mean of two readings on sample S-153. Column F is the standard deviation for sample S-153 calculated from the normal expression for standard deviation, i.e.

Square root ((sum (mean-reading)(mean-reading))/(N-1)) for N readings.

Column G is the standard deviation expressed as a percentage of the mean, i.e.

$$100 * \text{standard deviation/mean.}$$

Columns H, I and J are as E, F and G for sample S-74.

Element	A	B	C	D	E	F	G	H	I	J
Li	4.20	3.60	0.60	14.3	11.43	+/-0.71	6.2	32.21	+/-0.50	1.6
Rb	8.50	7.55	0.95	11.2	2.23	+/-0.01	0.6	27.24	+/-0.54	2.0
Sr	266.00	261.34	4.66	1.8	302.52	+/-2.11	0.7	348.24	-/-7.95	2.3
Y	14.00	10.96	3.04	21.7	19.60	+/-0.07	0.4	16.81	+/-0.45	2.7
Zr	108.00	91.10	16.90	15.6	83.65	+/-1.15	1.4	55.72	-/-0.33	0.6
Nb	19.20	20.60	-1.40	-7.3	4.45	+/-0.01	0.2	3.15	+/-0.08	2.5
Mo	0.87	55.34	-54.47	-62.61	1.11	+/-0.13	12.2	0.65	+/-0.06	9.9
Cs	0.57	0.57	0.00	0.0	0.11	+/-0.01	12.9	2.99	-/-0.03	0.9
Ba	61.00	46.93	14.07	23.1	63.11	+/-1.44	2.3	509.79	+/-0.86	0.2
La	9.89	9.00	0.89	9.0	9.32	+/-0.12	1.3	7.67	+/-0.07	0.9
Ce	26.00	26.80	-0.80	-3.1	21.76	+/-0.07	0.3	17.30	+/-0.08	0.5
Pr	3.40	3.76	-0.36	-10.6	2.94	+/-0.05	1.7	2.42	+/-0.01	0.6
Nd	19.20	18.22	0.98	5.1	13.22	+/-0.24	1.8	11.45	+/-0.18	1.6
Sm	4.50	4.44	0.06	1.3	3.37	+/-0.11	3.2	3.11	-/-0.02	0.7
Eu	1.39	1.44	-0.05	-3.6	1.09	+/-0.04	3.9	1.25	+/-0.00	0.0
Gd	4.00	4.08	-0.08	-2.0	3.81	+/-0.04	1.1	3.56	+/-0.02	0.6
Tb	0.51	0.55	-0.04	-7.8	0.60	+/-0.00	0.0	0.56	-/-0.02	3.8
Dy	2.90	3.07	-0.17	-5.9	3.66	+/-0.01	0.4	3.45	+/-0.01	0.2
Ho	0.49	0.52	-0.03	-6.1	0.77	+/-0.02	2.8	0.72	+/-0.01	1.0
Er	1.12	1.29	-0.17	-15.2	2.22	+/-0.03	1.3	2.02	+/-0.04	2.1
Tm	0.11	0.15	-0.04	-36.4	0.33	+/-0.01	2.2	0.28	+/-0.01	2.6
Yb	0.60	0.82	-0.22	-36.7	2.13	+/-0.02	1.0	1.74	+/-0.04	2.0
Lu	0.12	0.11	0.01	8.3	0.31	+/-0.00	0.0	0.25	+/-0.00	0.0
Hf	3.76	3.75	0.01	0.3	2.53	-/-0.04	1.7	1.74	+/-0.05	2.9
Ta	0.80	0.89	-0.09	-11.2	0.43	+/-0.01	1.7	0.29	+/-0.01	2.5
Tl	0.06	0.05	0.01	16.7	0.02	+/-0.01	47.1	0.11	+/-0.02	20.2
Pb	10.00	4.89	5.11	51.1	2.79	+/-0.04	1.5	2.76	+/-0.09	3.3
Bi	0.01	0.15	-0.14	-14	0.02	+/-0.01	70.7	0.06	+/-0.01	12.9
Th	0.93	0 82	0.11	11.8	1.23	+/-0.03	2.3	0.90	-/-0.02	2.4
U	0.24	0.32	-0.08	-33.3	0.65	+/-0.01	1.1	0.57	+/-0.01	1.2

Appendix 1: continued

XRF Data

Major and trace element XRF values are compared to the United States Geological Survey (USGS) standard diabase W-2. Trace elements are compared to the USGS standard andesite AGV-1. Column A is the assumed true value of the standard W-2. Column B is the mean of 14 measured analyses of this standard. Column C is the standard deviation. Column D is the difference between the standard value and the mean measured value. Column E is the assumed true value of the standard AGV-1. Column F is the mean of measured 14 analyses of this standard. Columns G and H are as C and D.

W-2

Element	A Standard	B Mean	C Std. Dev.	D Difference
SiO2	52.44	52.52	+/-0.10	0.08
TiO2	1.06	1.05	+/-0.01	0.01
Al2O3	15.35	15.21	+/-0.12	0.14
Fe2O3	10.76	10.31	+/-0.08	0.45
MnO	0.10	0.16	+/-0.00	0.06
MgO	6.37	6.50	+/-0.10	0.13
CaO	10.87	10.97	+/-0.07	0.10
Na2O	2.14	2.40	+/-0.24	0.26
K2O	0.63	0.64	+/-0.01	0.01
P2O5	0.13	0.12	+/-0.01	0.01
Ba	182.0	180.8	+/-5.8	1.2
Rb	20.0	21.8	+/-2.1	1.8
Sr	194.0	193.6	+/-4.2	0.4
Y	24.0	18.0	+/-1.7	6.0
Zr	94.0	90.2	+/-2.2	3.8
Nb	7.9	5.5	+/-0.7	2.4
Ga	20.0	18.4	+/-1.4	1.6
Zn	77.0	82.3	+/-1.1	5.3
Cu	103.0	109.3	+/-3.8	6.3
Ni	70.0	71.3	+/-2.1	1.3
V	262.0	262.3	+/-6.4	0.3
Cr	93.0	89.8	+/-3.8	3.3

AGV-1

Element	A Standard	B Mean	C Std. Dev.	D Difference
Ba	1226.0	1244.1	+/-11.6	18.1
Rb	67.3	67.6	+/-2.1	0.3
Sr	662.0	666.4	+/-5.0	4.4
Y	20.0	19.4	+/-1.0	0.6
Zr	227.0	247.5	+/-9.2	20.5
Nb	15.0	12.0	+/-1.1	3.0
Ga	20.0	19.1	+/-1.9	0.9
Zn	88.0	89.1	+/-1.5	1.1
Cu	60.0	60.9	+/-5.9	0.9
Ni	16.0	17.1	+/-1.7	1.1
V	121.0	123.4	+/-3.1	2.4
Cr	10.1	16.0	+/-3.7	5.9

Appendix 2: Microprobe data for chromite in samples from the ultramafic unit underlying the Northern Beaulieu River belt.

Analytical Methods:

Analyses were conducted using a JGEOL 733 electron microprobe equipped with four wavelength dispersive spectrometers (WDS) and an Oxford Link eXL energy dispersive system (EDS). The energy dispersive system was used for all elements. Resolution of the energy dispersive detector was 137ev at 5.9Kev. Each spectrum was acquired for 40 seconds with an accelerating voltage of 15 Kv and a beam current of 15nA. Probe spot size was approximately 1 micron. The raw data was corrected using a Link's ZAF correction program. Instrument calibration was performed on chromium metal. Instrument precision on cobalt metal (n=10) was +/-0.5% at 1 standard deviation. Accuracy for major elements was +/-1.5 to 2.0% relative. Geological standards were used as controls. Detection limits for most elements using the energy dispersive system range from approximately 0.1-0.3%.

% oxide	SiO2	TiO2	Al2O3	Cr2O3	FeO	MnO	MgO	CaO	ZnO	NiO	V2O5	Total
31-1-rim	--	--	--	5.63	89.16	--	--	--	--	0.69	--	95.48
31-1-int.	0.20	0.38	0.41	39.25	54.10	2.60	0.89	--	1.17	--	--	99.00
31-1-core	0.35	--	16.62	45.40	28.18	1.96	4.10	--	3.25	--	--	99.86
31-2-rim	0.21	--	--	4.18	90.41	--	--	--	--	--	--	94.80
31-2-int.	--	0.29	--	37.92	55.44	2.63	0.57	--	1.00	--	--	97.85
31-2-core	0.33	--	16.50	45.80	28.50	2.12	3.80	--	2.94	--	--	99.99
31-3-rim	--	0.26	--	37.12	56.63	2.63	0.55	--	--	--	--	97.19
31-3-int.	0.26	0.31	0.22	38.24	55.89	2.57	0.55	--	--	--	--	98.04
31-3-core	0.27	0.27	16.67	45.41	28.77	1.89	3.92	--	3.41	--	--	100.61
31-4-rim	0.26	--	--	6.07	88.55	--	0.22	--	--	--	--	95.10
31-4-int.	--	0.35	1.79	41.32	50.85	2.76	1.08	--	0.98	--	--	99.13
31-4-core	0.24	--	16.17	45.98	28.65	1.90	3.92	--	3.13	--	--	99.99
31-5-rim	0.24	0.31	0.26	38.73	55.05	2.69	0.76	--	0.84	--	--	98.88
31-5-int.	--	0.26	16.22	45.82	29.55	1.95	3.69	--	3.21	--	--	100.70
31-5-core	--	--	15.95	47.10	27.99	1.70	4.28	--	2.85	--	--	99.87
57-1-rim	--	--	--	--	94.15	--	--	--	--	--	0.34	94.49
57-1-int.	--	--	--	--	93.46	--	--	--	--	--	0.35	93.81
57-1-core	0.23	--	--	--	93.97	--	--	--	--	--	0.30	94.50
57-2-rim	40.60	1.30	11.48	--	33.43	--	2.42	4.86	--	--	--	94.09
57-2-core	0.29	--	--	--	93.95	--	--	--	--	--	0.35	94.59
57-3-rim	--	--	--	--	94.04	--	--	--	--	--	--	94.04
57-3-int.	27.35	--	8.52	--	62.85	--	--	0.18	--	--	--	98.90
57-3-core	0.22	--	--	--	93.61	--	--	--	--	--	0.37	94.20
57-4-rim	64.41	0.37	17.48	--	3.46	--	1.12	3.40	--	--	--	90.24
57-4-int.	0.27	--	--	--	93.52	--	--	--	--	--	--	93.79
57-4-core	0.30	--	--	--	94.46	--	--	--	--	--	--	94.76
60-1-rim	--	--	--	3.49	91.34	--	--	--	--	--	--	94.83
60-1-int.	--	0.26	--	36.63	58.43	2.06	0.56	--	0.89	--	--	98.83
60-1-core	0.30	--	15.15	44.60	31.55	1.84	3.01	--	3.32	--	--	99.77
60-2-rim	0.20	--	--	7.08	86.30	0.36	--	--	--	--	--	93.94
60-2-int.	0.30	--	0.35	37.86	56.54	2.24	0.66	--	1.01	--	--	98.96
60-2-core	0.27	0.32	15.68	44.77	30.75	1.72	3.16	--	3.38	--	--	100.05

60-3-rim	–	0.26	0.20	38.26	55.58	2.21	0.65	–	0.99	–	–	98.15
60-3-int.	6.35	–	0.26	33.93	56.83	1.96	4.76	–	0.84	–	–	104.93
60-3-core	–	0.38	0.70	40.75	52.58	2.30	0.80	–	1.18	0.59	–	99.28
60-4-rim	–	0.29	0.27	38.26	55.77	2.39	0.66	–	0.99	–	–	98.63
60-4-int.	–	0.39	1.00	40.05	53.20	2.04	1.02	–	1.17	–	–	98.87
60-4-core	–	0.50	0.87	39.55	53.76	1.99	0.90	–	1.38	–	–	98.95
60-5-rim	0.25	–	0.21	37.65	57.01	2.01	0.60	–	1.13	–	–	98.86
60-5-int.	0.23	0.48	0.76	39.46	54.01	2.17	0.82	–	1.29	–	–	99.22
60-5-core	0.32	–	15.02	44.25	31.99	2.05	2.87	–	3.82	–	–	100.32
60-6-rim	0.25	–	–	33.49	59.75	2.59	0.25	–	0.90	–	–	97.23
60-6-int.	0.22	0.32	0.64	38.70	54.54	2.25	0.73	–	0.83	–	–	98.23
60-6-core	0.34	0.22	15.71	45.19	30.07	1.93	3.27	–	3.21	–	–	99.94

Appendix 2: continued

Appendix 3: Major and trace element data from the ultramafic unit underlying the Northern Beaulieu River belt (ND)=no data

Sample	PLC-97-29	PLC-97-56	PLC-97-57	PLC-97-117	PLC-97-162	PLC-98-3
SiO2	46.05	46.78	46.97	44.95	45.72	41.34
TiO2	1.45	2.28	2.27	0.55	0.76	0.21
Al2O3	6.81	13.09	12.84	15.17	16.5	4.8
Fe2O3	16.18	20.53	20.44	12.26	11.97	11.3
MnO	0.25	0.31	0.28	0.18	0.18	0.13
MgO	17.07	4.94	4.74	13.25	9.42	29.72
CaO	9.71	9.36	9.01	9.76	10.58	3.68
Na2O	0.43	2.92	4.25	0.94	2.22	0.02
K2O	0.08	0.45	0.3	0.44	0.44	0.02
P2O5	0.12	0.25	0.25	0.04	0.06	0.03
LOI	4.14	0.39	0.39	3.45	2.71	7.78
Total	102.29	101.3	101.74	100.99	100.56	99.03
Cr	1928	55	56	567	347	3994
Ni	948	34	30	358	213	1531
Co	106	102	95	75	60	94
Sc	23	17	31	0	11	25
V	238	450	424	168	225	93
Cu	180	81	106	61	85	39
Pb	8	20	11	3	24	11
Zn	126	150	123	114	76	73
Rb	18	15	15	24	24	28
Ba	0	141	147	53	168	229
Sr	15	91	92	100	134	0
Ga	10	23	19	13	15	5
Nb	9.92	7.77	8.08	1.13	1.74	12
Zr	80	125	129	44	54	29
Y	15.84	54.69	55.77	11.73	15.92	11
Th	0.8	0.93	0.94	0.22	0.3	1
U	0.25	0.22	0.24	0.06	0.07	1
La	9.02	9.22	9.33	2.02	2.51	ND
Ce	22.4	25.02	24.32	4.72	6.35	ND
Pr	3.39	4	3.95	0.72	0.99	ND
Nd	15.22	19.79	19.76	3.44	4.97	ND
Sm	3.86	6.4	6.31	1.11	1.56	ND
Eu	1.3	1.83	1.9	0.48	0.6	ND
Gd	ND	ND	ND	ND	ND	ND
Tb	0.58	1.43	1.43	0.28	0.37	ND
Dy	3.48	9.63	9.7	1.9	2.54	ND
Ho	0.64	2.09	2.07	0.43	0.58	ND
Er	1.7	6.03	5.98	1.26	1.65	ND
Tm	0.22	0.89	0.88	0.19	0.25	ND
Yb	1.37	5.66	5.59	1.23	1.64	ND
Lu	0.2	0.87	0.86	0.19	0.27	ND

Appendix 4: Representative samples from the Point Lake, Northern Beaulieu River and Central Beaulieu River belts displaying various textures.

Texture	Peltier Formation (Point Lake belt)	Northern Beaulieu River belt	Central Beaulieu River belt
Aphanitic	C7-82 (mafic massive flow); C7-101 (pillowed flow)	C7-66 (pillowed flow); C7-139 (pillowed flow)	
Porphyritic			W9-51 (rhyolite flow)
Vitrophyric		C7-166 (dacite tuff)	
Glomeroporphyritic			W9-50 (rhyolite flow); C8-18 (rhyolite flow); C8-21 (mafic dyke)
Ophitic	C7-77 (mafic massive flow); C7-98 (mafic dyke); C7-100 (mafic sill)	C7-114 (mafic dyke); C7-118 (mafic dyke); C7-163 (mafic dyke); C8-4 (pillowed flow)	C8-27 (mafic dyke)
Subophitic		C8-6 (pillowed flow)	C8-32 (mafic dyke)
Intersertal		C7-45 (pillowed flow)	C8-29 (massive mafic flow)
Hyalopilitic		C7-51 (pillowed flow)	
Pilotaxitic			C8-34 (fragments in pillow breccia)
Micropoikilitic			W9-51 (rhyolite flow); W9-45 (rhyolite flow)
Intergranular	C7-99 (mafic dyke)		
Amygdaloidal	C7-84 (mafic massive flow)		C8-34 (fragments in pillow breccia); C8-36 (pillowed flow); C8-37 (pillowed flow); C8-38 (pillowed flow)
Nematoblastic (hornblende porphyroblasts)		C7-68 (pillowed flow); C7-73 (pillowed flow)	
Microcrystalline quartz (chert)		C7-150 (felsic tuff)	
Quartz-feldspar recrystallization of glass	C7-101 (pillowed flow)	C7-45 (pillowed flow); C7-169 (felsic tuff); C7-68 (pillowed flow)	C8-35 (matrix of pillow breccia); C8-39 (pillowed flow); C8-41 (mafic lobate flow)

BIBLIOGRAPHY

Abbott, D. 1996. Plumes and hotspots as sources of greenstone belts. Lithos, 37: 113-127.

Allan, J.F, and Gorton, M.P., 1992. Geochemistry of igneous rocks from legs 127 and 128, Sea of Japan. In: Tamaki, K., Suyehiro, K., Allan, J., and McWilliams. M., (Eds.), Proceedings of the Ocean Drilling Program Scientific Results, 127/128, Pt. 2: 905-929.

Allen, R.L., Lundström, I., Ripa, M., Simeonov, A., and Christofferson, H., 1996. Facies analysis of a 1.9 Ga, continental margin, back-arc, felsic caldera province with diverse Zn-Pb-Ag-(Cu-Au) sulfide and Fe oxide deposits, Bergslagen Region, Sweden. Economic Geology, 91: 979-1008.

Arculus, R.J. 1987. The significance of source versus process in the tectonic controls of magma genesis. Journal of Volcanology and Geothermal Research, 32: 1-12.

Arndt, N.T., 1991. High Ni in Archean tholeiites. Tectonophysics, 187: 411-420.

Aubele, J.C., Crumpler, L.S., and Elston, W.E., 1988. Vesicle zonation and vertical structure of basalt flows. Journal of Volcanology and Geothermal Research, 35: 349-374.

Ayres, L.D., and Peloquin, A.S., 2000. Subaqueous, Paleoproterozoic, metarhyolite dome-flow-cone complex, Flin Flon greenstone belt, Manitoba, Canada. Precambrian Research, 101: 211-235.

Ayres, J.C., and Watson, E.B. 1991. Solubility of apatite, monazite, zircon, and rutile in supercritical aqueous fluids with implications for subduction zone geochemistry. In: Tarney, J., Pickering, K.T., Knipe, R.J., and Dewey, J.F., (Eds.), The behaviour and influence of fluids in subduction zones. London, The Royal Society, 139-149.

Ballard, R.D., Holcomb, R.T., and van Andel, T.H., 1979. The Galapagos Rift at 86°W: 3. Sheet flows, collapse pits, and lava lakes of the rift valley. Journal of Geophysical Research, 84: 5407-5422.

Baragar, W.R.A., 1966. Geochemistry of the Yellowknife volcanic rocks. Canadian Journal of Earth Sciences, 3: 9-30.

Barley, M.E., 1986. Incompatible-element enrichment in Archean basalts: a consequence of contamination by older sialic crust rather than mantle heterogeneity. Geology, 14: 947-950.

Barley, M.E., 1987. The Archaean Whim Creek Belt, and ensialic fault-bounded basin in the Pilbara Block, Australia. Precambrian Research, 37: 199-215.

Barrett, T.J., and MacLean, W.H., 1997. Volcanic sequences, litho-geochemistry and hydrothermal alteration in some bimodal VMS systems. In: Barrie, C.T., and Hannington, M.D. (Eds.), Volcanic-associated massive sulfide deposits: processes and examples in modern and ancient settings. Geological Association of Canada and the Society of Economic Geologists Co-Sponsored Short Course: 105-133.

Batiza, R., and White, J.D.L., 2000. Submarine lavas and hyaloclastite. In: Sigurdsson, H., Houghton, B., McNutt, S.R., Rymer, H., and Stix, J. (Eds.). Encyclopedia of Volcanoes. Academic Press, San Diego, 361-381.

Beccaluva, L., Ohnenstetter, D., and Ohnenstetter, M., 1979. Geochemical discrimination between ocean-floor and island-arc tholeiites-application to some ophiolites. Canadian Journal of Earth Sciences, 16: 1874-1882.

Bickle, M.J., 1978. Heat loss from the Earth: a constraint on Archaean tectonics from the relation between geothermal gradients and the rate of plate production. Earth and Planetary Science Letters, 40: 301-315.

Bickle, M.J., 1986. Implications of melting for stabilisation of the lithosphere and heat loss in the Archaean. Earth and Planetary Science Letters, 80: 314-324.

Bleeker, W., Davis, B., and Villeneuve, M., 1997a. The Slave Province: evidence for contrasting crustal domains and a complex, multistage tectonic evolution. In: Cook, F., Erdmer, P. (Comps.), Slave-Northern Cordillera Lithospheric Evolution Transect and Cordilleran Tectonics Workshop Meeting (March 7-9), University of Calgary, Lithoprobe Report No. 56, pp. 36-37.

Bleeker, W., Villeneuve, M., and Bethune, K., 1997b. Thematic structural studies in the Slave Province, Northwest Territories: contrasting basement/cover relationships on western and southwestern flanks of the Sleepy Dragon Complex. In: Current Research 1997-C, Geological Survey of Canada, 27-37.

Bleeker, W., Ketchum, J.W.F., Jackson, V.A., and Villeneuve, M.E. 1999a. The Central Slave Basement Complex, Part I: its structural topology and autochthonous cover. Canadian Journal of Earth Sciences, 36: 1083-1109.

Bleeker, W., Ketchum, J.W.F., and Davis, W.J., 1999b. The Central Slave Basement Complex, Part II: age and tectonic significance of high-strain zones along the basement-cover contact. Canadian Journal of Earth Sciences, 36: 1111-1130.

Bleeker, W., Ketchum, J., Stern, R., Sircombe, K., and Davis, B., 2000. Crustal architecture of the Slave Craton. In: Cook, F. and Erdmer, P. (Compilers) Slave-Northern Cordillera Lithospheric Evolution (SNORCLE). Transect and Cordilleran Tectonics Workshop Meeting (February), University of Calgary, Lithoprobe Report No. 72, 25-26.

Bostock, H.H., 1980. Geology of the Itchen Lake area, District of Mackenzie, 76E(W/2) and part of 86H. Geological Survey of Canada Open File 338, 155 pp.

Bouma, A.H., 1962. Sedimentology of some flysch deposits: a graphic approach to facies interpretations. Elsevier, Amsterdam, 168 pp.

Bourgeois, J., and Leithold, E.L., 1984. Wave-worked conglomerates - depositional processes and criteria for recognition. In: Koster, E.H. and Steel, R.J. (Eds.), Sedimentology of Gravels and Conglomerates. Canadian Society of Petroleum Geologists Memoir 10: 331-343.

Bowring, S.A., and Williams, I.S., 1998. Priscoan (4.00-4.03 Ga) orthogneisses from northwestern Canada. Contributions to Mineralogy and Petrology, 134: 3-16.

Bowring, S.A., Williams, I.S., and Compston, W., 1989. 3.96 Ga gneisses from the Slave Province, Northwest Territories. Geology, 17: 969-1064.

Bruce, P.M., and Huppert, H.E., 1990. Solidification and melting along dykes by the laminar flow of basaltic magma. In: Ryan, M.P. (Ed.), Magma transport and storage. Wiley & Sons, Chichester, 87-101.

Busby-Spera, C.J., 1987. Lithofacies of deep marine basalts emplaced on a Jurassic backarc apron, Baja California (Mexico). Journal of Geology, 95: 671-686.

Busby-Spera, C.J., and White, J.D.L., 1987. Variation in peperite textures associated with differing host-sediment properties. Bulletin of Volcanology, 49: 765-775.

Carey, S., and Sigurdsson, H.A., 1984. A model of volcanogenic sedimentation in marginal basins. In: Kokelaar, B.P. and Howells, M.F. (Eds.), Marginal Basin Geology. Geological Society Special Publication No 16, 37-58.

Cas, R.A.F., 1992. Submarine volcanism: eruption styles, products, and relevance to understanding the host-rock successions to volcanic-hosted massive sulfide deposits. Economic Geology, 87: 511-541.

Chadwick, W.W. Jr., and Embley, R.W., 1994. Lava flows from a mid-1980s submarine eruption on the Cleft segment, Juan de Fuca Ridge. Journal of Geophysical Research, 99: 4761-4776.

Condie, K.C., 1986. Geochemistry and tectonic setting of early Proterozoic supracrustal rocks in the southwestern United States. Journal of Geology, 94: 845-864.

Condie, K.C. 1989. Plate Tectonics and Crustal Evolution. New York, Pergamon Press, 476 pp.

Condie, K.C., 1994. Greenstones through time. In: Condie, K.C. (Ed.), Archean Crustal Evolution. Developments in Precambrian Geology 11. Elsevier, 85-120.

Corcoran, P.L, 2000. Recognizing distinct portions of seamounts using volcanic facies analysis: examples from the Archean Slave Province, Northwest Territories, Canada. Precamb. Geol. 101, 237-261.

Corcoran, P.L., and Dostal, J.. 2001. Development of an ancient back-arc basin overlying continental crust: the Archean Peltier Formation, Northwest Territories. Canada. Journal of Geology, 109: 329-348.

Corcoran, P.L., and Mueller, W.U., in press. The effects of weathering, sorting and source composition in Archean high-relief basins: examples from the Slave Province, Northwest Territories. Canada. In: Altermann, W. and Corcoran, P.L. (Eds) Precambrian Sedimentary Environments: modern approach to ancient depositional systems. International Association of Sedimentologists Special Publication.

Corcoran, P.L., Mueller, W.U., and Chown, E.H.. 1998. Climatic and tectonic influences on fan deltas and wave- to tide-controlled shoreface deposits: evidence from the Archean Keskarrah Formation, Slave Province, Canada. Sedimentary Geology, 120: 125-152.

Corcoran, P.L., Mueller, W.U., and Padgham, W.A., 1999. Influence of tectonism and climate on lithofacies distribution and sandstone and conglomerate composition in the Archean Beaulieu Rapids Formation, Northwest Territories, Canada. Precambrian Research. 94: 175-204.

Cousens, B.L., 2000. Geochemistry of the Archean Kam Group, Yellowknife Greenstone Belt, Slave Province, Canada. Journal of Geology, 108: 181-197.

Cousens, B.L., and Allan, J.F., 1992. A Pb, Sr, and Nd isotopic study of basaltic rocks from the Sea of Japan. Legs 127/128. In: Tamaki. K. Suyehiro, K, Allan, J., and McWilliams, M.. (Eds.), Proceedings of the Ocean Drilling Program Scientific Results, 127/128, Pt. 2, 805-817.

Cousineau, P., and Dimroth, E., 1982. Interpretation of the relations between massive, pillowed and brecciated facies in an Archean submarine andesite volcano--Amulet Andesite, Rouyn-Noranda, Canada. Journal of Volcanology and Geothermal Research, 13: 83-102.

Covello, L., Roscoe, S.M., Donaldson. J.A., Roach, D.. and Fyson, W.K., 1988. Archean quartz arenite and ultramafic rocks at Beniah Lake, Slave structural province, N.W.T. In: Current Research Part C. Geological Survey of Canada Paper 88-1C: 223-232.

Cox, K.G., and Hawkesworth, C.J., 1985. Geochemical stratigraphy of the Deccan Traps at Mahabaleshwar, Western Ghats, India, with implications for open system magmatic processes. Journal of Petrology, 26: 355-377.

Cunningham, M.P., and Lambert, R.S.J., 1989. Petrochemistry of the Yellowknife volcanic suite at Yellowknife, NWT. Canadian Journal of Earth Sciences, 26: 1630-1646.

Davis, W.J., and Hegner, E., 1992. Neodymium isotopic evidence for the tectonic assembly of Late Archean crust in the Slave Province, northwest Canada. Contributions to Mineralogy and Petrology, 111: 493-504.

De Baar, H.J.W., Bacon, M.P., and Brewer, P.G., 1983. Rare-earth distributions with a positive Ce anomaly in the Western North Atlantic Ocean. Nature, 301: 324-327.

DePaolo, D.J., and Wasserburg, G.J., 1976. Nd isotopic variations and petrogenetic models. Geophysical Research Letters, 3: 249-252.

De Rosen-Spence, A. F., Provost, G., Dimroth, E., Gochnauer, K., and Owen, V., 1980. Archean subaqueous felsic flows, Rouyn-Noranda, Quebec, Canada, and their Quaternary equivalents. Precambrian Research, 12: 43-77.

Des Marais, D.J., 1994. The Archean atmosphere: its composition and fate. In: Condie, K.C. (Ed.), Archean Crustal Evolution: Developments in Precambrian Geology 11. Elsevier, Amsterdam, 528 pp.

Dewey J.F., 1980. Episodicity, sequence, and style at convergent plate boundaries. In: Strangway, D.W. (Ed.), The continental crust and its mineral deposits. Geological Society of Canada Special Paper 20: 553-573.

Dimroth, E., Cousineau, P., Leduc, M., and Sanschagrin, Y., 1978. Structure and organization of Archean subaqueous basalt flows, Rouyn-Noranda area, Quebec, Canada. Canadian Journal of Earth Sciences, 15: 902-918.

Dimroth, E., Imreh, L., Cousineau, P., Leduc, and M., Sanschagrin, Y., 1985. Paleogeographic analysis of mafic submarine flows and its use in the exploration for massive sulphide deposits. In: Ayres, L.D., Thurston, P.C., Card, K.D., and Weber, W. (Eds.), Evolution of Archean Supracrustal Sequences. Geological Association of Canada Special Paper 28, 203-222.

Dostal, J., and Corcoran, P.L. 1998. Evolution of the Slave Province as recorded by physical volcanology, trace elements and isotopic systematics of selected Archean greenstone belts along the Beniah Lake fault, Slave Province, Northwest Territories. DIAND EGS Report 98-11: 26 pp.

Dudas, F.O., Henderson, J.B., and Mortensen, J.K., 1990. U-Pb ages of zircon from the Anton Complex, southern Slave Province, Northwest Territories. In: Radiogenic age and isotope studies Report 3. Geological Survey of Canada Paper 89-2: 39-44.

Easton, R.M., 1984. Growth and evolution of volcanic edifices--with implications for Precambrian volcanoes. In: Easton, R.M., and Easton, M.G. (Eds.). Geological Association of Canada Short Course Notes 4: 1-40.

Easton, R.M., 1985. The nature and significance of pre-Yellowknife Supergroup rocks in the Point Lake area, Slave Structural Province, Canada. In: Ayres, L.D., Thurston, P.C., Card, K.D., and Weber, W., (Eds.), Evolution of Archean Supracrustal Sequences. Geological Association of Canada Special Paper 28: 153-167.

Easton, R.M., Boodle, R.L., and Zalusky, L., 1982. Evidence for gneissic basement to the Archean Yellowknife Supergroup in the Point Lake area, Slave Structural Province, District of Mackenzie, N.W.T. In: Current Research, Part B, Geological Survey of Canada Paper 82-1B: 33-41.

Eddy, C.A., Dilek, Y., Hurst, S., and Moores, E.M., 1998. Seamount formation and associated caldera complex and hydrothermal mineralization in ancient oceanic crust, Troodos ophiolite (Cyprus). Tectonophysics, 292: 189-210.

Fink, J.H., 1983. Structure and emplacement of a rhyolitic obsidian flow: Little Glass Mountain, Medicine Lake Highland, northern California. Geological Society of America Bulletin, 94: 362-380.

Fink, J.H., and Anderson, S.W., 2000. Lava domes and coulees. In: Sigurdsson, H., Houghton, B., McNutt, S.R., Rymer, H., and Stix, J. (Eds.), Encyclopedia of Volcanoes. Academic Press, San Diego, 307-319.

Fisher, R.V., 1960. Criteria for recognition of laharic breccias, southern Cascade Mountains, Washington. Geological Society of America Bulletin, 71: 127-132.

Fisher, R.V., 1961. Proposed classification of volcaniclastic sediments and rocks. Geological Society of America Bulletin, 72: 1409-1414.

Fisher, R.V., 1966. Rocks composed of volcanic fragments. Earth Science Reviews, 1: 287-298.

Fisher, R.V., 1984. Submarine volcaniclastic rocks. In: Kokelaar, B.P., and Howells, M.F. (Eds.), Marginal Basin Geology: volcanic and associated sedimentary and tectonic processes in modern and ancient marginal basins. Geological Society Special Publication No. 16: 5-27.

Fisher, R.V., and Schmincke, H.-U., 1984. Pyroclastic Rocks. Springer-Verlag, New York, 472 pp.

Fiske, R.S., and Matsuda, T., 1964. Submarine equivalents of ash flows in the Tokiwa Formation, Japan. American Journal of Science, 262: 76-106.

Floyd, P.A., 1989. Geochemical features of intra-plate oceanic plateau basalts. In: Saunders, A.D., and Norry, M.J. (Eds.), Magmatism in the Ocean Basins. Geological Society of London Special Publication 42: 215-230.

Fornari, D.J., Ryan, W.B.F., and Fox, P.J., 1985. Sea-floor lava fields on the East Pacific Rise. Geology, 13: 413-416.

Forslund, T., and Gudmundsson, A., 1991. Crustal spreading due to dikes and faults in southwest Iceland. Journal of Structural Geology, 13: 443-457.

Fritz, W.J., and Vanko, D.A., 1992. Geochemistry and origin of a black mudstone in a volcaniclastic environment, Ordovician Lower Rhyolitic Tuff Formation, North Wales, UK. Sedimentology, 39: 663-674.

Fryer, P., 1995. Geology of the Mariana Trough. In: Taylor, B. (Ed.), Backarc Basins: Tectonism and Magmatism. Plenum Press, New York, 237-279.

Gamble, J.A., and Wright, I.C., 1995. The Southern Havre Trough: geological structure and magma petrogenesis of an active backarc rift complex. In Taylor, B., (Ed.), Backarc Basins: tectonics and magmatism. New York, Plenum Press, 29-62.

Gamble, J.A., Wright, I.C., Woodhead, J.D., and McCulloch, M.T., 1995. Arc and back-arc geochemistry in the southern Kermadec arc-Ngatoro Basin and offshore Taupo Volcanic Zone, SW Pacific. In: Smellie, J.L. (Ed.), Volcanism associated with extension at consuming plate margins. Geological Society Special Publication No. 81: 193-212.

Gibson, H.L., 1999. Rhyolitic lava flows and domes. In: Physical volcanology: felsic volcanic processes, deposits and mineralization. Geological Association of Canada Short Course Notes: 31 pp.

Gibson, H., Morton, R., and Hudak, G., 1997. Subaqueous volcanism: environments and controls on VMS mineralization. In: Barrie, T.C., and Hannington, M.D. (Eds.), Volcanic-Associated Massive Sulfide Deposits: Processes and Examples in Modern and Ancient Settings. GAC-MDD-SEG co-sponsored short course, Geological Association of Canada/Mineralogical Association of Canada: 13-51.

Goodwin, A.M., 1977. Archean basin-cratonic complexes and the growth of Precambrian shields. Canadian Journal of Earth Sciences, 14: 2737-2759.

Goodwin, A.M., 1981. Archean plates and greenstone belts. In: Kroner, A. (Ed.), Precambrian Plate Tectonics. Amsterdam, Elsevier, 105-135.

Govindaraju, K., 1994. Compilation of working values and sample descriptions for 383 geostandards. Geostandards Newsletter, 18: 1-158.

Griffiths, R.W., and Fink, J.H., 1992. Solidification and morphology of submarine lavas: a dependence on extrusion rate. Journal of Geophysical Research, 97: 19729-19737.

Grove, T.L., 2000. Origin of magmas. In: Sigurdsson, H., Houghton, B., McNutt, S.R., Rymer, H., and Stix, J. (Eds.), Encyclopedia of Volcanoes. Academic Press, San Diego, 133-147.

Hamilton, W.B., 1995. Subduction systems and magmatism. In: Smellie, J.L. (Ed.), Volcanism associated with extension at consuming plate margins. Geological Society Special Publication No. 81: 3-28.

Hargreaves, R., and Ayres, L.D., 1979. Morphology of Archean metabasalt flows, Utik Lake, Manitoba. Canadian Journal of Earth Sciences, 16: 1452-1466.

Hart, B.S., and Plint, A.G., 1995. Gravelly shoreface and beachface deposits. In: A.G. Plint (Ed.) Sedimentary facies analysis. International Association of Sedimentologists Publication 22: 75-99.

Haskin, L.A., Haskin, M.A., Frey, F.A., and Wildman, T.R., 1968. Relative and absolute terrestrial abundances of the rare earths. In: Ahrens, L.H. (Ed.), Origina and distribution of the elements. Pergamon, Oxford: 889-911.

Hathway, B., 1994. Sedimentation and volcanism in an Oligocene-Miocene intra-oceanic arc and fore-arc, southwestern Viti Levu, Fiji. Journal of the Geological Society, London, 151: 499-514.

Hawkins, J.W. Jr., 1995. The geology of the Lau Basin. In: Taylor, B. (Ed.), Backarc Basins: Tectonism and Magmatism. Plenum Press, New York, 63-138.

Head, J.W. III, Wilson, L., and Smith, D.K., 1996. Mid-ocean ridge eruptive vent morphology and substructure: evidence for dike widths, eruption rates, and evolution of eruptions and axial volcanic ridges. Journal of Geophysical Research, 101: 28265-28280.

Hekinian, R., Thompson, G., and Bideau, D., 1989. Axial and off-axial heterogeneity of basaltic rocks from the East Pacific Rise at 12°35'N-12°51'N and 11°26'N-11°30'N. Journal of Geophysical Research, 94: 17437-17463.

Helmstaedt, H., King, J.E., and Boodle, R., 1980. Geology of the Banting and Walsh lakes map-areas, NTS 85 J/9. DIAND EGS 1980-5.

Helmstaedt, H., and Padgham, W., 1986. A new look at the stratigraphy of the Yellowknife Supergroup at Yellowknife, N.W.T.--implications for the age of gold-bearing shear zones and Archean basin evolution. Canadian Journal of Earth Sciences, 23: 454-475.

Helmstaedt, H., Padgham, W.A., and Brophy, J.A., 1986. Multiple dikes in Lower Kam Group, Yellowknife greenstone belt: evidence for Archean sea-floor spreading? Geology, 14: 562-566.

Henderson, J.B., 1970. Stratigraphy of the Yellowknife Supergroup, Yellowknife Bay-Prosperous Lake area, District of Mackenzie. Geological Survey of Canada Paper 70-26.

Henderson, J.B., 1975. Sedimentological studies of the Yellowknife Supergroup in the Slave Structural Province. Geological Survey of Canada Paper 75-1A: 325-330.

Henderson, J.B., 1981. Archean basin evolution in the Slave Province, Canada. In: Kroner, A. (Ed.) Precambrian Plate Tectonics. Amsterdam, Elsevier, 213-236.

Henderson, J.B., 1985. Geology of the Yellowknife-Hearne Lake area, District of Mackenzie: a segment across an Archean basin. Geological Survey of Canada Memoir 414.

Henderson, J.B., 1988. Geology, Keskarrah Bay Area, District of Mackenzie, Northwest Territories. Geological Survey of Canada Map 1679A, scale 1:50 000.

Henderson, J.B., 1998. Geology of the Keskarrah Bay Area, District of Mackenzie, Northwest Territories. Geological Survey of Canada Bulletin 527, 122 pp.

Henderson, J.B., and Brown, I.C., 1966. Geology and structure of the Yellowknife greenstone belt, District of Mackenzie. Geological Survey of Canada Bulletin 141.

Henderson, J.B., Loveridge, W.D. and Sullivan, R.W., 1982. A U-Pb study of zircon from granitic basement beneath the Yellowknife Supergroup, Point Lake, District of Mackenzie. In: Current Research, Part C. Geological Survey of Canada Paper 82-1C, 173-177.

Henderson, J.B., van Breemen, O., and Loveridge, W.D., 1987. Some U-Pb zircon ages from Archean basement, supracrustal and intrusive rocks, Yellowknife-Hearne Lake area, District of Mackenzie. In: Radiogenic Age and Isotopic Studies Report 1. Geological Survey of Canada Paper 87-2: 111-121.

Honma, H., Kusakabe, M., Kagami, H., Iizumi, S., Sakai, H., Kodama, Y., and Kimura, M., 1991. Major and trace element chemistry and D/H, $^{18}O/^{16}O$, $^{87}Sr/^{86}Sr$ and $^{143}Nd/^{144}Nd$ ratios of rocks from the spreading center of the Okinawa Trough, a marginal back-arc basin. Geochemical Journal, 25: 121-136.

Hooper, P.R., 2000. Flood basalt provinces. In: Sigurdsson, H., Houghton, B., McNutt, S.R., Rymer, H., and Stix, J. (Eds.), Encyclopedia of Volcanoes. Academic Press. San Diego, 345-359.

Howard, J.D., and Reineck, H.-E., 1981. Depositional facies of high-energy beach to offshore sequence: a comparison with a low-energy sequence. American Association of Petroleum Geologists Bulletin 65: 807-830.

Huijsmans, J.P.P., and Barton, M.. 1989. Geochemical evolution of two shield volcanoes from Santorini, Aegean Sea, Greece: evidence for zoned magma chambers from cyclic compositional variations. Journal of Petrology, 30: 583-625.

Hunter, A.G., 1998. Intracrustal controls on the coexistence of tholeiitic and calc-alkaline magma series at Aso Volcano, SW Japan. Journal of Petrology, 39: 1255-1284.

Hunter, A.G., and Blake, S., 1995. Petrogenetic evolution of a coexisting tholeiitic and calc-alkaline magma series: Towada volcano, Japan. Journal of Petrology. 36: 1579-1605.

Isachsen. C.E., 1992. U-Pb zircon geochronology of the Yellowknife Volcanic Belt and subjacent rocks. N.W.T.. Canada: constraints on the timing, duration, and mechanics of greenstone belt formation. Unpublished Ph.D. thesis, Washington University. St. Louis, 164 pp.

Isachsen, C.E., and Bowring, S.A.. 1994. Evolution of the Slave Craton. Geology. 22: 917-920.

Isachsen, C.E., and Bowring, S.A.. 1997. The Bell Lake group and Anton Complex: a basement - cover sequence beneath the Archean Yellowknife greenstone belt revealed and implicated in greenstone belt formation. Canadian Journal of Earth Sciences, 34: 169-189.

Isachsen, C.E., Bowring, S.A., and Padgham, W.A., 1991. U-Pb zircon geochronology of the Yellowknife volcanic belt, NWT, Canada: New constraints on the timing and duration of greenstone belt magmatism. Journal of Geology, 99: 55-67.

Jackson, V.A. 1984. Structure and metamorphism of the Keskarrah Bay area, Point Lake. N.W.T., second preliminary report. Contributions to Geology of Northwest Territories, v. 1, 47-54.

Jackson, V. A., 1996. Preliminary Geology of part of the Lower Supracrustal Succession in the Bell Lake Area (85 J/16). DIAND EGS Map 1996-17.

Jakes, P., and Gill, J., 1970. Rare earth elements and the island arc tholeiitic series. Earth and Planetary Science Letters, 9: 17-28.

Jakes, P., and White, A.J.R., 1972. Major and trace element abundances in volcanic rocks of orogenic areas. Geological Society of America Bulletin, 83: 29-40.

James, D.T., and Mortenson, J.K., 1992. An Archean metamorphic core complex in the southern Slave Province: basement-cover structural relations between the Sleepy Dragon Complex and the Yellowknife Supergroup. Canadian Journal of Earth Sciences, 29: 2133-2145.

Johnson, H.D., and Baldwin, C.T., 1996. Shallow clastic seas. In: Reading, H.G. (Ed.), Sedimentary Environments: processes, facies and stratigraphy. Blackwell Science: 232-280.

Johnson, H.D., and Levell, B.K., 1995. Sedimentology of a transgressive, estaurine sand complex: the Lower Cretaceous Woburn Sands (Lower Greensand), southern England. In: Plint, A.G. (Ed.) Sedimentary facies analysis. International Association of Sedimentologists Publication 22: 17-46.

Kano, K., Takeuchi, K., Yamamoto, T., and Hoshizumi, H., 1991. Subaqueous rhyolite block lavas in the Miocene Ushikiri Formation, Shimane Peninsula, SW Japan. Journal of Volcanology and Geothermal Research, 46: 241-253.

Kano, K., Yamamoto, T., and Takeuchi, K., 1993. A Miocene island-arc volcanic seamount: the Takashibiyama Formation, Shimane Peninsula, SW Japan. Journal of Volcanology and Geothermal Research, 59: 101-119.

Karig, D.E., 1971. Origin and development of marginal basins in the Western Pacific. Journal of Geophysical Research, 76: 2542-2561.

Karig, D.E., Anderson, R.N., and Bibee, L.D., 1978. Characteristics of back arc spreading in the Mariana Trough. Journal of Geophysical Research, 83: 1213-1226.

Kasting, J.F., 1993. Earth's early atmosphere. Science, 259: 920-926.

Kay, S.M., Kay, R.W., and Citron, G.P., 1982. Tectonic controls on tholeiitic and calc-alkaline magmatism in the Aleutian arc. Journal of Geophysical Research, 87: 4051-4072.

Kennish, M.J., Lutz, R.A., 1998. Morphology and distribution of lava flows on mid-ocean ridges: a review. Earth Science Reviews, 43: 63-90.

Kerr, A., Jenner, G.A., and Fryer, B.J., 1995. Sm-Nd isotopic geochemistry of Precambrian to Paleozoic granitoid suites and the deep-crustal structure of the southeast margin of the Newfoundland Appalachians. Canadian Journal of Earth Sciences, 32: 224-245.

Kerrich, R, and Wyman, D.A.. 1996. The trace element systematics of igneous rocks in mineral exploration: an overview. In: Wyman, D.A. (Ed.), Trace element geochemistry of volcanic rocks: applications for massive sulphide exploration. Geological Association of Canada Short Course Notes Volume 12: 1-50.

Ketchum, J., and Bleeker, W. 2000. New field and U-Pb data from the Central Slave Cover Group near Yellowknife and the Central Slave Basement Complex at Point Lake. In: Cook, F. and Erdmer, P. (Compilers). Slave-Northern Cordillera Lithospheric Evolution (SNORCLE). Transect and Cordilleran Tectonics Workshop Meeting (February), University of Calgary. Lithoprobe Report No. 72, 27-31.

Klein. G.D., 1985. The control of depositional depth. tectonic uplift, and volcanism on sedimentation processes in the back-arc basins of the western Pacific. Journal of Geology, 92: 1-25.

Kokelaar, P., 1986. Magma-water interactions in subaqueous and emergent basaltic volcanism. Bulletin of Volcanology, 48: 275-289.

Krapez. B.. and Barley, M.E.. 1987. Archaean strike-slip faulting and related ensialic basins: evidence from the Pilbara Block. Australia. Geological Magazine. 124: 555-567.

Krogh. T.E., and Gibbins. W.. 1978. U-Pb isotopic ages of basement and supracrustal rocks in the Point Lake area of the Slave Structural Province. Canada: Geological Association of Canada Abstract. p. 438.

Kusky. T.M.. 1989. Accretion of the Archean Slave Province. Geology. 17: 63-67.

Kusky. T.M.. 1990. Evidence for Archean ocean opening and closing in the southern Slave Province. Tectonics. 9: 1533-1563.

Kusky, T.M., 1991. Structural development of an Archean orogen, western Point Lake. Northwest Territories. Tectonics, 10: 820-841.

Kusky. T.M.. and Kidd, W.S.F.. 1992. Remnants of an Archean oceanic plateau, Belingwe greenstone belt, Zimbabwe. Geology, 20: 43-46.

Lafrance. B., Mueller, W.U.. Daigneault, R., and Dupras, N.. 2000. Evolution of a submerged composite arc volcano: volcanology and geochemistry of the Normétal volcanic complex. Abitibi greenstone belt, Québec, Canada. Precambrian Research. 101: 277-311.

Lambert, M.B., 1988. Cameron River and Beaulieu River volcanic belts of the Archean Yellowknife Supergroup, District of Mackenzie, Northwest Territories. Geological Survey of Canada Bulletin 382: 145 pp.

Lambert, M.B., Ernst, R.E., and Dudas, F.O.L., 1992. Archean mafic dyke swarms near the Cameron River and Beaulieu River volcanic belts and their implications for tectonic modeling of the Slave Province. Northwest Territories. Canadian Journal of Earth Sciences, 29: 2226-2248.

Lambert, M.B., and van Breemen, O., 1991. U-Pb zircon ages from the Sleepy Dragon Metamorphic Complex and a new occurrence of basement within the Meander Lake Plutonic Suite, Slave Province, N.W.T. In: Radiogenic age and isotopic studies: report 4. Geological Survey of Canada Paper 90-2: 79-84.

Leitch, E.C., 1984. Marginal basins of the SW Pacific and the preservation and recognition of their ancient analogues: a review. In: Kokelaar, B.P., and Howells. M.F. (Eds.), Marginal Basin Geology. Geological Society of London Special Publication, 16: 97-108.

Letouzey, J., and Kimura, M., 1985. Okinawa Trough genesis: structure and evolution of a backarc basin developed in a continent. Marine Petroleum Geology. 2: 111-130.

Leybourne, M.I., Van Wagoner, N.A., and Ayres. L.D., 1997. Chemical stratigraphy and petrogenesis of the Early Proterozoic Amisk Lake volcanic sequence, Flin Flon-Snow Lake greenstone belt. Canada: Journal of Petrology. 38: 1541-1564.

Lonsdale, P., and Batiza, R., 1980. Hyaloclastite and lava flows on young seamounts examined with a submersible. Geological Society of America Bulletin. 91: 545-554.

Lowe, D.R., 1982. Sediment gravity flows: II. Depositional models with special reference to the deposits of high-density turbidity currents. Journal of Sedimentary Petrology. 52: 279-297.

Lowe, D.R., 1988. Suspended-load fallout rate as an independent variable in the analysis of current structures. Sedimentology. 35: 765-776.

Lowe, D.R., 1994. Archean greenstone-related sedimentary rocks. In: Condie, K.C. (Ed.), Archean crustal evolution. Developments in Precambrian Geology 11, Elsevier: 121-169.

Mackenzie, D., and Bickle, M.J., 1988. The volume and composition of melt generated by extension of the lithosphere. Journal of Petrology, 29: 625-679.

MacLachlan, K., and Helmstaedt, H., 1995. Geology and geochemistry of an Archean mafic dyke complex in the Chan Formation: basis for a revised plate-tectonic model of the Yellowknife greenstone belt. Canadian Journal of Earth Sciences, 32: 614-630.

Manetti, P., Peccerillo, A., and Poli, G. 1979. REE distribution in Upper Cretaceous calc-alkaline and shoshonitic volcanic rocks from eastern Srednogorie (Bulgaria). Chemical Geology, 26: 51-63.

McGlynn, J.C., and Henderson, J.B.. 1970. Archean volcanism and sedimentation in the Slave Province. In: Baer, A.J. (Ed.), Symposium on basins and geosynclines of the Canadian Shield. Geological Survey of Canada Paper 70-40: 31-44.

McKenzie, D.. and O'Nions. R.K., 1991. Partial melt distributions from inversion of rare earth element concentrations. Journal of Petrology, 32: 1021-1091.

McMillan, K., Cross. R.W., and Long, P.E.. 1987. Two-stage vesiculation in the Cohassett flow of the Grande Ronde Basalt, south-central Washington. Geology, 15: 809-812.

McPhie, J.. 1995. A Pliocene basaltic seamount: Ba Volcanic Group at Rakiraki, Fiji. Journal of Volcanology and Geothermal Research, 64: 193-210.

McPhie. J., Doyle. M., and Allen. R.. 1993. Volcanic textures: a guide to the interpretation of textures in volcanic rocks. Centre for Ore Deposit and Exploration Studies, University of Tasmania, Tasmania, 198 pp.

Miller. C.A.. Barton. M.. Hanson, R.E.. and Fleming, T.H., 1994. An Early Cretaceous volcanic arc/marginal basin transition zone, Peninsula Hardy. southernmost Chile. Journal of Volcanology and Geothermal Research. 63: 33-58.

Mitchell. A.H.. and Reading, H.G.. 1971. Evolution of island arcs. Journal of Geology, 79: 253-284.

Miyashiro, A.. 1974. Volcanic rock series in island arcs and active continental margins. American Journal of Science. 274: 321-355.

Moore, J.G., 1975. Mechanism of formation of pillow lava. American Scientist, 63: 269-277.

Moore, J.G., and Lockwood, J.P.. 1978. Spreading cracks on pillow lava. Journal of Geology, 86: 661-671.

Moore, J.G.. and Schilling, J.-G.. 1973. Vesicles. water, and sulfur in Reykjanes Ridge Basalts. Contributions to Mineralogy and Petrology, 41: 105-118.

Moores. E. M., and Twiss, R.J.. 1995. Tectonics. W.H. Freeman and Company, New York, 415 pp.

Mortensen. J.K., Henderson, J.B., Jackson, V.A.. and Padgham, W.A., 1992. U-Pb geochronology of Yellowknife Supergroup felsic volcanic rocks in the Russell Lake

and Clan Lake areas, southwestern Slave Province, N.W.T. In: Radiogenic age and isotopic studies 5, Geological Survey of Canada Paper 91-2, 1-7.

Mueller, W., 1991. Volcanism and related slope to shallow marine volcaniclastic sedimentation: an Archean example, Chibougamau, Quebec, Canada. Precambrian Research, 49: 1-22.

Mueller, W.U., Bowring, S.A., Corcoran, P.L., and Pickett, C., 1998. Unconformities, major faults and the evolution of volcano-sedimentary basins on the Slave craton. In: Cook, F., Erdmer, P. (Comps.), Slave-Northern Cordillera Lithospheric Evolution Transect and Cordilleran Tectonics Workshop Meeting (March 6-8), Simon Fraser University, Lithoprobe Report No. 64: 15-16.

Mueller, W.U., and Corcoran, P.L., 1998. Late-orogenic basins in the Archaean Superior Province, Canada : characteristics and inferences. Sedimentary Geology, 120 : 177-203.

Mueller, W.U., and Corcoran, P.L., in press. Volcanic and sedimentary processes operating on a marginal continental arc: evidence from the Archean Raquette Lake Formation, Slave Province, Canada. Sedimentary Geology.

Mueller, W.U., Corcoran, P.L., and Donaldson, J.A., in press. Sedimentology of a tide- and wave-influenced high energy Archean coastline: the Jackson Lake Formation, Slave Province, Canada. In: Altermann, W. and Corcoran, P.L. (Eds) Precambrian Sedimentary Environments: modern approach to ancient depositional systems. International Association of Sedimentologists Special Publication.

Mueller, W.U., Corcoran, P.L., Simard, R.L., and Mortensen, J.K., 2001. Continental arc-backarc evolution : the 2650-2710 Ma volcano-sedimentary sequences in the central Slave Province. In: Cook, F., and Erdmer, P. (Comps.), Slave-Northern Cordillera Lithospheric Evolution Transect and Cordilleran Tectonics Workshop Meeting (February 22-25), Pacific Geoscience Centre, Lithoprobe Report No. 79: 12-17.

Mueller, W., and Donaldson, J.A., 1992. A felsic feeder dyke swarm formed under the sea: the Archean Hunter Mine Group, south-central Abitibi belt, Quebec, Canada. Bulletin of Volcanology, 54: 117-134.

Mueller, W.U., Mortensen, J.K., Corcoran, P.L., and Simard, R.L., 2000. Constraints on the geological evolution at Point and Beniah Lakes, Northwest Territories: results from preliminary U-Pb zircon age determinations. In: Cook, F. and Erdmer, P. (Compilers) Slave-Northern Cordillera Lithospheric Evolution (SNORCLE). Transect and Cordilleran Tectonics Workshop Meeting (February), University of Calgary, Lithoprobe Report No. 72, 8-10.

Nisbet, E.G., and Fowler, C.M.R., 1983. Model for Archean plate tectonics. Geology, 11: 376-379.

Nohda, S., and Wasserburg, G.J., 1986. Trends of Sr and Nd isotopes through time near the Japan Sea in northeastern Japan. Earth and Planetary Science Letters, 78: 157-167.

Northrup, C.J., Isachsen, C., and Bowring, S.A., 1999. Field relations, U-Pb geochronology and Sm-Nd isotope geochemistry of the Point Lake greenstone belt and adjacent gneisses, central Slave craton, N.W.T., Canada. Canadian Journal of Earth Sciences, 36: 1043-1059.

Orton, G.J., 1996. Volcanic environments. In: Reading, H.G. (Ed.), Sedimentary Environments: processes, facies and stratigraphy. Blackwell Science, Oxford, 485-567.

Padgham, W.A., 1980. An Archean ignimbrite at Yellowknife and its relationship to the Kam Formation basalts. Precambrian Research, 12: 99-113.

Padgham, W.A., 1985. Observations and speculations on supracrustal successions in the Slave Structural Province. In: Ayers, L.D., Thurston, P.C., Card, K.D., and Weber, W., (Eds.) Evolution of Archean Supracrustal Sequences. Geological Association of Canada Special Paper 28, 133-152.

Padgham, W.A., 1987. The Yellowknife volcanic belt: setting and stratigraphy. In: Padgham, W.A. (Ed.), Yellowknife guide book. Mineral Deposits Division, Geological Survey of Canada: 11-19.

Padgham, W.A., and Fyson, W.K., 1992. The Slave Province: a distinct Archean craton. Canadian Journal of Earth Sciences, 29: 2072-2086.

Pearce, J.A., 1982. Trace element characteristics of lavas from destructive plate boundaries. In: Thorpe, R.S. (Ed.), Andesites. New York, John Wiley & Sons, 525-548.

Pearce, J.A., 1996. A user's guide to basalt discrimination diagrams. In: Wyman, D.A. (Ed.), Trace element geochemistry of volcanic rocks: applications for massive sulphide exploration. Geological Association of Canada Short Course Notes Volume 12: 79-113.

Pearce, J.A., Harris, N.B., and Tindle, A.G., 1984. Trace element discrimination for the tectonic interpretation of granitic rocks. Journal of Petrology, 23: 956-983.

Pearce, J.A., and Norry, M.J., 1979. Petrogenetic implications of Ti, Zr, Y, and Nb variations in volcanic rocks. Contributions to Mineralogy and Petrology, 69: 33-47.

Pearce, J.A., and Parkinson, I.J., 1993. Trace element models for mantle melting: applications to volcanic arc petrogenesis. Geological Society of London Special Publications, 76: 373-403.

Perfit, M.R., and Davidson, J.P., 2000. Plate tectonics and volcanism. In: Sigurdsson, H., Houghton, B., McNutt, S.R., Rymer, H., and Stix, J. (Eds.), Encyclopedia of Volcanoes. Academic Press, San Diego, 89-113.

Perfit, M.R., Gust, D.A., Bence, A.E., Arculus, R.J., and Taylor, S.R., 1980. Chemical characteristics of island-arc basalts: implications for mantle sources. Chemical Geology, 30: 227-256.

Polat, A., Kerrich, R., and Wyman, D.A., 1998. The late Archean Schreiber-Hemlo and White River-Dayohessarah greenstone belts, Superior Province: collages of oceanic plateaus, oceanic arcs, and subduction-accretion complexes. Tectonophysics, 289: 295-326.

Pouclet, A., and Bellon, H., 1992. Geochemistry and isotopic composition of volcanic rocks from the Yamato Basin: Hole 794D, Sea of Japan. In: Tamaki, K. Suyehiro, K, Allan, J., and McWilliams, M. (Eds.), Proceedings of the Ocean Drilling Program Scientific Results, 127/128, Pt. 2, 779-789.

Pouclet, A., Lee, J.-S., Vidal, P., Cousens, B., and Bellon, H., 1994. Cretaceous to Cenozoic volcanism in South Korea and in the Sea of Japan: magmatic constraints on the opening of the back-arc basin. In: Smellie, J.L. (Ed.) Volcanism Associated with Extension at Consuming Plate Margins. Geological Society of London, U.K., 169-191.

Reinson, G.E. 1984. Barrier island and associated strand-plain systems. In: Walker, R.G. (Ed.), Facies models (2nd edition). Geoscience Canada Reprint Series 1, 119-140.

Relf, C., Chouinard, A., Sandeman, H., and Villeneuve, M., 1994. Contact relationships between the Anialik River volcanic belt and the Kangguyak gneiss belt, northwestern Slave Province, Northwest Territories. In: Current Research 1994-C, Geological Survey of Canada, 49-59.

Relf, C., Sandeman, H.A., and Villeneuve, M.E., 1999. Tectonic and thermal history of the Anialik River area, northwestern Slave Province, Canada. Canadian Journal of Earth Sciences, 36: 1207-1226.

Richards, M.A., Jones, D.L., Duncan, R.A., and DePaolo, D.J., 1991. A mantle plume initiation model for the Wrangellia flood basalts and other oceanic plateaus. Science, 254: 263-267.

Roach, D., 1990. Geology of the Beniah Lake Area NTS 85 P/8. DIAND EGS Map 1990-2, scale 1:50 000.

Robertson, A., and Degnan, P., 1994. The Dras arc Complex: lithofacies and reconstruction of a Late Cretaceous oceanic volcanic arc in the Indus Suture Zone, Ladakh Himalaya. Sedimentary Geology, 92: 117-145.

Robillard, I., Francis, D., and Ludden, J.N., 1992. The relationship between E- and N-type magmas in the Baffin Bay lavas. Contributions to Mineralogy and Petrology, 112: 230-241.

Rogers, N., and Hawkesworth, C., 2000. Composition of magmas. In: Sigurdsson, H. (Ed.) Encyclopedia of Volcanoes. San Diego, Academic Press, 115-131.

Rolland, Y., Pêcher, A., and Picard, C., 2000. Middle Cretaceous back-arc formation and arc evolution along the Asian margin: the Shyok Suture Zone in northern Ladakh (NW Himalaya). Tectonophysics, 325: 145-173.

Rollinson, H., 1993. Using geochemical data: evaluation, presentation, interpretation. Addison Wesley Longman Limited, England, 352 pp.

Roscoe, S. M., Stubley, M., and Roach, D., 1989. Archean quartz arenites and pyritic paleoplacers in the Beaulieu River supracrustal belt, Slave Structural Province, N.W.T. In: Current Research. Geological Survey of Canada Paper 89-1C: 199-214.

Sahagian, D., 1985. Bubble migration and coalescence during the solidification of basaltic lava flows. Journal of Geology, 93: 205-211.

Sajona, F.G., Maury, R.C., Pubellier, M., Leterrier, J., Bellon, H., and Cotton, J., 2000. Magmatic source enrichment by slab-derived melts in a young post-collision setting, central Mindanao (Philippines). Lithos, 54: 173-206.

Sato, H., and Amano, K., 1991. Relationship between tecetonics, volcanism, sedimentation and basin development. Late Cenozoic, central part of Northern Honshu, Japan. Sedimentary Geology, 74: 323-343.

Saunders, A.D., and Tarney, J., 1984. Geochemical characteristics of basaltic volcanism within back-arc basins. In: Kokelaar, B.P, and Howells, M.F. (Eds.) Marginal Basin Geology. Geological Society of London Special Publication16: 59-76.

Schmidt, R., and Schmincke, H.-U., 2000. Seamounts and island building. In: Sigurdsson, H. (Ed.) Encyclopedia of Volcanoes. San Diego, Academic Press, 383-402.

Schmincke, H.-U., 1967. Fused tuff and peperites in south central Washington. Geological Society of America Bulletin, 78: 319-330.

Scutter, C.R., Cas, R.A.F., and Moore, C.L., 1998. Facies architecture and origin of a submarine rhyolitic lava flow-dome complex, Ponza, Italy. Journal of Geophysical Research, 103: 27551-27566.

Shervais, J.W., 1982. Ti-V plots and the petrogenesis of odern and ophiolitic lavas. Earth and Planetary Science Letters, 59: 101-118.

Sibuet, J.-C., Hsu, S.-K., Shyu, C.-T., and Liu, C.-S., 1995. Structural and kinematic evolutions of the Okinawa Trough backarc basin. In: Taylor, B. (Ed.) Backarc Basins: tectonics and magmatism. New York, Plenum Press, 343-379.

Simard, R.-L., 2000. Étude pétrographique et géochimique de trois intrusions porphyriques le long de la faille de Beniah Lake, Province de l'Esclave, Territoires du Nord-Ouest. BSc. thesis. Université du Québec à Chicoutimi, 67 p.

Smith, D.K., and Cann, J.R., 1992. The role of seamount volcanism in crustal construction at the Mid-Atlantic Ridge (24°-30°N). Journal of Geophysical Research, 97: 1645-1658.

Smith, G.A., 1991. Facies sequences and geometries in continental volcaniclastic sediments. In: Fisher, R.V., and Smith, G.A. (Eds.), Sedimentation in Volcanic Settings. Society for Sedimentary Geology Special Publication 45: 109-121.

Smith, J.R., Taylor, B., Malahoff, A., Petersen, L., 1990. Submarine volcanism in the Simusi Rift, Izu-Bonin arc. Earth and Planetary Science Letters, 100: 148-160.

Smith, T.L., and Batiza, R., 1989. New field and laboratory evidence for the origin of hyaloclastite flows on seamount summits. Bulletin of Volcanology, 51: 96-114.

Sohn, Y.K., 1995. Geology of Tok Island, Korea: eruptive and depositional processes of a shoaling to emergent island volcano. Bulletin of Volcanology, 56: 660-674.

Spray, J.G., 1985. Dynamothermal transition zone between Archaean greenstone and granitoid gneiss at Lake Dundas, Western Australia. Journal of Structural Geology, 7: 187-203.

Staudigel, H., and Schminke, H.-U., 1984. The Pliocene seamount series of La Palma/Canary Islands. Journal of Volcanology and Geothermal Research, 89: 11195-11215.

Storey, M., Mahoney, J.J., Kroenke, L.W., and Saunders, A.D., 1991. Are oceanic plateaus sites of komatiite formation? Geology, 19: 376-379.

Stubley, M., 1989. Geology of the Spencer Lake area; parts of NTS 85 P/1,2. DIAND EGS Map 1989-12, scale 1:50 000.

Sun, S-S., and McDonough, W.F., 1989. Chemical and isotopic systematics of oceanic basalts: implications for mantle composition and processes. In: Saunders, A.D., and Norry, M.J. (Eds.) Magmatism in the Ocean Basins. Geological Society of London Special Publication 42: 313-345.

Sylvester, P.J., Attoh, K., and Schulz, K.J., 1987. Tectonic setting of late Archean bimodal volcanism in the Michipicoten (Wawa) greenstone belt, Ontario. Canadian Journal of Earth Sciences, 24: 1120-1134.

Taira, A., Pickering, K.T., Windley, B.F., and Soh, W., 1992. Accretion of Japanese island arcs and implications for the origin of Archean greenstone belts. Tectonics, 11: 1224-1244.

Tamaki, K., 1995. Opening tectonics of the Japan Sea: In Taylor, B., (Ed.), Backarc Basins: tectonics and magmatism. New York, Plenum Press, 407-420.

Tarney, J., and Windley, B.F., 1981. Marginal basins through geological time. Philosophical Transactions of the Royal Society of London. A301: 217-232.

Thorpe, R.I., Cumming, G.L., and Mortensen, J.K., 1992. A significant Pb isotope boundary in the Slave Province and its probable relation to ancient basement in the western Slave Province. Geological Survey Open File 2484: 179-184.

Thurston, P.C., 1994. Archean volcanic patterns. In: Condie, K.C., (Ed.) Archean Crustal Evolution. Developments in Precambrian Geology 11. Elsevier. 45-84.

Thurston, P.C., and Chivers, K.M., 1990. Secular variation in greenstone sequence development emphasizing Superior Province, Canada. Precambrian Research. 46: 21-58.

van Breemen, O., Davis, W.J., and King, J.E., 1992. Temporal distribution of granitoid plutonic rocks in the Archean Slave Province, northwest Canadian Shield. Canadian Journal of Earth Sciences. 20: 2186-2199.

van Breemen, O., Henderson, J.R., Jefferson, C.W., Johnstone, R.M., and Stern, R., 1994. U-Pb age and Sm-Nd isotopic studies in Archean Hood River and Torp Lake supracrustal belts, northern Slave Province, Northwest Territories. In: Radiogenic Age and Isotopic Studies Report 8, Geological Survey of Canada Paper 1994-F: 1-16.

Viereck, L.G., Griffin, B.J., Schmincke, H.-U., and Pritchard, R.G., 1982. Volcaniclastic rocks of the Reydarfjordur Drill Hole, eastern Iceland. 2. Alteration. Journal of Geophysical Research. 87: 6459-6476.

Villeneuve, M.E., 1994. Correlating within and between Slave Province greenstone belts using U-Pb dating. DIAND Exploration Overview: p. 60.

Walker, G.P.L., 1992. Morphometric study of pillow-size spectrum among pillow lavas. Bulletin of Volcanology, 54: 459-474.

Walker, G.P.L., 1993. Basaltic-volcano systems. In: Prichard, H.M., Alabaster, T., Harris, N.B.W., Neary. C.R. (Eds.), Magmatic processes and plate tectonics. Geological SocietymSpecial Publication No. 76: 3-38.

Walker, G.P.L., 2000. Basaltic volcanoes and volcanic systems. In: Sigurdsson. H. (Ed.) Encyclopedia of Volcanoes. San Diego, Academic Press, 283-289.

Wells. G., Bryan, W.B., and Pearce, T.H., 1979. Comparative morphology of ancient and modern pillow lavas. Journal of Geology, 87: 427-440.

Wharton, M.R., Hathway, B., and Colley. H., 1995. Volcanism associated with extension in an Oligocene-Miocene arc. southwestern Viji Levu, Fiji. In: Smellie. J.L. (Ed.), Volcanism Associated with Extension at Consuming Plate Margins. Geological Society of London. Special Publication 81. 95- 114.

Wilson. M.. 1989. Igneous Petrogenesis: a global tectonic approach. London. Chapman and Hall, 466 pp.

Windley. B.F.. 1995. The Evolving Continents. John Wiley and Sons, Chichester. 526 pp.

Yamagishi. H.. 1991. Morphological and sedimentological characteristics of the Neogene submarine coherent lavas and hyaloclastites in Southwest Hokkaido, Japan. Sedimentary Geology. 74: 5-23.

Yamagishi. H.. 1994. Subaqueous volcanic rocks. Hokkaido University Press, Japan. 195 pp.

Yamagishi. H.. and Dimroth. E.. 1985. A comparison of Miocene and Archean rhyolite hyaloclastites: evidence for a hot and fluid rhyolite lava. Journal of Volcanology and Geothermal Research. 23: 337-355.

Yamagishi, H., Sakamoto, I., and Ishii. J.. 1989. Internal structures of pillow lobes of Cenozoic and Mesozoic pillow lavas in and around Hokkaido. Proceedings of the Hokkaido Tokai University, Science and Engineering 2: 107-118.

Young, G.M., 1991. The geologic record of glaciation: relevance to the climatic history of the Earth. Geoscience Canada 18: 100-108.